SUPRAMOLECULAR COORDINATION CHEMISTRY OF PHOSPHORUS, ARSENIC, ANTIMONY, AND BISMUTH WITH ORGANOTHIOLATES

by

VIRGINIA MAY CANGELOSI

A DISSERTATION

Presented to the Department of Chemistry
and the Graduate School of the University of Oregon
in partial fulfillment of the requirements
for the degree of
Doctor of Philosophy

September 2010

University of Oregon Graduate School

Confirmation of Approval and Acceptance of Dissertation prepared by:

Virginia Cangelosi

Title:

"Supramolecular Coordination Chemistry of Phosphorus, Arsenic, Antimony, and Bismuth with Organothiolates"

This dissertation has been accepted and approved in partial fulfillment of the requirements for the Doctor of Philosophy degree in the Department of Chemistry by:

James Hutchison, Chairperson, Chemistry
Darren Johnson, Member, Chemistry
Catherine Page, Member, Chemistry
Michael Haley, Member, Chemistry
Scott Bridgham, Outside Member, Biology

and Richard Linton, Vice President for Research and Graduate Studies/Dean of the Graduate School for the University of Oregon.

September 4, 2010

Original approval signatures are on file with the Graduate School and the University of Oregon Libraries.

An Abstract of the Dissertation of

Virginia May Cangelosi for the degree of Doctor of Philosophy

in the Department of Chemistry to be taken September 2010

Title: SUPRAMOLECULAR COORDINATION CHEMISTRY OF PHOSPHORUS, ARSENIC, ANTIMONY, AND BISMUTH WITH ORGANOTHIOLATES

Approved: _____
Darren W. Johnson

The ever-expanding field of supramolecular chemistry has recently incorporated use of the main group ions. This dissertation presents a supramolecular approach to the coordination chemistry of the Group 15 elements, with a special emphasis on arsenic (As). Arsenic is ubiquitous in our environment, contaminates the drinking water of large human populations, and is a worldwide health concern. Arsenic's legendary toxicity is thought to be due to its thiophilicity and the stability of arsenic-thiolate bonds within proteins. Chapter I is a review of the current literature on the kinetics, thermodynamics, and supramolecular chemistry of the As(III)-thiolate bond and reveals that the stability and lability of the bond make it well-suited for supramolecular chemistry. The remainder of the dissertation explains our supramolecular design strategies for the As(III) ion with thiolate ligands, then expands the approach to the Group 15 elements phosphorus, antimony, and bismuth.

Chapter II presents an approach to controlling diastereoselectivity in the self-assembly of supramolecular $As_2L_2Cl_2$ macrocycles using *intramolecular* steric interactions. Chapter III expands upon this approach by using *intermolecular* steric interactions to control diastereoselectivity and dimer formation of $As_2L_2Cl_2$ macrocycles. Chapter IV gives insight into the self-assembly of these $As_2L_2Cl_2$ macrocycles by identifying several reaction intermediates and kinetic mistakes that form during the course of the reaction. In Chapter V the application of our design strategy to the heavier Group 15 elements of antimony and bismuth is shown through the presentation of E_2L_3 cryptands (E = As, Sb, Bi). Additionally, a Group 15 "transmetallation" reaction is explained which allows, for the first time, the preparation of the elusive P_2L_3 cryptand. Chapter VI further examines the transmetallation reaction, the solution isomerism of the E_2L_3 cryptands, and presents three heterometallic $EE'L_3$ cryptands. Finally, Chapter VII briefly concludes this dissertation and provides some potential future directions for the project.

This dissertation includes co-authored material and previously published results.

CURRICULUM VITAE

NAME OF AUTHOR: Virginia May Cangelosi

PLACE OF BIRTH: Grand Rapids, MI

DATE OF BIRTH: November 24, 1982

GRADUATE AND UNDERGRADUATE SCHOOLS ATTENDED:

University of Oregon, Eugene, OR
Albion College, Albion, MI
University of Wollongong, Wollongong, NSW, Australia

DEGREES AWARDED:

Doctor of Philosophy, Chemistry, 2010, University of Oregon
Bachelor of Arts, Chemistry, 2005, Albion College

AREAS OF SPECIAL INTEREST:

Supramolecular Chemistry
Main Group Coordination Chemistry

PROFESSIONAL EXPERIENCE:

Graduate Research Assistant, University of Oregon, 2006-2010
Graduate Teaching Fellow, University of Oregon, 2005-2010

GRANTS, AWARDS AND HONORS:

National Science Foundation GK12 Fellowship, 2007-2010
Department of Education GAANN Fellowship, 2007-2010
University of Oregon Women in Technology and Science Travel Award, 2010
American Chemical Society Travel Award, 2008

PUBLICATIONS:

Cangelosi, V. M.; Carter, T. G.; Crossland, J. L.; Zakharov, L. N.; Johnson, D. W. "Self-Assembled E_2L_3 Cryptands (E = P, As, Sb, Bi): Transmetallation, Homo- and Heterometallic Assemblies, and Conformational Isomerism" *submitted to Inorg. Chem.*

Cangelosi, V. M.; Pitt, M. A.; Vickaryous, W. J.; Allen, C. A.; Zakharov, L. N.; Johnson, D. W. "Design Considerations for the Group 15 Elements: The Pnictogen···π Interaction as a Complementary Component in Supramolecular Assembly Design" *Cryst. Growth Des.* **2010**, *in press*.

Lindquist, N. R.; Carter, T. C.; Cangelosi, V. M.; Zakharov, L. N.; Johnson, D. W. "Three's Company: Co-crystallization of a Self-Assembled S_4 Metallacyclophane with Two Diastereomeric Metallacycle Intermediates" *Chem. Commun.* **2010**, *46*, 3505-3507.

Cangelosi, V. M.; Zakharov, L. N.; Crossland, J. L.; Franklin, B. C.; Johnson, D. W. "A Surprising "Folded-In" Conformation of a Self-Assembled Arsenic-Thiolate Macrocycle" *Cryst. Growth Des.* **2010**, *10*, 1471-1473.

Cangelosi, V. M.; Zakharov, L. N.; Johnson, D. W. "Supramolecular "Transmetalation" Leads to an Unusual Self-Assembled P_2L_3 Cryptand" *Angew. Chem., Int. Ed.* **2010**, 1248-1251.

Cangelosi, V. M.; Carter, T. C.; Zakharov, L. N.; Johnson, D. W. "Observation of Reaction Intermediates and Kinetic Mistakes in a Remarkably Slow Self-Assembly Reaction" *Chem. Commun.* **2009**, 5606-5608.

Allen, C. A.; Cangelosi, V. M.; Zakharov, L. N.; Johnson, D. W. "Supramolecular Organization Using Multiple Secondary Bonding Interactions" *Cryst. Growth Des.* **2009**, *9*, 3011-3013.

Cangelosi, V. M.; Zakharov, L.N.; Fontenot, S. A.; Pitt, M. A.; Johnson, D. W. "Host-Guest Interactions in a Series of $As_2L_2Cl_2$ Macrocycles" *Dalton Trans.* **2008**, 3447-3453.

Cangelosi, V. M.; Sather, A. C.; Zakharov, L. N.; Berryman, O. B.; Johnson, D. W. "Diastereoselectivity in the Self-Assembly of $As_2L_2Cl_2$ Macrocycles is Directed by the As-π Interaction" *Inorg. Chem.* **2007**, *46*, 9278-9284.

Carter, T. G.; Vickaryous, W. J.; Cangelosi, V. M.; Johnson, D. W. "Supramolecular Arsenic Coordination Chemistry" *Comments on Inorg. Chem.* **2007**, *28*, 97-122.

ACKNOWLEDGMENTS

First and foremost I would like to thank my advisor Darren Johnson for the support and encouragement he has provided me throughout the last five years. His excitement for chemistry is contagious and the mentoring he provided is indispensible. He has managed to build a very fun and supportive lab environment by not ignoring the importance of interpersonal relationships and team building with barbeques, poker, and a little lab competition (aka fantasy football). I've especially appreciated the unquestioning acceptance that he has shown me over the last several months while lab work has been impossible. Additionally, I would like to thank my thesis committee chair Jim Hutchison and members Mike Haley, Cathy Page, and Scott Bridgham for their guidance and time. I also appreciate the quick, insightful, and kind feedback on crystals from Lev Zakharov. His structures have been an integral part of my research and this project could not have advanced without them. Funding from the Department of Education GAANN, NSF GK12, and the University of Oregon are acknowledged.

I have been lucky to work with an eclectic group of lab mates whom have helped me to grow professionally and personally. Specifically, I have enjoyed input and help from the toxics group: Tim Carter, Sean Fontenot, and Jake Vickaryous. Corinne Allen went above-and-beyond what I expected of her as "my undergrad" and I look forward to seeing her future success. Finally, in the last couple months, Justin Crossland has been a great help in wrapping up several key experiments.

Outside of my lab, I have been privileged to befriend a number of motivational, inspirational, and fun cohorts. My fellow classmates made the first two years of grad school hoop-jumping a lot more enjoyable. I've enjoyed getting some outside perspective from Lallie McKenzie and Elsa Johnson. The professional development and mentoring that I have gotten from Women in Graduate Sciences members, specifically Suzanne Buck, has been appreciated.

Lastly, I would like to thank my friends and family. I'm glad to have spent much of my free time with Rachel and Charlie Swor and Lauren and Ian Moody. My parents, Mark and Gloria, and my siblings, Margie, Carrie, Terry and Elena, have been very supportive over the last five years. Finally, John, thank you for sharing Oregon with me.

To John and our final grad school experiment. I hope she turns out like her dad.

TABLE OF CONTENTS

Chapter Page

Chapter Page

Chapter Page

Chapter Page

Chapter Page

Chapter Page

LIST OF FIGURES

Figure Page

Figure Page

Figure Page

LIST OF TABLES

LIST OF SCHEMES

Scheme Page

CHAPTER I

Scheme Page

LIST OF CHARTS

CHAPTER I

KINETICS, THERMODYNAMICS, AND STRUCTURE OF THE ARSENIC(III)-THIOLATE BOND

General Overview

This dissertation describes the supramolecular chemistry which occurs between rigid dithiol and dithiolate ligands and the Group 15 elements (P, As, Sb, and Bi). The majority of the work in this document focuses on the utilization of the dynamic arsenic-thiolate bond for self-assembly, but later chapters (V and VI) apply these lessons to phosphorus, antimony and bismuth as well. Chapter I sets the stage for the utilization of the As(III)-thiolate bond in self-assembly by reviewing the kinetics, stability, preferred structure, and published supramolecular chemistry of the bond. Chapters II and III (published, co-authored) describe how steric interactions can be used to promote stereoselectivity in the self-assembly of arsenic-containing macrocycles. Chapter IV (published, co-authored) explores the self-assembly process, giving insight into the kinetics of the As-S bond and supramolecular assembly. Chapters V (published, co-authored) and VI (co-authored) apply these lessons in As-S chemistry to other Group 15 elements. The reactivity, dynamic solution behavior, and structures of a series of Group

15 element-containing cryptands are described. Chapter VII is a brief conclusion that further ties together these chapters and suggests some potential future experiments.

Chapter I surveys the literature on the As(III)-thiolate bond. The strength and lability of this bond are implicated in the toxicity of arsenic, yet the mechanism(s) of arsenic toxicity are not fully understood. This chapter begins with a brief overview of arsenic as a worldwide drinking water contaminant and the implications of arsenic contamination on human health. Next, the kinetics and thermodynamics of the As(III)-thiolate bond are reviewed. It is revealed found that the bond is kinetically labile, but thermodynamically stable. The following section explores the preferred geometry of As(III)-thiolate complexes by presenting a representative sample of crystal structures containing As(III)-thiolate bonds. Finally, the use of the As(III)-thiolate bond in protein mimics and supramolecular assemblies is reported.

Introduction

Arsenic (As) is infamous for its toxicity and its presence in drinking water is a worldwide health problem. There have already been several excellent reviews on arsenic's toxicity,[1,2] distribution,[3] water chemistry,[4] and metabolism.[5] Here, we will review the As(III)-thiolate bond, thought to play a critical role in arsenic's toxicity. Specifically, we aim to learn about the stability and lability of the As(III)-thiolate (herein referred to as As-S) bond by looking at relevant examples from the literature that report on the kinetics, thermodynamics and structure of the bond. While many examples are

pulled from the biochemical literature, this is not an exhaustive review of biologically relevant As-containing molecules. This chapter will wrap with an overview of how the As-S bond has been used in supramolecular design strategies.

Arsenic is the 20th most common element on the planet[3] and, consequently, is ubiquitous in the environment. Arsenic occurs naturally in over 300 types of minerals, many of which also contain sulfur, and is released into the air and water during natural weathering processes.[6] Once a part of the groundwater cycle, arsenic can easily spread. Dangerously high levels of arsenic in drinking water[7] are a worldwide problem, especially affecting highly populated regions in Asia, Europe, and North and South America.[2,4,8] The World Health Organization recommends a maximum of 10 μg As per liter of drinking water, yet these limits are severely exceeded in many natural water sources, including, but not limited to, those in Bangladesh,[9,10] Vietnam,[11] and the western and New England regions of the United States of America.[12]

While arsenic is naturally occurring, it can also be introduced into a local environment by human activities such as coal burning,[13] mining,[14] and the use of poultry litter as a fertilizer.[15] Arsenic has also been used medicinally throughout history.[16] Currently, it can be found in treatments for African sleeping sickness (melarsoprol)[17] and acute promyelocytic leukemia (arsenic trioxide).[18] Unfortunately, treatment with arsenic-containing drugs is not without risk. In fact 4-8% of individuals treated with melarsoprol die from the treatment.[19] Acute exposure to arsenic is fatal, hence its use as a poison,[16,20] even to this day.[21] However, many more people are affected by long term exposure to

low levels of arsenic in their drinking water. In 2000, a risk assessment was carried out investigating bladder, liver and lung cancer caused by exposure to arsenic in drinking water. It was found that consumption of water containing 50 μg/L arsenic led to an increased risk of cancer and, therefore, a limit set at that level is not protective of human health.[22] Regular exposure to arsenic in drinking water has been correlated with increased rates of skin, liver, kidney, colon, bladder, and lung cancer[23] as well as lesions on the hands and feet,[24] hematologic disorders, diabetes, developmental and neurological disorders, and cardiovascular disease.[25]

Arsenic toxicity has been shown to be heavily dependent on its speciation.[4] In an aqueous environment, arsenic typically exists as the arsenate (As(V)) species H_3AsO_4 (**1**), $H_2AsO_4^{1-}$ (**2**), and $HAsO_4^{2-}$ (**3**) (Chart 1).[26] However, in vivo, arsenate is reduced to arsenite (As(III)) (**4**) which is more toxic.[27] In humans, arsenite is known to go through a series of methylation steps, with monomethylarsenite (MMA, **5**) and dimethylarsenite (DMA, **6**) being excreted in urine (Chart 1).[28] Methylation is not necessarily a detoxification pathway, though; MMA is known to be more toxic than arsenite.[29]

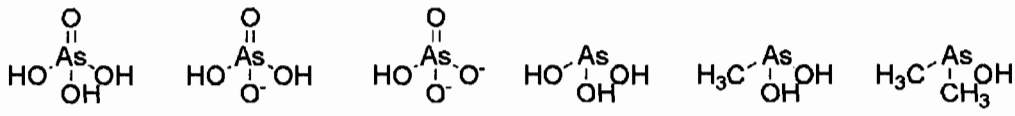

1 **2** **3** **4** MMA **5** DMA **6**

Chart 1. Common arsenic species.

While arsenic's toxicity is legendary, its mechanism of toxicity is not well understood, probably because arsenic interacts with so many different biomolecules in vivo. Arsenic is very thiophilic and strong As(III)-thiolate bonding between arsenite and cysteine has been known and studied since at least the 1920s.[30,31] Glutathione (GSH, **7**) is thought to play an important role in arsenic detoxification (Chart 2).[27] Consequently As(III)-GSH adducts, such as $As(GS)_3$ (**8**) have been well studied[32-34] by NMR[35] and mass spectrometry.[36,37]

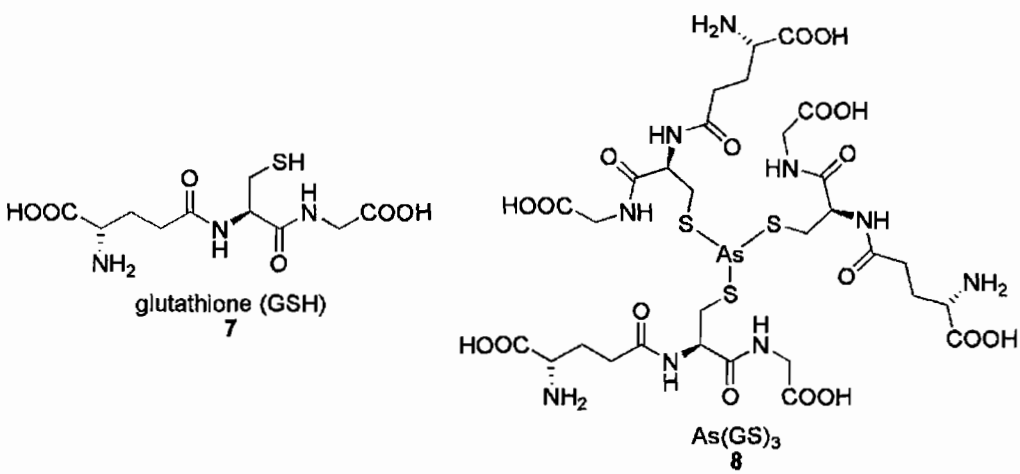

Chart 2. Structures of glutathione (**7**) and $As(GS)_3$ (**8**).

Arsenic can cause changes to the secondary structure of cysteine-containing proteins upon binding,[38] inhibiting their functions.[39] Arsenic has been shown to bind to metallothionein,[40-48] hemoglobin,[49] ArsR protein,[50,51] galectin-1 and thioredoxin peroxidase II,[52,53] GLUT4,[54] tubulin and Actin.[55] In 2009, Yan and co-workers used an

affinity selection technique to identify over 70 proteins in human lung carcinoma cells alone that bind arsenic.[56] This chapter summarizes the current understanding of the As-S bond – knowledge that is vital to understanding arsenic's mode of toxicity.

Kinetics of the As(III)-Thiolate (As-S) Bond

The rates by which As(III)-thiolate complexes react are important for understanding As-toxicity and its use in supramolecular assemblies. However, there are limited examples of in-depth kinetic analysis of the As-S bond.

Kinetics for Small Biomolecule-Arsenic Adducts

One of the first experiments on the kinetics of the As-S bond was carried out by Zahler and Cleland in the late 1960s.[57] Rate constants for the formation and dissociation of complexes of biologically-relevant dithiols (Chart 3) with arsenite were measured in the course of designing a sensing assay for disulfide groups. For dithiothreitol (DTT, **9**) the rate constant for complex formation was found to be $k_{on} = 4.7 \times 10^2$ $sec^{-1}M^{-1}$ and the rate constant for complex dissociation was found to be $k_{off} = 1.5 \times 10^{-4}$ sec^{-1}. Similarly, these rate constants were found to be $k_{on} = 4.5 \times 10^2$ $sec^{-1}M^{-1}$ and $k_{off} = 1.7 \times 10^{-4}$ sec^{-1} for dithioerythritol (DTE, **10**), $k_{on} = 1.2 \times 10^3$ $sec^{-1}M^{-1}$ and 5.7×10^{-4} sec^{-1} for 1,3-dithioglycerol (**11**), and $k_{on} = 3.0 \times 10^2$ $sec^{-1}M^{-1}$ and $k_{off} = 7.7 \times 10^{-5}$ sec^{-1} for 1,2-dithioglycerol (**12**). It should be noted that these rates were calculated for the *complex* formation which includes two As-S bonds and, in the case of DTT and possibly the

others, an intramolecular As-O bond.[58] Individual As-S bond formation and dissociation are expected to be significantly faster, especially if the second As-S bond forms cooperatively.

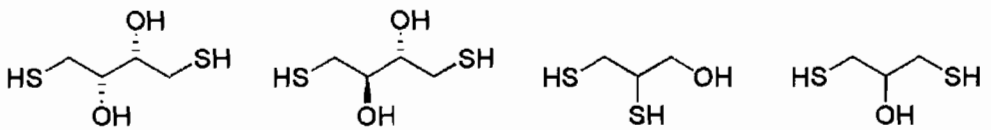

Chart 3. Biomolecules used in kinetic experiments by Zahler and Cleland.[57]

Kinetics of the As-S Bond Within Nanoreactors

Recently, rate constants have been obtained by Bayley and co-workers for the formation and dissociation of As-S bonds using single-molecule techniques.[59,60] By binding 4-sulfophenylarsonous acid (**13**) (Figure 1a) to a cysteine residue at position 117 within an α-hemolysin pore, kinetic measurements were carried out on the reversible formation and dissociation of the As-S bond. In their first experiment, the pore was modified to contain just one cysteine residue[59] and rate constants were found to be k_{on} = 2.0×10^4 $M^{-1}s^{-1}$ for the forming of an As-S bond and $k_{off} = 1.4$ s^{-1} for the breaking of that bond. This gave an overall formation constant of $k_f = 1.4 \times 10^4$ M^{-1} at 24 °C. These rate constants were for a single As-S bond and are markedly faster than those observed for the multiple bonds involved in complex formation by Zahler and Cleland.[57]

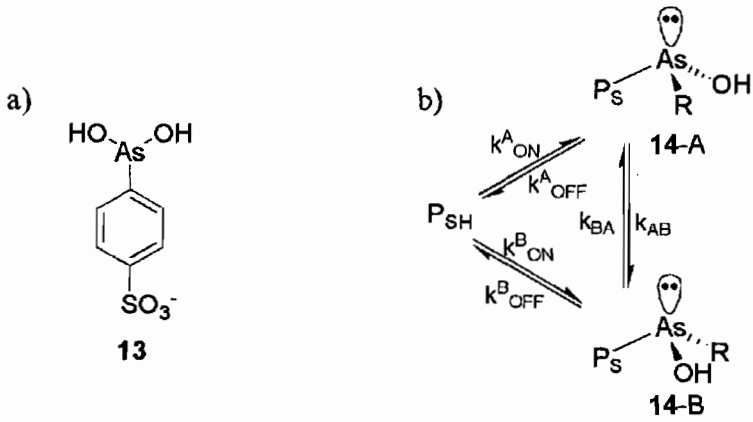

Figure 1. Structure of 4-sulfophenylarsonous acid (**13**) (a) and kinetic scheme showing binding of arsenic within pore to give isomeric products **14**-A and **14**-B (b).[60]

Moving the cysteine residue to position 137 revealed that two isomers (**14**-A and **14**-B) formed upon reaction of **13** with the nanoreactor (Figure 1b).[60] These isomers formed with slightly different rate constants of $k_{on} = 1.4 \times 10^4$ and 5.9×10^3 $M^{-1}s^{-1}$ and dissociated with rate constants of $k_{off} = 1.5$ and 0.40 s^{-1} for **14**-A and **14**-B, respectively. The overall formation constants of $k_f = 9.3 \times 10^3$ and 1.5×10^4 M^{-1} are similar to that observed when the cysteine residue was at position 117. These rate constants were expected to be similar to those in solution and, to test this, the authors carried out magnetization-transfer NMR spectroscopy experiments on a 2:1 GSH-4-sulfophenylarsonous acid adduct. A rate constant of 4.7 s^{-1} at 30 °C was found for GSH exchange, which was approximately the same as the rate of As-S bond dissociation in the nanoreactor.

Kinetics of As-S Bonds Within Proteins

As-toxicity is usually linked to the loss of cellular function that occurs upon As-cysteine binding in folded proteins. Arsenite (**4**), MMA (**5**), and an aryl arsenical bind cysteine residues in *un*folded proteins preferentially over GSH (**7**), likely leading to a loss in protein function.[61] The reaction of reduced riboflavin binding (Rfb) protein with excess MMA was monitored by fluorescence quenching on a stopped-flow instrument and it was found that 60% of the decrease in fluorescence occurred in the initial fast phase of the reaction. Pseudo-first order conditions yielded a second-order association rate constant of 2.35×10^3 $M^{-1}s^{-1}$. This was on the same order of magnitude as the rates found by Bayley and co-workers for As-S bond formation in a nanoreactor.[60]

Significant work has been carried out on the consequences of binding of arsenic to metallothioneins,[41-48] but only those with contributions to the kinetics of the As-S bond will be discussed here. The recombinant human metallothionein (rhMT) isoform 1a protein binds arsenic in the α (As_3S_{cys11}) and β (As_3S_{cys9}) domains (Figure 2). Time- and temperature-resolved electrospray mass spectrometry was used to conduct a complete kinetic analysis of the reaction of these isolated domains with As(III).[62] At pH 3.5 and room temperature, the individual rate constants were found to be 5.5, 6.3, and 3.9 $M^{-1}s^{-1}$ for the first, second, and third binding events to the α-domain and 3.6, 2.0, and 0.6 $M^{-1}s^{-1}$ for the β-domain. These rate constants are significantly slower than those in the unfolded Rfb proteins[61] and Bayley's nanoreactor.[60] Respectively, the activation energies were measured at 7.9, 6.9, and 5.5 kcal/mol for the α-domain and 7.6, 8.4, and 6.9 kcal/mol for

the β-domain. In each case, the activation entropies were negative (between -30.4 and -39.4 kcal/mol) and the activation enthalpies were positive (between 4.8 and 7.9 kcal/mol) giving very consistent activation free energies of between 16.3 and 17.4 kcal/mol at 25 °C.

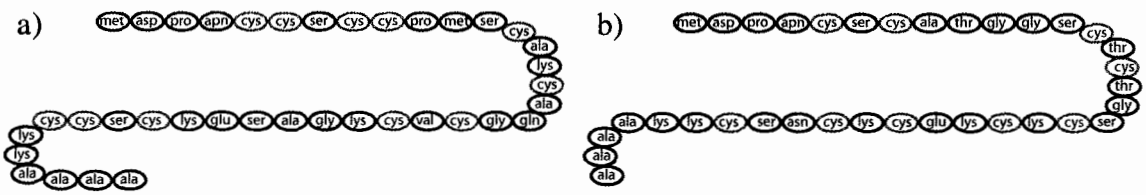

Figure 2. Recombinant human α-domain (a) and β-domain (b).[62]

Next, this electrospray mass spectrometry analysis was extended to the complete, two domain rhMT isoform 1a protein and the results were compared to those for the isolated domains.[63] It was found that the complete protein binds As(III) faster initially and that each successive binding event occurs slower, which implies a non-cooperative mechanism. Sequential rate constants for the binding events were found to be k = 25, 24, 29, 14, 8.7, and 3.7 $M^{-1}s^{-1}$. The authors attributed the faster binding in the complete protein to the larger number of binding sites for arsenic (six compared to three for each domain). Activation energies were found to be 3.3 kcal/mol for the first event and 5.3 kcal/mol for each subsequent event. Again, the activation entropies were negative (between -33.0 and -42.5 kcal/mol) and the activation enthalpies were positive (between

2.9 and 6.0 kcal/mol) giving very consistent activation free energies of between 15.3 and 16.5 kcal/mol at 25 °C. The authors concluded that increasing the number of equivalent binding sites in a protein increased the rate at which metals bind, implying that metallothionein may have evolved two sites in order to scavenge metals more efficiently.

The two domain *F. vesiculosus* metallothionein, found in seaweed, was also subjected to kinetic analysis upon As-binding.[64] Rate constants of 19.8 and 1.4 $M^{-1}s^{-1}$ were found for the γ domain and 16.3, 9.1 and 2.2 $M^{-1}s^{-1}$ for the β domain and the authors concluded that the length of the interdomain linker in multi-domain metallothioneins had a direct effect on the rate of binding metals. Again, there were similar activation energies (8.1 and 7.9 kcal/mol for the γ domain and 7.6, 8.4, and 6.5 kcal/mol for the β domain) with an average of 7.6 kcal/mol. Activation entropies (between -26.8 and -36.6 kcal/mol with average $\Delta S^{\ddagger}$ = -30.8 kcal/mol), activation enthalpies (between 6.0 and 7.9 kcal/mol with average $\Delta H^{\ddagger}$ = 7.2 kcal/mol), and activation free energies (between 15.5 and 17.2 kcal/mol with average $\Delta G^{\ddagger}$ = 16.5 kJ/mol) were similar to those found for the transition state in the human form of the protein.

More recently, this kinetic analysis has been extended to two three-domain proteins: recombinant βββ and ααα human metallothionein 1a, which contain 27 and 33 cysteine residues respectively.[65] Arsenic binding was found to be noncooperative at 198 K, with rate constants of 40, 36, 37, 26, 27, 17, 12, 6, and 1 $M^{-1}s^{-1}$ for the βββ protein and 52, 45, 46, 42, 38, 36, 29, 25, 14, and 6 $M^{-1}s^{-1}$ for the ααα protein.

Thermodynamics of the As(III)-Thiolate (As-S) Bond

As with the kinetic studies, much of the thermodynamic data on the As-S bond comes from biologically-relevant examples. In addition to measuring rate constants, Zahler and Cleland measured dissociation constants for arsenite-dithiolate adducts during the design of their free thiol sensing assay (Chart 3).[57] These dissociation constants can be converted to stability constants for comparison to the more recent literature. They concluded that, surprisingly, the five-membered ring adduct with 1,2-dithioglycerol (**11**) was the most stable with $K = 3.8 \times 10^6\ M^{-1}$, followed by two seven-membered ring adducts with DTT (**9**) ($K = 3.0 \times 10^6\ M^{-1}$) and DTE (**10**) ($K = 2.7 \times 10^6\ M^{-1}$). Finally, the six-membered ring adduct with 1,3-dithioglycerol (**12**) was the least stable ($K = 2.0 \times 10^6\ M^{-1}$). It has since been shown that the As-DTT complex is actually bicyclic in structure, not the seven-membered ring that the authors proposed. This does not mean that there is any problem with the stability constants reported for these complexes, but that correlations between ring size and stability cannot be drawn.

These results directly contradict Whittaker's previous experiments in which dithiols (**15**) with varying spacer lengths were tested to see which would reactivate pigeon brain pyruvate oxidase most effectively after poisoning with lewisite (**16**) (Scheme 1).[66] Stability constants were not reported, but the relative stability of the lewisite-adducts (**17**) with rings of varying size were reported. The authors concluded that rings containing five, six, and 9-13 atoms were the most stable. Larger rings and those containing seven or eight atoms were the least stable. However, disulfides in the

pigeon brain mince could have oxidized dithiols to varying degrees and dithiobutane has the lowest redox potential of the series giving a possible explanation for the discrepancy in S-As-S-containing ring stabilities. Several monothiols were found to be less stable than the rings and the enzyme-lewisite adduct.

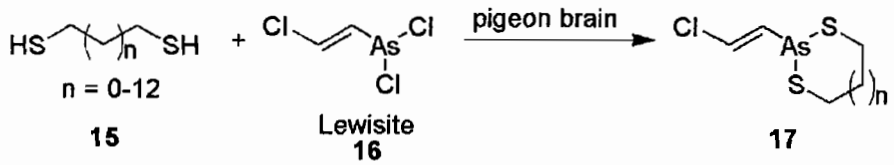

Scheme 1. Reaction of alkyl-spaced dithiols with lewisite in pigeon brain mince.[66]

The relative stabilities of several other monothiolate and dithiolate adducts of arsenite have also been reported. NMR spectroscopy showed exchange when dimercaptosuccinic acid (DMSA, **18**) was added to a solution of a $(glutathione)_3$-arsenite complex ($As(GS)_3$) (**8**) (Scheme 2),[35,67] further establishing the greater stability of dithiolate-arsenite adducts over monothiolate-arsenite adducts.[68] Additionally, DMSA was shown to form a more stable complex (**19**) (five-membered ring) with arsenite than was DTE (**10**) (seven-membered ring) (Scheme 3). This is in agreement with both Zahler and Cleland's[57] and Whittaker's[66] results.

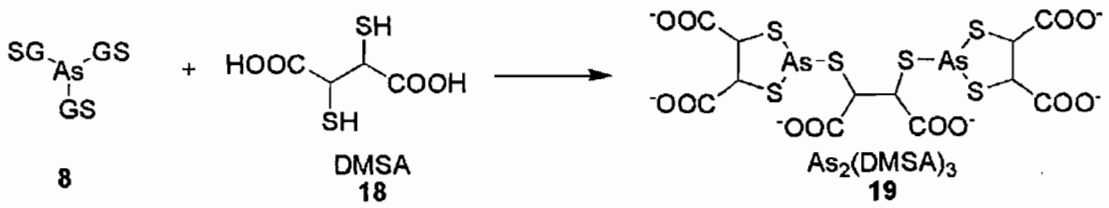

Scheme 2. Ligand-exchange reaction of $As(GS)_3$ (**8**) with DMSA (**18**).[35,67]

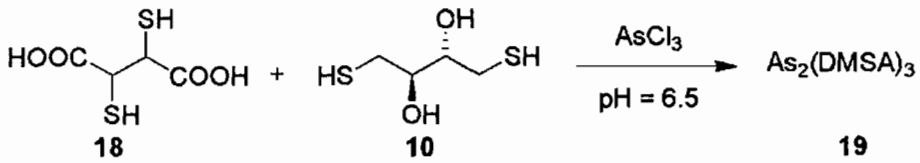

Scheme 3. Competition experiment of DMSA (**18**) with DTE (**10**).[35,67]

While these results indicate that monothiolate-arsenic adducts are not as stable as dithiolate adducts, they are still thought to be an important part of the arsenic detoxification route in many animals. Studying the stability of glutathione adducts with arsenite and MMA in rat bile revealed that neither $As(GS)_3$, nor $CH_3As(GS)_2$, is stable under physiological conditions.[69] However, As-treated rats had increased concentrations of glutathione present in their bile and it was found that both adducts were stabilized in a GSH concentration-dependent manner.

In 2004, Pereira-Maia et al. monitored potentiometric and spectroscopic titrations of cysteine (**20**) and glutathione (**7**) with sodium arsenite. The stability constants for the adducts that formed were log K = 29.84 for $As(Cys)_3$ (**21**), log K = 12.01 for $As(Cys)(OH)_2^-$ (**22**), log K = 32.0 for $As(GS)_3^{3-}$ (**8**), and log K = 10 for $As(GS)(OH)_2^{2-}$ (**23**) (Schemes 4 and 5).[70]

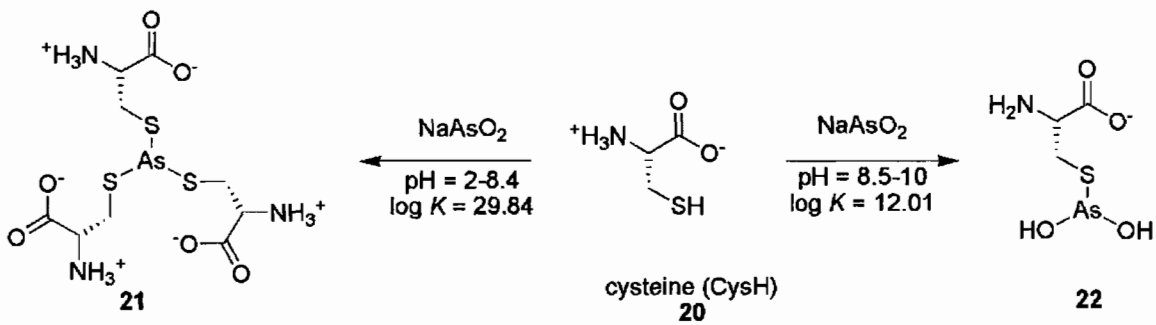

Scheme 4. Reaction of sodium arsenite with cysteine.[70]

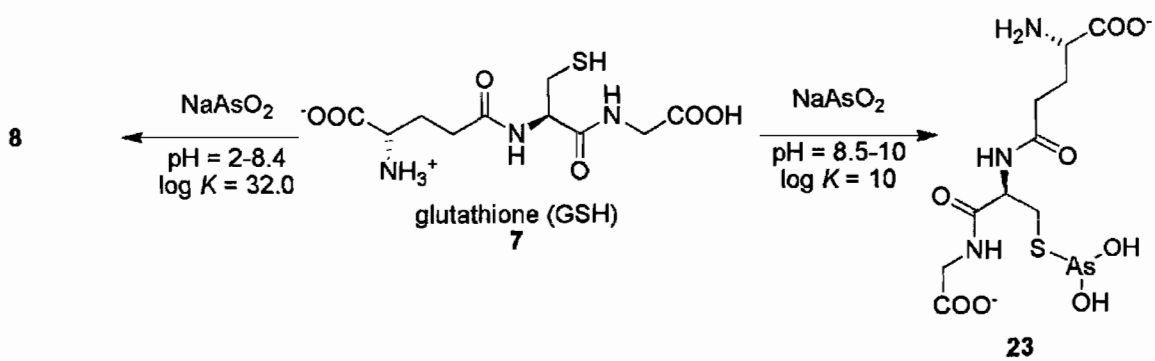

Scheme 5. Reaction of sodium arsenite with glutathione.[70]

These stability constants are inconsistent with those reported the following year by Wilcox et al. for the $As(GS)_3^{3-}$ (**8**).[71] Using near-UV absorption spectroscopy and isothermal titration calorimetry (ITC), the thermodynamics of arsenite and MMA coordinated by GSH (**7**), DMSA (**18**), dihydrolipoic acid (DHLA, **24**), and DTT (**10**) (Scheme 6) were quantified. Based on their spectroscopic data, they concluded that neither arsenite nor MMA formed particularly stable complexes (**8**, **25**) with GSH ($\beta = 1.0 \times 10^7$ for arsenite and $\beta = 2.3 \times 10^7$ for MMA), but that arsenite and DHLA do form a very stable 2:3 complex (**26**) ($\beta = 4 \times 10^{18}$). Other than this arsenite-DHLA adduct, MMA complexes ($K = 2.7 \times 10^5$ for 1:1 complex with DMSA (**27**), $K = 3.2 \times 10^6$ for 1:1 complex with DHLA (**28**), and $K = 2.0 \times 10^6$ for 1:1 complex (**29**) with DTT) were found to be more stable than arsenite complexes ($\beta = 5 \times 10^9$ for 1:2 complex with DMSA (**19**), $\beta = 4 \times 10^{18}$ for 2:3 complex (**26**) with DHLA, and $K = 1.1 \times 10^6$ for 1:1 complex (**30**) with DTT).

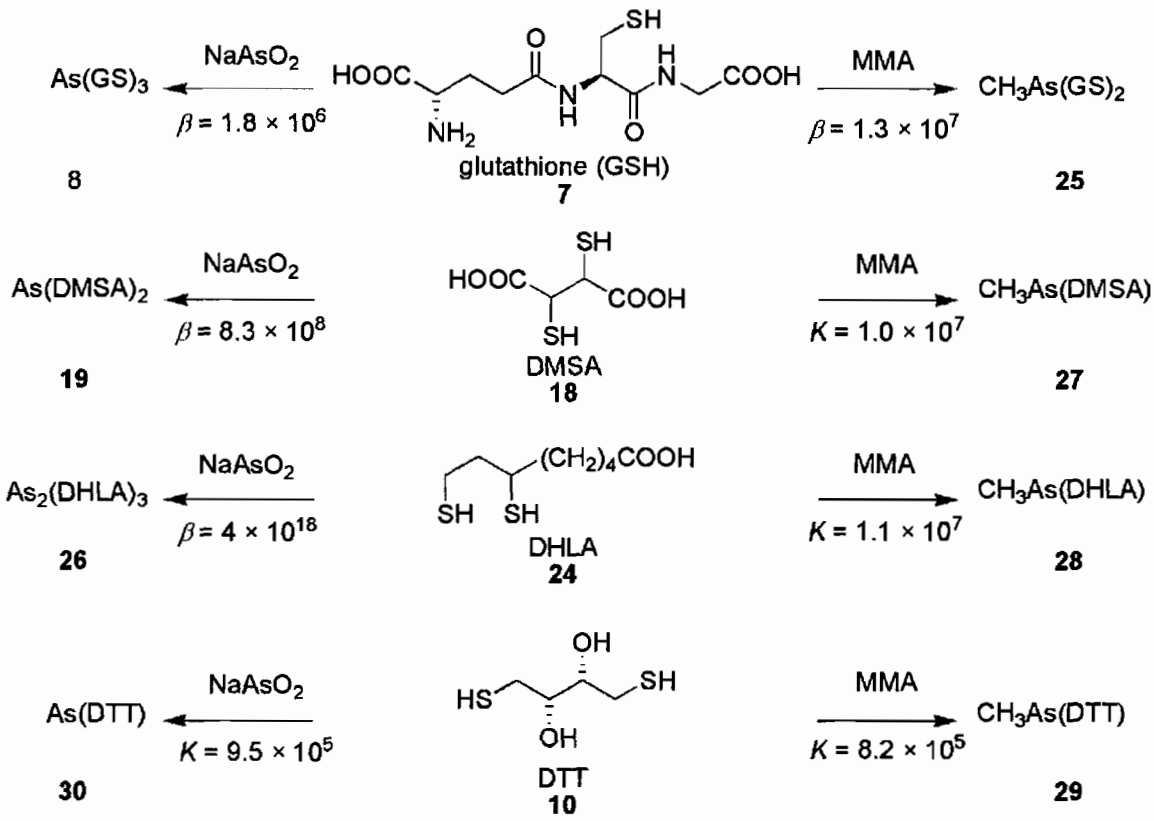

Scheme 6. Stability constants of complexes reported by Wilcox.[71] All values are taken from ITC data except for $As_2(DHLA)_3$.

Calorimetric data was obtained under almost identical conditions and the binding constants compare well with those obtained by spectroscopy ($\beta = 1.8 \times 10^6$ for **8**, $\beta = 8.3 \times 10^8$ for **19**, $\beta = 2.1 \times 10^5$ for **26**, and $K = 9.5 \times 10^5$ for **30**, $\beta = 1.3 \times 10^7$ for **25**, $K = 1.0 \times 10^7$ for **27**, $K = 1.1 \times 10^7$ for **28**, and $K = 8.2 \times 10^5$ for **29**). The most glaring discrepancy between UV and ITC results are the stability constants calculated for **26**, but the authors conclude that ITC cannot accurately account for the 2:3 stoichiometry and that the optical data is more accurate in this case. ITC also revealed thermodynamic

parameters for the formation of each of these As(III)-thiolate complexes. In general, it was found that formation became increasingly entropically unfavorable as ring size was increased. However, in each case the formation of the As-S bonds was exothermic and the formation of the complexes was favorable.

As previously mentioned, these results do not agree with those reported by Pereira-Maia et al.[70] However, the stability constant reported here by Wilcox for **30** (K = 1 x 10^6) does agree closely with that reported by Zahler and Cleland (K = 3 x 10^6 M^{-1}), despite the use of very different methods of measurement.[57] Wilcox's measurements also agree with previous observations that DMSA will extract As(III) from glutathione.[35,67]

Glutathione will form fully saturated complexes of arsenite, MMA, and DMA on a size-exclusion column with glutathione buffer under conditions resembling those within hepatocyte cytosol.[32,33] Temperature-dependent retention behavior of these arsenic compounds revealed that the As-S bonds in $CH_3As(SG)_2$ (**25**) and $(CH_3)_2As(SG)$ are more stable than those in $As(SG)_3$ (**8**).

Thermodynamics and Kinetics of Inversion at the As-Center

In some cases, As(III)-thiolate complexes exist as stereoisomers due to the stereochemistry at the As-center. The lone pair of electrons on $As(III)R_3$ compounds is stereochemically active due to the high barrier to inversion. Pyramidal inversion of this lone pair of electrons is known to be higher in energy in arsines than in amines or phosphines.[72,73] The first experimental measurement of the pyramidal inversion energy

of an arsine was carried out on ethylmethylphenylarsine (**31**) and found to be $\Delta G^{\ddagger}$ = 42-46 kcal/mol at 218 °C (Scheme 7).[74] This is significantly higher than the energy requirement that had been previously calculated for lone pair inversion in arsines.[75,76] A rate constant of 1.4×10^{-6} sec^{-1} was reported for the pyramidal inversion.

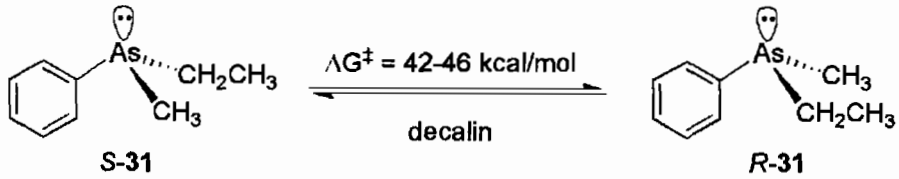

S-31 *R*-31

Scheme 7. Pyramidal inversion of ethylmethylphenylarsine (**31**).[74]

While pyramidal inversion is very slow, inversion at the arsenic center can also occur by the breaking and reforming of bonds to arsenic. In As(III)-S and As(III)-Cl complexes, inversion can occur through the breaking and reforming of As-S[60,77,78] (Scheme 8) or As-Cl[79] (Scheme 9) bonds, respectively. Either of these routes to inversion is expected to be faster and lower in energy than inversion of the lone pair.

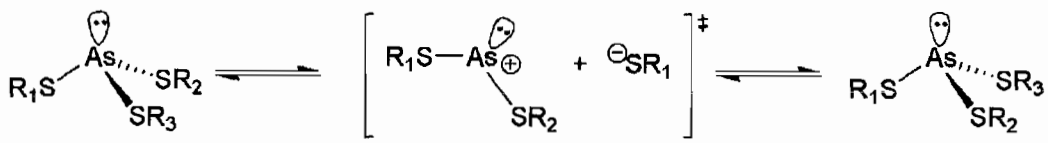

Scheme 8. Inversion by the breaking/reforming of As-S bond.

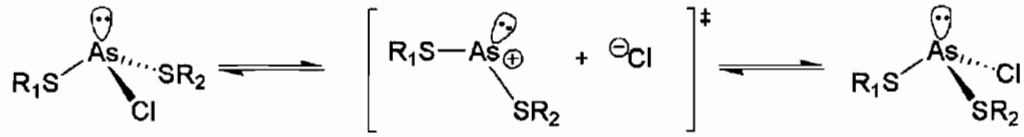

Scheme 9. Inversion by the breaking/reforming of As-Cl bond.

The first experimental measurements of the energy of inversion for compounds containing As-S bonds was carried out on several dithiarsolanes using ^{1}H NMR spectroscopy.[80] Here, the barriers were measured assuming coalescence at the highest temperature attained (197 °C). However, coalescence, or even line broadening, was not actually observed and consequently the reported values for the barrier to inversion are lower limits and the actual barriers can be expected to be significantly higher. The lower limit was measured as $\Delta G^{\ddagger} = 26$ kcal/mol for both PhAs(SCH_2CHMeS) (**32**) in chloroform and PhAs(S-*i*-$C_3H_7)_2$ in benzene (Scheme 10).

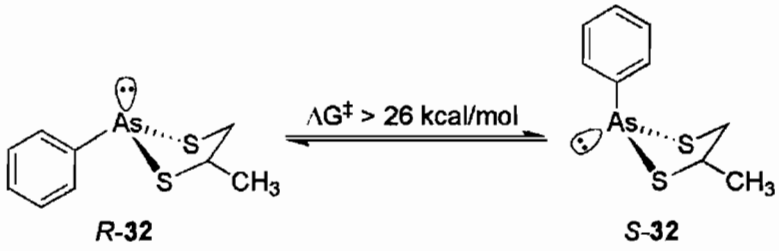

R-**32** *S*-**32**

Scheme 10. Inversion of **32**.[80]

Compounds with stereoisomers at the As-center are not necessarily energetically equivalent. Configurational isomers of arsenicals with different thermodynamic stabilities have been reported[81] as have several examples[79,82,83] of isomeric As-containing macrocycles. The latter will be discussed in detail in the "Supramolecular Arsenic Chemistry" section below.

In order to study the interconversion of stereoisomers, six-membered S-As-S-containing heterocycles were examined.[77] When crystals of the (2*RS*,4*RS*)-**33** isomer were dissolved in chloroform, they slowly (over several days at room temperature) converted to an equilibrium mixture consisting of 84% of that isomer and 16% of the (2*SR*,4*RS*)-**33** isomer (Scheme 11). In methanol, this conversion was much faster and gave a final ratio of 85:15, corresponding to a $\Delta G° = 1.0 \pm 0.2$ kcal/mol and an inversion energy of $\Delta G^{‡} = 26$ kcal/mol at 25 °C. Again, it was concluded that inversion occurred through the breaking and reforming of As-S bonds, not pyramidal inversion at the As-center. Because the rates of inversion were faster in methanol than in chloroform, the authors interpreted the inversion to occur by acid catalysis.

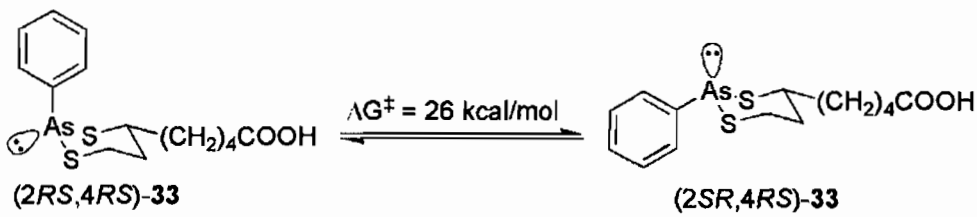

(2*RS*,4*RS*)-**33** (2*SR*,4*RS*)-**33**

Scheme 11. Inversion of **33**.[77]

Five- and six-membered isomeric rings containing S-As-S units were found to interconvert.[78] A double irradiation NMR experiment was used to obtain rate constants for interconversion between the geometric isomers. The phenyldichloroarsine adduct of 1,3-dimercapto-2-propanol, **34**, was found to exchange with rates of $k_1 = 0.419\ s^{-1}$ and $k_2 = 1.588\ s^{-1}$ at 298 K (Scheme 12). Activation energies for this exchange were measured at 10.25 kcal/mol for E_{a1} and 8.83 kcal/mol for E_{a2}. For the 1,2-dimercaptopropane adduct, **35**, rates of $k_1 = 0.975\ s^{-1}$ and $k_2 = 2.273\ s^{-1}$ at 295 K and activation energies of 13.66 kcal/mol for E_{a1} and 13.36 kcal/mol for E_{a2} were measured (Scheme 13), revealing that the five-membered ring is slightly more stable than the six-membered ring. Additionally, it was found that the exchange rates increased with increasing concentration of adduct or HCl and were affected by the addition of excess phenyldichloroarsine, but not by excess ligand. In both cases inversion occurred through the breaking and reforming of an As-S bond.

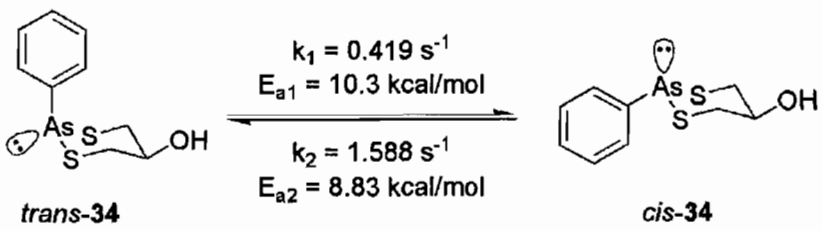

Scheme 12. Inversion of **34**.[78]

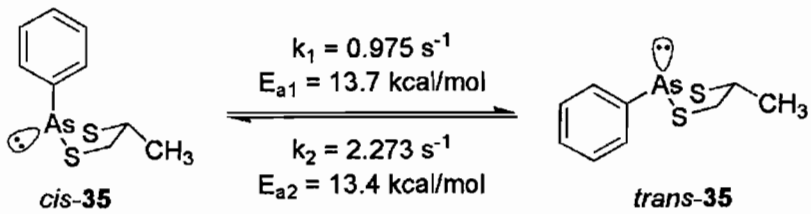

Scheme 13. Inversion of **35**.[78]

The kinetic analysis of the As-S bond within a nanoreactor by Bayley et al. also contained data on the rate constants for inversion between the two isomers.[60] They found that inversion occurred slowly relative to the breakdown of the As-S bond and less than 8% of all bond-breaking and forming events resulted in inversion. Inversion between isomers **14**-A and **14**-B occurred with rate constants of $k_{AB} = 7.1 \times 10^{-2}$ and $k_{BA} = 4.9 \times 10^{-2}$ s^{-1} (as compared to $k_{off} = 1.5$ and 0.4 s^{-1}) (Figure 1). The authors concluded that the process of inversion was based on an As-S bond breaking/reforming mechanism.

Preferred Geometries for As(III)-Thiolate Complexes

2004[84] and 2005[85] searches of the Cambridge Structural Database (CSD) revealed only 59 examples of crystal structures in which an As(III) ion was coordinated by one or more organic thiolate ligands. Of these, only 14 contained an As(III) ion that was also bonded to a carbon. This chapter will not cover every structure in the database, but will present a representative set of examples. These examples show that when bound by thiolates, As(III) typically has a predictable trigonal pyramidal coordination geometry which features a stereochemically active lone pair of electrons (Chart 4, left). However,

secondary bonding interactions (SBIs) between arsenic[86] and aryl rings[87-90] or heteroatoms such as oxygen,[85] sulfur,[91,92] or the halogens[93] can cause distortion of this preferred geometry. Extreme distortion results in a trigonal bipyramidal geometry around the arsenic atom (Chart 4, left center).

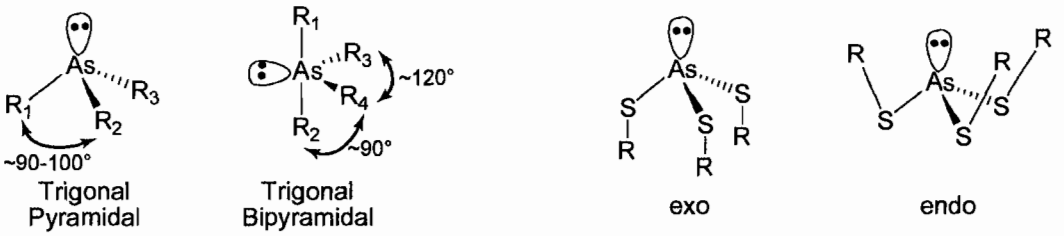

Chart 4. Common geometries (left) and conformations (right) for As(III)thiolate compounds.

Arsenic can also sit in either an endo or exo position relative to the ligands bound to it (Chart 4, right). When in the exo position, the lone pair of electrons on arsenic is relatively exposed as a result of the positioning of the thiolate ligands. In the endo configuration, the lone pair is "protected" and points in the same direction as the S-C bonds of the thiolate ligands. Examples of arsenic in both the endo and exo positions have been observed and in each case may result from steric bulk or SBIs. Like so many features of crystal structures, the positioning of arsenic could also be a simple consequence of crystal packing forces. The following examples of As(III)-thiolate complexes are organized based on the identity of the atoms bound directly to arsenic. The vast majority of examples come from X-ray crystal structures, but NMR, IR, and

EXAFS spectroscopy have all be used to glean structural information of arsenic complexes.

Trithiolate Complexes

The X-ray crystal structure of tri(phenylthio)arsine (**36**) shows that it is C_3-symmetric and has an As-S bond length of 2.24 Å and a S-As-S angle of 96° (Figure 3).[94] The As-center sits in the endo conformation, possibly because this orientation minimizes steric interactions between the ligands. A comparison was drawn between the C_3 solid-state structure to the time-average C_{3v} solution structure in which the As-center is also believed be in the shielded endo conformation.[95]

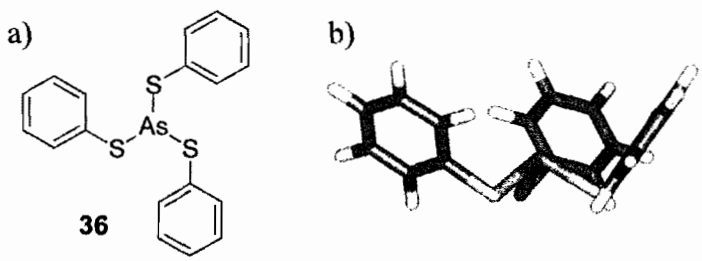

Figure 3. Cartoon (a) and stick (b) representations of the X-ray crystal structure of **36**.[94]

The treatment of N-(2-mercaptoethyl)-1,8-naphthalimide with $AsCl_3$ and base gave **37** (Figure 4).[85] The final structure of **37** is trigonal pyramidal but somewhat distorted due to steric interactions which allow only one weak As···O SBI with arsenic to

form. This interaction causes no elongation of the As-S bonds (2.23, 2.24, and 2.24 Å), but the S-As-S bond angles are far from equal (95, 96, 106°). The endo conformation of the As-center in this example may result from this SBI.

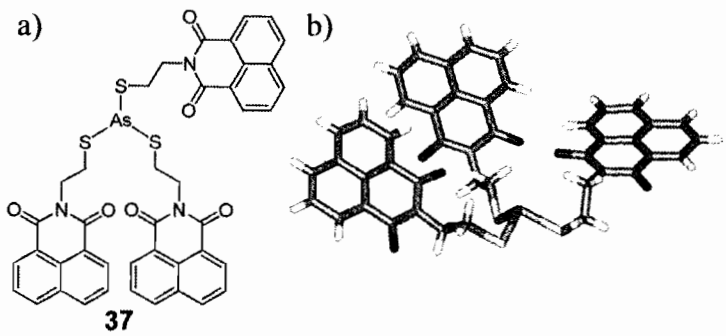

Figure 4. Cartoon (a) and stick (b) representations of the X-ray crystal structure of **37**.[85]

Recently, the structures of three new trithiolate arsenic complexes were reported (Chart 5, Figure 5).[96,97] Compound **38** contained two five-membered rings linked covalently by an -SCH_2CH_2S- unit with As-S distances ranging between 2.23 and 2.27 Å and S-As-S bond angles between 93 and 102°.[96] The longest bonds and widest angles around arsenic involved those sulfur atoms that were not a part of a ring system. Compound **39** contained three pentafluorophenylthiolate ligands bound to arsenic (Chart 5, Figure 5)[96] Unlike its non-fluorinated analogue **36**,[94] this complex did not crystallize with C_3 symmetry. Instead, unequal S-As-S angles of 88, 98, and 99° were reported. Additionally, As-S distances (2.26-2.27 Å) were slightly longer than in **36** (2.24 Å),

suggesting that electronic effects can influence the length of As-S bonds. In the solid state structures of both **39** and **36**, the As-center was in the endo conformation.

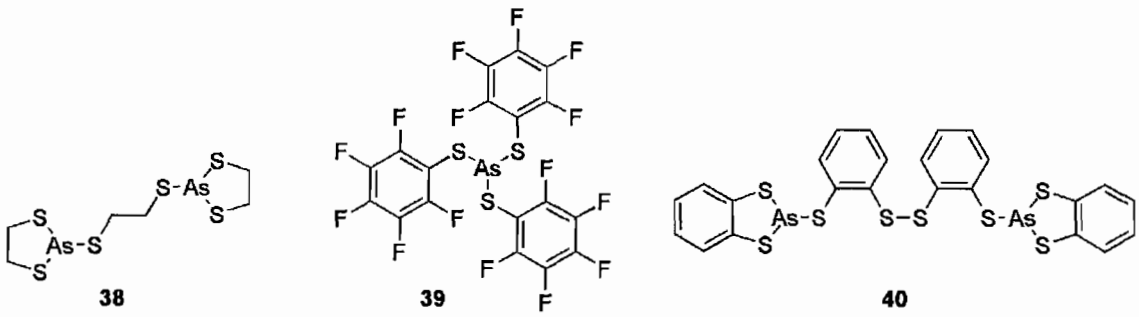

Chart 5. Trithiolate structures.[96,97]

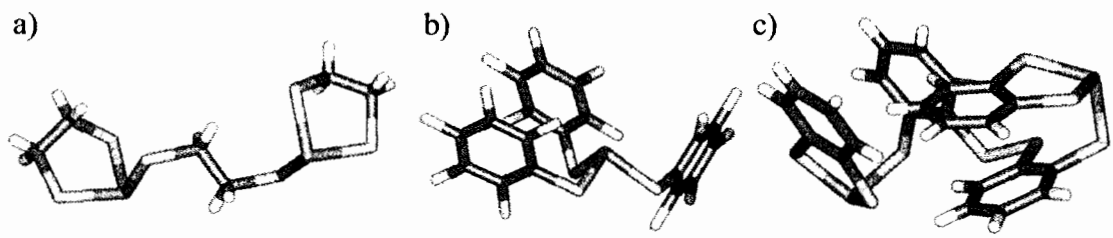

Figure 5. Stick-representations of the X-ray crystal structures of **38** (a), **39** (b), and **40** (c).[96,97]

A third structure, **40**, was reported separately (Chart 5, Figure 5).[97] Here, an unusual disulfide linkage was tethered between two arsenic centers. Angles and distances around the As-center were very similar to those observed in **38**, with As-S bond

lengths of 2.23, 2.25, and 2.29 Å and S-As-S angles of 92, 103, and 104°. The slightly wider bond angles for **40** were likely due to the difference in length of the hydrocarbon backbones between **39** and **40**. **38**, **39**, and **40** had trigonal pyramidal geometry and the As-centers in **38** and **40** were in the exo conformation.

The simple arsenic trithiolate complex **41** was prepared by the treatment of 2-mercaptomethylnaphthalene with $AsCl_3$ (Figure 6) in the presence of base.[98] As-S distances (2.23, 2.24, 2.25 Å) and S-As-S angles (95, 98, 102°) were in the typical range for a trigonal pyramidal arsenic center. Asymmetry around the As-center resulted from SBIs in the solid state. A single As···π SBI to one ligand and π-π stacking of the naphthalene rings were observed. Here, the As-center is in neither the exo nor the endo conformation, with two ligands positioned toward the arsenic lone pair and one positioned away from it.

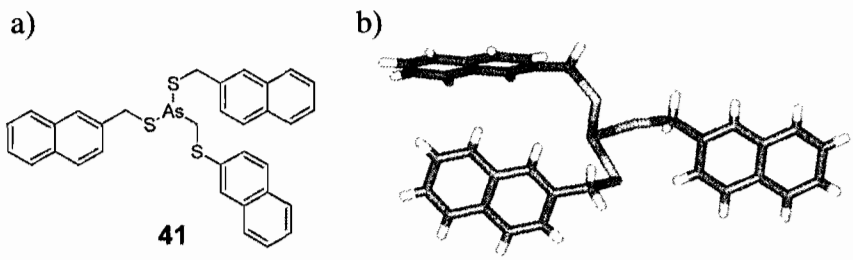

Figure 6. Cartoon (a) and stick-representation (b) of the X-ray crystal structure of **41**.[98]

In each of the examples reported above, As-S distances were between 2.23 and 2.29 Å and S-As-S angles were between 92 and 106°. When no SBIs were present in the

solid state, the bond angles were equal, or close to it, and the geometry was clearly trigonal pyramidal. SBIs distorted the symmetry and angles around the As-center, giving the geometry some degree of trigonal bipyramidalism. The structures suggested that there is no general preference for either the endo or exo conformation at the As-center in trithiolate complexes. In each case the observed orientation seemed to be due to steric interactions, SBIs, or crystal packing forces, although some subtle electronic "donor-acceptor" type interactions may be involved.

Halo-Arsenic Dithiolate Complexes

While preparing **37**, crystals of **42** were also isolated (Figure 7). Here, As-S bond lengths of 2.22 and 2.23 Å were observed. These were just slightly shorter than the As-S bonds in **37**, likely a result of the electron-withdrawing ability of the chloride ligand. The S-As-S of 92° was smaller than those observed in **37**, probably because the steric bulk of chlorine caused S-As-Cl bond angles of 98 and 101°.[85] The As-center is in the endo conformation and arsenic is involved in one short As···O SBI.

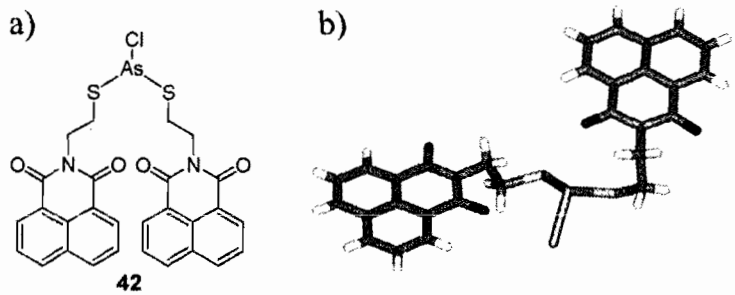

42

Figure 7. Cartoon (a) and stick-representation (b) of the crystal structure of **42**.[85]

Five new XAs(SRS) structures where X = Cl or I and R = $(CH_2)_2$, $(CH_2)_3$, or $(CH_2C_6H_4CH_2)$ were recently reported (Chart 6, Figure 8).[96] These five, six, and seven-membered S-As-S ring complexes allowed insight into the effects of halogen identity and ring size. Compound **43**, a five-membered ring with chloride substitution on arsenic, had an S-As-S angle of 93° and S-As-Cl angles of 98°. Replacement of chloride with iodide gave compound **44**. Here, the angles were very similar to those in **43**, showing that identity of the terminal halide had very little effect on the structure of the ring, despite being in the axial position. The six-membered, chloro-substituted compound **45** had a significantly wider S-As-S bond angle of 102°, suggesting slight ring strain. Again, there were similar bond angles in the iodinated compound **46**. In the seven-membered ring **47**, a S-As-S bond angle of 105° suggested increased ring strain. Based on these observations, strain increased with ring size. These results were in line with previous observations that in S-As-S-containing ring systems, five-membered rings are more stable than seven-membered rings.[35,67] In each case, arsenic was trigonal pyramidal and exo and the halide was found to be in the axial position with respect to the ring, likely due to the anomeric effect.

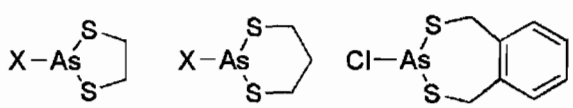

43 X = Cl
44 X = I

45 X = Cl
46 X = I

47

Chart 6. Halo-arsenic dithiolate rings structures.[96]

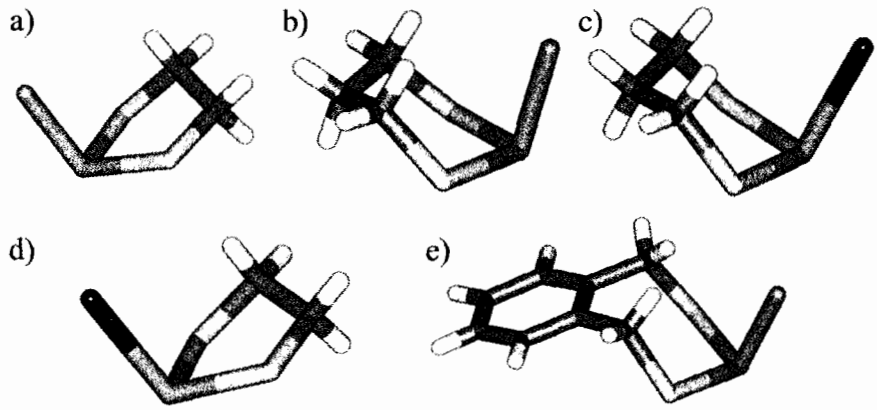

Figure 8. Stick-representations of crystal structures of **43** (a), **45** (b), **46** (c), **44** (d), and **47** (e).[96]

A different polymorph of **43** was previously reported which had slightly different angles and distances. As-S bonds were 2.19 and 2.23 Å, the S-As-S angle was 93.5°, and the S-As-Cl angles were 98 and 100°.[99]

In the solid-state, a greater range of bond distances and angles is exhibited by halo-arsenic dithiolate complexes than by trithiolate complexes. This could be a consequence of steric and electronic differences between substituents and/or the ring strain observed in many of the examples. As-S distances between 2.19 and 2.27 Å, S-As-S angles between 87 and 105° and S-As-X angles between 97 and 101° were typical. The identity of the halide, X, did not seem to affect bond distances and angles, but ring size did. Again, both endo and exo conformations were observed at the trigonal pyramidal As-centers.

Organic Dithiolate Complexes

Organic dithiolate arsenic complexes containing $CAsS_2$ units have been structurally characterized to some degree. As-S distances of 2.25 and 2.26 Å, an S-As-S angle of 99°, and S-As-C angles of 95 and 96° were observed in the crystal structure of 1,3-dithia-2-phenylarsino-[3]ferrocenophane (**48**).[100] These measurements show that despite its close proximity to arsenic, the ferrocene unit did not affect arsenic's exo trigonal pyramidal geometry (Figure 9). The X-ray crystal structure of a tolylarsenic-BAL (British Anti-Lewisite) complex (**49**) (Figure 10) revealed a five-membered ring in which the As-S distances (2.23 Å) , S-As-S angle (93°) and S-As-C angles (98 and 101°) were in the typical range.[101] Arsenic, in the endo position, did not take part in any SBIs, despite the availability of the alcohol oxygen.

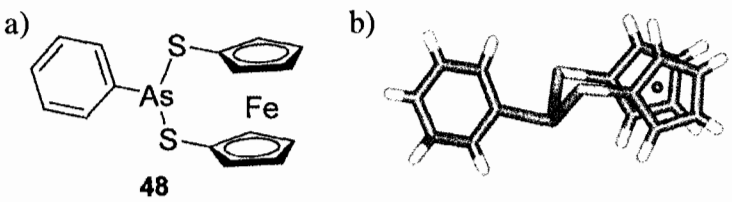

Figure 9. Cartoon (a) and stick (b) representations of **48**.[100]

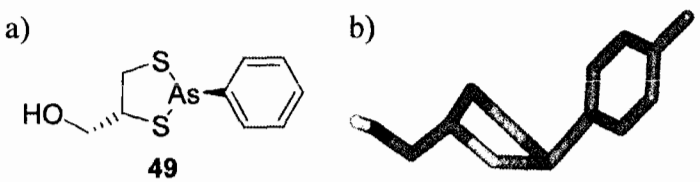

Figure 10. Cartoon (a) and stick (b) representations of **49**.[101]

The biologically relevant structure of a phenyl As-lipoic acid derivative, **50**, contained an AsS_2C_3 six-membered ring in the chair conformation.[77] The As-center was in the exo conformation and the phenyl group on arsenic was in the expected axial position (Figure 11). This example reiterates the axial preference for substituents on the arsenic atom in rings that was seen above for compounds **43-47**.[96,97] This preference has also been observed in solution for six-membered rings containing S-As-S or O-As-O units.[102] In the solid state structure of **50** there were no SBIs involving arsenic which was in the endo conformation with trigonal pyramidal geometry. The bond lengths and angles around arsenic fell into the typical range for aryl-AsS_2 moieties. As-S distances of 2.23 Å, an S-As-S angle of 99°, and S-As-C angles of 99 and 101° were observed.

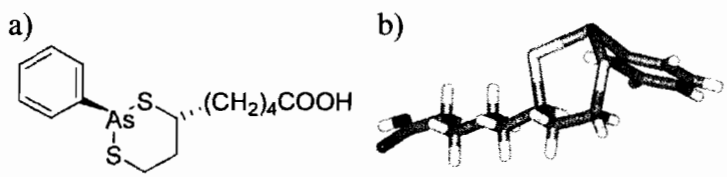

50

Figure 11. Cartoon (a) and stick (b) representations of the X-ray crystal structure of **50**.[77]

In each case reported above, the geometry at arsenic was trigonal pyramidal. For organic dithiolate arsenic complexes, As-S distances in the range of 2.23 to 2.26, S-As-S angles between 93 and 99°, and S-As-C angles between 95 and 101° were typical. Both endo and exo conformations were observed. It should be noted that these angles and

distances seem to be typical for the $CAsS_2$ trigonal pyramidal unit, even if the sulfur atom is not part of a thiolate ligand. For instance, the As-S distances in realgar (As_4S_4) are 2.21 Å and in arsenic trisulfide (As_2S_3) are 2.25 Å.[103] A table of known As-S bond lengths in cluster compounds has been previously reported and will not be discussed here.[104] However, a few more recent examples will be. The phenyl arsenic sulfide tetramer (**51**) has As-S distances of 2.26 Å, S-As-S angles of 102° and S-As-C angles of 94 and 96 (Chart 7).[105] Due to the steric crowding of four phenyl units, each occupies an equatorial, rather than axial position. The crystal structure of diphenyldiarsenic trisulfide (**52**) has As-S distances of 2.25 Å, an S-As-S angle of 98°, and S-As-C angles of 100 and 101°.[106] Rings **53** and **54** have similar structural features.[107]

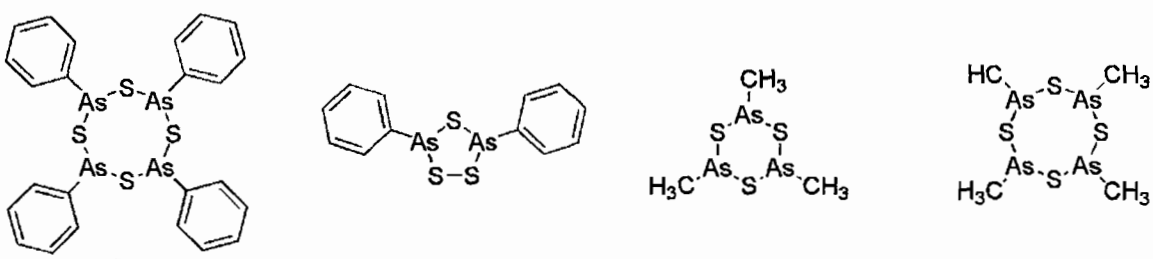

Chart 7. Cartoon representations of structures **51**,[105] **52**,[106] **53**,[107] and **54**.[107]

Heteroatom-Arsenic Dithiolate Complexes

The X-ray crystal structure of the As-DTT adduct (**30**) showed that, surprisingly, the complex was not the seven-membered ring hypothesized by Zahler and Cleland,[57] but

a bicyclic structure in which one of the oxygens on DTT was bound directly to arsenic (Figure 12).[58] Despite the strain in **30**, As-S bond distances were typical (2.23 and 2.24 Å). However, the bond angles were affected by the strain and by SBIs between arsenic and the sulfur atoms on neighboring molecules. This resulted in a geometry around arsenic that was intermediate between trigonal pyramidal and octahedral. The S-As-O angle in the five-membered ring was only 89°, while the S-As-O angle in the six-membered ring was significantly wider at 97°. The S-As-S angle in the seven-membered ring was 101°. Based on these results, it seems possible that the arsenite complexes of dithioerythritol (**10**), 1,2-dithioglycerol (**11**), and 1,3-dithioglycerol (**12**) also have covalent bonds between an oxygen atom within the ligand framework and bicyclic structures.

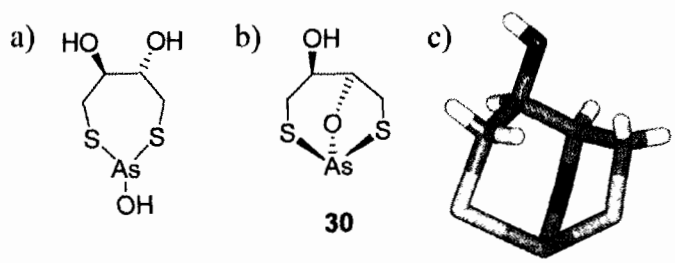

Figure 12. Cartoon representation of the incorrect[57] (a) and correct (b) structures of the As-DTT adduct **30**. Stick representation of the X-ray crystal structure of **30** (c).[58]

Burford and co-workers have mainly focused their efforts on the preparation and characterization of arsonium cations which are beyond the scope of this review. However, they have also presented several examples of crystal structures containing As-S units in neutral molecules.[99,108,109] In **55**, the N,S,Cl coordination-sphere around arsenic was slightly distorted from trigonal pyramidal by a SBI with chlorine in a neighboring molecule (Figure 13).[108] The As-S bond length was unaffected (2.20 Å).

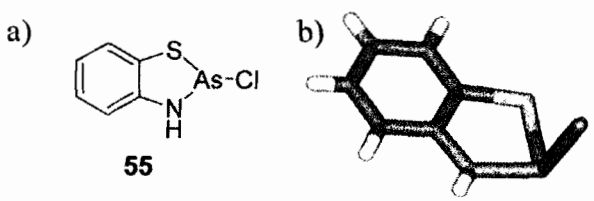

55

Figure 13. Cartoon (a) and stick (b) representations of the X-ray crystal structure of **55**.[108]

Non-Trigonal Pyramidal Geometries

A series of As(III)-thiolate containing metallocanes (eight-membered rings: $X(CH_2CH_2S)_2AsR$, X = O or S) with a range of trigonal pyramidal to trigonal bipyramidal geometries has been reviewed previously by Moya-Cabrera et al.[110] and will not be repeated here. However, since Moya-Cabrera's review was published, the crystal structures of a series of $S(C_6H_4S)_2AsX$ where X = Cl (**56**), Br (**57**), and I (**58**) were reported (Chart 8, Figure 14).[111] The primary coordination spheres have the classic

trigonal pyramidal geometry. However, intramolecular transannular S→As SBIs gave the complexes trigonal bipyramidal geometries. The authors evaluated the influence of the S→As interaction on the geometry using the donor-acceptor bond length method described by Holmes[112-114] and the Pauling-type bond order of that interaction.[115-117] They found that the complexes actually had hybrid geometries and were each between 64-67% trigonal bipyramidal and 36-33% trigonal pyramidal. The S→As bond orders were between 0.19 and 0.21. As-S distances were long for halo-arsenic dithiolate complexes, between 2.27 and 2.29 Å. The S-As-S angles were wide, between 103 and 104°, likely a steric effect of the S→As SBI. Finally, S-As-X angles were between 87 and 88°. The small difference in angles here indicates that the identity of the halogen had only a slight effect on bond angles and distances.

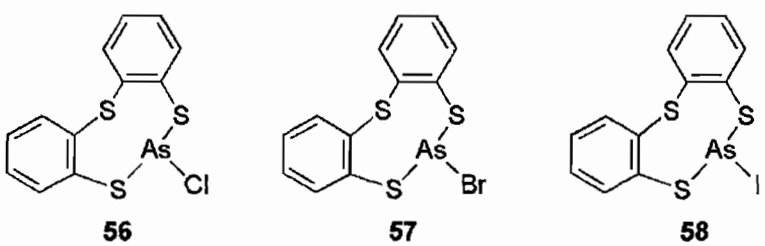

56 **57** **58**

Chart 8. $S(C_6H_4S)_2AsX$ structures **56-58**.

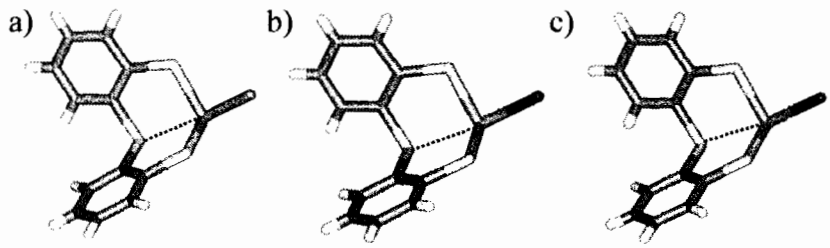

Figure 14. Stick representations of the X-ray crystal structures of **56** (a), **57** (b), and **58**.[111] S→As secondary bonding interactions are shown with dashed lines.

The X-ray crystal structure of the unusual, biologically-relevant, four-coordinate As(III)-N,S complex **59** (Figure 15) was recently reported.[118] Upon treatment with $AsCl_3$, an N,S-containing benzothiazoline ligand (**60**) reacted to form **59** (Scheme 14). The equatorial plane of **59** included N, I, and the lone pair, while the axial positions were occupied by S and N, making the geometry at the As-center trigonal bipyramidal. The As-S bond distance of 2.29 Å was similar to those observed in three-coordinate thiolate complexes. The equatorial location of the lone pair in this structure was consistent with other four-coordinate As(III)-thiolate structures.[119-123]

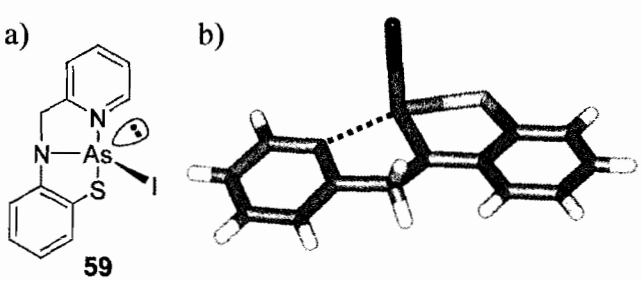

59

Figure 15. Cartoon (a) and stick (b) representations of the X-ray crystal structure of **59**. The axial N-S bond is represented by a dotted line.[118]

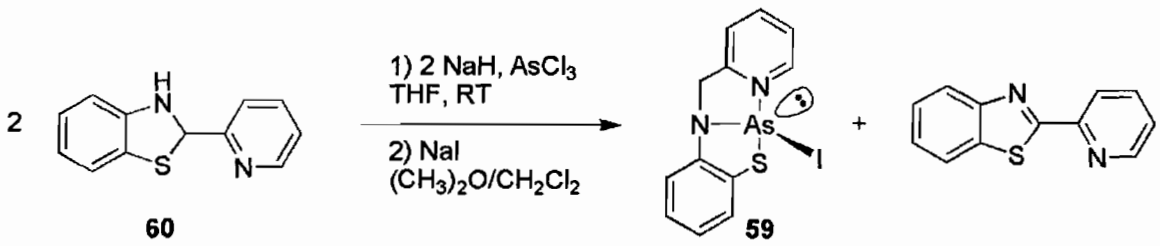

60 59

Scheme 14. Synthesis of **59**.

Protein Mimics and Supramolecular Arsenic-Thiolate Chemistry

Protein Mimics

Arsenic has been shown to bind a number of cysteine-containing proteins, but As-protein adducts are difficult to study. One way around this problem is to study As-polypeptide interactions in protein mimics.[124,125] The well-studied peptide helix bundles from the TRI family are known to aggregate in two-helix bundles at low pH and three-helix bundles at high pH.[126] Cysteine was substituted onto the peptide at position 16 and an excess of sodium arsenite was added at both low and high pHs (Figure 16). For both, electrospray and MALDI mass spectrometry showed that the product was the three-helix coiled coil bound to arsenic (**60**), suggesting that the trigonal binding preferences of arsenic can overcome the preference of the peptide to exist as a two-helix bundle at low pH. An As-S bond length of 2.25 Å was determined by EXAFS spectroscopy. Similar results were obtained when using a peptide substituted in position 12 despite unfavorable rotameric forms of the cysteine in this position. These results demonstrate that the

thiophilicity of arsenic is great enough to cause distortion and aggregation in certain biopolymers.[127]

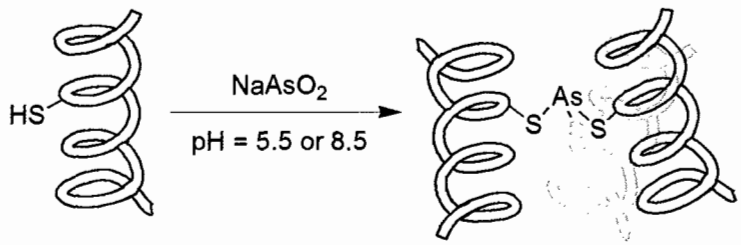

60

Figure 16. Cartoon representation of synthesis of As-coordinated three-helix coil (**60**).[124,125]

Using a slightly different peptide, Coil Ser with cysteine in position 9 (CSL9C), Pecoraro et al. were able to determine the crystal structure of the triply bound $As(CSL9C)_3$ (**61**) to 1.8 Å resolution (Figure 17a).[128] A mean As-S distance of 2.28 Å and S-As-S angles of 91, 92, and 88° were found. These angles are slightly smaller than those observed for typical small molecule trithiolate arsenic complexes and this could be due to peptide aggregation or side chain rotamer effects. The As-center was in the endo conformation within the coiled coil, with arsenic's lone pair of electrons and the cysteine carbons all lying below the plane of the sulfur atoms (Figure 17b). While this conformation is not uncommon in small molecule As(III)-thiolate complexes,[85,94] the exo conformation is also often observed.[96-98] This is a rare example of a structurally characterized As-containing biomolecule and the environment around arsenic matches that proposed for arsenic in Ars-R and Ars-D arsenic-resistance regulatory proteins.[50]

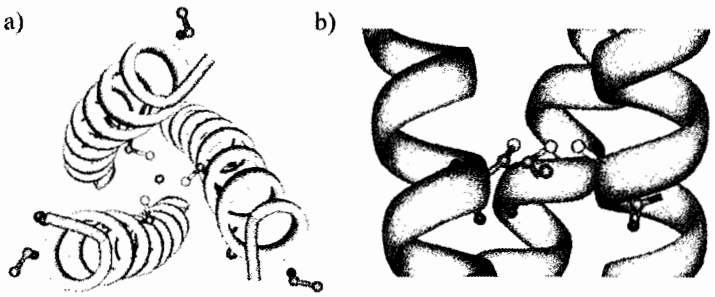

Figure 17. Representations of the X-ray crystal structure of **61** from the top down (a) and side (b).[128]

The effects of arsenic binding to a single α-helix has also been reported.[129] A family of peptides with two cysteine residues in the *i*, *i*+1, *i*+2, *i*+3, and *i*+4 positions was treated with MMA and the structural effects of 1:1 binding were studied by circular dichroism (CD) spectroscopy. Destabilization and structural alteration were found to occur in all cases except for the helix with residues in the *i*, *i*+4 positions (Figure 18). In this case, stabilization was found to occur by enhancement of the helical structure. Dissociation constants were found to range from 1.5-19.8 × 10^{-9} M, suggesting that the location of the cysteine residues had little effect on the tight As-binding regardless of the structural consequences. Association constants ranging from 1.1-2.8 × 10^{4} $M^{-1}s^{-1}$ were also reported.

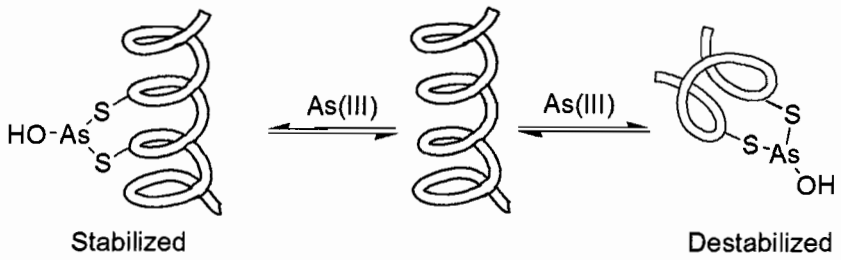

Figure 18. Cartoon representation of As(III) binding to an α-helix causing stabilization or destabilization depending on location of cysteine residues.[129]

The effects of arsenic binding to modified β-hairpins has also been studied.[38] Four model hairpins, each with a cysteine incorporated at two positions, were treated with MMA and studied by CD, NMR, and UV-vis spectroscopy. It was found the arsenic binding could stabilize or destabilize the hairpin structure. Similarly to the results for α-helical binding, this stabilization/destabilization was dependent on the location of the cysteine residues. Binding was found to occur rapidly. Association rate constants were measured between 1.0-2.2 × 10^4 $M^{-1}s^{-1}$ no matter the location of residues or structural reorganization upon binding. Equilibrium dissociation constants of 1.3-10.6 × 10^{-9} M were also reported.

Supramolecular Chemistry

Supramolecular chemistry is the study of dynamic molecules assembled of multiple components through reversible interactions.[130,131] These interactions are often hydrogen bonds[132,133] or labile metal-ligand bonds,[134,135] but can also include π-π,[136] cation-π,[137] and CH-π[138] interactions and take advantage of hydrophobic and solvophobic

effects.[138] Typically, the design of metal-organic assemblies involves incorporation of the highly studied and well-behaved transition metals. However, a recent resurgence of the main group elements[139,140] has led to interest in the use of main group ions in metal-directed self-assembly.[141]

As a component in supramolecular assemblies, As(III) has much to offer. In addition to the favorable thermodynamics and kinetics of the As-S bond discussed earlier in this chapter, arsenic can take part in secondary bonding interactions with heteroatoms such as oxygen,[85] sulfur,[91,92] and the halogens,[93] as well as with electron-rich aromatic rings through As···π interactions.[87-90] Finally, trigonal pyramidal bonding geometries and endohedral functionality are unusual in supramolecular assemblies. As(III) supplies both.[142]

Arsenic-Containing Cryptands

The first reported use of As(III) as a directing ion for supramolecular self-assembly involved the treatment of a rigid phenyl-spaced dithiolate ligand (L^{2-}) with $AsCl_3$, resulting in the formation of As_2L_3 (**62**) in high yields (Figure 19).[84] This showed for the first time that the As-S bond is labile enough for the self-assembly of discrete species. This example also has several interesting features. First, in the crystal structure, each As-center was in the endo conformation with its lone pairs of electrons pointing directly into the cavity. This could have been due in part to favorable As···π interactions with the ligands. Second, the cryptand was remarkably stable; air, water, excess ligand,

competing metal ions, and even heating to reflux in $CHCl_3$ in the presence of trifluoroacetic acid or *p*-toluenesulfonic acid caused no decomposition or reaction. This suggests that the supramolecular chelate structure imparted additional stability onto the assembly beyond what was expected for the individual As-S bonds. The observed As-S bond lengths of 2.25 Å and S-As-S angles of 95° were within the typical range for non-constrained S-As-S units, showing that the chelating effects of the ligands did not disturb the geometry around the As-center.

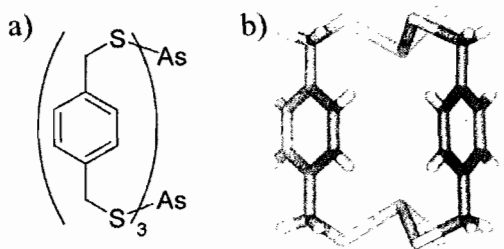

62

Figure 19. Cartoon (a) and stick (b) representations of the X-ray crystal structure of **62**.[84]

Since this initial discovery, the structures of two other As_2L_3 cryptands have been reported. The preparation of **63**, a cryptand with an extended diphenylmethane spacer, allowed comparison of the crystal structure (Figure 20) with a DFT-calculated structure run at the B3LYP/6-31+G* level.[143] These two structures were shown to be very similar, except that DFT did not predict As···π interactions. This was not surprising, as the Bi···π interaction is not correctly interpreted by DFT.[144] Again, in this crystal structure, As-S distances between 2.23 and 2.25 Å were within the typical range. S-As-S angles ranged

from 91-103° showing that this structure clearly lacked the C_3 symmetry of the **62**. The loss of symmetry here appeared to be due to edge-to-face aromatic interactions in the crystal packing; NMR spectroscopy revealed a time-averaged symmetric structure in solution.

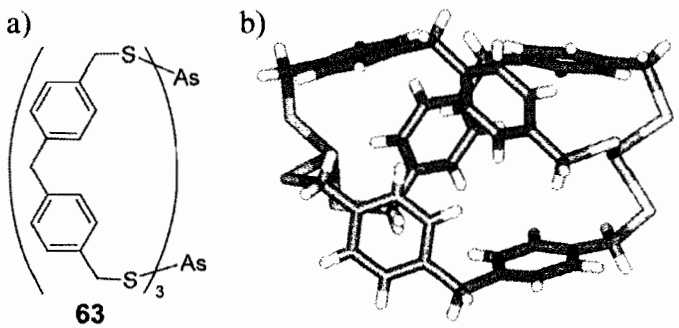

Figure 20. Cartoon (a) and stick (b) representations of the X-ray crystal structure of **63**.[143]

In the crystal structure of the naphthyl-spaced As_2L_3 cryptand **64**, the As···As distance was very similar to that in **62**, but the cavity of the assembly was far more sterically congested (Figure 21).[145] This had little effect on the endo trigonal pyramidal geometry around the As-center. Again, As-S distances of 2.25 Å and S-As-S angles of 94° were reported. This cryptand was prepared by an unconventional route; the Sb_2L_3 congener (**65**) was transmetallated with $AsCl_3$, resulting in complete conversion to As_2L_3. This reaction highlighted the relative stability of the As-S and Sb-S bonds. In solution, a small percentage of the As_2L_3 cryptand rearranged to a less-symmetric structure in which one ligand was folded in the opposite direction of the other two. The conversion between

the symmetric and asymmetric structures likely occured when an As-S bond breaks and reforms, again showing the lability of the As-S bond.[146] This cryptand will be described in further detail in Chapters V and VI.

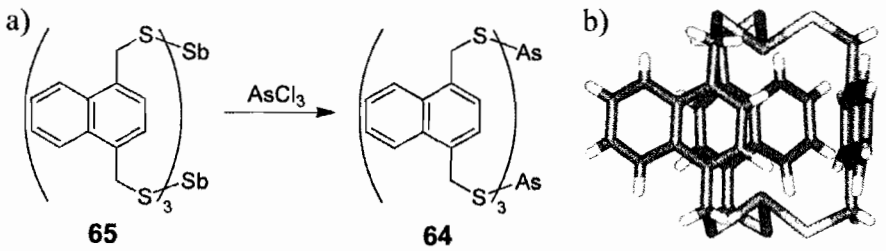

Figure 21. Schematic cartoon showing transmetallation reaction (a) and stick representation of the X-ray crystal structure of **64** (b).[145]

Arsenic-Containing Macrocycles

$As_2L_2Cl_2$ macrocycles, intermediates in the formation of As_2L_3 cryptands, were prepared directly from rigid dithiol ligands (H_2L) and $AsCl_3$. Crystal structures of **66**, a macrocycle prepared from the phenyl-spaced ligand used in **62**, revealed that the As-centers again were in the endo conformation and were involved in As···π interactions (Figure 22).[82] Two isomers, *syn* and *anti*, were observed in the solid state and in solution. As-S distances of 2.22 and 2.23 Å, S-As-S angles of 87 and 90° and S-As-Cl angles of 100 and 101° were observed. These angles were similar to those previously reported for halo-arsenic dithiolate structures.[85,96] While the two isomers could be isolated separately

in the solid state, dissolving one in chloroform led to an equilibrium ~1:1 mixture of both isomers within five minutes.

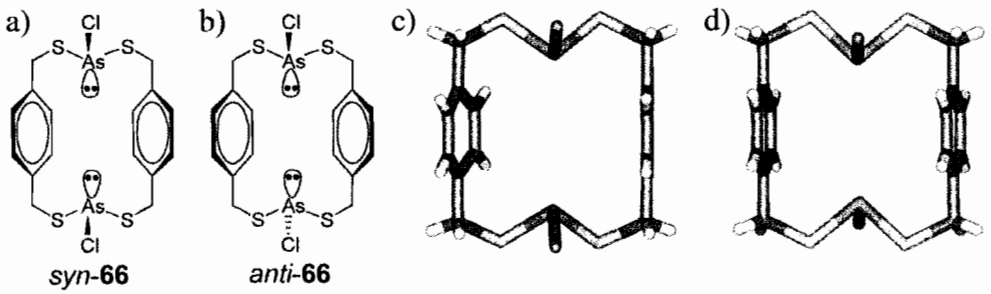

Figure 22. Cartoon and stick representations of the X-ray crystal structure of *syn*-**66** (a,c) and *anti*-**66** (b,d).[82]

The *syn*-to-*anti* ratio of macrocycles **67**, **68**, and **69** was controlled by use of rationally-placed steric bulk in the dithiol ligands.[79] A series of conformationally isomeric naphthyl-spaced ligands were prepared and treated with $AsCl_3$ resulting in macrocycle assembly (Figure 23). Crystal structures and NMR spectroscopy revealed diastereomeric excesses of the less sterically-congested isomers. Again, interconversion between isomers was found to be fast (equilibrium was reached within minutes of dissolving crystals of a single isomer). However, NMR samples heated to 135 °C showed no coalescence and EXSY experiments showed no exchange, implying that interconversion was slow on the NMR timescale. Interconversion likely occurred through the breaking of the As-S bond (Figure 7), but could also occur through As-Cl bond (Figure 8) breaking and reforming. As-S distances of 2.22 Å, S-As-S angles of 86-

90° and S-As-Cl angles of 97-102° were observed in each macrocycle around the endo-positioned As(III) ions. This system is further described in Chapter II.

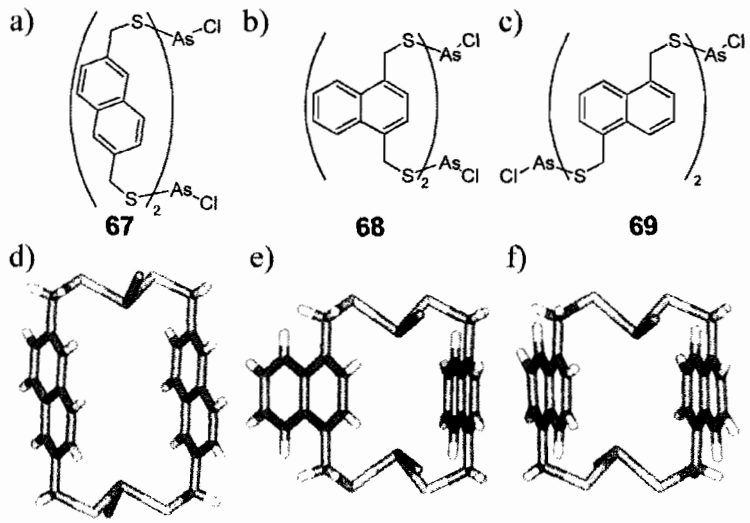

Figure 23. Cartoon and stick representations of the X-ray crystal structures of **67** (a,d), **68** (b,e), and **69** (c,f).

The diastereomeric excess was similarly controlled using methyl groups to impart steric control (Figure 24).[83] In the *anti* 2,5-substituted macrocycle **70**, the As-centers were in the endo conformation with their lone pairs of electrons pointing directly toward each other. As-S distances of 2.21 Å, S-As-S angles of 86°, and S-As-Cl angles of 100 and 102° were observed. However, in the 2,3-substituted macrocycle (**71**), one As-center was not in the expected position. Rather than having its lone pair pointing directly toward the other As(III) ion, it was folded into the macrocyclic cavity to fill the space. Previously, this was observed in the crystal structure of a conformer of **68** not shown in

Figure 23.[79] Even in these "folded-in" or "imploded" structures, typical bond distances and angles were observed. For the folded in S_2AsCl unit, As-S distances were 2.21 and 2.22 Å, S-As-S angles were 88° and S-As-Cl angles were 98, 101 and 104.°

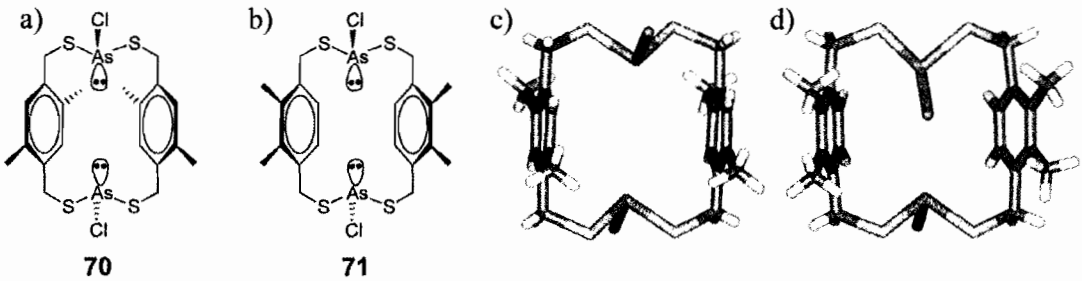

Figure 24. Cartoon and stick representations of the X-ray crystal structures of **70** (a,c) and **71** (b,d).[83]

The *syn*-to-*anti* ratio of macrocycle **72** was controlled in the solid state (Figure 25a).[142] When **72** was crystallized from $CHCl_3$ or C_6H_6, the *anti*-macrocycle crystallized exclusively (Figure 25b) as a result of intramolecular steric interactions between the chloride ligands and the methoxy groups on the organic ligand. However, when crystals were grown from larger solvents such as toluene or *p*-xylene, two molecules of **72** were found to dimerize around one solvent molecule. *p*-xylene filled the cavity of the dimer, causing the bulky chloride ligands to point away from the cavity. This resulted in the exclusive crystallization of *syn*-**72** (Figure 25c). Toluene, which is slightly smaller than *p*-xylene, was not able to fill the cavity of the dimer as effectively. Although the dimer still formed, **72** crystallized as a mixture of *syn* and *anti* isomers (Figure 25d, only the *syn-syn* dimer is shown). Overall, the size of the guest played an important role in the

syn-to-*anti* ratio of **72** as well as whether or not dimerization occurred. As-S distances in these structures ranged from 2.13-2.24 Å and S-As-S angles ranged from 87-93°. S-As-Cl had a wide range from 87-111°. More on this diastereoselective system can be found in Chapter III.

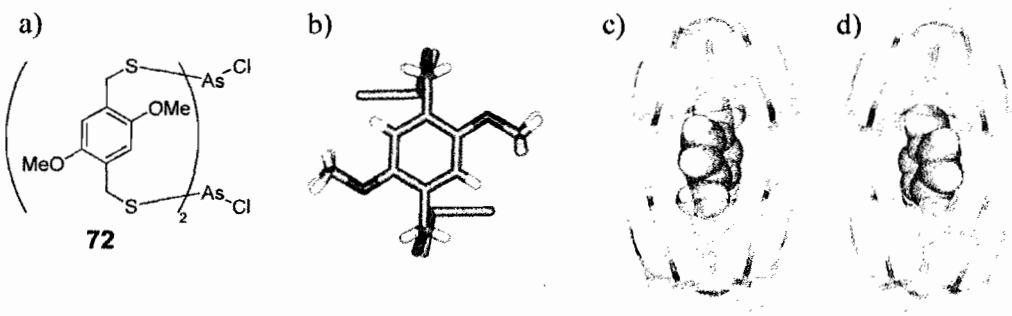

Figure 25. Cartoon (a) and stick representations of the X-ray crystal structures of *anti*-**72** (b), [(*syn*-**72**)$_2$·*p*-xylene] (c), and [(*syn*-**72**)$_2$·toluene] (d).[142]

Several other macrocycles which partially host aromatic guests have been prepared from dithiol ligands containing biphenyl (**73**) and *trans*-stilbene (**74**) spacers (Figure 26).[142] Here, As-S distances ranged from 2.11 to 2.21 Å, S-As-S angles from 88-92°, and S-As-Cl angles from 95-103°. **73** and **74** are described in further detail in Chapter III. In an attempt to increase the volume of the cavity, 1,4-bis(mercaptoethyl)benzene was incorporated into macrocycle **75**. In this structure, As-S distances of 2.21 Å, S-As-S angles of 93°, and S-As-Cl angles of 100 and 102° were observed.[98] The tetramethyl-substituted phenyl-spaced macrocycle **76** was also

reported[147] with As-S distances of 2.21 and 2.22 Å, S-As-S angles of 86°, and S-As-Cl angles of 100°. This structure can be found in Chapter IV.

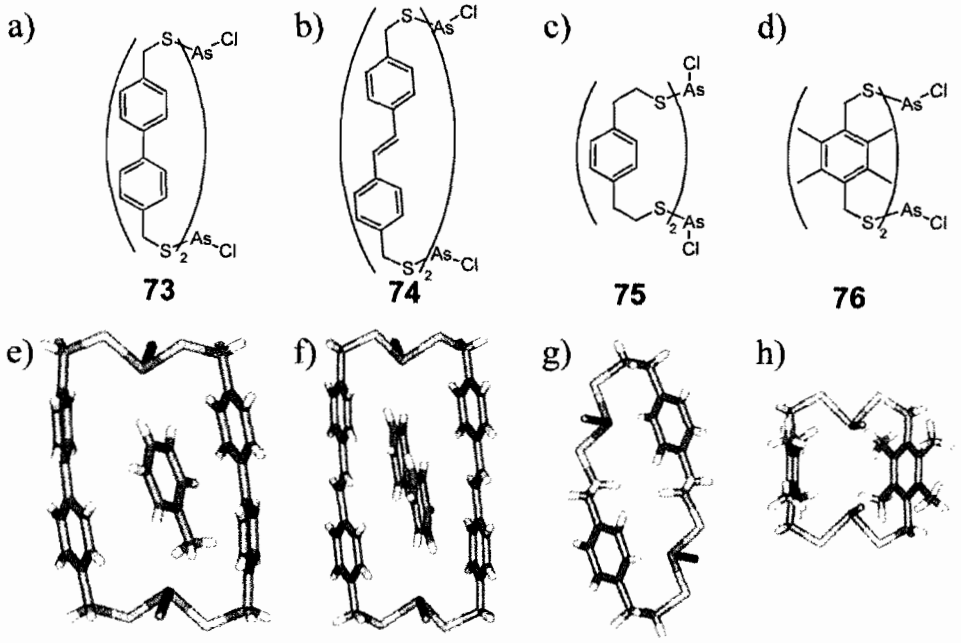

Figure 26. Cartoon and stick representations of the X-ray crystal structures of **73** (a,e),[142] **74** (b,f),[142] **75** (c,g),[98] and **76** (d,h).[147]

In addition to structural data, $As_2L_2Cl_2$ macrocycles have given insight into the self-assembly process.[147] Most transition metal-ligand complexes form within minutes and their assembly can only be monitored by stopped-flow experiments. As-S kinetics in our systems are relatively slow. For example, it took a week for the assembly of $As_2L_2Cl_2$ macrocycles **62** and **73** to reach equilibrium. This allowed monitoring by ^{1}H NMR spectroscopy and MALDI mass spectrometry. Intermediates (Scheme 15) and oligomeric

mistakes which corrected themselves over the course of the self-assembly process (Chart 9) were observed. Additionally, an As_2LCl_4 intermediate (**77**) was crystallized (Figure 27) with As-S bond distances of 2.22 Å and S-As-Cl bond angles of 89 and 102°. The large difference in angles here were caused by an As···O SBI with the ligand's methoxy ether. More detail on these experiments can be found in Chapter IV.

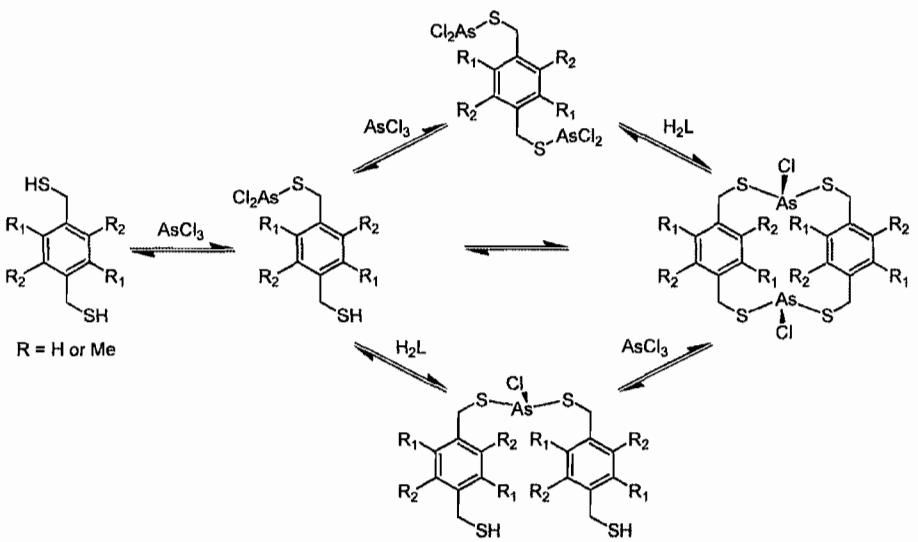

Scheme 15. Intermediates in the self-assembly of $As_2L_2Cl_2$ macrocycles.[147]

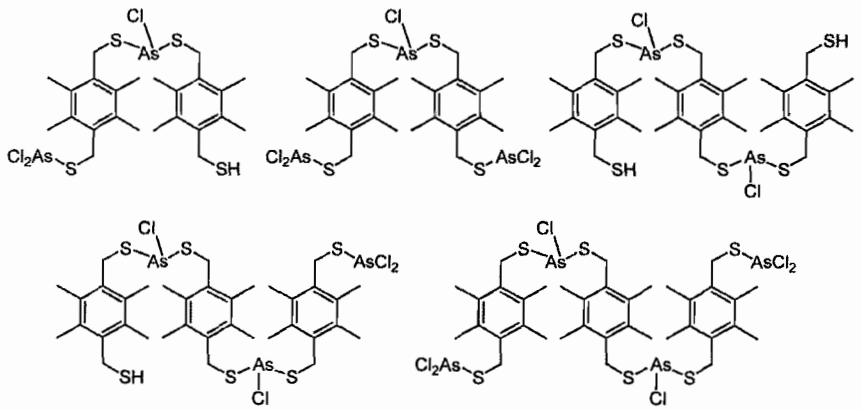

Chart 9. Kinetic mistakes observed in the self-assembly of $As_2L_2Cl_2$ macrocycles.[147]

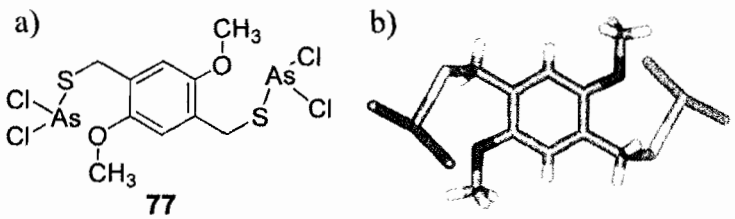

Figure 27. Cartoon (a) and stick (b) representations of the X-ray crystal structures of **77**.[147]

Higher-Order Structures

The first tetranuclear As-containing supramolecular assembly, **78**, was prepared using a tetrathiol ligand.[148] In the crystal structure of this S_4-symmetric $As_4L_2Cl_4$ metallocryptand, As-S distances of 2.22 and 2.23 Å, S-As-S angles of 90°, and S-As-Cl angles of 97 and 103° were observed (Figure 28). The AsS_2Cl centers in this structure were in the same endo and trigonal pyramidal conformation that is observed for every As-containing supramolecular assembly reported to date. Two isomeric As_2LCl_2

intermediates *cis*-**79** and *trans*-**79** were also isolated. Their crystal structures revealed As-S distances of 2.22-2.25 Å, S-As-S angles of 104-107°, and S-As-Cl angles of 97-99° (Figure 29). These intermediates contained seven-membered AsS_2C_4 rings that were very similar structurally to **47**. The distances and angles for **47** were within the range observed here and in both structures the As(III) ions were trigonal pyramidal and exo.

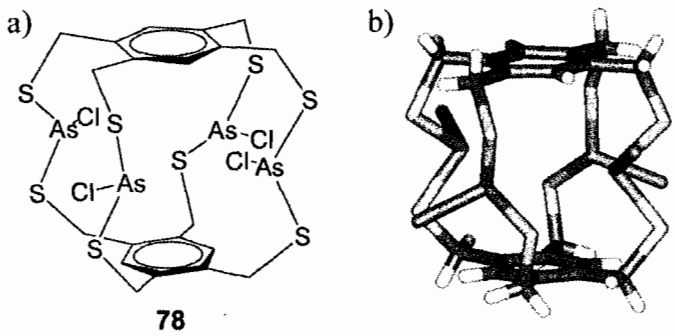

Figure 28. Cartoon (a) and stick (b) representations of the X-ray crystal structures of **78**.

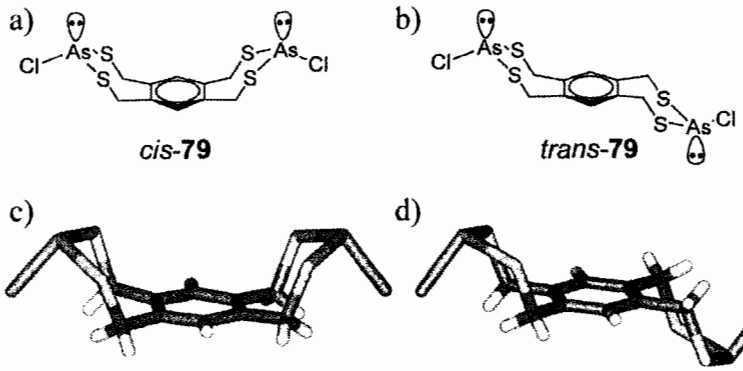

Figure 29. Cartoon and stick representations of the X-ray crystal structures of *cis*-**79** (a,c) and *trans*-**79** (b,d).

Conclusions

The kinetics, thermodynamics, structure, and supramolecular chemistry of the As(III)-thiolate bond were reviewed. All As-S-containing biomolecules were not comprehensively covered, but those which have reported kinetics, thermodynamics, or crystal structures were included. It was shown that the As-S bond is labile, with rate constants for bond formation ranging from 10^3-10^4 $M^{-1}s^{-1}$. Bond dissociation was found to be slower and on the order of 1-10 s^{-1}. Stability constants for As-containing complexes were reported and the thermodynamics and kinetics of S-As-S-containing rings were compared. It was also shown that thiolate-bound As(III) prefers a trigonal pyramidal geometry but substituent identity and secondary bonding interactions can affect the bond distances and angles. When SBIs were involved, trigonal bipyramidal geometries were observed. Arsenic-containing protein mimics and the chemistry of the As-S bond in a supramolecular context were also reviewed.

Bridge to Chapter II

Chapter I reviewed the kinetics, thermodynamics, preferred structure, and supramolecular chemistry of the As(III)-thiolate bond. It was seen that the bond is thermodynamically stable, yet kinetically labile enough to allow for the formation of discrete supramolecular assemblies. The preferred geometry of As(III)-thiolate complexes was found to be trigonal pyramidal at the As-center and the rates and thermodynamics of inversion at the As-center were explored in the context of

interconversion between isomers. In Chapter II, a supramolecular design strategy is applied to the As(III)-thiolate bond, allowing for the synthesis and characterization of a series of $As_2L_2Cl_2$ macrocycles. The ratio of isomers is controlled by the strategic placement of intramolecular steric bulk and the interconversion between isomers is explored.

CHAPTER II

DIASTEREOSELECTIVITY IN THE SELF-ASSEMBLY OF $As_2L_2Cl_2$ MACROCYCLES IS DIRECTED BY THE As-π INTERACTION

This chapter presents the diastereoselective self-assembly of a series of $As_2L_2Cl_2$ macrocycles in which the diastereomeric excess is controlled by intramolecular steric interactions. This co-authored work was previously published (*Inorganic Chemistry*, **2007**, *46*, 9278-9284, © American Chemical Society).[1] The synthesis and solution characterization of $As_2(\mathbf{L}^{1,5})_2Cl_2$ was carried out by Aaron C. Sather. The X-ray crystal structures of $As_2(\mathbf{L}^{2,6})_2Cl_2$ and $As_2(\mathbf{L}^{1,4})_2Cl_2$ were solved by Dr. Lev N. Zakharov and of $As_2(\mathbf{L}^{1,5})_2Cl_2$ by Dr. Orion B. Berryman. Professor Darren W. Johnson provided intellectual input and editorial assistance. I carried out the synthesis and solution characterization of $As_2(\mathbf{L}^{2,6})_2Cl_2$ and $As_2(\mathbf{L}^{1,4})_2Cl_2$ and wrote the manuscript.

Introduction

The use of main group ions as directing elements in metal-ligand self-assembly reactions is rare, and few predictive design strategies for forming self-assembled supramolecular main group compounds exist.[2-4] We have recently developed a strategy

to synthesize self-assembled dinuclear arsenic-containing structures[5,6] that are stabilized by arsenic-π interactions.[7,8] $As_2L_2Cl_2$ (H_2L = *p*-bis(mercaptomethyl)benzene) macrocyclic assemblies synthesized by this strategy exist in equilibrium as a statistical mixture of *syn* and *anti* diastereomers (Scheme 1), in which the arsenic-π interaction directs the arsenic atoms into the macrocyclic cavity formed by the arene rings of the ligands.

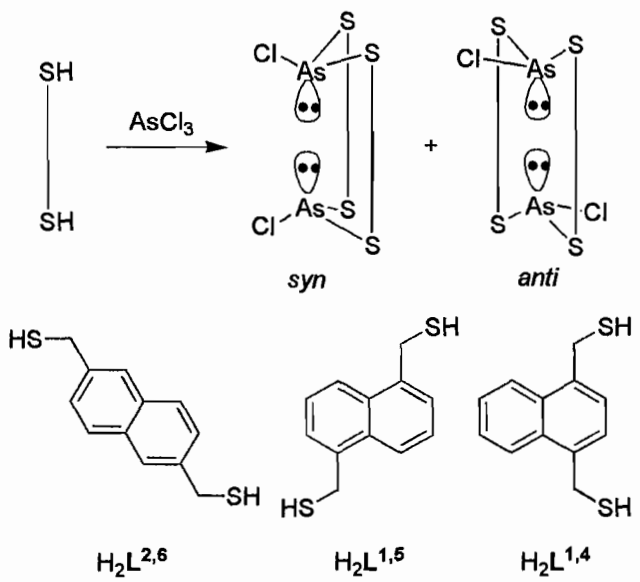

Scheme 1. The self-assembly of $As_2L_2Cl_2$ macrocycles. In the *syn* macrocycle both chlorine atoms are on the same side of the arsenic atoms. In the *anti* macrocycle the chlorine atoms are on opposite sides of the macrocyclic cavity.

Metal-ligand self-assembly reactions that can lead to two or more possible diastereomers typically proceed diastereoselectively.[9,10] To the best of our knowledge, only a few examples exist of metal-ligand self-assembly reactions that provide a mixture of diastereomers: 1) in rare instances multiple diastereomeric M_4L_6 tetrahedra (*T*, C_3 or

S_4) exist in equilibrium,[11] and 2) diastereomeric excess (*de*) values have been reported in the formation of host-guest *complexes* in which two enantiomers of a chiral guest have different binding affinities within two enantiomers of a chiral host molecule.[12]

We now show that the *de* of self-assembled arsenic-containing macrocycles can be controlled by the appropriate choice of achiral, isomeric dithiol ligands (Scheme 1). This demonstrates the generality of our design strategy for forming $As_2L_2Cl_2$ macrocycles and shows an unusual example of multiple supramolecular interactions (reversible As-S bond formation and As-π interactions) acting in tandem to dictate the stereochemical outcome of a self-assembly reaction.

Results and Discussion

Scheme 1 illustrates a series of isomeric bis(mercaptomethyl)naphthalene ligands that form equilibrium mixtures of diastereomeric macrocycles when combined with $AsCl_3$ in solution. Depending on the choice of ligand, either no *de* is observed ($H_2\mathbf{L}^{2,6}$), the *syn*-isomer is favored ($H_2\mathbf{L}^{1,4}$) or the *anti*-isomer ($H_2\mathbf{L}^{1,5}$) is favored. The naphthalene rings of these ligands provide added steric bulk to the macrocyclic cavity (compared to $H_2\mathbf{L}$), which forces either the chlorine or sulfur atoms into close proximity with these aromatic backbones (Figure 1). The repulsive interaction between the electron-rich chlorine atoms coordinated to arsenic and the aromatic rings of the ligand causes the diastereomer that positions the chlorine atoms farthest away from the arene rings to form in excess. The result is a predictable strategy that controls the *syn*-to-*anti* ratio of the self-assembly reaction based on the shape of the ligand.

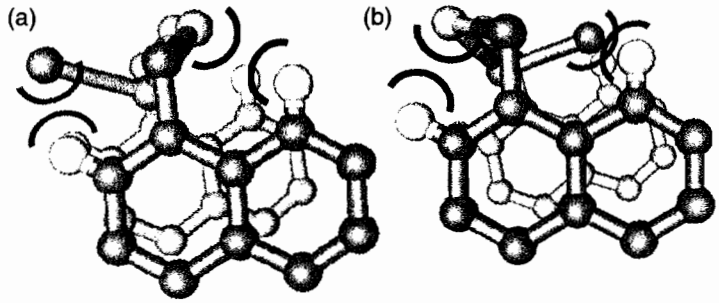

Figure 1. Partial ball and stick models showing two conformations for this molecule with the chlorine atom pointing away from (a) and toward (b) the hydrocarbon backbone. Possible points for steric repulsion are marked in red (with chlorine) and blue (with sulfur).

To test the stereocontrol of these self-assembly reactions, three regioisomers of bis(mercaptomethyl)naphthalene were prepared with mercaptomethyl substituents in the 2,6-, 1,5- and 1,4-positions. It was predicted that $H_2\mathbf{L}^{1,5}$ would give mostly *anti*-product, $H_2\mathbf{L}^{1,4}$ would give mostly *syn*-product, and $H_2\mathbf{L}^{2,6}$ would show no preference. These predictions result from the minimization of unfavorable steric repulsions (Figure 1b) exhibited in both *anti*-$As_2(\mathbf{L}^{1,5})_2Cl_2$ and *syn*-$As_2(\mathbf{L}^{1,4})_2Cl_2$ in which the chlorine atoms are directed away from the sterically-congested macrocyclic cavity (Figure 2). Conversely, $As_2(\mathbf{L}^{2,6})_2Cl_2$ should show no such preference: the chlorine atom is directed away from the macrocycle in both diastereomers. When $AsCl_3$ is added to a chloroform solution of each ligand, $As_2L_2Cl_2$ macrocycles self-assemble in each case, showing that our design strategy[5,6] for forming these macrocycles is general despite the differences in geometry of these ligands.

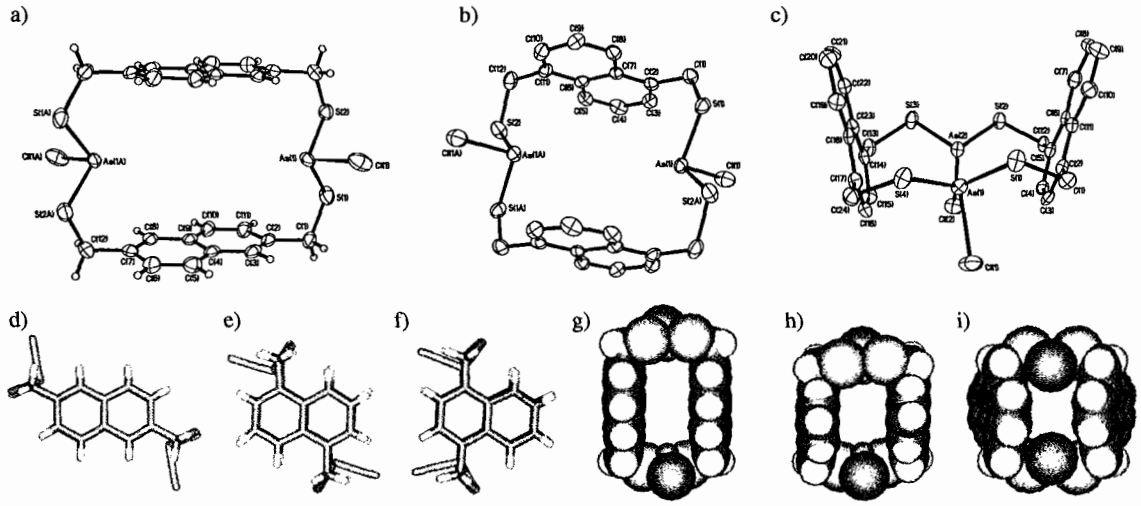

Figure 2. ORTEP (30% probability ellipsoids), wireframe, and space filling representations of single-crystal X-ray structures for *anti*-$As_2(\mathbf{L}^{2,6})_2Cl_2$ (a,d,g), *anti*-$As_2(\mathbf{L}^{1,5})_2Cl_2$ (b,e,h) and *syn*-$As_2(\mathbf{L}^{1,4})_2Cl_2{\cdot}CHCl_3$ macrocycles (c,f,i). Carbon is shown in black, hydrogen in white, sulfur in yellow, chlorine in green, and arsenic in purple. The ligands are planar within 0.02 Å. The angle between the average planes of the ligands is 28 Å in $As_2(\mathbf{L}^{1,4})_2Cl_2{\cdot}CHCl_3$ and 0 Å in $As_2(\mathbf{L}^{2,6})_2Cl_2$ and $As_2(\mathbf{L}^{1,5})_2Cl_2$. Hydrogens (a,b,c) and cocrystallized $CHCl_3$ (c,f,i) are omitted for clarity, and only one of the six $As_2(\mathbf{L}^{1,4})_2Cl_2$ macrocycles contained in the asymmetric unit is shown for brevity (c,f,i).

Single crystal X-ray diffraction studies confirm that each macrocycle consists of two arsenic atoms spanned by two bridging ligands that create a cavity that is roughly 6 Å across (Figure 2, Tables 1 and 2). Each arsenic atom also remains coordinated by a lone chlorine atom that is not displaced when the reactions are performed in the absence of base.[5,6] Each structure reveals that As-π interactions are influencing the stereochemistry of the assemblies by directing arsenic, and thus its coordination sphere, into the macrocyclic cavities of the complexes. Only one of the two possible diastereomers of each macrocycle crystallizes out of chloroform: *anti*-$As_2(\mathbf{L}^{2,6})_2Cl_2$ (Figure 2a,d, Table 1),

anti-$As_2(L^{1,5})_2Cl_2$ (Figure 2b,e), and *syn*-$As_2(L^{1,4})_2Cl_2 \cdot CHCl_3$[a] (Figure 2c,f, Table 1). Although the As•••As distances in these structures vary widely (7.45, 5.64 and 4.66 Å, respectively), the As•••C distances between the As atom and the nearest C atom in the naphthalene rings (3.30, 3.22 and 3.14 Å, respectively) consistently indicate the presence of As-π interactions (Table 2).[8,14]

Table 1. Crystallographic Data and Refinement Parameters for $As_2(L^{2,6})_2Cl_2$, $As_2(L^{1,5})_2Cl_2$, $As_2(L^{1,4})_2Cl_2 \cdot CHCl_3$, and $As_2(L^{1,4})_2Cl_2 \cdot C_6H_6$.

	$As_2(L^{2,6})_2Cl_2$	$As_2(L^{1,5})_2Cl_2$	$As_2(L^{1,4})_2Cl_2 \cdot CHCl_3$	$As_2(L^{1,4})_2Cl_2 \cdot C_6H_6$
empirical formula	$C_{24}H_{20}As_2Cl_2S_4$	$C_{24}H_{20}As_2Cl_2S_4$	$C_{25}H_{21}As_2Cl_5S_4$	$C_{30}H_{26}As_2Cl_2S_4$
formula weight	657.38	657.38	776.75	735.49
temperature (K)	153(2)	173(2)	173(2)	173(2)
wavelength (Å)	0.71073	0.71073	0.71073	0.71073
space group	$P2_1/n$	$P2_1/c$	P-1	$P2_1/n$
a (Å)	6.395(1)	6.813(4)	19.313(4)	10.3332(7)
b (Å)	19.675(4)	19.08(1)	19.923(4)	34.375(2)
c (Å)	10.967(2)	10.277(6)	24.508(5)	17.859(1)
α (°)	90	90	78.110(4)	90
β (°)	106.817(3)	107.79(1)	78.860(5)	98.965(1)
γ (°)	90	90	89.183(5)	90
volume (Å^3)	1320.8(5)	1272.5(14)	9050(3)	6266.3(7)
Z, Z'	2, 0.5	4, 1	12, 6	8,2
D_{calcd} (mg/m^3)	1.653	1.716	1.710	1.559
μ (cm^{-1})	0.3061	0.3177	0.2951	0.2590
N measd	10816	6949	102535	53433
N ind [R_{int}]	2322 [0.0264]	2750 [0.0816]	39214 [0.0953]	11027 [0.0315]
N obs [$I > 2\sigma(I)$]	1904	1632	19406	9741
no. of params	145	145	1937	708
goodness-of-fit on F^2	1.053	1.037	0.981	1.260
R1/wR2 [$I > 2\sigma(I)$]	0.0486/0.1226	0.0816/0.1779	0.0687/0.1278	0.0577/0.1155
R1/wR2 (all data)	0.0603/0.1314	0.1482/0.2138	0.1577/0.1646	0.0657/0.1185

[a] *syn*-$As_2(L^{1,4})_2Cl_2$ crystallizes exclusively out of chloroform with six macrocycles present in the asymmetric unit. The six *syn*-macrocycles vary slightly in their conformations. A full description of the structural details and refinement are in the Experimental Section. A roughly 3:1 mixture of *syn*-to-*anti*-$As_2(L^{1,4})_2Cl_2 \cdot C_6H_6$ crystallizes out of benzene. Full details of the modeling of the disorder are contained in the Experimental Section.

Table 2. Selected Bond Lengths (Å) and Angles (°).

$As_2(\mathbf{L}^{2,6})_2Cl_2$		$As_2(\mathbf{L}^{1,5})_2Cl_2$	
As(1)-S(1)	2.1987(16)	As(1)-S(2A)	2.210(3)
As(1)-S(2)	2.2078(15)	As(1)-S(1)	2.215(3)
As(1)-Cl(1)	2.2494(18)	As(1)-Cl(1)	2.237(3)
S(1)-As(1)-S(2)	89.33(6)	S(2A)-As(1)-S(1)	85.81(10)
S(1)-As(1)-Cl(1)	100.42(7)	S(2A)-As(1)-Cl(1)	100.99(12)
S(2)-As(1)-Cl(1)	98.74(6)	S(1)-As(1)-Cl(1)	102.16(11)
C(1)-S(1)-As(1)	99.4(2)	C(1)-S(1)-As(1)	102.1(3)
C(12)-S(2)-As(1A)	98.89(19)	C(12)-S(2)-As(1A)	102.1(3)
syn(1)-$As_2(\mathbf{L}^{1,4})_2Cl_2{\cdot}C_6H_6$[a] and *anti*(1)-$As_2(\mathbf{L}^{1,4})_2Cl_2{\cdot}C_6H_6$[a]		*syn*(2)-$As_2(\mathbf{L}^{1,4})_2Cl_2{\cdot}C_6H_6$ and *anti*(2)-$As_2(\mathbf{L}^{1,4})_2Cl_2{\cdot}C_6H_6$[a]	
As(1A)-S(4A)	2.208(2)	As(1)-S(1)	2.2021(15)
As(1A)-S(1A)	2.2109(17)	As(1)-S(4)	2.2077(16)
As(1A)-Cl(1A)	2.255(2)	As(1)-Cl(1)	2.223(2)
As(2A)-S(2A)	2.2112(19)	As(2)-S(2)	2.2158(15)
As(2A)-S(2B)	*2.055(15)*		
As(2A)-S(3A)	2.2027(17)	As(2)-S(3)	2.2198(16)
As(2A)-S(3B)	*2.167(12)*		
As(2A)-Cl(2A)	2.2757(19)	As(2)-Cl(2)	2.261(3)
As(2A)-Cl(2B)	*2.295(14)*	*As(2)-Cl(2')*	*2.286(4)*
S(4A)-As(1A)-S(1A)	87.07(7)	S(1)-As(1)-S(4)	89.68(6)
S(4A)-As(1A)-Cl(1A)	101.01(10)	S(1)-As(1)-Cl(1)	100.71(9)
S(1A)-As(1A)-Cl(1A)	102.42(9)	S(4)-As(1)-Cl(1)	99.84(9)
S(2A)-As(2A)-S(3A)	89.31(7)	S(2)-As(2)-S(3)	88.06(6)
S(2B)-As(2A)-S(3B)	*100.6(6)*		
S(2A)-As(2A)-Cl(2A)	96.91(8)	S(2)-As(2)-Cl(2)	101.75(8)
S(2B)-As(2A)-Cl(2B)	*100.4(7)*	*S(2)-As(2)-Cl(2')*	*103.85(10)*
S(3A)-As(2A)-Cl(2A)	100.14(8)	S(3)-As(2)-Cl(2)	97.00(11)
S(3B)-As(2A)-Cl(2B)	*99.7(6)*	*S(3)-As(2)-Cl(2')*	*97.93(11)*
C(1A)-S(1A)-As(1A)	101.5(2)	C(1)-S(1)-As(1)	100.0(2)
C(12A)-S(2A)-As(2A)	98.4(2)	C(12)-S(2)-As(2)	101.33(19)
C(12A)-S(2B)-As(2A)	*97.6(2)*		
C(13A)-S(3A)-As(2A)	101.3(2)	C(13)-S(3)-As(2)	99.3(2)
C(13A)-S(3B)-As(2A)	*107.3(2)*		
C(24A)-S(4A)-As(1A)	100.3(2)	C(24)-S(4)-As(1)	98.1(2)

[a] This structure contains two macrocycles in the asymmetric unit, both of which are disordered over *syn* and *anti* conformations (denoted *syn*(1), *anti*(1), *syn*(2) and *anti*(2)). *anti*(1) and *anti*(2) refer to the two conformers of the *anti*-macrocycle present in the disordered structure (see Figure 6). The structure *anti*(2) results from disorder of the chlorine atom that is bonded to As(2) over two sites: Cl(2) and Cl(2'). The structure *anti*(1) results from disorder of the chlorine and sulfur atoms bonded to As(2a) in the other macrocycle. The bond distances and angles for the *anti*-isomers are italicized in the table.

Table 2 (continued).

$As_2(L^{1,4})_2Cl_2 \cdot CHCl_3$[b]			
As(1)-S(4)	2.216(2)	S(1)-As(1)-Cl(1)	100.78(10)
As(1)-S(1)	2.227(2)	S(3)-As(2)-S(2)	88.77(8)
As(1)-Cl(1)	2.246(2)	S(3)-As(2)-Cl(2)	100.43(9)
As(2)-S(3)	2.224(2)	S(2)-As(2)-Cl(2)	101.88(9)
As(2)-S(2)	2.227(2)	C(1)-S(1)-As(1)	99.9(3)
As(2)-Cl(2)	2.240(2)	C(12)-S(2)-As(2)	99.2(3)
S(4)-As(1)-S(1)	89.53(8)	C(13)-S(3)-As(2)	99.0(3)
S(4)-As(1)-Cl(1)	100.39(9)	C(24)-S(4)-As(1)	100.2(3)

[b] Data from only one of six conformers is shown for brevity.

Each macrocycle exists as a mixture of diastereomers in differing amounts, in solution. A nearly equal mixture of *syn*- and *anti*-$As_2(L^{2,6})_2Cl_2$ macrocycles is observed in solution (*de* = 9%) by ^1H NMR spectroscopy (Figure 3a). The ^1H NMR spectrum of this mixture reveals that the methylene protons of each diastereomer appear as an AB quartet.

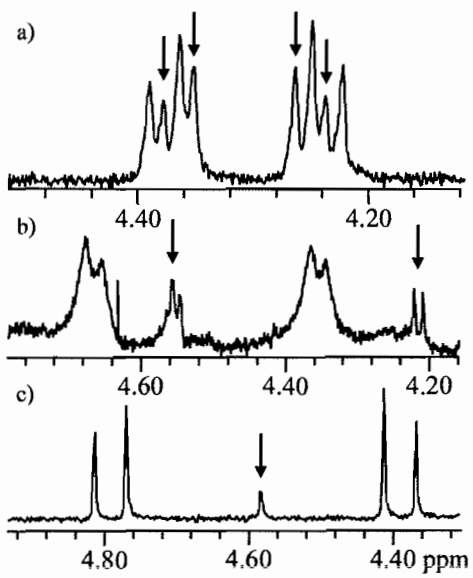

Figure 3. Methylene region of the ^1H NMR spectra (in ppm) of $As_2L_2Cl_2$ macrocycles with arrows marking the least thermodynamically stable isomers. The equilibrium mixtures of *syn*- and *anti*-$As_2(L^{2,6})_2Cl_2$ (a), $As_2(L^{1,5})_2Cl_2$ (b), and $As_2(L^{1,4})_2Cl_2$ (c) at 25 °C are shown.

In the ^{1}H NMR spectrum obtained by dissolving single crystals of *anti*-$As_2(\mathbf{L}^{1,5})_2Cl_2$, it is clear that there is a large excess of one diastereomer, presumably the *anti*-isomer (Figure 3b).[b] The *de* was calculated to be 85%, although the low solubility of the complex, as shown by the noisy NMR spectrum (obtained from an overnight scan of a saturated solution on a 600 MHz spectrometer), leads to a high error in this value.

A large excess of *syn*-isomer is observed in solution for the $As_2(\mathbf{L}^{1,4})_2Cl_2$ macrocycles (*de* = 90%) (Figure 3c). In this case the *anti*-macrocycle appears as a singlet in the center of the *syn*-AB quartet. Variable temperature NMR spectroscopy revealed that at high temperatures this singlet splits into the AB quartet expected for the geminal methylene protons (Figure 4). At room temperature, the methylene resonances are coincidental, and as a result do not split each other. As the temperature is raised, these resonances shift slightly, are no longer coincidental, and split into the characteristic AB quartet. Interestingly, as the temperature is raised the *de* decreases, reminiscent of organic reactions in which *de*'s are typically optimized by performing reactions at lower temperatures.[c,15] This indicates that the *anti*-macrocycle is entropically favored over the *syn*-isomer. In a related supramolecular example, Stang and co-workers have reported that a mixture of self-assembled macrocyclic dimers and trimers exists in a temperature-dependent equilibrium favoring the entropically-preferred dimer at higher temperatures.[16]

---

[b] For each macrocycle, single crystals of one diastereomer were dissolved and thermodynamic equilibrium is quickly reached (<5 min).

[c] This is similar to the established case of organic addition reactions, which can exhibit temperature dependent *de*'s when the enthalpically and entropically favored products are not the same.[15]

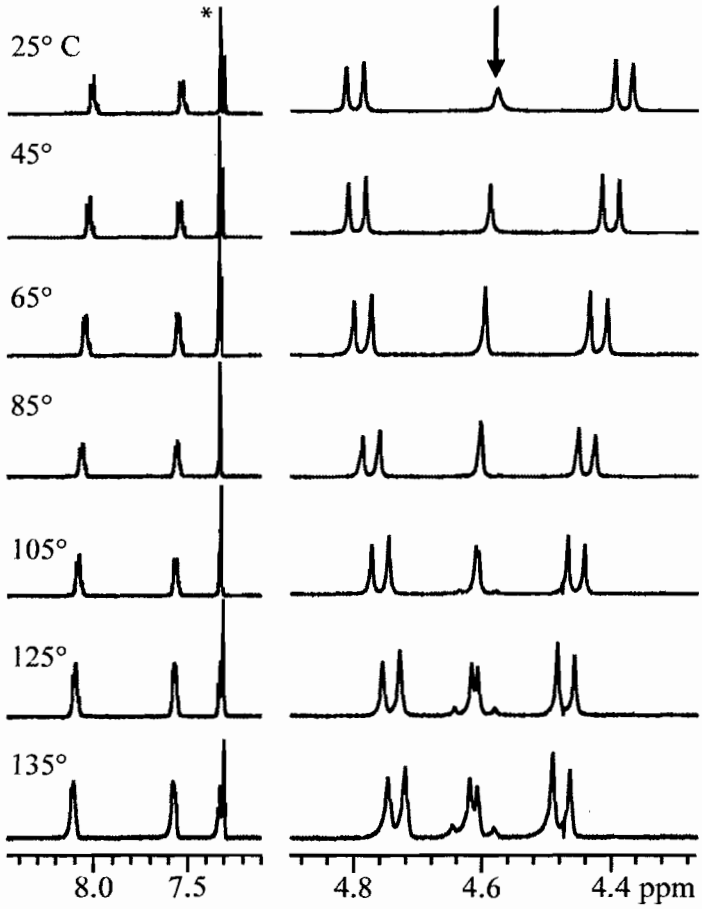

Figure 4. Variable temperature ^{1}H NMR spectra (in ppm) for $As_2(\mathbf{L}^{1,4})_2Cl_2$ macrocycles with the arrow marking the resonances for the methylene protons of the *anti*-diastereomer. The resonance with the * corresponds to $CHCl_3$.

Variable temperature ^{1}H NMR spectroscopic experiments were also carried out on the $As_2(\mathbf{L}^{2,6})_2Cl_2$ macrocycles and revealed incomplete coalescence at temperatures up to 135 °C, suggesting that the interconversion between *syn*- and *anti*-isomers is slow on the NMR timescale (Figure 5). As the sample is heated, the *syn* and *anti* resonances shift to a point where they overlap, making a quantitative measurement of the *de* at temperatures

above 45 °C impossible. EXSY experiments confirmed that conversion between diastereomers is slow on the NMR timescale for both $As_2(\mathbf{L}^{2,6})_2Cl_2$ and $As_2(\mathbf{L}^{1,4})_2Cl_2$ at room temperature on a 400 MHz spectrometer.

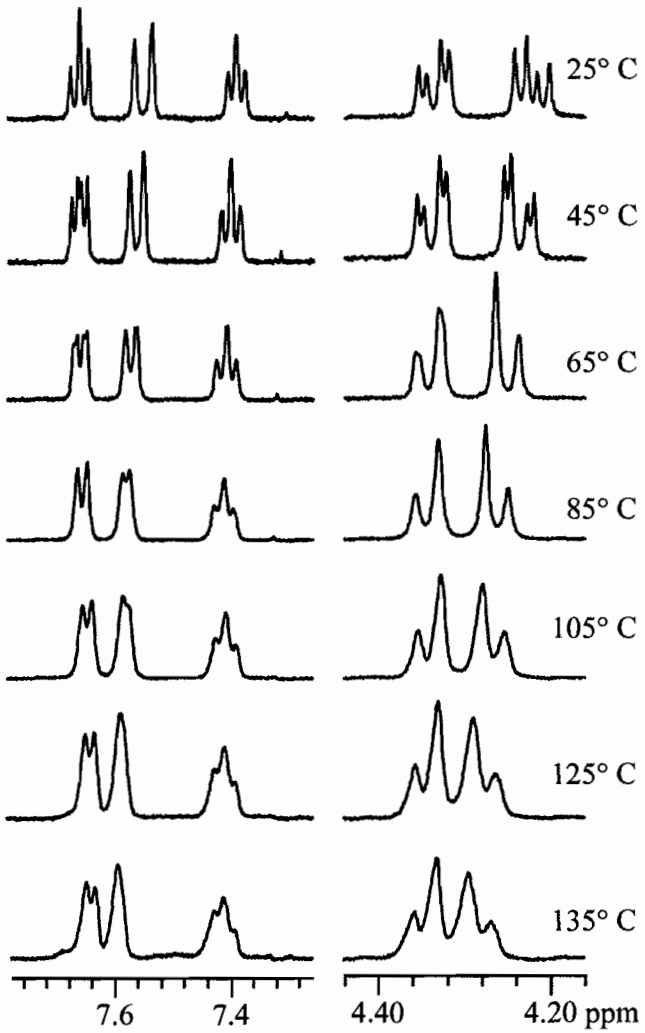

Figure 5. Variable temperature ^1H NMR spectra (in ppm) for $As_2(\mathbf{L}^{2,6})_2Cl_2$ macrocycles.

Mechanism of Interconversion

We previously showed that the interconversion of *syn*-to-*anti* macrocycles is not occurring by 1) pyramidal inversion of one As(III) center, 2) complete ligand dissociation, or 3) HCl-catalyzed inversion for the following reasons.[6] First, the barrier to arsine inversion is too high to occur at room temperature, making pyramidal inversion followed by bond rotation an unlikely route for interconversion.[d,17,18] Second, complete ligand exchange was not observed for a related mixture of $As_2\mathbf{L}_2Cl_2$ macrocycles ($H_2\mathbf{L}$ = bis(mercaptomethyl)benzene).[6] Finally, hydrochloric acid, a side-product of macrocycle formation, is known to cause racemization of chiral arsines[19,20] and was initially thought to be involved in the interconversion of *syn*-to-*anti* macrocycles. However, when crystals of exclusively one diastereomer are dissolved in chloroform that has been neutralized with basic alumina to remove any traces of HCl, interconversion still occurs rapidly to give an equilibrium mixture of diastereomers.[6] Having shown that arsine inversion, complete ligand dissociation, and HCl-catalyzed racemization are unlikely to be involved in the interconversion of *syn*-to-*anti* macrocycles, a new mechanism based on the disproportionation of two arsenic centers is proposed.

X-ray crystal data reveal that when crystals of $As_2(\mathbf{L}^{1,4})_2Cl_2$ are grown by slow diffusion of pentane into benzene, they contain two conformers of both the *syn*-

---

[d] The barrier to pyramidal inversion was found to be 39 kcal/mol for AsH_3, 45 kcal/mol for AsF_3,[17] and at least 42 kcal/mol for chiral arsines.[18]

macrocycle and the *anti*-macrocycle (Figure 6). In the *anti*(2)-conformer shown in Figure 6c, the chlorine atom is pointing into the cavity with an As-Cl distance of 2.286(4) and a short As-Cl contact to the other arsenic center of 3.54 Å. This non-bonding distance is shorter than the sum of the van der Waals radii for arsenic and chlorine (3.80 Å). Based on this structure, and the knowledge that $AsCl_3$ can disproportionate into $AsCl_2^+$ and $AsCl_4^-$,[e,21-22] it is reasonable that the interconversion of *syn*-to-*anti* macrocycles could occur by disproportionation of two arsenic centers. This interconversion could occur intramolecularly through a zwitterionic intermediate (Scheme 2), or intermolecularly. We are currently studying this interconversion mechanism to determine 1) if the halide ligand is involved in the interconversion, 2) how the halide ligand affects the rate of interconversion, and 3) if the rate depends on halide concentration. Furthermore, it is possible that partial ligand dissociation (breakage of only one As-S bond) could result in interconversion. The results of these studies will be reported in due course.

---

[e] $AsCl_3$ is known to disproportionate into $AsCl_2^+$ and $AsCl_4^-$.[21,22] It seems plausible that AsL_2Cl complexes (where L = thiolate) could also disproportionate into AsL_2^+ and $AsL_2Cl_2^-$ ions. Upon the reformation of AsL_2Cl, inversion at the arsenic center can occur. In the anionic form, either chloride ligand could leave with equal likelihood, scrambling the stereochemistry at arsenic. Conversely, in the planar cation, the incoming chloride could either attack above or below the plane of the complex leading to two different configurations at arsenic. This mechanism of interconversion could occur *intra- or intermolecularly* in $As_2L_2Cl_2$ macrocycles.

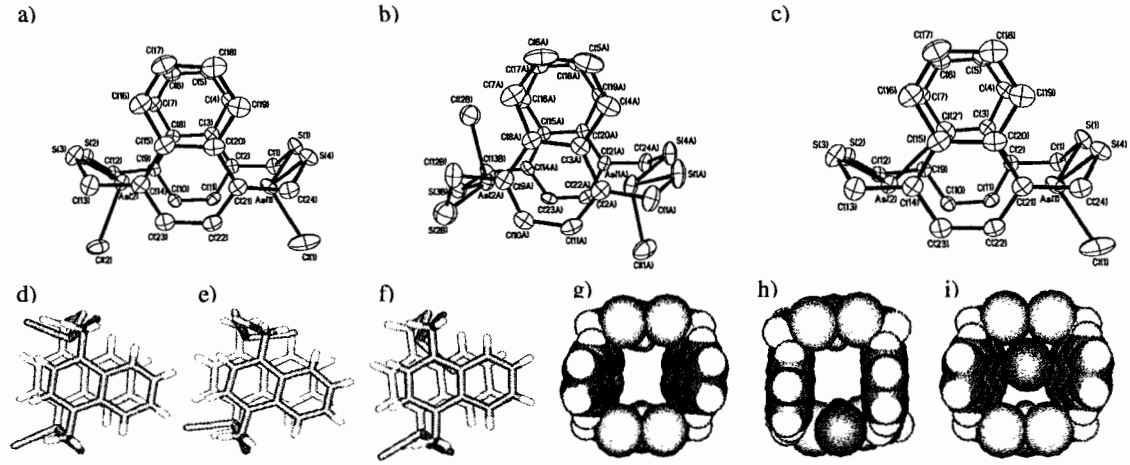

Figure 6. ORTEP (30% probability ellipsoids), wireframe, and space filling representations of three conformers found in the crystal structure of $As_2(\mathbf{L}^{1,4})_2Cl_2{\cdot}C_6H_6$: *syn*(1)-$As_2(\mathbf{L}^{1,4})_2Cl_2{\cdot}C_6H_6$ (a,d,g), *anti*(1)-$As_2(\mathbf{L}^{1,4})_2Cl_2{\cdot}C_6H_6$ (b,e,h) and *anti*(2)-$As_2(\mathbf{L}^{1,4})_2Cl_2{\cdot}C_6H_6$ (c,f,i) macrocycles. The ligands are planar within 0.03 Å. The dihedral angle between the average planes of the ligands in the isomers are different: 7.4 Å in *anti*(1)-$As_2(\mathbf{L}^{1,4})_2Cl_2{\cdot}C_6H_6$ (b,e,h) and 36.0Å in both *syn*- $As_2(\mathbf{L}^{1,4})_2Cl_2{\cdot}C_6H_6$ (a,d,g) and *anti*(2)-$As_2(\mathbf{L}^{1,4})_2Cl_2{\cdot}C_6H_6$ (c,f,i). Cocrystallized C_6H_6 (a-i) and hydrogens (a,b,c) are omitted for clarity.

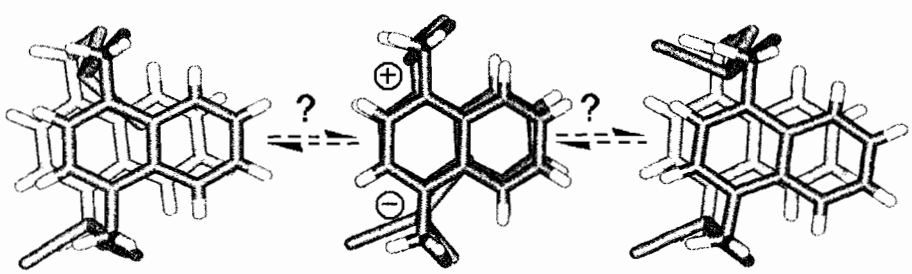

Scheme 2. Proposed mechanism for the intramolecular disproportionation leading to interconversion between *syn*- and *anti*-macrocycles.

Conclusion

In summary, this study represents an unusual example of a self-assembly reaction in which the *de* is controlled in a predictable manner through the use of achiral, isomeric ligands. The As-π interaction acts as the directing force for the self-assembly of $As_2L_2Cl_2$ macrocycles that exist as an equilibrium mixture of both "*syn*" and "*anti*" diastereomers in solution. By controlling the *syn*-to-*anti* ratio of our $As_2L_2Cl_2$ macrocycles in solution, we gain some understanding of how these macrocycles could act as synthons for larger assemblies. We are currently pursuing this goal, as well as designing macrocycles with improved diastereocontrol and studying the mechanism of *syn*-to-*anti* interconversion.

Experimental Section

General Procedures

^{1}H NMR spectra were measured using a Varian INOVA-500 spectrometer operating at 500.11 MHz ($As_2(\mathbf{L}^{2,6})_2Cl_2$ and $As_2(\mathbf{L}^{1,4})_2Cl_2$) and a Varian INOVA-600 spectrometer operating at 599.98 MHz ($As_2(\mathbf{L}^{1,5})_2Cl_2$). All variable temperature experiments were carried out on the Varian INOVA-500 spectrometer on compounds dissolved in 1,1,2,2-tetrachloroethane-d_2. Spectra were referenced using either TMS or the residual solvent resonances as internal standards. Single crystal X-ray diffraction studies were performed on a Bruker SMART APEX diffractometer. Commercially available reagents were used as received. All ligands were prepared following a modified literature procedure.[13]

^{1}H NMR spectroscopy revealed complete transformation (>99% yield) of ligand and $AsCl_3$ to macrocycles $As_2(\mathbf{L}^{2,6})_2Cl_2$ and $As_2(\mathbf{L}^{1,4})_2Cl_2$. (This was not measurable for $As_2(\mathbf{L}^{1,5})_2Cl_2$ due to poor product solubility). The reported yields below are for isolated single-crystals. *Caution: Arsenic compounds are hazardous and should be handled with care!* (This accounts for the small scale of the reactions reported herein.)

Synthetic Procedures

2,6-bis(bromomethyl)naphthalene. 2,6-dimethylnaphthalene (1.34 g, 8.59 mmol), *N*-bromosuccinimide (4.84 g, 25.8 mmol), benzoyl peroxide (859 mg, 0.221 mmol) and dry chloroform (50 mL) were stirred together and degassed to give a yellow suspension. The reaction mixture was heated under N_2 at 55 °C for 12 h. Chloroform (25 mL) was added and the solution was washed with 2 M HCl (2 × 25 mL), then 2 M NaOH (2 × 25 mL). The solvent was evaporated to yield an off-white powder. This powder was purified by trituration with acetone to yield a white solid (1.34 g, 4.27 mmol, 50%). ^{1}H NMR ($CDCl_3$): δ 7.82 (s, 2H, C*H*), 7.82 (d, 2H, C*H*, J = 8.5 Hz), 7.54 (d, 2H, C*H*, J = 8.5 Hz), 4.67 (s, 4H, CH_2).

2,6-bis(mercaptomethyl)naphthalene ($H_2\mathbf{L}^{2,6}$). 2,6-bis(bromomethyl)naphthalene (1.09 g, 3.47 mmol) and thiourea (803 mg, 10.6 mmol) were heated to reflux in 1:1 v/v CH_2Cl_2/acetone (60 mL) for 1 h 15 min. The solvent was evaporated and the resulting white salt was washed with acetone, dried overnight by vacuum filtration, and then degassed. Degassed 2 M NaOH (30 mL) was transferred via cannula onto the salt and the solution was stirred under N_2 at 80 °C for 2 h. The solution

was acidified with 6 M HCl and extracted with CH_2Cl_2 (3 × 30 mL). The organic layer was washed with 0.5 M HCl, dried with $MgSO_4$, and concentrated to yield a white solid (510 mg, 2.31 mmol, 67%). ^{1}H NMR ($CDCl_3$): δ 7.78 (d, 2H, C*H*, J = 8.2 Hz), 7.72 (s, 2H, C*H*), 7.48 (dd, 2H, C*H*, *J* = 8.5 Hz, *J* = 1.8 Hz), 3.91 (d, 4H, CH_2, *J* = 7.6 Hz), 1.81 (t, 2H, S*H*, *J* = 7.6 Hz).

$As_2(L^{2,6})_2Cl_2$. $AsCl_3$ (6.37 μL, 0.0746 mmol) was added slowly to a solution of $H_2L^{2,6}$ (16.5 mg, 0.0746 mmol) in $CDCl_3$ (5 mL) to yield a solution containing only a mixture of *syn-* and *anti-* diastereomers in a ratio of 1.7:1 after three days. Single crystals were grown by slow vapor diffusion of pentane into a $CHCl_3$ solution of $As_2(L^{2,6})_2Cl_2$ yielding colorless crystals after 3 days (4.7 mg, 0.0072 mmol, 19%). *syn*-$As_2(L^{2,6})_2Cl_2$: ^{1}H NMR (300 MHz, $CDCl_3$) δ 7.64 (d, 2H, C*H*, J = 8.8 Hz), 7.56 (s, 2H, C*H*), 7.35 (m, 2H, C*H*), 4.26 (ABq, CH_2, 4H, *J* = 12.9 Hz). *anti*-$As_2(L^{2,6})_2Cl_2$: ^{1}H NMR ($CDCl_3$) δ 7.63 (d, 2H, C*H*, *J* = 8.5 Hz), 7.51 (s, 2H, C*H*), 7.38 (m, 2H, C*H*), 4.25 (ABq, CH_2, 4H, *J* = 12.9 Hz).

1,5-bis(bromomethyl)naphthalene. 1,5-dimethylnaphthalene (10.0 g, 64.0 mmol), *N*-bromosuccinimide (34.2 g, 192 mmol) and benzoyl peroxide (1.55 g, 6.40 mmol) were dissolved in dry chloroform (250 mL) in a 500 mL 3-neck flask and degassed. The reaction mixture was heated under N_2 at 50 °C for 3 h 15 min. The solution was cooled to room temperature and half of the solvent was evaporated, causing a white precipitate to crash out of solution. This precipitate was removed by vacuum filtration and washed with 2 M HCl (2 × 30 mL), 2 M NaOH (2 × 30 mL), brine, and dried with $MgSO_4$ to yield a white powder as the crude product (14.4 g, 45.9 mmol,

72%). ^{1}H NMR ($CDCl_3$): δ 8.19 (d, 2H, C*H*, *J* = 8 Hz), 7.58 (m, 4H, C*H*), 4.96 (s, 4H, CH_2).

1,5-bis(mercaptomethyl)naphthalene (H_2**L**^{1,5}). 1,5-bis(bromomethyl)naphthalene (14.3 g, 45.4 mmol) and thiourea (13.9 g, 182 mmol) were heated to reflux in acetone (500 mL) for 1 h 15 min. The solvent was removed by vacuum filtration and the resulting white salt was washed with acetone to yield a white salt. The salt was then placed under N_2 in a 500 mL 3-neck flask equipped with a stir bar. Degassed 2 M NaOH (300 mL) was transferred via cannula onto the salt and the solution was stirred under N_2 at reflux for 2 h. After cooling to room temperature, the solution was acidified with concentrated HCl and extracted with CH_2Cl_2 (3 × 50 mL). The organic layer was washed with H_2O, dried with $MgSO_4$, and concentrated to yield a white solid (8.28, 37.4 mmol, 82%). ^{1}H NMR ($CDCl_3$): δ 8.04 (m, 2H, C*H*), 7.49 (m, 2H, C*H*), 4.21 (d, 4H, CH_2, J = 7.4 Hz), 1.88 (t, 2H, S*H*, J = 7.4 Hz).

As$_2$(L^{1,5})$_2$Cl$_2$. $AsCl_3$ (5.13 μL, 0.0601 mmol) was added slowly to a solution of H_2**L**^{1,5} (13.3 mg, 0.0601 mmol) in $CHCl_3$ (5 mL) and mixed well causing white crystals to crash out of solution that were suitable for single crystal X-ray structure determination (52.0 mg, 0.079 mmol, 35%). Sparingly soluble crystals were dissolved in CD_2Cl_2 and the ^{1}H NMR spectrum was collected over 10 hours: ^{1}H NMR (600 MHz, CD_2Cl_2) δ 7.98 (d, C*H*, *J* = 8.2 Hz), 7.37 (m, C*H*), 7.33 (m, C*H*), 7.24 (m, C*H*), 7.18 (m, C*H*), 4.51 (ABq, CH_2, *J* = 12 Hz), 4.39, (ABq, CH_2, *J* = 4 Hz).

1,4-bis(bromomethyl)naphthalene. 1,4-dimethylnaphthalene (4.42 g, 28.3 mmol) was dissolved in dry chloroform (150 mL) and degassed. Under active N_2, *N*-

bromosuccinimide (15.0 g, 84.5 mmol) and benzoyl peroxide (690 mg, 2.85 mmol) were added and the suspension was degassed to give a yellow suspension. The reaction mixture was heated under N_2 at 55 °C for 6 h. The solution was cooled to room temperature and then washed with 2 M HCl (2 × 15 mL), 2M NaOH (2 × 20 mL), brine, and dried with $MgSO_4$. The solvent was evaporated to yield an off-white powder as the crude product (9.50 g, 28.3 mmol, >99%). ^{1}H NMR ($CDCl_3$): δ 8.22 (m, 2H, C*H*), 7.67 (m, 2H, C*H*), 7.49 (s, 2H, C*H*), 4.94 (s, 4H, CH_2).

1,4-bis(mercaptomethyl)naphthalene ($H_2\mathbf{L}^{1,4}$). 1,4-bis(bromomethyl)naphthalene (4.00 g, 12.7 mmol) and thiourea (2.92 g, 38.5 mmol) were heated to reflux in 3:2 v/v $CHCl_3$/acetone (250 mL) for 16 h. The solvent was removed by vacuum filtration and the resulting white salt was washed with acetone and dried for 1 h 30 min by vacuum filtration to yield a pale yellow salt (5.92 g, 12.7 mmol, >99%). The salt was then placed under N_2 in a 500 mL 3-neck flask equipped with a stir bar. Degassed 2 M NaOH (200 mL) was transferred via cannula onto the salt and the solution was stirred under N_2 at 80 °C for 2 h. After cooling to room temperature, the solution was acidified with concentrated HCl and extracted with CH_2Cl_2 (3 × 50 mL). The organic layer was washed with H_2O, dried with $MgSO_4$, and concentrated to yield a yellow solid (2.06, 9.31 mmol, 73%). ^{1}H NMR ($CDCl_3$): δ 8.14 (m, 2H, C*H*), 7.60 (m, 2H, C*H*), 7.38 (s, 2H, C*H*), 4.19 (d, 4H, CH_2, J = 7.0 Hz), 1.88 (t, 2H, S*H*, J = 7.0 Hz).

$As_2(\mathbf{L}^{1,4})_2Cl_2$. $AsCl_3$ (17.4 μL, 0.203 mmol) was added slowly to a solution of $H_2\mathbf{L}^{1,4}$ (45.0 mg, 0.203 mmol) in $CHCl_3$ (15 mL) and mixed well to yield a solution of *syn* and *anti* diastereomers in a ratio of 20:1. Slow diffusion of pentane into a chloroform

solution of the complex yielded clear, colorless crystals that were suitable for structure determination using single crystal X-ray diffraction methods (6.9 mg, 0.010 mmol, 10%). Single crystals were also obtained by slow diffusion of pentane into a benzene solution of the complex. Single crystals were dissolved in $CDCl_3$: *syn*-$As_2(\mathbf{L}^{1,4})_2Cl_2$: ^1H NMR (500 MHz, $CDCl_3$) δ 8.03 (m, 4H, C*H*), 7.53 (m, 4H, C*H*), 7.32 (s, 4H, C*H*), 4.58 (ABq, 16H, CH_2, J = 13.2 Hz). *anti*-$As_2(\mathbf{L}^{1,4})_2Cl_2$: ^1H NMR (500 MHz, $CDCl_3$) δ 8.00 (m, 4H, C*H*), 7.47 (m, 4H, C*H*), 7.28 (s, 4H, C*H*), 4.57 (s, 16H, CH_2).

X-Ray Crystallography

All data was collected on a Bruker SMART APEX CCD diffractometer using Mo Kα radiation at 153 K ($As_2\mathbf{L}^{2,6}{}_2Cl_2$) or 173 K ($As_2(\mathbf{L}^{1,5})_2Cl_2$, $As_2(\mathbf{L}^{1,4})_2Cl_2{\cdot}CHCl_3$ and $As_2(\mathbf{L}^{1,4})_2Cl_2{\cdot}C_6H_6$). The crystallographic data, details of the data collections, and refinements of the structures are given in the CIF files. The absorption corrections for each structure were applied by SADABS. The structures were solved using direct methods or the Patterson function, completed by subsequent difference Fourier syntheses, and refined by full matrix least-squares procedures on F^2. In each of the structures, all non-H atoms were refined with anisotropic thermal parameters except the disordered C and Cl atoms in solvent $CHCl_3$ molecules in $As_2(\mathbf{L}^{1,4})_2Cl_2$. H atoms were treated in calculated positions. All calculations were performed by the Bruker SHELXTL package.

Some additional comments about the X-ray structure of $As_2(\mathbf{L}^{1,4})_2Cl_2{\cdot}CHCl_3$ should be noted. The crystal structure of this compound was determined as triclinic

(space group *P*-1, unit cell a = 19.313(4), b = 19.923(4), c = 24.508(5) Å, α= 78.110(4), β= 78.860(5), γ= 89.183(5)° with six symmetrically independent structural units, each containing the macrocycle and one $CHCl_3$ molecule. Checking these crystals for possible twins by CELL_NOW[23] showed that the crystals could contain a twin which consists of four domains with the same unit cell (a = 10.494, b = 17.351, c = 17.616 Å, α= 105.80, β= 92.98, γ= 95.98° but different orientations. Our attempts to solve this structure as a twin or in a monoclinic system failed (the fact that parameters a, b and angles α, β are close to each other indicates such a possibility). However, it was possible to solve and perform refinements to the crystal structure of $As_2(\mathbf{L}^{1,4})_2Cl_2{\cdot}CHCl_3$ in space group *P*-1 with six independent molecules. All non-H atoms in $As_2(\mathbf{L}^{1,4})_2Cl_2{\cdot}CHCl_3$ were refined with anisotropic thermal parameters. The geometry of all six independent molecules, the anisotropic thermal parameters for each of the atoms, and the packing of the molecules in the crystal structure are all reasonable. Four of the six symmetrically independent solvent $CHCl_3$ molecules are disordered over two positions with opposite orientations. All six macrocyclic molecules have a *syn*-configuration and the geometrical parameters in all of the molecules are close. The X-ray data for $As_2(\mathbf{L}^{1,4})_2Cl_2{\cdot}CHCl_3$ confirm the connectivity and stereochemistry of this macrocycle as reported in the manuscript.

There are two symmetrically independent molecules $As_2(\mathbf{L}^{1,4})_2Cl_2$ in the crystal structure of $As_2(\mathbf{L}^{1,4})_2Cl_2{\cdot}C_6H_6$. One of the Cl atoms in one of them and the S_2AsCl fragment in another one are disordered over two positions (in ratio 41/59 and 88/12, respectively) corresponding to *anti*-$As_2(\mathbf{L}^{1,4})_2Cl_2$, and *syn*-$As_2(\mathbf{L}^{1,4})_2Cl_2{\cdot}$ isomers,

respectively. Thus the X-ray data show that both *anti*- and *syn*-isomers are in the crystal structure of $As_2(\mathbf{L}^{1,4})_2Cl_2 \cdot C_6H_6$.

Crystallographic Information Files for each of these structures are available on the ACS website at pubs.acs.org.

Bridge to Chapter III

Chapter II reported on a series of $As_2L_2Cl_2$ macrocycles prepared from constitutionally isomeric naphthalene dithiol ligands. The diastereomeric excess, or *syn*-to-*anti* ratio, was controlled by the ligand choice; *intramolecular* steric interaction resulted in preference for one isomer over the other. In Chapter III, several different $As_2L_2Cl_2$ macrocyclic complexes are reported. In one example, the *syn*-to-*anti* ratio is controlled *intermolecularly*, through steric interactions in the solid state. In the absence of a suitable guest molecule, the macrocycle crystallizes as the *anti* isomer exclusively. However, if toluene or *p*-xylene is present during the crystallization process, two macrocycles dimerize around one solvent molecule, creating an inclusion complex. *p*-xylene causes the exclusive crystallization of the *syn* isomer, while inclusion of the smaller toluene molecule results in a mixture of *syn* and *anti* conformations.

CHAPTER III

HOST-GUEST INTERACTIONS IN A SERIES OF SELF-ASSEMBLED $As_2L_2Cl_2$ MACROCYCLES

This chapter presents solid-state evidence for the diastereoselective self-assembly of a series of $As_2L_2Cl_2$ macrocycles in which the diastereomeric excess is controlled by intermolecular steric interactions with solvent molecules. This co-authored work was previously published (*Dalton Transactions*, **2008**, 3447-3453, © Royal Society of Chemistry).[1] Sean A. Fontenot performed the synthesis of $As_2(\mathbf{1})_2Cl_2$ and $As_2(\mathbf{2})_2Cl_2$ and assisted in writing the manuscript. X-ray crystallography was carried out by Dr. Lev N. Zakharov. Dr. Melanie A. Pitt performed calculations on cavity volumes. Professor Darren W. Johnson provided intellectual input and editorial assistance. I synthesized each isomer of $As_2(\mathbf{3})_2Cl_2$, performed cavity volume calculations, and wrote the majority of the manuscript.

Introduction

The use of main-group elements as components in metal-ligand supramolecular assemblies is not common, and has led to new structure types that are inaccessible using the more traditional transition metals.[2] Self-assembled from metal ions and multidentate

organic ligands, metal-ligand supramolecular assemblies are dynamic systems,[3-6] often capable of encapsulating guest molecules within their three-dimensional cavities. The walls of these cavities usually consist of phenyl rings causing the cavity interiors to be highly hydrophobic, an environment that can differ significantly from that of the solvent outside the cavity. It is difficult, but also of great interest, to spice up these bland interiors by preparing cavities with endohedral functionality.[7] Guest molecules can interact specifically with inward-directed functional groups,[8] potentially increasing the selectivity of the cavity and the likelihood of reaction or catalysis within that cavity. Unfortunately, endohedral functionalization is synthetically very challenging. Gibb and co-workers have demonstrated this challenge by showing that reactive sites on the exterior of a cavitand are more likely to react than reactive sites within the cavitand.[9,10] As one elegant example of inward-directed functionality, Rebek and co-workers have prepared bowl-shaped cavitands with functional groups that dangle over the bowl-opening,[11-13] allowing them to trap reactive intermediates that are not normally observable on the NMR timescale.[14]

While many of these systems require extensive synthesis, *self-assembled* arsenic-ligand supramolecular[a,15] structures provide easy access to inherently endohedrally-functionalized hosts: the As(III) lone-pairs point into the host's cavity. We are exploring inclusion complexes of these hosts that are uniquely suited for unusual host-guest interactions.

---

[a] These self-assembled supramolecular systems could also be reasonably described as dynamic covalent systems.

Arsenic(III) has an unusual, but predictable, trigonal pyramidal coordination geometry that features a stereochemically active lone-pair when coordinated by sulfur-based ligands. Our laboratory has shown that this geometry can be targeted in the self-assembly of $As_2L_2Cl_2$ macrocycles (where L = a rigid dithiolate) from $AsCl_3$ and dithiol ligands.[16-17] In the solid state, the arsenic atoms in these macrocycles sit within the macrocyclic cavity, partially due to the As-π interaction. This causes the lone-pair of electrons on each arsenic atom to point directly into the cavity, which, when combined with the electron-rich aromatic ligand walls, results in a Lewis-basic interior for the macrocyclic cavity. Unfortunately, all $As_2L_2Cl_2$ macrocycles reported to date are too small to host any guest molecules, and no interactions of potential guests with the unusual Lewis-basic interiors of these cavities have been observed. In this chapter, the single crystal X-ray structures for three macrocycles with larger cavities are reported, and their inclusion complexes with aromatic guests are described. In one case, guest inclusion drives the crystallization of the sterically-hindered isomer of a macrocycle into a dimeric "capsule" around that guest.

Results and Discussion

$AsCl_3$ and dithiol ligands H_2**1**, H_2**2**, and H_2**3** self-assemble into *syn-* and *anti-* $As_2L_2Cl_2$ macrocycles (Scheme 1). These macrocycles were crystallized as inclusion complexes with a variety of aromatic guests (Table 1). In each case it was found that guest inclusion does not affect the As-π interaction, an attractive electrostatic interaction between Lewis-acidic As(III) and Lewis-basic aromatic rings.[18-20] While the presence of

this interaction results in arsenic lone pairs within the macrocyclic cavities, the strong As-π interactions shelter the lone-pairs from interacting with the guests. However, guests do dictate their host's structure, and in fact, host-guest interactions can even be used to provide diastereocontrol in the self-assembly reactions in some cases.

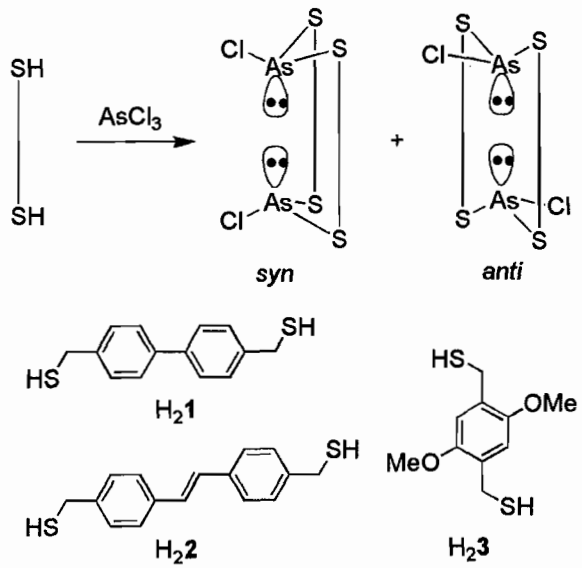

Scheme 1. Self-assembly of $As_2L_2Cl_2$ macrocycles. In the *syn*-$As_2L_2Cl_2$ macrocycles, both chlorine atoms are on the same side of the macrocyclic cavity while in the *anti*-$As_2L_2Cl_2$ macrocycles, the chlorine atoms are on opposite sides.

Table 1. Crystallographic Data and Refinement Parameters for $As_2\mathbf{1}_2Cl_2$, $As_2\mathbf{2}_2Cl_2$, and $As_2\mathbf{3}_2Cl_2$.

	½ [$As_2\mathbf{1}_2Cl_2$ ·toluene]	[*anti*-$As_2\mathbf{2}_2Cl_2$ ·benzene]	*anti*-$As_2\mathbf{3}_2Cl_2$	½ [(*syn*-$As_2\mathbf{3}_2Cl_2)_2$ ·toluene]	½ [(*syn*-$As_2\mathbf{3}_2Cl_2)_2$ · *p*-xylene]
Formula	$C_{21}H_{20}AsClS_2$	$C_{38}H_{34}As_2Cl_2S_4$	$C_{20}H_{24}As_2Cl_2O_4S_4$	$C_{23.50}H_{28}As_2Cl_2O_4S_4$	$C_{24}H_{29}As_2Cl_2O_4S_4$
Formula weight	446.86	839.63	677.37	723.44	730.45
Temperature (K)	173(2)	173(2)	173(2)	173(2)	173(2)
Wavelength (Å)	0.71073	0.71073	0.71073	0.71073	0.71073
Crystal system	Triclinic	Monoclinic	Triclinic	Monoclinic	Monoclinic
Space group	P-1	$P2_1/c$	P-1	$P2_1$	$P2_1/c$
a (Å)	9.3876(7)	15.404(7)	8.4805(11)	13.8813(13)	13.9458(17)
b (Å)	9.6322(8)	6.395(3)	9.3290(12)	9.8378(9)	9.8297(12)
c (Å)	12.0300(9)	19.576(8)	9.6719(12)	21.764(2)	21.814(3)
α (°)	107.6460(10)	90	117.4210(10)	90	90
β (°)	99.3000(10)	104.071(5)	101.198(2)	90.202(2)	90.784(2)
γ (°)	101.4170(10)	90	98.034(2)	90	90
Volume ($Å^3$)	987.09(13)	1870.5(14)	642.79(14)	2972.1(5)	2990.0(6)
Z, *Z'*	2, 1	2, 0.5	1, 0.5	4, 2	4, 1
D_{calcd} (mg/m^3)	1.503	1.491	1.750	1.617	1.623
μ (cm^{-1})	0.2070	0.2179	0. 3158	0.2738	0.2722
F(000)	456	856	340	1460	1476
Crystal size (mm)	0.18 × 0.16 × 0.12	0.19 × 0.14 × 0.02	0.27 × 0.14 × 0.10	0.32 × 0.26 × 0.08	0.18 × 0.14 × 0.10
Index ranges	$-12 \le h \le 12$, $-12 \le k \le 12$, $-15 \le l \le 15$	$-18 \le h \le 18$, $-7 \le k \le 7$, $-23 \le l \le 23$	$-10 \le h \le 10$, $-11 \le k \le 11$, $-12 \le l \le 12$	$-17 \le h \le 17$, $-12 \le k \le 12$, $-27 \le l \le 27$	$-13 \le h \le 17$, $-8 \le k \le 12$, $-27 \le l \le 26$
Reflections collected	11379	12553	5920	33472	14607
Independent reflections [R_{int}]	4453 [0.0211]	3268 [0.1021]	2713 [0.0131]	12933 [0.0186]	6483 [0.0309]
Data/restraints/ parameters	4438/0/318	3268/0/208	2713/0/193	12933/11/643	6483/4/371
Goodness-of-fit on F^2	1.103	1.122	1.031	1.045	1.134
R1/wR2 [$I > 2\sigma(I)$]	0.0382/ 0.0876	0.0897/ 0.2091	0.0280/ 0.0692	0.0516/ 0.1469	0.0713/ 0.1340
R1/wR2 (all data)	0.0450/ 0.0910	0.1412/ 0.2356	0.0316/ 0.0713	0.0615/ 0.1550	0.0985/ 0.1440
Largest diff. peak and hole/e $Å^{-3}$	0.926; -0.489	1.294; -1.428	0.661; -0.399	1.155; -0.772	1.037/-1.096

anti-$As_2\mathbf{1}_2Cl_2$

4,4'-Bis(mercaptomethyl)biphenyl ($H_2\mathbf{1}$) was designed to form macrocycles with cavities that are *tall* enough along the As-As axis to host small guest molecules. $As_2\mathbf{1}_2Cl_2$ was prepared by mixing $H_2\mathbf{1}$ with $AsCl_3$ in toluene. X-ray quality crystals of the [*anti*-$As_2\mathbf{1}_2Cl_2$·toluene] inclusion complex were obtained by the slow diffusion of hexanes into a toluene solution of $As_2\mathbf{1}_2Cl_2$.[b] In the crystal structure, the observed As-C_{aryl} distances, the shortest of which is 3.24 Å, reveal intramolecular As-π interactions (Figure 1a). However, no interactions between the arsenic atoms and the toluene guest molecule are observed. The distances (~3.5 Å) between the closest carbon atoms in the biphenyl

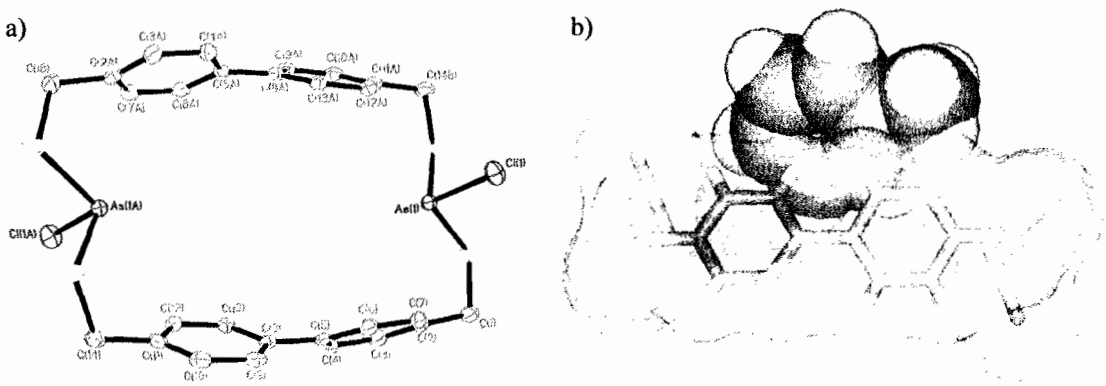

Figure 1. ORTEP (30% probability ellipsoids) representation of single-crystal X-ray structure of *anti*-$As_2\mathbf{1}_2Cl_2$ (a) and space-filling representation (b) of single-crystal X-ray structure of the [$As_2\mathbf{1}_2Cl_2$·toluene] inclusion complex. Only one position for disordered groups is shown for clarity.

---

[b] Crystals were obtained only when toluene or benzene were present, although the crystals grown from benzene were not of X-ray quality. The following solvents did not yield single crystals; presumably, they were not appropriately sized to serve as guests: CH_2Cl_2, $CHCl_3$, *p*-xylene, mesitylene, and THF.

ligands and toluene indicate the presence of π-π stacking between host and guest. The biphenyl ligands bow out slightly, presumably to accommodate the toluene guest. A search of the Cambridge Structural Database[21] reveals that this degree of bending is within the observed range for biphenyl moieties in known structures. All S-As-S, S-As-Cl, and C-S-As angles are within the typical range observed for $As_2L_2Cl_2$ macrocycles (Table 2).[15,17]

Table 2. Selected bond lengths (Å) and angles (°).

[(*syn*-As_2**3**$_2Cl_2)_2$·toluene]		[(*syn*-As_2**3**$_2Cl_2)_2$·*p*-xylene]	
As(1)-S(1)	2.203(2)	As(1)-S(1)	2.2140(2)
As(1)-S(4)	2.214(2)	As(1)-S(3)	2.199(2)
As(1)-Cl(1)	2.248(2)	As(1)-Cl(1)	2.246(2)
As(2)-S(2)	2.220(3)	As(2)-S(2)	2.245(5)
As(2)-S(3)	2.244(3)	As(2)-S(4)	2.218(5)
As(2)-Cl(2)	2.232(3)	As(2)-Cl(2)	2.235(7)
As(2A)-S(2A)	2.13(2)	As(2A)-S(2)	2.105(2)
As(2A)-S(3A)	2.13(3)	As(2A)-S(4)	2.177(1)
As(2A)-Cl(2A)	2.336(1)	As(2A)-Cl(2A)	2.24(2)
As(3)-S(5)	2.192(2)	S(3)-As(1)-S(1)	87.80(8)
As(3)-S(8)	2.212(2)	S(3)-As(1)-Cl(1)	103.22(1)
As(3)-Cl(3)	2.247(2)	S(1)-As(1)-Cl(1)	100.27(8)
As(4)-S(7)	2.201(3)	C(1)-S(1)-As(1)	100.1(2)
As(4)-S(6)	2.209(3)	C(11)-S(3)-As(1)	102.4(3)
As(4)-Cl(4)	2.248(3)	S(4)-As(2)-S(2)	87.58(2)
As(4A)-S(6A)	2.13(5)	Cl(2)-As(2)-S(2)	101.8(2)
As(4A)-S(7A)	2.32(3)	S(4)-As(2)-Cl(2)	102.8(3)
As(4A)-Cl(4A)	2.254(2)	C(8)-S(2)-As(2)	103.0(3)
S(1)-As(1)-S(4)	87.79(8)	C(18)-S(4)-As(2)	101.7(3)
S(1)-As(1)-Cl(1)	102.93(1)	S(2)-As(2A)-S(4)	92.3(7)
S(4)-As(1)-Cl(1)	100.74(9)	S(2)-As(2A)-Cl(2A)	99.9(8)

Table 2 continued.

C(1)-S(1)-As(1)	102.5(3)
C(18)-S(4)-As(1)	99.5(2)
S(2)-As(2)-S(3)	88.47(1)
S(2)-As(2)-Cl(2)	100.14(1)
S(3)-As(2)-Cl(2)	101.88(1)
C(8)-S(2)-As(2)	100.0(2)
C(11)-S(3)-As(2)	101.4(3)
S(3A)-As(2A)-S(2A)	93.0(8)
S(2A)-As(2A)-Cl(2A)	93.1(6)
S(3A)-As(2A)-Cl(2A)	88.4(8)
C(8)-S(2A)-As(2A)	100.7(3)
C(11)-S(3A)-As(2A)	103.2(3)
S(5)-As(3)-S(8)	88.47(9)
S(5)-As(3)-Cl(3)	102.02(1)
S(8)-As(3)-Cl(3)	99.47(9)
C(21)-S(5)-As(3)	103.1(3)
C(38)-S(8)-As(3)	100.3(2)
S(7)-As(4)-S(6)	87.83(1)
S(6)-As(4)-Cl(4)	100.64(1)
S(7)-As(4)-Cl(4)	101.94(1)
C(28)-S(6)-As(4)	103.7(3)
C(31)-S(7)-As(4)	102.3(3)
S(6A)-As(4A)-S(7A)	86.8(1)
S(6A)-As(4A)-Cl(4A)	110.8(1)
Cl(4A)-As(4A)-S(7A)	105.9(1)
C(28)-S(6A)-As(4A)	94.3(5)
C(31)-S(7A)-As(4A)	99.4(5)

anti-$As_2\mathbf{3}_2Cl_2$	
As(1)-S(1)	2.2182(7)
As(1)-S(2)#3	2.2018(8)
As(1)-Cl(1)	2.2586(8)
S(2)#3-As(1)-S(1)	86.76(3)
S(2)#3-As(1)-Cl(1)	101.50(4)
S(1)-As(1)-Cl(1)	102.73(3)
C(1)-S(1)-As(1)	102.92(9)
C(10)-S(2)-As(1)#3	103.85(1)
S(4)-As(2A)-Cl(2A)	86.7(2)
C(8)-S(2)-As(2A)	103.7(4)
C(18)-S(4)-As(2A)	105.6(6)

$[As_2\mathbf{1}_2Cl_2$·toluene]	
As(1)-S(1)	2.1922(9)
As(1)-S(2)	2.2125(9)
As(1)-Cl(1)	2.2524(9)
As(1)-S(1A)	2.185(6)
As(1)-S(2A)	2.110(6)
As(1)-Cl(1A)	2.464(8)
S(1)-As(1)-S(2)	88.19(3)
S(1)-As(1)-Cl(1)	101.63(4)
S(2)-As(1)-Cl(1)	101.23(4)
C(1)-S(1)-As(1)	103.37(1)
C(14)#1-S(2)-As(1)	101.12(1)
S(1A)-As(1)-S(2A)	92.4(3)
S(1A)-As(1)-Cl(1A)	94.9(3)
S(2A)-As(1)-Cl(1A)	95.4(3)
As(1)-S(1A)-C(1)	104.5(3)
As(1)-S(2A)-C(14A)#1	93.1(3)

[*anti*-$As_2\mathbf{2}_2Cl_2$·benzene]	
As(1)-S(1)	2.204(3)
As(1)-S(2)	2.213(3)
As(1)-Cl(1)	2.244(4)
S(1)-As(1)-S(2)	87.52(1)
S(1)-As(1)-Cl(1)	102.69(2)
S(2)-As(1)-Cl(1)	98.77(2)
C(1)-S(1)-As(1)	102.9(4)
C(16)#2-S(2)-As(1)	99.5(4)

Symmetry Codes: #1-x+2, -y+2, -z+2; #2-x, -y+1, -z; -x, -y, -z+2. Disordered atoms in the second positions are indicated with the symbol A.

anti-$As_2\mathbf{2}_2Cl_2$

4,4'-Bis(mercaptomethyl)-*trans*-stilbene ($H_2\mathbf{2}$) is longer than $H_2\mathbf{1}$ and was designed to form macrocycles with even *taller* cavities. $As_2\mathbf{2}_2Cl_2$ was prepared by mixing $H_2\mathbf{2}$ with $AsCl_3$ in CH_2Cl_2. X-ray quality crystals of [*anti*-$As_2\mathbf{2}_2Cl_2$·benzene] were obtained by the slow diffusion of benzene layered on top of a CH_2Cl_2 solution of macrocycle.[c] The crystal structure reveals the presence of intramolecular As-π interactions as evidenced by short As-C_{aryl} contacts, the shortest of which is 3.23 Å (Figure 2a). A slight bowing of the stilbene ligands is observed, allowing guest inclusion. No unusual bond angles are observed (Table 2) suggesting that there is not much strain imposed on the macrocycle by the guest molecules. One benzene molecule per macrocycle is present, but is shared with a neighboring macrocycle, so that each macrocycle partially hosts two guests and each guest is partially encapsulated by two macrocycles (Figure 2c). Alternating macrocycles and benzene molecules form infinite chains of π-π stacked host-guest assemblies (Figure 2b).

---

[c] Crystals were not obtained when an aromatic solvent molecule was not present. The crystals grown from benzene were of X-ray quality, but those obtained from toluene, mesitylene, and *p*-xylene were not. The following solvents were not appropriately sized to serve as guests: CH_2Cl_2, $CHCl_3$, THF, DCE, TCE.

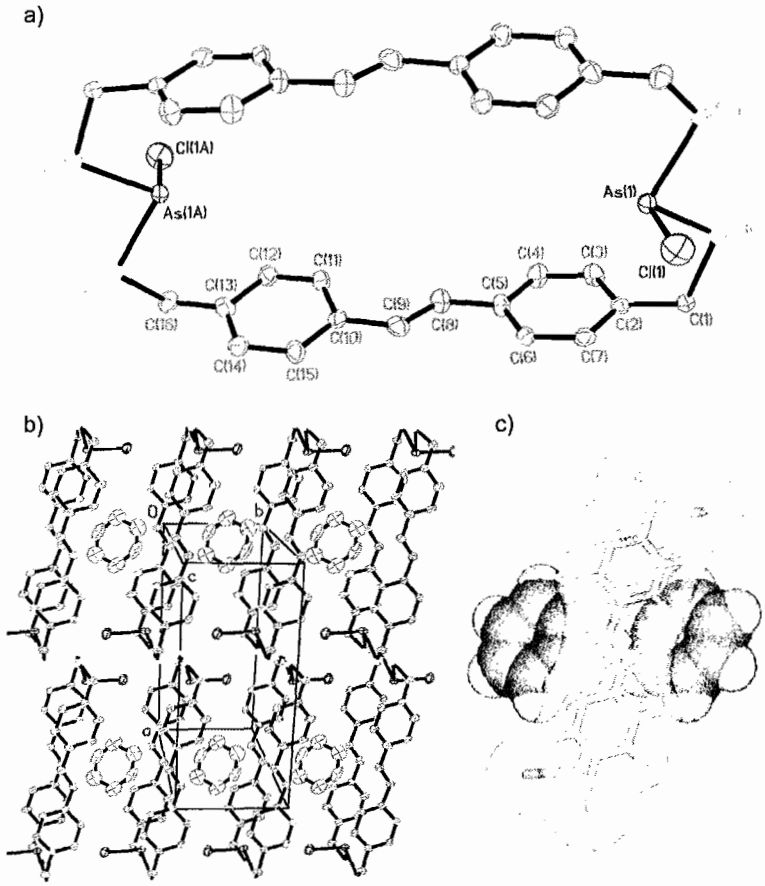

Figure 2. ORTEP (30% probability ellipsoids) representations of single-crystal X-ray structure of *anti*-$As_2\mathbf{2}_2Cl_2$ (a) and the packing diagram of [*anti*-$As_2\mathbf{2}_2Cl_2$·benzene] along the macrocyclic axis (b). Space-filling representation of single-crystal X-ray structure of the [*anti*-$As_2\mathbf{2}_2Cl_2$·benzene] inclusion complex (c).

$As_2\mathbf{3}_2Cl_2$

1,4-Dimethoxy-2,5-bis(mercaptomethyl)benzene ($H_2\mathbf{3}$) was designed to be used in the preparation of macrocycles that are *wide* but not *tall*. The methoxy groups on this ligand expand the macrocyclic cavity. $As_2\mathbf{3}_2Cl_2$ was prepared by mixing $H_2\mathbf{3}$ with $AsCl_3$ in chloroform, benzene, toluene, or *p*-xylene. The solvent used for crystallization

becomes the guest in the inclusion complex and dictates whether *anti*-$As_2\mathbf{3}_2Cl_2$, [(*syn*-$As_2\mathbf{3}_2Cl_2)_2$·guest], or [(*syn*-$As_2\mathbf{3}_2Cl_2$)(*anti*-$As_2\mathbf{3}_2Cl_2$)·guest] crystallizes.[d]

[($As_2\mathbf{3}_2Cl_2)_2$·Guest] Dimers

If $As_2\mathbf{3}_2Cl_2$ is crystallized from *p*-xylene a [(*syn*-$As_2\mathbf{3}_2Cl_2)_2$·*p*-xylene] inclusion complex is observed (Figure 3). In this structure, the organic ligand backbones are at a slight angle (31.5°) to each other resulting in an opening of one side of the macrocycle and a closing of the other. The chlorine ligands of *syn*-$As_2\mathbf{3}_2Cl_2$ are directed toward the sterically hindered closed end of the macrocycle, which defines the tapered end of a bowl-shaped structure. The open ends of two adjacent macrocycles are sandwiched together to form a cavity with an interior volume of ca. 216 $Å^3$.[e,22] Within each macrocycle, the two organic ligands can be eclipsed (methoxy groups on both ligands aligned) or staggered, and both species exist within the crystal structure (the disorder was modeled showing 73% of the eclipsed structure is present). For ease of viewing, only the eclipsed structures are shown.

If $As_2\mathbf{3}_2Cl_2$ is crystallized from toluene a mixture of homo- and hetero-dimers forms: [(*syn*-$As_2\mathbf{3}_2Cl_2)_2$·toluene] and [(*syn*-$As_2\mathbf{3}_2Cl_2$)(*anti*-$As_2\mathbf{3}_2Cl_2$)·toluene]. The

---

[d] The following molecules were screened as guests, but were not found to drive dimer formation: *p*-dimethoxybenzene, hydroquinone, *p*-benzenedimethanol, *p*-xylenediamine, phenol, bromobenzene, iodobenzene, mesitylene, 1,2,3-trimethylbenzene, cyclohexane, 1,4-cyanobenzene, and *m*-xylene. In each case, either the *anti*-$As_2\mathbf{3}_2Cl_2$ macrocycle or nothing crystallized from solution. Crystallization from *o*-xylene resulted in an [($As_2\mathbf{3}_2Cl_2)_2$·*o*-xylene] dimer that was highly disordered in the solid state.

[e] Cavities were measured using solvent (1.4 Å) surfaces. The cavity volume was estimated as the difference between the volume of the [(*syn*-$As_2\mathbf{3}_2Cl_2)_2$·*p*-xylene] host-guest complex and the volume of the *p*-xylene guest. By this calculation, *p*-xylene fills 46% of the cavity.

structure of these dimers is very similar to that of the [(*syn*-As_2**3**$_2Cl_2)_2$·*p*-xylene] dimer with a 29.9° angle between the organic ligand backbones and an interior volume of ca. 184 Å^3.[f,22] With the decrease in symmetry in the guest molecules from *p*-xylene to toluene comes a decrease in the symmetry of the dimer. While [(*syn*-As_2**3**$_2Cl_2)_2$·*p*-xylene] is disordered only in the orientation of the methoxy groups and the position of a As-Cl fragment, the toluene-containing dimer contains a mixture of *syn* and *anti* macrocycles, disordered methoxy groups, and a disordered toluene guest (see Experimental section for details on the modelling of the disorder).

Guest inclusion in the dimer can be accomplished without destroying the strong As-π interaction. The shortest As-C_{aryl} contact (3.26 Å and 3.22 Å for toluene and *p*-xylene guests respectively) is significantly less than the sum of the van der Waals radii for arsenic (2.0 Å) and a phenyl carbon (1.7 Å). The As-As distances (4.83 and 4.86 Å for toluene guest and 4.89 and 4.74 Å for *p*-xylene guest) within each macrocycle of the dimer are significantly longer than the As-As distance in the *anti*-macrocycle (see below), showing that the macrocycle is sufficiently flexible to accommodate guest molecules. The guest molecules are oriented in the cavity to best fill the space with the methyl groups on each guest pointing into the cavity of one or both components of the dimer (Figure 3b,d). There are no obvious π-π or CH-π interactions between the host and guest molecules – only van der Waals interactions.

---

[f] Cavities were measured using solvent (1.4 Å) surfaces. The cavity volume was again estimated as the difference between the volume of the [(*syn*-As_2**3**$_2Cl_2)_2$·toluene] complex and the volume of toluene. By this calculation, toluene fills 45% of the cavity.

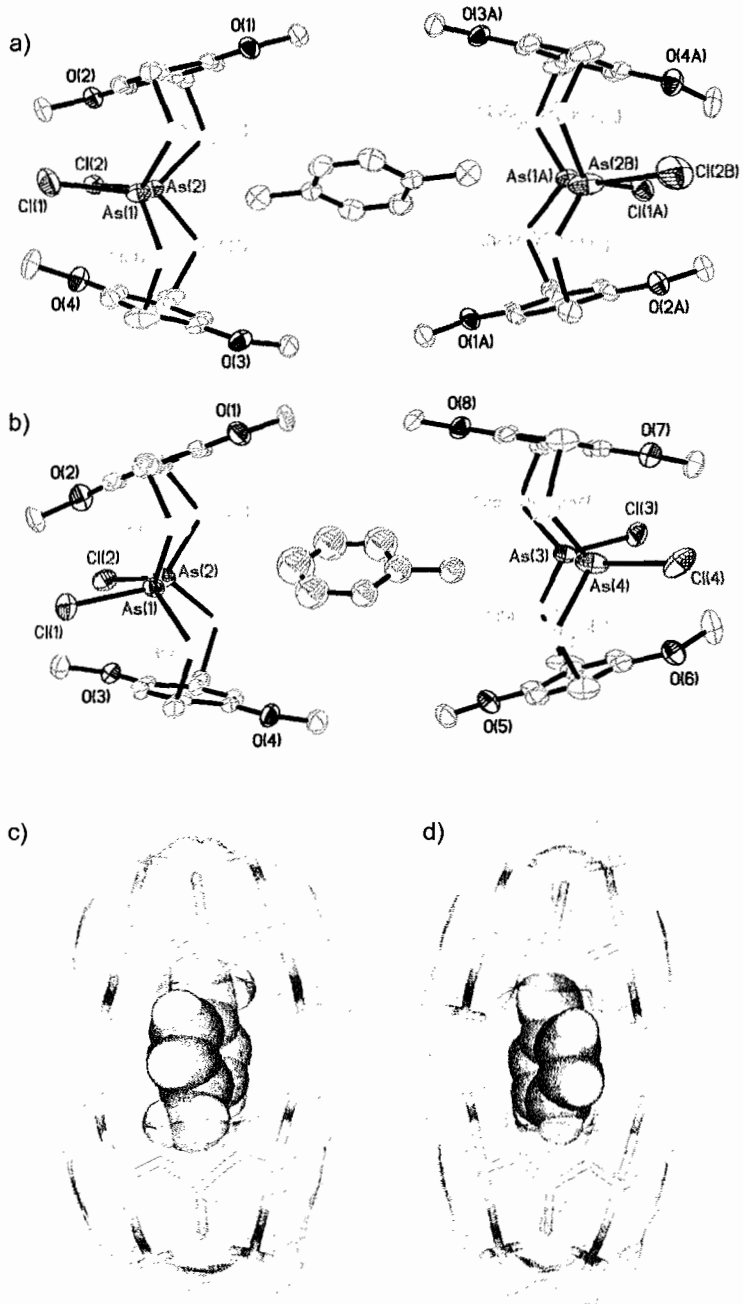

Figure 3. ORTEP (30% probability ellipsoids) and space-filling representations of the single-crystal X-ray structure of [(*syn*-$As_2\mathbf{3}_2Cl_2)_2$·*p*-xylene] (a,c) and [(*syn*-$As_2\mathbf{3}_2Cl_2)_2$·toluene] (b,d) inclusion complexes. Only one position for disordered groups is shown for clarity.

*anti-As_2**3**$_2Cl_2$*

If appropriately-sized guest molecules are not present during the crystallization process, *anti*-As_2**3**$_2Cl_2$ crystallizes exclusively. *anti*-As_2**3**$_2Cl_2$ is observed when crystals are grown from chloroform or benzene, both of which are apparently too small or of the wrong shape to satisfactorily fill the cavity of the (As_2**3**$_2Cl_2)_2$ dimer. In the *anti*-As_2**3**$_2Cl_2$ solid-state structure (Figure 4a), the two organic ligands that make up the macrocycle are parallel and the methoxy groups of each ligand are aligned. The chlorine ligands on each arsenic atom are directed away from the sterically bulky methoxy groups. The expanded cavity is filled by the methoxy groups of neighboring macrocycles and face-to-face π-π stacking occurs between neighboring macrocycles (C_{aryl}-C_{aryl} distance of 3.56 Å) (Figure 4b-c).

In this structure, the As-π interaction is completely unaffected by guest molecules as none are present. The As-C_{aryl} distance of 3.11 Å for *anti*-As_2**3**$_2Cl_2$ is the shortest contact for any $As_2L_2Cl_2$ macrocycle that has been reported to date.[15,17] This As-π interaction is shorter, and presumably stronger, than those previously observed because the aryl rings in this system are more electron rich due to the electron donating methoxy substituents.

Structural Trends in $As_2L_2Cl_2$ Macrocycles

Analysis of the five crystal structures obtained for As_2**1**$_2Cl_2$, As_2**2**$_2Cl_2$, and As_2**3**$_2Cl_2$ gives insight into the ability of these macrocycles to host guest molecules. Each macrocycle is too small to completely encapsulate a guest molecule, but is large enough

to partially host one while maintaining As-π interactions. $As_2\mathbf{2}_2Cl_2$ has a longer cavity than $As_2\mathbf{1}_2Cl_2$ and this difference in size is reflected in the number of solvent molecules that each can host. While $As_2\mathbf{1}_2Cl_2$ partially hosts one toluene molecule, each $As_2\mathbf{2}_2Cl_2$ macrocycle partially hosts two benzene molecules. In either case guest inclusion results in a slight bowing of the organic ligands. In the $As_2\mathbf{3}_2Cl_2$ macrocycle, the organic ligands do not deviate from planarity to accommodate a guest molecule, but rather the macrocycle walls tilt out of parallel allowing one end of the macrocyclic cavity to open up and a guest molecule to fill the void. In each case it is shown that guest inclusion dictates the structure—and in some cases drives diastereoselectivity in the self-assembly—of the macrocycle.

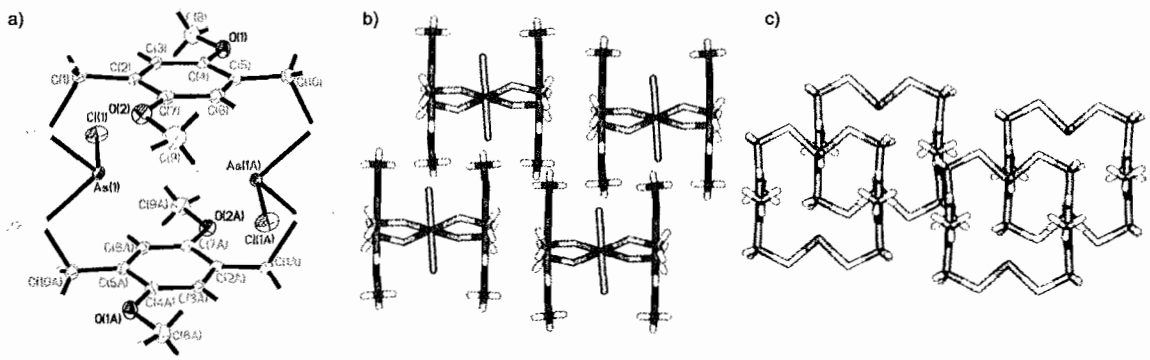

Figure 4. ORTEP (30% probability ellipsoids) representation of single-crystal X-ray structure of *anti*-$As_2\mathbf{3}_2Cl_2$ (a). Stick representation showing the packing of *anti*-$As_2\mathbf{3}_2Cl_2$ in the crystal structure from top (b) and side views (c).

Conclusion

In this paper, five new X-ray crystal structures were presented for three new $As_2L_2Cl_2$ macrocycles. In each example, appropriately sized aromatic solvent molecules fill the macrocyclic cavity. In the case of $As_2\mathbf{3}_2Cl_2$, choice of guest molecule allows stereocontrol over which diastereomer is crystallized. Larger guest molecules (toluene, *p*-xylene) are encapsulated by an $[(As_2\mathbf{3}_2Cl_2)_2\cdot guest]$ inclusion complex, while smaller guest molecules (chloroform, benzene) are too small to fill the dimer cavity forcing *anti*-$As_2\mathbf{3}_2Cl_2$ to crystallize exclusively. When the guest is *p*-xylene, the dimer consists of only *anti* macrocycles, and when the guest is toluene, the structure contains and mixture of *anti-anti* and *syn-anti* dimers. We have shown that larger dithiol ligands will predictably form expanded $As_2L_2Cl_2$ macrocycles with spacious cavities; even larger ligands are needed for complete encapsulation of a guest or the formation of kinetically stable inclusion complexes in solution. We will continue these studies by exploring the possibility of "threading" a guest molecule through the cavity of these macrocycle to make rotaxanes and synthetically linking macrocycles to give larger assemblies.

Experimental Section

General Procedures

^{1}H NMR spectra were measured using a Varian INOVA-300 spectrometer operating at 299.935 MHz. *J* values are given in Hz. Commercially available reagents were used as received. $H_2\mathbf{1}$[23] and $H_2\mathbf{3}$[24,25] were prepared following modified literature procedures. Complete transformation (>99% yield) of ligand and $AsCl_3$ to macrocycles is

revealed by ^{1}H NMR spectroscopy. Isolated single-crystal yields are reported. *Caution: Arsenic compounds are highly toxic and should be handled with care!*

Synthetic Procedures

4,4'-bis(mercaptomethyl)biphenyl ($H_2$1). Procedure is modified from that which was previously reported.[23] 4,4'-bis(chloromethyl)biphenyl (2.00 g, 7.96 mmol) was dissolved in solution of absolute ethanol (30 mL) and acetone (4 mL). Thiourea (1.31 g, 17.2 mmol) was added and the solution was heated to reflux for 3 hours. The off-white precipitate was filtered, washed with acetone, and dried under vacuum (3.01g, 7.46 mmol, 93%). A 3-neck round bottom flack was charged with this precipitate (1.04 g, 2.58 mmol), equipped with a stir bar and condenser, and placed under a N_2 atmosphere. Degassed 2 M NaOH (30 mL) was added via cannula and the mixture was heated to 80 °C for 4 hours. The cloudy solution was cooled to room temperature and degassed 4 M HCl (20 mL) was added via cannula. Precipitate formed as the acid was added and pH paper was used to verify that the solution was acidic (pH < 3). The reaction mixture was extracted with CH_2Cl_2 (3 × 20 mL) and the combined organics were dried over sodium sulfate and evaporated to dryness to yield a white powder (373 mg, 1.51 mmol, 59%). δ_H(300 MHz; $CDCl_3$; Me_4Si) 7.54 (d, 4 H, CH, *J* 4.5), 7.39 (d, 4 H, CH, *J* 7.8), 3.79 (d, 4 H, CH_2, *J* 7.5), 1.80 (t, 2 H, SH, *J* 7.5); δ_C(75 MHz; $CDCl_3$) 140.4, 139.7, 128.6, 127.5, 28.9, which matched the values reported in the literature.

$As_2$1$_2Cl_2$. $AsCl_3$ (4.0 μL, 0.047 mmol) was added to $H_2$1 (12.7 mg, 0.0475 mmol)

in toluene (4 mL). Gold-colored X-ray quality crystals[g] of the *anti* macrocycle were obtained after 5 days by the diffusion of hexanes into this solution at 4 °C (1.5 mg, 4.1 μmol, 17%). Dissolving the crystals yields a solution of both *syn* and *anti* macrocycles. δ_H(300 MHz; $CDCl_3$; Me_4Si) 7.13 (d, 8 H, CH, *J* 7.8), 7.04 (d, 8 H, CH, *J* 9.3), 4.24 (ABq, 4 H, CH_2, *J* 13), 4.23 (ABq, 4 H, CH_2, *J* 13).

4,4'-bis(mercaptomethyl)-*trans*-stilbene[h,26] ($H_2$2). 4,4'-bis(bromomethyl)-*trans*-stilbene[27,28] (903 mg, 2.69 mmol) was dissolved in solution of absolute ethanol (20 mL) and acetone (3 mL). Thiourea (613 mg, 8.06 mmol) was added and the solution was heated to reflux for 4 hours. The off-white precipitate was filtered, washed with acetone, and dried under vacuum (1.07 g, 2.07 mmol, 77%). A 3-neck round bottom flask was charged with this precipitate (200 mg, 386 mmol), equipped with a stir bar and condenser, and placed under a N_2 atmosphere. Degassed 2 M NaOH solution (30 mL) was added via a cannula, and the resulting mixture was heated to 80 °C for 4 hours. The cloudy solution was cooled to room temperature, and degassed 4 M HCl (20 mL) was added via a cannula. Precipitate formed as the acid was added and pH paper was used to verify that the solution was acidic (pH < 3). The reaction mixture was extracted with CH_2Cl_2 (3 × 20 mL) and the combined organics were dried over sodium sulfate and evaporated to dryness to yield a white powder (43.0 mg, 158 mmol, 41%). mp 156.4-158.1 °C; δ_H(300 MHz; $CDCl_3$; Me_4Si) 7.46 (d, 4 H, CH, *J* 8.1), 7.31 (d, 4 H, CH, *J* 8.1),

---

[g] CCDC reference number 676182.

[h] While use of this ligand has been reported previously,[26] no synthetic details or characterization data is available.

7.07 (s, 2 H, HC=CH), 3.74 (d, 4 H, CH_2, *J* 7.2), 1.76 (t, 2 H, SH, *J* 7.2); δ_C(75 MHz; $CDCl_3$) 140.7, 136.3, 128.6, 128.3, 127.0, 29.0; *m/z* (EI) 272 (58%, M^+), 239 (100, M - SH), and 206 (58, M – 2 × SH).

$As_2\mathbf{2}_2Cl_2$. $AsCl_3$ (4.0 μL, 0.047 mmol) was added to a solution of H_2**2** (12.7 mg, 0.0475 mmol) in CH_2Cl_2 (4 mL). Pale yellow X-ray quality crystals[i] were obtained after 5 days by layering of benzene on top of this CH_2Cl_2 solution at 4 °C (1.0 mg, 2.5 μmol, 12%). Dissolving the crystals yields a solution of both *syn* and *anti* macrocycles. δ_H(300 MHz; $CDCl_3$; Me_4Si) 7.07 (d, 8 H, CH, *J* 7.5), 7.01 (d, 8 H, CH, *J* 7.2), 6.97 (s, 4 H, HC=CH), 4.17 (ABq, 4 H, CH_2, *J* 13), 4.16 (ABq, 4 H, CH_2, *J* 13).

1,4-dimethoxy-2,5-bis(mercaptomethyl)benzene ($H_2$3). Procedure is modified from that which was previously reported.[30] 1,4-bis(methoxy)-2,5-bis(chloromethyl)benzene (251 mg, 1.07 mmol) and thiourea (275 mg, 3.62 mmol) were heated to reflux in acetone (40 mL) for 4 h. The solvent was evaporated to yield an off-white salt. The salt was transferred to a 3-neck round-bottom flask and placed under N_2. Degassed 2 M NaOH (50 mL) was transferred via cannula onto the salt and the solution was stirred under N_2 at 80 °C for 7 h. This solution was acidified using 6 M HCl under N_2, then extracted with CH_2Cl_2 (4 × 20 mL). The organic layer was washed with water (25 mL) and brine (25 mL) and the solvent was evaporated to yield a white solid (120 mg, 0.521 mmol, 49%). δ_H(300 MHz; $CDCl_3$; Me_4Si) 6.81 (s, 2 H, CH), 3.85 (s, 6 H, CH_3),

---

[i] CCDC reference number 676181.

3.71 (d, 4 H, CH_2, *J* 7.9), 1.96 (t, 2 H, SH, *J* 7.9), which matched the values reported in the literature.

$As_2\mathbf{3}_2Cl_2$. $AsCl_3$ (15.3 μL, 0.179 mmol) was added to a solution of $H_2\mathbf{3}$ (41.2 mg, 0.179 mmol) in *p*-xylene (10 mL) to yield a mixture of four macrocycle isomers. Colorless single crystals of [(*syn*-$As_2\mathbf{3}_2Cl_2)_2$·*p*-xylene][j] were grown by the slow diffusion of pentane into a *p*-xylene solution of $As_2\mathbf{3}_2Cl_2$ after 6 days (5.19 mg, 3.55 μmol, 7.9%). δ_H(300 MHz; $CDCl_3$; Me_4Si) 6.80 (m, 2 H, CH), 4.52 (m, 4 H, CH_2), 3.79 (m, 6 H, CH_3). Replacing *p*-xylene with toluene or chloroform as the solvent yielded [($As_2\mathbf{3}_2Cl_2)_2$·toluene][k] and *anti*-$As_2\mathbf{3}_2Cl_2$,[l] respectively.

Volume Calculations using GRASP[31]

The cavity volume of the [($As_2\mathbf{3}_2Cl_2)_2$·toluene] dimer was also calculated using the software package GRASP and found to be 164 $Å^3$. The large apertures in the plane of the sulfur atoms were "capped" for the calculation by the addition of a non-covalently bound anthracene units on each side. This "capping" is expected to cause the volume to be slightly underestimated.

---

[j] CCDC reference number 676184.

[k] CCDC reference number 676185.

[l] CCDC reference number 676183.

X-Ray Crystallography

All X-ray diffraction data were collected on a Bruker Smart Apex difractometer at 173 K using MoKα radiation ($\lambda = 0.71073$ Å). Absorption corrections were applied by SADABS.[29] Crystal structures were solved by direct methods. The crystal structure of [(*syn*-$As_2\mathbf{3}_2Cl_2)_2$·*p*-xylene] was determined to be in the monoclinic space group $P2_1/c$. Crystals of [$(As_2\mathbf{3}_2Cl_2)_2$·toluene] are also monoclinic with unit cells that are close to that of [(*syn*-$As_2\mathbf{3}_2Cl_2)_2$·*p*-xylene]. However, for the crystal structure of [$(As_2\mathbf{3}_2Cl_2)_2$·toluene] there are several hundred non-zero *hkl*-type reflections which are inconsistent with a *c* glide plane. Therefore, the structure was solved in space group $P2_1$. The collected data suggested that the crystal of [$(As_2\mathbf{3}_2Cl_2)_2$·toluene] was a racemic twin with a 30/70 ratio of the two phases. The disorder presumably arises from the mismatched symmetry of the macrocycle and the solvent guest molecules in [$(As_2\mathbf{3}_2Cl_2)_2$·toluene] and [(*syn*-$As_2\mathbf{3}_2Cl_2)_2$·*p*-xylene], the latter of which is centrosymmetric. Two of the four S_2AsCl fragments in [$(As_2\mathbf{3}_2Cl_2)_2$·toluene] are also disordered over two positions with opposite orientations of the As-Cl bonds. Thus in the structure there are two types of molecules with *syn* and *anti* configurations in 88:12 and 91:9 ratios for the two independent molecules. Toluene guest molecules in [$(As_2\mathbf{3}_2Cl_2)_2$·toluene] are disordered over two positions in a 50:50 ratio. One of two AsCl fragments in each macrocycle in [(*syn*-$As_2\mathbf{3}_2Cl_2)_2$·*p*-xylene] is also disordered over two positions. In contrast to [$(As_2\mathbf{3}_2Cl_2)_2$·toluene], all molecules in [(*syn*-$As_2\mathbf{3}_2Cl_2)_2$·*p*-xylene] have a *syn* configuration. The disorder of the AsCl group in [(*syn*-$As_2\mathbf{3}_2Cl_2)_2$·*p*-xylene] results from the two positions for the As atom, one above and one below the average plane of the

connected -$CH_2S\cdots SCH_2$- groups. The -OMe groups in [$(As_2\mathbf{3}_2Cl_2)_2$·toluene] and [(*syn*-$As_2\mathbf{3}_2Cl_2)_2$·*p*-xylene] are disordered over two positions corresponding to two opposite orientations for the benzene rings of the ligand, resulting in macrocycles that are eclipsed or staggered. The ratios of the occupancies for these two positions are 73:27 in [(*syn*-$As_2\mathbf{3}_2Cl_2)_2$·*p*-xylene] and 84:16 and 62:38 for the two symmetrically independent molecules in [$(As_2\mathbf{3}_2Cl_2)_2$·toluene]. In [*anti*-$As_2\mathbf{1}_2Cl_2$·toluene] both S_2AsCl fragments are disordered over two positions with opposite orientations of the As-Cl bonds in a ratio of 82/18. Non-H atoms in all structures were refined with anisotropic thermal parameters. H atoms in [$(As_2\mathbf{3}_2Cl_2)_2$·toluene], [(*syn*-$As_2\mathbf{3}_2Cl_2)_2$·*p*-xylene] and [*anti*-$As_2\mathbf{2}_2Cl_2$·benzene] were refined in calculated positions in a rigid group model. In [*anti*-$As_2\mathbf{3}_2Cl_2$] and [*anti*-$As_2\mathbf{1}_2Cl_2$·toluene] H atoms were found on the residual electron density map and refined with isotropic thermal parameters, except those at the CH_2 groups connected to the disordered fragments which were treated in calculated positions. Disordered fragments were refined with restrictions; standard distances of bonds were used in the refinement as targets for corresponding chemical bonds and atoms disordered in similar positions were refined with the same thermal parameters. All calculations were performed using the Bruker SHELXTL 6.10 package.[32]

Disorder in Crystal Structures

Disorder in the crystal structures is shown in Figure 5.

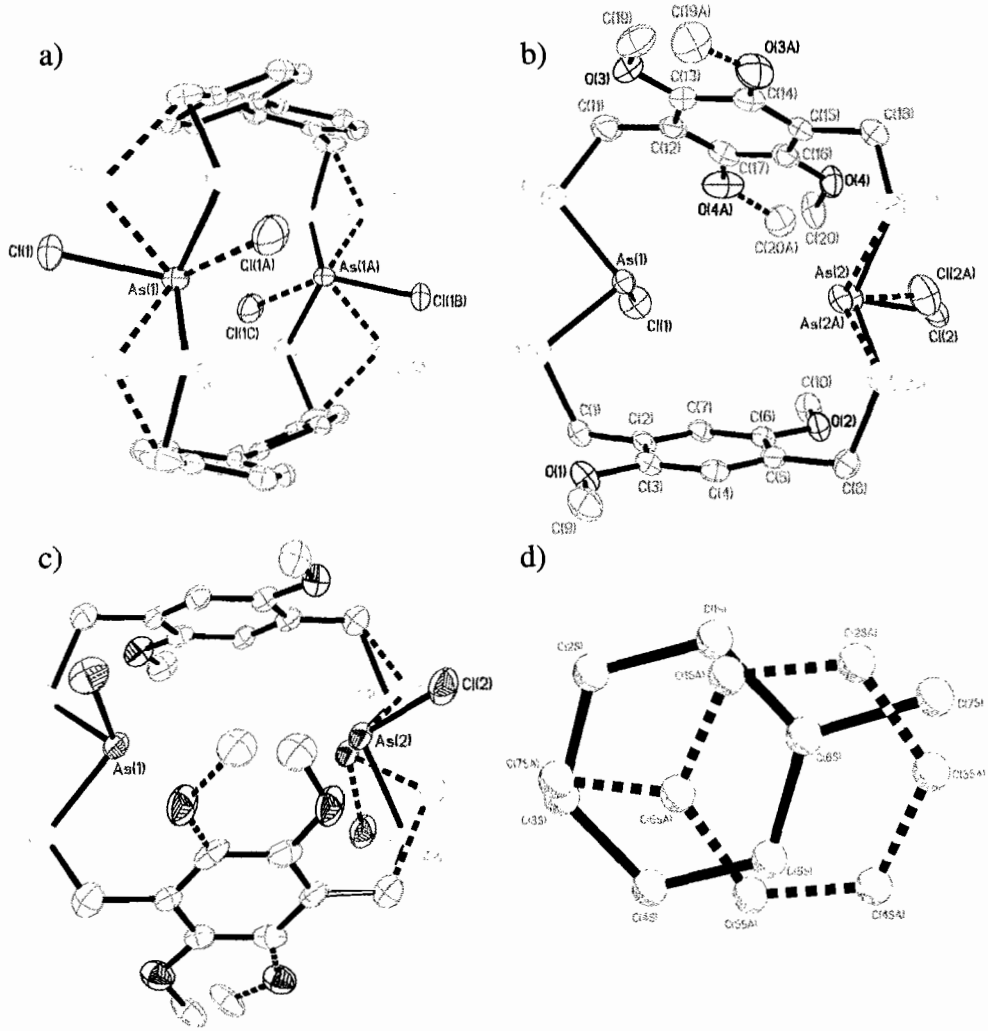

Figure 5. ORTEP (30% probability ellipsoids) representations of the disorder of the macrocycles in the X-ray crystal structures of $As_2\mathbf{1}_2Cl_2$ (a), $[(As_2\mathbf{3}_2Cl_2)_2 \cdot p\text{-xylene}]$ (b), and $[(As_2\mathbf{3}_2Cl_2)_2 \cdot \text{toluene}]$ (c). Ball and stick representation of the disorder of toluene in the X-ray crystal structure of $[(As_2\mathbf{3}_2Cl_2)_2 \cdot \text{toluene}]$ (d).

Measurement of Bend in Biphenyl Ligand

The bend of the biphenyl ligands in the X-ray crystal structure of $As_2\mathbf{1}_2Cl_2$ was compared to that of 4,4'-substituted biphenyl moieties in other molecules. To measure

this bend, the ligand was represented as a set of five lines, drawn between the following carbons: C1-C2, C2-C5, C5-C8, C8-C11, C11-C14. The angles formed at the intersections of these lines were measured using the Bruker SHELXTL 6.10 software.[32] A Cambridge Crystal Structure Database[21] search yielded 91 structures containing the 4,4'-substituted biphenyl moiety and the measurement procedure was repeated on a selection of similar structures. These measurements yielded angles similar to those found in $As_2\mathbf{1}_2Cl_2$.

Bridge to Chapter IV

Chapters II and III reported the synthesis and characterization of $As_2L_2Cl_2$ macrocycles in which the *syn*-to-*anti* ratio was controlled by steric bulk intra- or intermolecularly. The self-assembly of these macrocycles in the observed ratios is necessarily a dynamic process that involves the self-correction and reassembly of pieces to get to the thermodynamically stable product. In Chapter IV, this self-assembly process is monitored and analyzed using ^{1}H NMR spectroscopy, MALDI mass spectrometry, and X-ray diffraction. Several intermediates to the final product are observed and characterized, suggesting multiple pathways to the final product. Additionally, oligomeric "kinetic mistakes" are observed which are corrected during the self-assembly process.

CHAPTER IV

OBSERVATION OF REACTION INTERMEDIATES AND KINETIC MISTAKES IN A REMARKABLY SLOW SELF-ASSEMBLY REACTION

This chapter presents solution and solid-state evidence for several intermediates and oligomeric "mistakes" that form during the normal course of metal-ligand self-assembly. This co-authored work was previously published (*Chemical Communications*, **2009**, 5606-5608, © Royal Society of Chemistry).[1] MALDI mass spectrometry was carried out by Dr. Timothy G. Carter. Dr. Lev N. Zakharov performed all X-ray crystallography experiments. Professor Darren W. Johnson provided intellectual input and editorial assistance on the manuscript. I performed all synthesis, crystal growth, NMR studies, and wrote the manuscript.

Introduction

Self-assembly is the most efficient route to prepare discrete supramolecules,[2,3] but the complexity of the dynamic self-assembly process is still poorly understood.[4] It is generally accepted that this process involves the correction of misconnections and random oligomeric errors, quickly leading from kinetic intermediates to the discrete, thermodynamic product. Despite this widespread assumption, there exist only a few

examples of the observation of oligomeric errors ("kinetic mistakes") and in these cases they are not structurally characterized.[5] Additional examples involving the observation of self-assembly intermediates exist, but because most of these reactions between metals (M) and organic ligands (L) occur spontaneously and quickly, it is difficult to observe kinetic intermediates that form prior to the final thermodynamic product.[6] Intermediates have been observed during the titration of one component (M or L) into the other, but this approach is limited in that only the *equilibrium* product of each titration is observed in solution.[7,8] Rarely are kinetic intermediates stable enough to isolate from solution.[8,9]

Since the speed by which self-assembly reactions occur precludes the observation of intermediates and kinetic mistakes, slowing down the process could allow a better understanding of metal-directed assembly. This may ultimately lead to the ability to incorporate design features and specific properties into supramolecular assemblies with greater predictability. Paradoxically, for the self-assembly of discrete species to occur in a reasonable amount of time, fast kinetics are required in the forming and breaking of individual supramolecular interactions (typically either labile metal-ligand bonds or H-bonds). In this chapter, we describe the relatively slow self-assembly of M_2L_2 supramolecular macrocycles. This reaction occurs over the course of several days which allows for the observation and identification of several intermediate species and kinetic mistakes along the pathway to macrocycle formation.

Results and Discussion

A mixture of *syn* and *anti*-$As_2L_2Cl_2$ macrocycles form in solution over the course of several days (Scheme 1) when rigid dithiol ligands $H_2\mathbf{L}^{a}$,[10] $H_2\mathbf{L}^{b}$ and $H_2\mathbf{L}^{c}$[11] are individually treated with arsenic trichloride. X-ray quality crystals of *syn*-$As_2\mathbf{L}^{b}{}_2Cl_2$ were grown by diffusion of pentane into a solution of $As_2\mathbf{L}^{b}{}_2Cl_2$ in chloroform. The crystal structure (Figure 1a,b) reveals an As-As distance of 4.45 Å and a distance of 4.26 to 7.45 Å between the methyl carbons on opposite ligands, leaving a small cavity that is devoid of a guest.

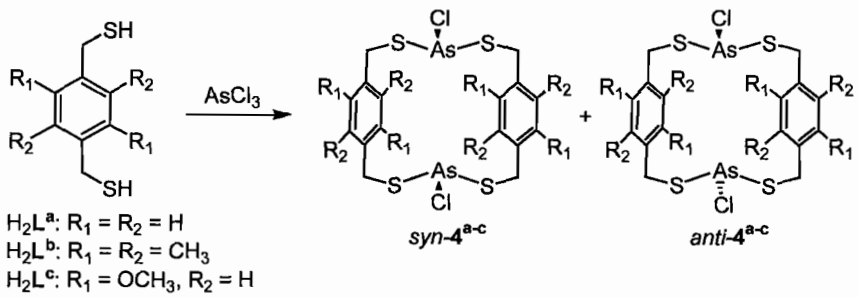

Scheme 1. Ligands and $As_2L_2Cl_2$ macrocycles. Both chlorine atoms are on the same side of the macrocyclic cavity in the *syn* macrocycle and on opposite sides in the *anti* macrocycle.

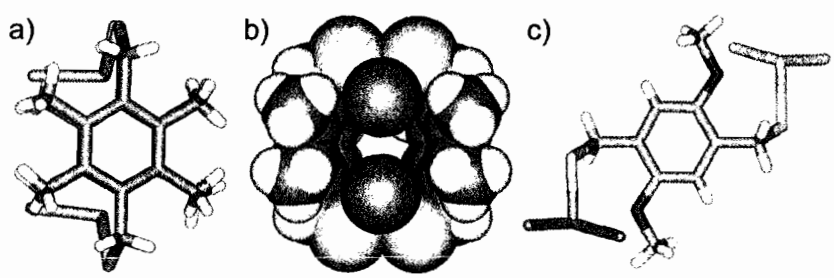

Figure 1. X-ray crystal structure representations of $As_2(\mathbf{L}^{a})_2Cl_2$ (stick) (a), $As_2(\mathbf{L}^{b})_2Cl_2$ (van der Waals radii) (b), and $As_2\mathbf{L}^{c}Cl_4$ (stick) (c).

When $As_2\mathbf{L}^{a}{}_2Cl_2$ ($\mathbf{4}^{a}$) and $As_2\mathbf{L}^{b}{}_2Cl_2$ ($\mathbf{4}^{b}$) are prepared in *d*-chloroform, the reaction progress can be monitored by observing the changes to the methylene region of the ^{1}H NMR spectrum (Figure 2 for $\mathbf{4}^{a}$ and Appendix A for $\mathbf{4}^{b}$). In each case, as H_2L is consumed, its resonances are replaced with those corresponding to several different reaction intermediates. These, in turn, are replaced with the resonances for **4**, the fully formed macrocycles. While several of the methylene region resonances overlap, it was possible to identify three of these intermediate species by symmetry. The first species observed upon treatment of H_2L with $AsCl_3$ is $HL(AsCl_2)$ (**1**), which appears as a doublet for the unbound ($C\mathbf{H}_2SH$) end and a singlet for the bound ($C\mathbf{H}_2S(AsCl_2)$) end. The next observed species is HL(AsCl)LH (**2**) which appears as an ABq for the bound (($C\mathbf{H}_2S)_2AsCl$) end and a doublet for the unbound ($C\mathbf{H}_2SH$) end, which is coincidental with the resonance for H_2L or **1**. The third species that can be identified by ^{1}H NMR is $L(AsCl_2)_2$ (**3**), which appears downfield as a singlet since the ligand symmetrically spans two As centers.

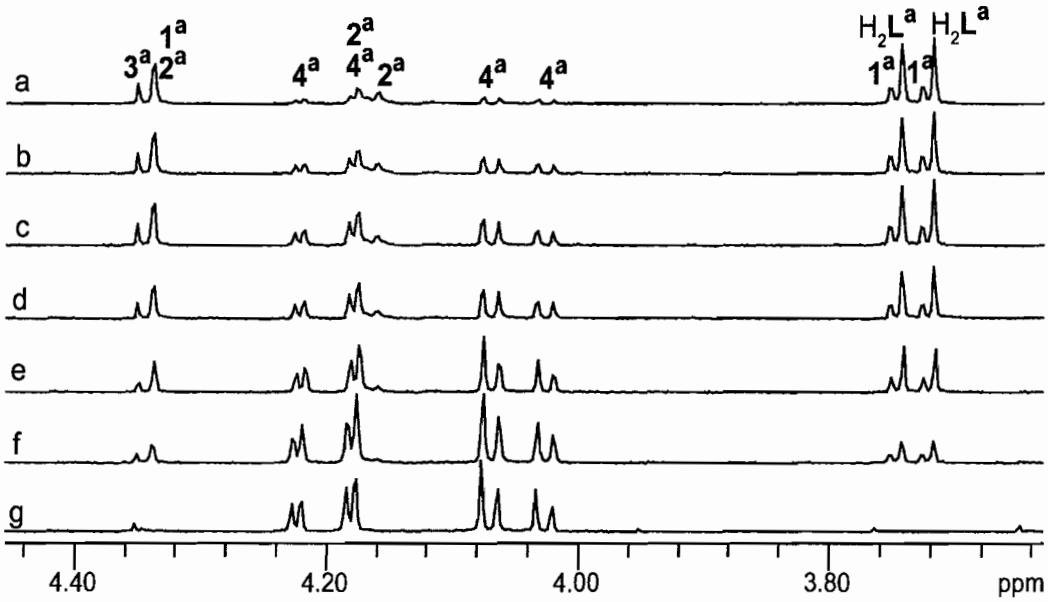

Figure 2. CH_2 region of ^1H NMR spectra of reaction of $H_2\mathbf{L}^a$ with $AsCl_3$ after 35 (a), 81 (b), 122 (c), 186 (d), 366 (e), 1378 (f), and 5650 (g) minutes. Structures of $\mathbf{1}^a$-$\mathbf{4}^a$ are shown in Scheme 2.

The identities of $\mathbf{1}^b$ – $\mathbf{4}^b$ were also confirmed by MALDI-MS ([$\mathbf{1}^b$+Na+2H]$^+$, 394.9, calc 394.9; [$\mathbf{2}^b$+Na+4H]$^+$, 587.0, calc 587.1; [$\mathbf{3}^b$+Na]$^+$, 536.8, calc 536.8; [$\mathbf{4}^b$+Na]$^+$, 690.9, calc 690.9), when $As_2L_2Cl_2$ was prepared from $H_2\mathbf{L}^b$. These species could either be intermediates or kinetic mistakes that are corrected in the self-assembly of $As_2L_2Cl_2$ (**4**). It is possible that the self-assembly reaction is occurring simultaneously through several competing pathways, as outlined in Scheme 2.[a,b]

---

[a] Unfortunately the slow kinetics and complexity of the reaction do not allow for the measurement of rate constants. EXSY NMR experiments were carried out on the reaction of $AsCl_3$ with a monofunctional model ligand (2-mercaptomethylnaphthalene) at 120 °C, but no ligand exchange was observed.

[b] **2** and **3** could be both intermediates and kinetic mistakes.

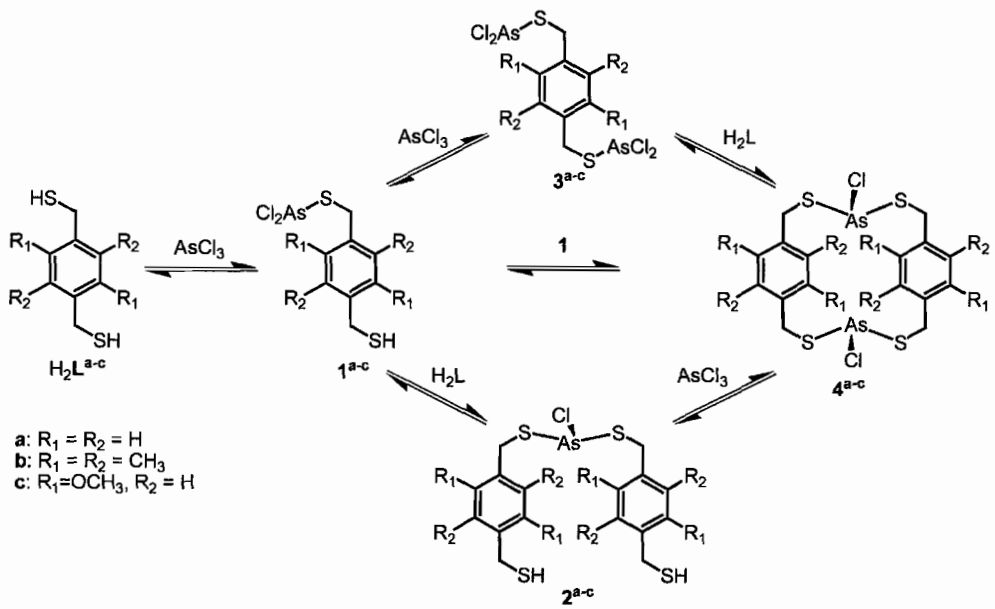

Scheme 2. Self-assembly of $As_2L_2Cl_2$.

While the overlapping resonances of H_2L, **1**, **2**, **3**, and $As_2L_2Cl_2$ (**4**) make it difficult to accurately integrate the NMR spectra, it is clear that at least one additional discrete species exists in solution,[c] likely a larger oligomeric kinetic mistake. These kinetic mistakes could easily form reversibly in the free-for-all chaos of the self-assembly reaction and then equilibrate to $As_2L_2Cl_2$. After 5 minutes, and under the same conditions as the NMR experiments, several oligomeric species (Chart 1) were identified by MALDI-MS ([$\mathbf{5}^{\mathbf{b}}$+Na+2H]$^+$, 728.9, calc 728.9; [$\mathbf{6}^{\mathbf{b}}$+Na]$^+$, 870.7, calc 870.7; [$\mathbf{7}^{\mathbf{b}}$+Na+4H]$^+$, 921.0, calc 921.0; [$\mathbf{8}^{\mathbf{b}}$+Na+2H]$^+$, 1062.8, calc 1062.9; [$\mathbf{9}^{\mathbf{b}}$+Na]$^+$, 1206.7, calc 1204.7). After 30 minutes, they are no longer observed. These species could be

[c] The *ABqs* in the ^{1}H NMR corresponding to $\mathbf{2}^{\mathbf{a}}$ and $\mathbf{4}^{\mathbf{a}}$ overlap. However, before the signal for $\mathbf{4}^{\mathbf{a}}$ becomes prominent, the asymmetry of the signal is clear, suggesting an overlapping resonance. The signal for $\mathbf{2}^{\mathbf{b}}$ is clearly an *ABq* (see Appendix A).

expected to have ^{1}H NMR resonances that overlap with the other intermediates. We do not know for sure that every one of these oligomeric species is present in solution during the reaction, as they could be formed as a concentration effect upon evaporation of the MALDI sample, yet after 30 minutes they are no longer observed by MALDI. It is clear that some kinetic mistakes are corrected during the course of the reaction because everything remains soluble and all resonances except those for $As_2L_2Cl_2$ disappear eventually. These oligomeric species observed by MALDI MS are the most likely culprits.

The isolation of compounds **1-3** was unsuccessful until prepared with a ligand containing additional coordinating groups (methyl ether in $H_2\mathbf{L}^c$). While macrocycle was typically isolated by crystallization of the reaction mixture of $H_2\mathbf{L}^c$ and $AsCl_3$, one attempt led to the isolation of $\mathbf{3}^c$ (Figure 1c). The intermediate is stabilized by As···O secondary bonding interactions[12] and crystal packing is dictated by the As···π interaction.[13] This experiment further supports the idea that structure **3** is an intermediate or a kinetic mistake in the self-assembly of $As_2L_2Cl_2$.

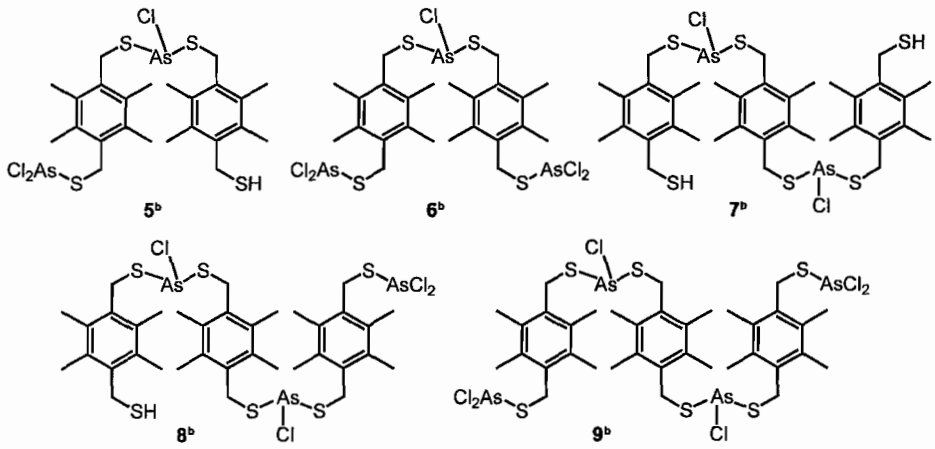

Chart 1. Oligomeric kinetic mistakes.

Conclusion

In conclusion, we have shown a metal-directed self-assembly reaction in which several intermediates and kinetic mistakes can be identified. This provides insight into the complexity of the self-assembly process—as revealed by the multiple possible pathways—even for a simple dinuclear species. While most self-assembly reactions occur too quickly to observe without stopped-flow kinetics, the dynamic covalent[14] nature of the As-S bond and the steric bulk of the ligands make this reaction slow enough to observe by ^{1}H NMR, providing exquisite structural detail. This shows that supramolecular chemistry based on main group elements not only leads to new structure types,[15] but also can add valuable insight into the nature of self-assembly, which could be applicable to understanding the formation of nanoparticles,[16] polymers[17] and monolayers[18] by self-assembly.

Experimental Section

General Procedures

Commercially available reagents were used as received. Literature procedures were followed to prepare $H_2\mathbf{L}^{a}$,[19] $H_2\mathbf{L}^{b}$,[20] and $H_2\mathbf{L}^{c}$.[11] *Caution: Arsenic compounds are hazardous and should be handled with caution!* ^{1}H NMR spectra were measured using a Varian INOVA-300 spectrometer. Spectra were referenced using the residual $CHCl_3$ solvent resonance as an internal standard.

Synthetic Procedures

$As_2\mathbf{L}^{a}{}_2Cl_2$ (4^{a}). 1,4-bis(mercaptomethyl)benzene ($H_2\mathbf{L}^{a}$, 16.1 mg, 94.9 μmol) was dissolved in 2.0 mL $CDCl_3$ in a scintillation vial. In a separate vial, $AsCl_3$ (94.8 μmol, 8.09 μL) was dissolved in 2.0 mL $CDCl_3$. The $AsCl_3$ solution was added to the solution containing ligand and mixed well (T = 0). An aliquot was transferred to an NMR tube and monitored by ^{1}H NMR.

$As_2\mathbf{L}^{b}{}_2Cl_2$ (4^{b}). 1,4-bis(mercaptomethyl)durene ($H_2\mathbf{L}^{b}$, 14.0 mg, 61.8 μmol) was dissolved in 4.0 mL $CDCl_3$ in a scintillation vial. $AsCl_3$ (61.8 μmol, 5.28 μL) was added and the solution was mixed well (T = 0). An aliquot was transferred to an NMR tube and monitored by ^{1}H NMR spectroscopy (see Appendix A for spectra). Colorless X-ray quality crystals were grown by the slow diffusion of pentane into a $CHCl_3$ solution of $As_2\mathbf{L}^{b}{}_2Cl_2$. Crystallographic Data: $C_{24}H_{32}As_2Cl_2S_4$, M = 669.48, 0.16 × 0.14 × 0.10 mm, T = 293 K, Triclinic, space group P-1, a = 8.4667(7) Å, b = 10.6932(9) Å, c = 17.0485(15) Å, α = 87.852(2)°, β = 77.066(2)°, γ = 68.0790(10)°, V = 1393.8(2) Å^3, Z =

2, D_c = 1.595 Mg/m^3, μ = 2.901 mm^{-1}, F(000) = 680, $2\theta_{max}$ = 27.00°, 15620 reflections (-10 ≤ h ≤ 10, -13 ≤ k ≤ 13, -21 ≤ l ≤ 21), 6027 independent reflections [R_{int} = 0.0306], R_1 = 0.0624, wR_2 = 0.1638 and GOF = 1.033 for 6027 reflections (298 parameters) with $I > 2\sigma(I)$, R_1 = 0.0945, wR_2 = 0.1892 and GOF = 1.033 for all reflections, max/min residual electron density +1.741/-0.704 eÅ^3, CCDC: 741267.

$As_2L^cCl_4$ (3^c). $AsCl_3$ (3.44 μL, 0.0404 mmol) was added slowly to a solution of 2,5-bis(mercaptomethyl)-1,4-dimethoxybenzene (H_2L^c) (9.30 mg, 0.0404 mmol) in $CHCl_3$ (4 mL) and mixed well. An aliquot of the solution was transferred into a vial and layered with pentane. Slow diffusion of pentane into this solution yielded colorless crystals after one week. Crystallographic Data: $C_{10}H_{12}As_2Cl_4O_2S$, M = 519.96, 0.27 × 0.22 × 0.14 mm, T = 173(2) K, monoclinic, space group $P2_1/c$, a = 8.1642(8) Å, b = 11.7354(12) Å, c = 9.2996(9) Å, γ = 106.451(2)°, V = 854.52(15) Å^3, Z = 2, D_c = 2.021 Mg/m^3, μ = 4.775 mm^{-1}, F(000) = 508, $2\theta_{max}$ = 28.19°, 9618 reflections (-10 ≤ h ≤ 10, -13 ≤ k ≤ 13, -21 ≤ l ≤ 21), 2030 independent reflections [R_{int} = 0.0194], R_1 = 0.0202, wR_2 = 0.0547 and GOF = 1.039 for 2030 reflections (115 parameters) with $I > 2\sigma(I)$, R_1 = 0.0212, wR_2 = 0.0554 and GOF = 1.039 for all reflections, max/min residual electron density +0.490/-0.222 eÅ^3, CCDC: 741266.

Mass Spectrometry Experiments

Laser Desorption Ionization experiments on H_2L^b with $AsCl_3$ were performed on a Waters Micromass Q-TOF MALDI mass spectrometer (Milford, MA USA) using V-

Optics in positive ionization mode. Samples were prepared by spotting NMR solutions ($CDCl_3$) containing the analyte directly onto the sample plate, without the use of a matrix, at various time intervals ranging from T = 0 to T = 2 hrs after the addition of $AsCl_3$. Initial spectra where nearly devoid of macrocycle $\mathbf{4}^{\mathbf{b}}$ and contained mostly $M_n\mathbf{L}_m$ species. After sampling at T = 30 minutes, macrocycle $\mathbf{4}^{\mathbf{b}}$ was the prominent species detected. Sodium adducts of the species of interest most likely resulted from the direct laser desorption technique. Additionally, multiply protonated thiols $(M+2H+Na)^+$ were observed for species containing single thiols while $(M+4H+Na)^+$ were observed for those containing two thiols.[21] Ligands capped with arsenic (no free thiols) flew as $(M+Na)^+$ and did not contain additional protons. See Appendix A for MALDI data.

X- Ray Crystallography

Diffraction intensities for $As_2\mathbf{L}^{\mathbf{c}}Cl_4$ were collected at 173 K on a Bruker Apex diffractometer using MoKα radiation λ= 0.71073 Å. Crystals of $As_2(\mathbf{L}^{\mathbf{b}})_2Cl_2$ crack at low temperatures, so X-ray diffraction data for this compound was collected at room temperature, 293 K. Space groups were determined based on systematic absences ($As_2\mathbf{L}^{\mathbf{c}}Cl_4$) and intensity statistics ($As_2(\mathbf{L}^{\mathbf{b}})_2Cl_2$). Absorption corrections were applied by SADABS. Structures were solved by direct methods and standard Fourier techniques and refined on F^2 using full matrix least-squares procedures. Non-H atoms were refined with anisotropic thermal parameters. H atoms in $As_2\mathbf{L}^{\mathbf{c}}Cl_4$ were found on the F-map and refined with isotropic thermal parameters. H atoms in $As_2(\mathbf{L}^{\mathbf{b}})_2Cl_2$ were refined in calculated positions in a rigid group model. All calculations were performed by the

Bruker SHELXTL package. Single crystal X-ray diffraction studies were performed on a Bruker SMART APEX diffractometer.

Bridge to Chapter V

In Chapter IV, the dynamic nature of the self-assembly process was examined for $As_2L_2Cl_2$ macrocycles. Chapter V involves the same theme of dynamic self-assembly, but focuses on a new reaction (transmetallation) and a new structure type (E_2L_3 cryptands). In Chapter V, a series of E_2L_3 (E = P, As, Sb, Bi) cryptands are presented and their structures are compared in the solid state and in solution. While Sb_2L_3 and Bi_2L_3 were prepared by self-assembly, As_2L_3 and P_2L_3 were prepared by a transmetallation reaction from Sb_2L_3. This is a rare example of transmetallation used in a supramolecular context and it allows for the preparation of a previously inaccessible structure type (P_2L_3).

CHAPTER V

"SUPRAMOLECULAR TRANSMETALLATION" LEADS TO AN UNUSUAL SELF-ASSEMBLED P_2L_3 CRYPTAND

This chapter presents a series of E_2L_3 (E = P, As, Sb, Bi) cryptands and the transmetallation reaction that allowed access to our first P-containing assembly. This co-authored work was previously published (*Angewandte Chemie, International Edition* **2010**, 1248-1251, ©WILEY-VCH Verlag GmbH & Co).[1] All X-ray crystallography was carried out by Dr. Lev N. Zakharov. Professor Darren W. Johnson provided intellectual and editorial contributions. I carried out all synthesis, crystal growth, NMR experiments, and wrote the manuscript.

Introduction

Transmetallation is common in biochemical,[2] inorganic[3] and organometallic synthesis,[4] but has been largely overlooked by supramolecular chemists as a synthetic technique for preparing discrete assemblies.[5] The self-assembly of complex, multi-component metal-organic supramolecules[6] occurs by the breaking and reforming of reversible metal-ligand bonds[7] and in some cases through dynamic covalent chemistry.[8] These dynamic bonds also allow for the reshuffling of components within "fully-formed"

complexes, as revealed by ligand exchange studies.[9] The introduction or removal of guest molecules can cause rearrangement to higher or lower-order structures, which also necessitates the breaking and reforming of bonds.[10] Transmetallation, which can occur upon the addition of a second type of metal, is a less common display of the dynamic nature of these assemblies.[9c,11,a] Here, we report a "transmetallation" reaction of an antimony-containing cryptand with arsenic and, remarkably, phosphorus to provide a previously unattainable P_2L_3 cryptand. In this reaction, P-S bonds behave reversibly like typical metal-ligand bonds within supramolecular assemblies suggesting a potentially new motif for dynamic covalent chemistry.

Results and Discussion

A rigid dithiol ligand, 1,4-bis(mercaptomethyl)naphthalene (H_2**L**),[12] was treated with a pnictogen trichloride (ECl_3, E = As, Sb, Bi) and base resulting in self-assembly to the corresponding cryptands, E_2**L**$_3$ (Scheme 1). While our group has previously prepared As-[13] and Sb[14]-containing cryptands by a similar synthetic route, this is one of the first known examples of a Bi-containing supramolecular complex.[15] X-ray quality crystals were grown by layering chloroform solutions of each cryptand with acetonitrile (Figure 1). The structure of each cryptand is very similar, with apparent C_{3h} symmetry and only slight variations in ligand position. In each case, the pnictogen atoms are positioned

---

[a] The term "transmetallation" is typically used in an organometallic context, but references 9c and 11d refer to metal-exchange processes in metal-ligand complexes as transmetallation reactions.

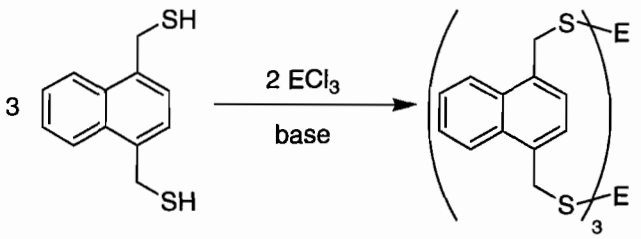

Scheme 1. The self-assembly of E_2L_3 (E = As, Sb, Bi) cryptands.

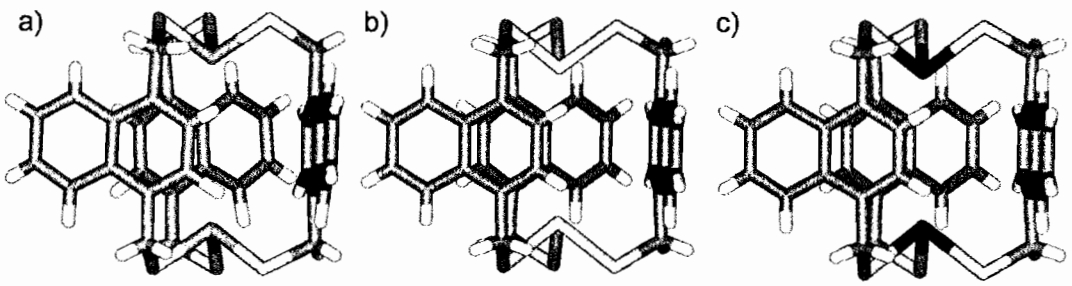

Figure 1. Stick representations of X-ray crystal structures of As_2L_3 (a), Sb_2L_3 (b), and Bi_2L_3 (c). Arsenic atoms are shown in purple, antimony in teal, bismuth in blue, sulfur in yellow, carbon in gray and hydrogen in white.

within the cavity, with the lone pairs of electrons on the two atoms pointing toward each other. The E···E distance decreases from As_2L_3 (5.11 Å) to Sb_2L_3 (4.83 Å) to Bi_2L_3 (4.68 Å), and the difference is compensated for in the increasing E-S bond distances and S-E-S angles. In each case, the pnictogen atoms are also involved in attractive E···π interactions,[16] as evidenced by E···C_{aryl} contacts of less than the sum of the van der Waals

radii.[b] In solution, these cryptands display similar, but distinct, ^{1}H NMR resonances with splitting (*ABq* for the methylene protons) which suggests that the ligands are "locked" into place as they are seen in the crystal structure, rather than flipping back and forth quickly (Figure 2).

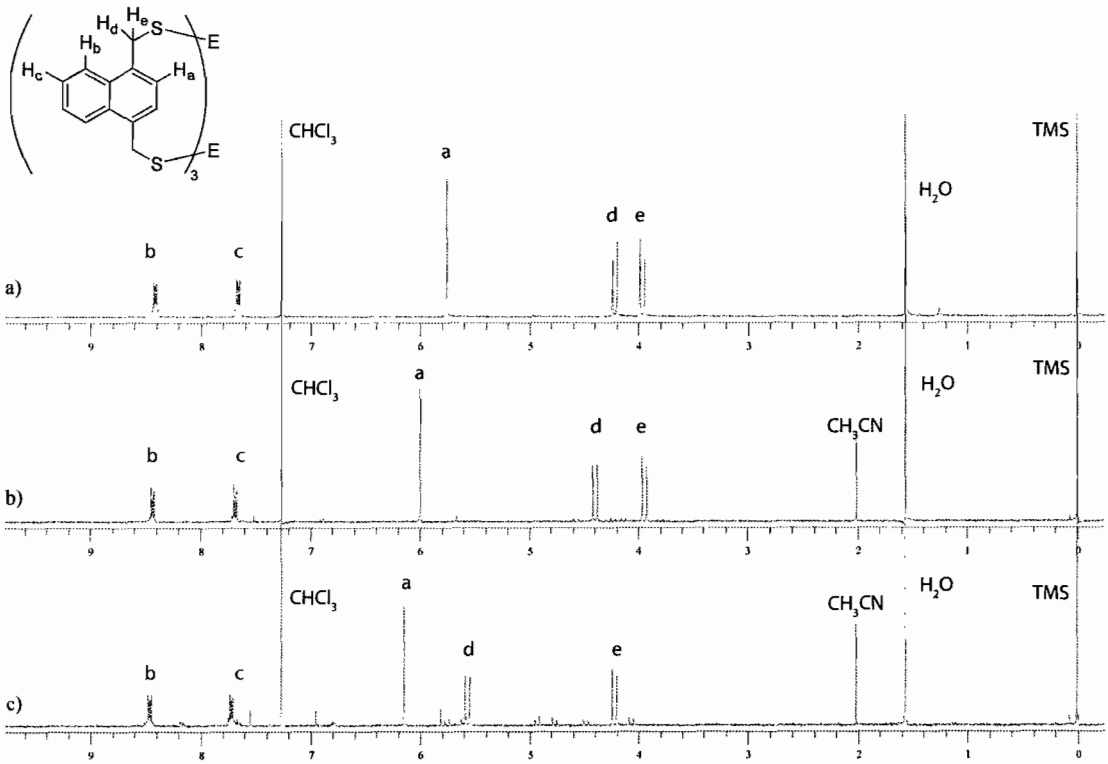

Figure 2. ^{1}H NMR spectra in $CDCl_3$ for $As_2\mathbf{L}_3$ (a), $Sb_2\mathbf{L}_3$ (b), and $Bi_2\mathbf{L}_3$ (c) taken on 300 MHz spectrometer with TMS as an internal reference.

[b] The two closest E···C_{aryl} contacts are 3.30 and 3.58 Å for As, 3.34 and 3.58 Å for Sb, and 3.36 and 3.55 Å for Bi.

To compare the stability of the complexes, transmetallation reactions were carried out and monitored by ^{1}H NMR spectroscopy. Crystals of $Sb_2\mathbf{L}_3$ were dissolved in $CDCl_3$ and two equivalents of $AsCl_3$ were added (Scheme 2). Within 30 minutes, all the $Sb_2\mathbf{L}_3$ was consumed and a white solid precipitated out of solution which was likely a coordination polymer incorporating both Sb and As. NMR spectroscopy identified two of the initial soluble reaction products (Figure 3). The first is the previously reported $As_2\mathbf{L}_2Cl_2$ macrocycle,[12] which is converted to $As_2\mathbf{L}_3$ as the precipitate redissolves and more ligand becomes available for reaction. This suggests that $As_2\mathbf{L}_2Cl_2$ is an intermediate in the self-assembly of $As_2\mathbf{L}_3$. The second species, a heterometallic $AsSb\mathbf{L}_3$ cryptand,[c] is relatively short lived as the Sb atom is quickly replaced with As. After five days, the only species left in solution are $As_2\mathbf{L}_3$ and trace $As_2\mathbf{L}_2Cl_2$.

Similarly, $Bi_2\mathbf{L}_3$ was treated with $AsCl_3$ and $SbCl_3$. In each case, a reaction occurred immediately resulting in a white precipitate. Over time, $As_2\mathbf{L}_2Cl_2$ and $Sb_2\mathbf{L}_2Cl_2$ were formed and identified by NMR spectroscopy, but the precipitate never completely

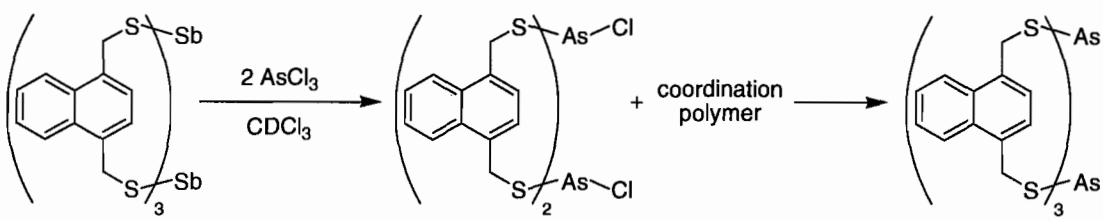

Scheme 2. Transmetallation of $Sb_2\mathbf{L}_3$ to $As_2\mathbf{L}_3$.

[c] A procedure for preparing heterometallic $AsSb\mathbf{L}_3$ independently is reported in Chapter VI.

redissolved and the reaction was not driven to completion as in the case of $Sb_2\mathbf{L}_3$ → $As_2\mathbf{L}_3$. A control reaction was carried out in which an excess of $SbCl_3$ was added to $As_2\mathbf{L}_3$, but no reaction occurred even after several days at elevated temperatures. Given that self-assembly reactions such as these are typically under thermodynamic

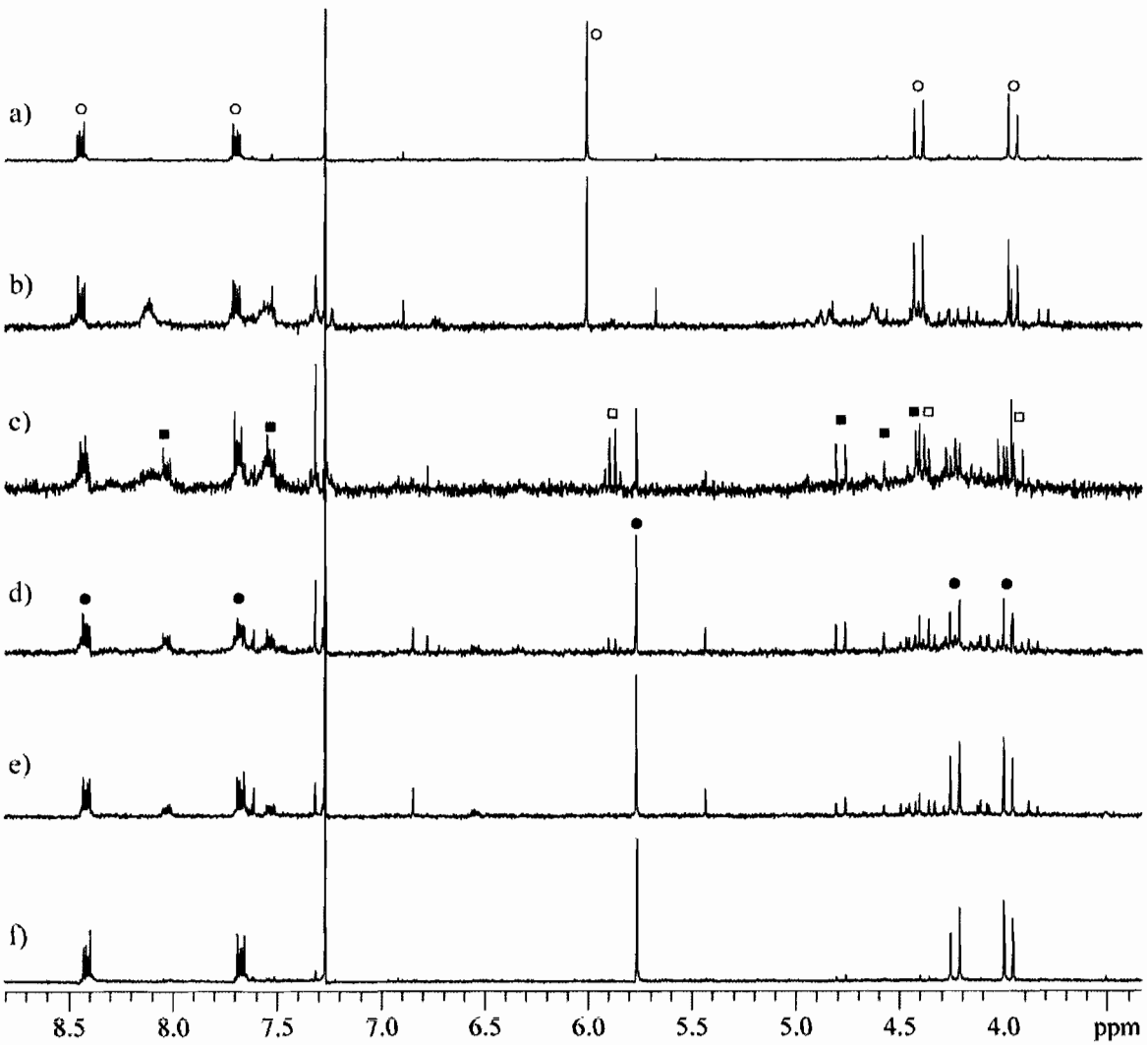

Figure 3. ^{1}H NMR spectra for the reaction of $Sb_2\mathbf{L}_3$ (a) with $AsCl_3$ after 10 min (b), 32 min (c), 1 hr 25 min (d), 7 hr (e), and 5 days (f). $Sb_2\mathbf{L}_3$ is marked ○, $AsSb\mathbf{L}_3$ □, $As_2\mathbf{L}_2Cl_2$ ■, and $As_2\mathbf{L}_3$ ●.

control, it seems that $As_2\mathbf{L}_3$ is more stable than $Sb_2\mathbf{L}_3$ which is more stable than $Bi_2\mathbf{L}_3$. While the energies of E(III)-S bonds have not been reported, they are likely the driving force for this transmetallation. The presumed byproduct of transmetallation is ECl_3 (where E is the metal that was removed) and E(III)-Cl bonds decrease in strength moving from As-Cl to Sb-Cl to Bi-Cl.[17]

The success of this transmetallation reaction led us to believe that this route might allow access to P-containing supramolecular complexes, which we have been unable to prepare by any other route. $Sb_2\mathbf{L}_3$ was dissolved in $CDCl_3$, PBr_3 was added to the NMR tube, and a white solid precipitated out of solution. While this precipitate did not completely redissolve, several new resonances appeared in the ^1H NMR spectrum after

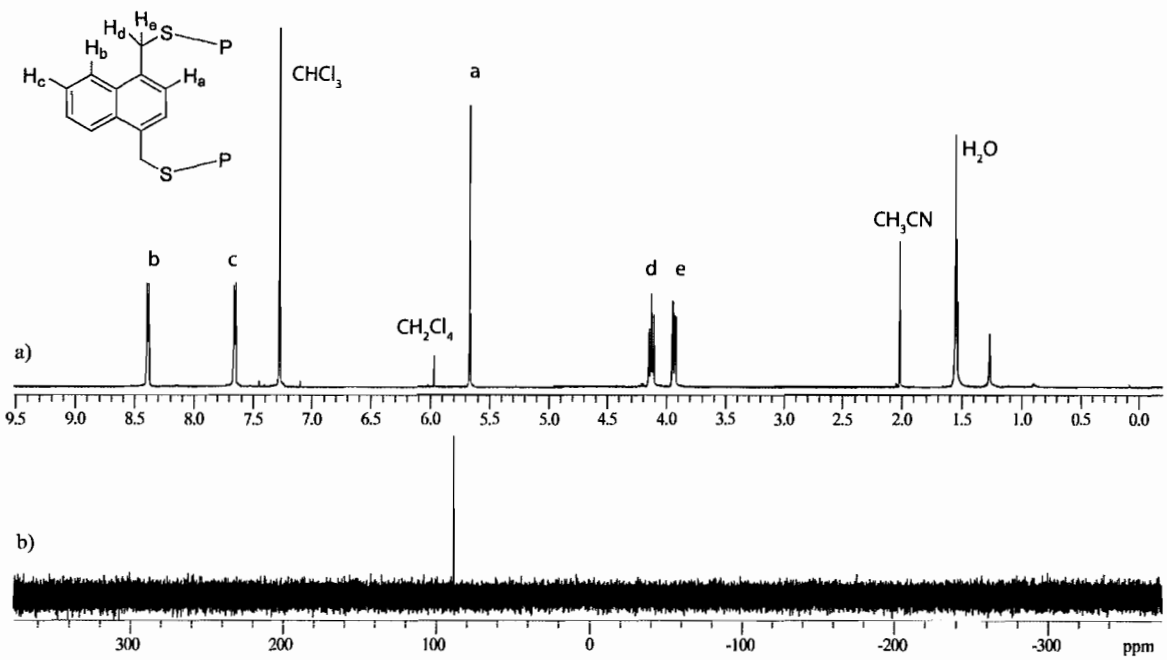

Figure 4. ^1H (a) and ^{31}P (b) NMR spectra of $P_2\mathbf{L}_3$ in $CDCl_3$ taken on 600 MHz spectrometer and referenced to $CHCl_3$ and external H_3PO_4, respectively.

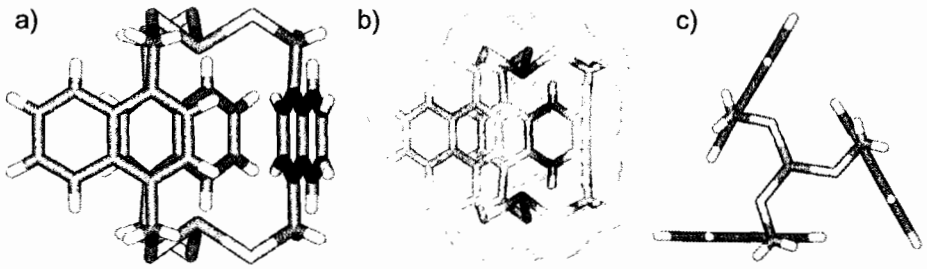

Figure 5. Representations of X-ray crystal structure of P_2L_3 as stick figure, side view (a), with van der Waals surface (b), and stick figure, top view (c). Phosphorus atoms are shown in orange.

two days which correspond to P_2L_3 (Figure 4). Crystals of this cryptand were grown by layering this solution with acetonitrile (Figure 5). The X-ray structure reveals that the phosphorus atoms are sitting slightly within the cavity with their lone pairs of electrons pointing in, filling the same position as the metals Sb and Bi and the metalloid As. While no favorable P···π interactions are expected, the P···C_{aryl} close contacts (3.25 and 3.54 Å) are less than the sum of the van der Waals radii (3.6 Å). The geometry of the ligand is well suited for this bis(trithiophosphite): all of the ligands are in a preferred *gauche* conformation[18] and the S-P-S angle (96.5°) is only slightly smaller than that for other reported trithiophosphites.[19] With a P···P distance of 5.49 Å, P_2L_3 has a small, empty cavity.[d,20] Attempts to fill that cavity with BH_3 or Au^{+} [21] have thus far resulted in no reaction and P_2L_3 is surprisingly air-stable for a trithiophosphite. This suggests that P's

---

[d] Cavities were measured using solvent (0.7 Å) surfaces inWebLab ViewerPro 4.0, December 1, 2000 release. The cavity volume was estimated as the difference between the volume of the P_2L_3 cryptand filled with a proton and the P_2L_3 cryptand with a void cavity. This was found to be 15 $Å^3$.

lone pairs are not inverting in solution, but are locked into their endohedral positions as observed in the crystal structure, in effect protecting the phosphorus atoms from further reaction or decomposition. Currently, we are working to expand the size of the cavity and use similar cryptands as *trans*-directing phosphine ligands.

Conclusion

We have shown in a supramolecular context that thiolate ligands prefer As over Sb over Bi. Surprisingly, an Sb-containing cryptand can be "transmetallated" with P, resulting in a previously inaccessible $P_2\mathbf{L}_3$ cryptand in which P acts like the "metal" in a metal-ligand self-assembly reaction. All of the $E_2\mathbf{L}_3$ cryptands have a propeller twist due to intramolecular edge-to-face aromatic interactions, yet are achiral due to an internal plane of symmetry (C_{3h} point group). Heterometallic analogs would provide interesting examples of chiral supramolecular assemblies, and in the case of P-containing cryptands, these chiral assemblies could act as *trans*-directing ligands for a metal guest. The facile transmetallation of these stable, yet labile, supramolecular main group assemblies suggests that transmetallation is another synthetic tool for supramolecular chemists seeking to prepare otherwise inaccessible assemblies. Such hosts offer applications in molecular machines,[11b] catalysis, and sensing.[11a] Furthermore, the As- and P-based assemblies are unusually stable compared to mononuclear analogs. If the Bi-containing cryptands display similar stability, are applications as materials precursors, catalysts and radiopharmaceuticals[22] possible?

Experimental Section

General Procedures

NMR spectra were obtained on a Varian INOVA 300-MHz spectrometer in $CDCl_3$ at 25 °C and referenced to the residual solvent peak unless otherwise noted. ^{31}P NMR was referenced to external H_3PO_4 (0 ppm). Commercially available reagents were used as received.

Synthetic Procedures

Bi_2L_3. H_2L (40.3 mg, 0.182 mmol) and $BiCl_3$ (36.4 mg, 0.115 mmol) were dissolved in MeOH (10 mL) and THF (40 mL) and stirred at 25 °C under N_2. DIPEA (301 μL, 1.82 mmol) was added and the solution turned bright yellow. After 6 hr, the solution was washed with H_2O and 2 M NaOH, dried with brine and $MgSO_4$, and then filtered. The yellow filtrate was layered with CH_3CN. After two weeks, the solvent was decanted yielding small orange needles (4.42 mg, 5.69 μmol, 10% crystalline yield). ^1H NMR: δ 8.45 (m, 6H, CH), 7.71 (m, 6H, CH), 6.14 (s, 6H, CH), 5.56 (d, 6H, CH_2, J = 13.0 Hz), 4.21 (d, 6H, CH_2, J = 13.0 Hz). Crystallographic Data for Bi_2L_3: $C_{38}H_{33}Bi_2NS_6$, M = 1113.97, 0.14 × 0.10 × 0.06 mm, T = 173(2) K, hexagonal, space group $P6_3/m$, $a = b$ = 11.5547(3) Å, c = 16.1081(10) Å, V = 1862.48(13) Å3, Z = 2, D_c = 1.986 Mg/m3, μ = 9.801 mm-1, $F(000)$ = 1060, $2\theta_{max}$ = 54.00°, 13673 reflections, 1412 independent reflections [R_{int} = 0.0355], $R1$ = 0.0242, $wR2$ = 0.0613 and GOF = 1.026 for 1412 reflections (67 parameters) with $I > 2\sigma(I)$, $R1$ = 0.0291, $wR2$ = 0.0640 and GOF = 1.026 for all reflections, max/min residual electron density +1.061/-0.349 eÅ^3.

Sb_2L_3. H_2L (0.237 g, 1.08 mmol) and $SbCl_3$ (0.164 g, 0.720 mmol) were dissolved in $CHCl_3$ (125 mL) and stirred at 50 °C under N_2. Diisopropylethylamine (DIPEA, 1.78 mL, 10.8 mmol) was added. After 1.5 hr, the solution was cooled to 25 °C, washed with 2 M HCl and H_2O, dried with $MgSO_4$, and concentrated in vacuo to yield a white powder. This powder was redissolved in $CHCl_3$ (30 mL), filtered, and layered with CH_3CN. After one week, the solution was decanted to yield colorless needles (0.167 g, 0.186 mmol, 52% crystalline yield). ^{1}H NMR: δ 8.43 (m, 6H, CH), 7.67 (m, 6H, CH), 5.99 (s, 6H, CH), 4.40 (d, 6H, CH_2, J = 12.7 Hz), 3.94 (d, 6H, CH_2, J = 12.7 Hz). Crystallographic Data for Sb_2L_3: $C_{38}H_{33}NSb_2S_6$, M = 939.51, 0.18 × 0.12 × 0.08 mm, T = 173(2) K, hexagonal, space group $P6_3/m$, $a = b$ = 11.5114(5) Å, c = 16.1142(10) Å, V = 1849.25(16) Å3, Z = 2, D_c = 1.687 Mg/m3, μ = 1.829 mm-1, $F(000)$ = 932, $2\theta_{max}$ = 54.00°, 20890 reflections, 1403 independent reflections [R_{int} = 0.0321], $R1$ = 0.0228, $wR2$ = 0.0600 and GOF = 1.073 for 1403 reflections (67 parameters) with $I > 2\sigma(I)$, $R1$ = 0.0234, $wR2$ = 0.0605 and GOF = 1.073 for all reflections, max/min residual electron density +0.763/-0.205 eÅ^3.

As_2L_3. $Sb_2L_3 \cdot CH_3CN$ (24.9 mg, 26.5 μmol) was dissolved in $CDCl_3$ (9 mL) and treated with $AsCl_3$ (4.52 μL, 53.0 μmol). An aliquot was transferred to an NMR tube and monitored until it reached ~99% conversion to As_2L_3. After one week, this aliquot was returned to the bulk solution and layered with pentane. After two weeks, the solution was decanted, yielding colorless needles of $As_2L_3 \cdot CH_3CN$ (9.49 mg, 11.2 μmol, 42% crystalline yield). X-ray quality crystals were grown by layering a solution of As_2L_3 with pentane. ^{1}H NMR: δ 8.41 (m, 6H, CH), 7.66 (m, 6H, CH), 5.75 (s, 6H, CH), 4.21 (d, 6H,

CH_2, J = 13.0 Hz), 3.96 (d, 6H, CH_2, J = 13.0 Hz); ^{13}C NMR (500 MHz): δ 133.4 (C), 131.7 (C), 126.2 (CH), 125.9 (CH), 125.3 (CH), 33.6 (CH_2). Crystallographic Data for As_2L_3: $C_{38}H_{32}As_2Cl_6S_6$, M = 1043.54, 0.21 × 0.14 × 0.08 mm, T = 173 K, cubic, space group $P2_13$, $a = b = c$ = 16.3746(3) Å, V = 4390.48(14) Å3, Z = 4, D_c = 1.579 Mg/m3, μ = 2.201 mm-1, $F(000)$ = 2096, $2\theta_{max}$ = 54.00°, 49649 reflections, 3216 independent reflections [R_{int} = 0.0526], $R1$ = 0.0355, $wR2$ = 0.0949 and GOF = 1.064 for 3216 reflections (197 parameters) with $I > 2\sigma(I)$, $R1$ = 0.0380, $wR2$ = 0.0971 and GOF = 1.064 for all reflections, the Flack parameter is 0.017(12), max/min residual electron density +1.028/-0.584 eÅ^3.

P_2L_3. Sb_2L_3 (51.7 mg, 57.6 μmol) was dissolved in dry 1,1,2,2-tetrachloroethane (20 mL) and stirred at 80 °C under N_2. The solution was treated with PBr_3 (12.0 μL, 127 μmol). After 3 days, the solution was concentrated in vacuo to 12 mL, then filtered and layered with CH_3CN. After two weeks, the solution was decanted, yielding X-ray quality colorless needles of P_2L_3 in very low yield. ^{1}H NMR (600 MHz): δ 8.38 (m, 6H, CH), 7.65 (m, 6H, CH), 5.66 (s, 6H, CH), 4.15 (d, 3H, CH_2, J = 12.8 Hz), 4.11 (d, 3H, CH_2, J = 13.3 Hz), 3.94 (d, 3H, CH_2, J = 13.3 Hz), 3.92 (d, 3H, CH_2, J = 12.8 Hz); ^{31}P NMR (600 MHz): δ 88.4. Crystallographic Data for P_2L_3: $C_{38}H_{33}NP_2S_6$, M = 757.95, 0.07 × 0.04 × 0.02 mm, T = 173(2) K, hexagonal, space group $P6_3/m$, $a = b$ = 11.2442(18) Å, c = 16.219(6) Å, V = 1775.8(7) Å3, Z = 2, D_c = 1.418 Mg/m3, μ = 0.506 mm-1, $F(000)$ = 788, $2\theta_{max}$ = 54.00°, 5011 reflections, 1334 independent reflections [R_{int} = 0.0935], $R1$ = 0.0561, $wR2$ = 0.1121 and GOF = 0.996 for 1334 reflections (87 parameters) with $I >$

$2\sigma(I)$, $R1 = 0.0879$, $wR2 = 0.1257$ and GOF = 0.996 for all reflections, max/min residual electron density +0.467/-0.396 eÅ^3.

X-Ray Crystallography

Diffraction intensities for $As_2\mathbf{L}_3$, $Sb_2\mathbf{L}_3$, $Bi_2\mathbf{L}_3$, and $P_2\mathbf{L}_3$ were collected at 173(2) K on a Bruker Apex CCD diffractometer using MoKα radiation λ = 0.71073 Å. Space groups were determined based on systematic absences. Absorption corrections were applied by SADABS.[23] Structures were solved by direct methods and Fourier techniques and refined on F^2 using full matrix least-squares procedures. All non-H atoms were refined with anisotropic thermal parameters. All H atoms in $As_2\mathbf{L}_3$, $Sb_2\mathbf{L}_3$, and $Bi_2\mathbf{L}_3$ were refined in calculated positions in a rigid group model. H atoms in $P_2\mathbf{L}_3$ were found from the F-map and refined with isotropic thermal parameters. In the crystal structures of $Sb_2\mathbf{L}_3$, $Bi_2\mathbf{L}_3$, and $P_2\mathbf{L}_3$ there is a solvent molecule, CH_3CN, disordered over two positions related by a mirror plane which was treated by SQUEEZE.[24] Corrections of the X-ray data by SQUEEZE (41, 38 and 44 electron/cell, respectively for $Sb_2\mathbf{L}_3$, $Bi_2\mathbf{L}_3$, and $P_2\mathbf{L}_3$) are close to the required values of 44 electrons/cell for two molecules in the full unit cells. All calculations were performed by the Bruker SHELXTL (v. 6.10) package.[25] CCDC 753593 – 753596 contain the supplementary crystallographic data for this chapter. These data can be obtained free of charge from The Cambridge Crystallographic Data Centre via www.ccdc.cam.ac.uk/data_request/cif.

Bridge to Chapter VI

Chapter V presented a series of E_2L_3 (E = P, As, Sb, Bi) cryptands and a new supramolecular transmetallation. Chapter VI expands upon this work by examining these cryptands in further detail. Trends in the solid-state and solution structures are further analyzed. The structure of an asymmetric conformer of the cryptand, observed only in solution, is elucidated. Furthermore, three new heterometallic cryptands ($PSbL_3$, $AsSbL_3$, and $AsBiL_3$) are prepared and their solid-state and solution structures analyzed.

CHAPTER VI

SELF-ASSEMBLED E_2L_3 CRYPTANDS (E = P, As, Sb, Bi): TRANSMETALLATION, HOMO- AND HETEROMETALLIC ASSEMBLIES, AND CONFORMATIONAL ISOMERISM

Chapter VI gives a deeper look into the E_2L_3 (E = P, As, Sb, Bi) cryptands presented in Chapter V. Their solid-state structures are further compared and their conformational isomerism in solution is described. Additionally, the synthesis and characterization of three heterometallic $EE'L_3$ cryptands are presented. This co-authored manuscript has been submitted as an article to *Inorganic Chemistry*.[1] Dr. Timothy G. Carter carried out liquid chromatography mass spectrometry experiments. Dr. Justin L. Crossland carried out one self-sorting NMR experiment and performed electrospray mass spectrometry characterization of the heterometallic cryptands. All X-ray crystallography was carried out by Dr. Lev N. Zakharov. Professor Darren W. Johnson provided intellectual and editorial contributions. I carried out the synthesis, crystal growth, and NMR experiments on all cryptands and wrote the manuscript.

Introduction

The Group 15 elements range in structure, property, and application as one

descends from the nonmetals nitrogen and phosphorus—essential to life—to the toxic metalloids arsenic and antimony, to the metal bismuth, the heaviest of all stable elements offering emerging applications in therapeutics and materials science.[2] While they are often overlooked in favor of the transition metals for supramolecular design, the main group elements, Group 15 in particular, can be used to prepare a variety of supramolecular structure types by metal-directed self-assembly.[3-11] When bound by thiolates in the E(III) oxidation state, P, As, Sb, and Bi each have a trigonal pyramidal geometry and a stereochemically active lone pair of electrons. Previously, our group has shown that each of these elements can be positioned interchangeably within self-assembled E_2L_3 cryptands.[12] Here, we expand upon this work by presenting their dynamic solution behavior, "transmetallation" chemistry, and three new examples of chiral, heterometallic $EE'L_3$ cryptands.

Heterometallic assemblies are relatively rare and most offer ligands with unique binding sites specific for each type of metal based on that metal's preferred coordination number, geometry, charge, hard/soft binding site, or electronic discrimination[13-22] or are prepared by stepwise synthesis.[23] However, the Group 15 elements within the cryptands reported here are bound by the same coordination sphere of three thiolates revealing a surprising *lack* of selectivity, implying that self-sorting may be at play. This series of homo- and heterometallic cryptands allows for the direct comparison of preferred bond angles and distances for E-S bonds within a confined supramolecular system. Furthermore, this series of cryptands exemplifies the dynamic nature of main group "metal"-ligand self-assembly through the synthesis, transmetallation and solution

behavior of the cryptands, including the surprising observation of a stable, asymmetric conformation of the E_2L_3 cryptands.

These self-assembled main group complexes are reminiscent of organic cyclophanes (or heterophanes), where an -S-E-S- group substitutes for a heteroatom or a –C-X-C- unit. Our As_2L_3 cryptands[11a,11f,12] are structurally similar to bicyclophanes,[24] specifically the π-prismands, and our recently reported As_4L_2 complex[11j] is remarkably similar to tetrathia[3.3.3.3]cyclophane.[25] However, our assemblies differ from their organic analogues by synthesis from a self-assembly reaction rather than a stepwise synthesis, resulting in typically high yields. Additionally, organic prismands lack the conformational isomerism and transmetallation properties exhibited by the main group congeners. This new generation of metallacyclophanes and metallacycles could allow access to new structure types and dynamic host-guest interactions.[26]

Results and Discussion

Symmetric and Asymmetric E_2L_3 Cryptands

Previously, our laboratory reported a series of $E_2\mathbf{L}_3$ cryptands (where E = P, As, Sb, Bi) that were prepared by self-assembly reactions (Scheme 1).[12] When $H_2\mathbf{L}$ was mixed with $AsCl_3$, $SbCl_3$, or $BiCl_3$ in chloroform and the HCl byproduct was removed with base, $E_2\mathbf{L}_3$ was formed. $Sb_2\mathbf{L}_3$ and $Bi_2\mathbf{L}_3$ were prepared in the presence of excess diisopropylethylamine (DIPEA), while $As_2\mathbf{L}_3$ was prepared in the presence of KOH. A

transmetallation[a] reaction could also be used to prepare As_2L_3, and "transmetallation" was the only effective route to form P_2L_3 (Scheme 2). Transmetallation occurred when Sb_2L_3 was treated with $AsCl_3$ or PBr_3 and As_2L_3 or P_2L_3 formed, respectively. For Sb_2L_3 → As_2L_3, the reaction was shown to be quantitative by ^1H NMR spectroscopy.

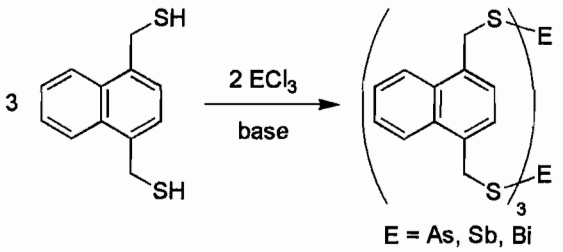

Scheme 1. Self-assembly of E_2L_3 cryptands. DIPEA was used as the base for E = Sb or Bi, while KOH was used for E = As.

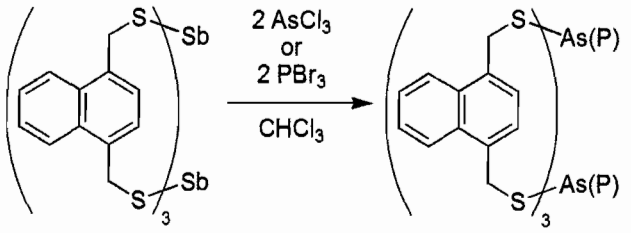

Scheme 2. Transmetallation of Sb_2L_3.

[a] Transmetallation is used to describe the replacement of one Group 15 element with another, even when the replacement is not a metal as in the case of As (metalloid) and P (non-metal). This language is consistent with our previous communication[12] on the topic.

Solid-State Structures. We previously communicated the supramolecular transmetallation reaction that allowed for the synthesis of these cryptands (Chapter V).[12] This chapter provides a thorough structural analysis (solid-state and solution) of these systems in the context of three additional new heterometallic assemblies described in subsequent sections and describes a surprising conformational isomerism for these cryptands in solution. X-ray quality crystals of the complexes were grown by the slow diffusion of acetonitrile (P_2L_3, Sb_2L_3 and Bi_2L_3) or pentane (As_2L_3) into a chloroform solution of cryptand. The structures for these symmetric cryptands are remarkably similar (Figure 1); the only significant differences are in the position of the pnictogen atoms, the

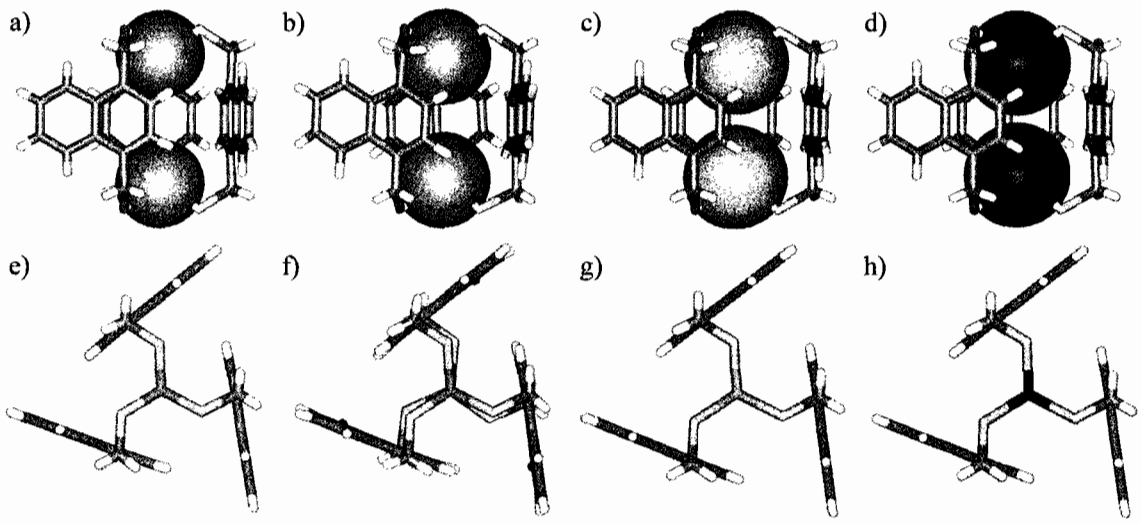

Figure 1. Stick and space-filling representations of the X-ray crystal structures of symmetric cryptands P_2L_3 (a, e), As_2L_3 (b, f), Sb_2L_3 (c, g) and Bi_2L_3 (d, h). Phosphorus is shown in orange, arsenic in purple, antimony in teal, bismuth in blue, sulfur in yellow, carbon in gray and hydrogen in white.

E-S bond distances, and S-E-S bond angles (Table 1). With increasing atomic mass comes an increase in E-S bond length and a decrease in the E···E distance. These differences are compensated for by the decreasing S-E-S angle, allowing the ligands to maintain almost identical positions in each cryptand (Figure 2). This trend is expected as the extent of s-character in the E-S bonds decreases going down the group. Searching the Cambridge Structural Database (CSD) for pnictogens bonded to three sulfur atoms in unconstrained systems reveals that this supramolecular coordination is not greatly affecting the bonding geometry of the pnictogens. In each of the E_2L_3 structures, the E-S distance is slightly shorter than, but within 0.1 Å of the CSD average. The S-E-S bond angles in the E_2L_3 structures are slightly larger than the CSD average, but within a couple degrees (and not out of the normal range).

Table 1. Select Distances and Bond Angles for E_2L_3 Cryptands.

	P_2L_3	As_2L_3	Sb_2L_3	Bi_2L_3
E···E (Å)	5.491	5.108	4.827	4.683
E-S (Å)	2.1182(12)	2.2514(10)	2.4206(5)	2.5157(10)
CSD average E-S (Å)	2.144	2.298	2.470	2.592
S-E-S (°)	96.52(5)	94.00(4)	91.456(18)	90.84(3)
CSD average S-E-S (°)	95.24	91.35	91.09	90.71
E···C_{aryl} (Å)	3.251 3.544	3.300 3.577	3.343 3.584	3.358 3.548

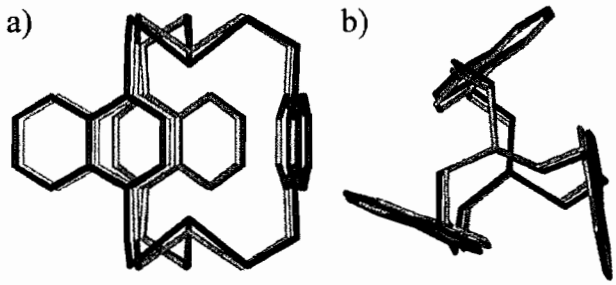

Figure 2. Overlayed stick-representations of the X-ray crystal structures of the symmetric cryptands P_2L_3 (orange) and Bi_2L_3 (blue) from side (a) and top-down (b) views.

Six E···π interactions stabilize each of the As_2L_3, Sb_2L_3, and Bi_2L_3 cryptands. The E···π interaction is an attractive interaction involving dispersion forces and the donation of π-electrons from the aryl ring into a σ* orbital on E.[27-30] In P_2L_3, the six shortest P···C_{aryl} contacts are also shorter than the sum of the van der Waals radii (3.5 Å), but no attractive P···π interactions are known or expected.[b,31] Each symmetric E_2L_3 cryptand possesses crystallographic C_{3h} symmetry, except As_2L_3, which is slightly offset and has C_3 crystallographic symmetry. This could be a result of the As···π interactions causing the ligands to twist more to allow the metals to sit deeper within the cavity, or it could be a consequence of crystal packing. The E···π interaction is known to be stronger for the larger pnictogens, typically resulting in a *decrease* in the E···C_{aryl} distance (Figure 3).[30]

---

[b] η^6-arene complexation to phosphenium cations is known, but very rare.[31] The CSD was searched for P···π contacts of less than the sum of the van der Waals radii for P and C, turning up 20 hits. However, no correlation between contact distance and angle was observed. See Appendix B for further detail.

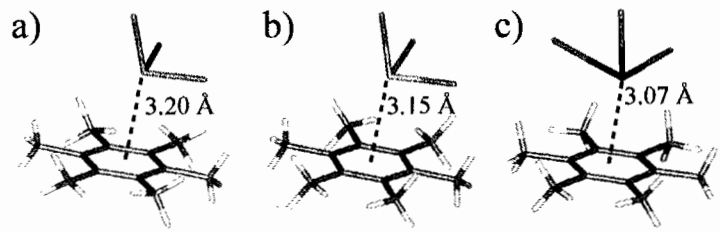

Figure 3. Stick representations of crystal structures of $AsCl_3$ (a),[32] $SbCl_3$ (b),[33] and $BiCl_3$ (c)[34] cocrystallized with hexamethylbenzene, reported by Schmidbaur and co-workers. The dashed lines represent the short E···π interactions (distances to ring centroids are shown in each case).

However, the opposite trend is observed here. In these supramolecular cryptands, the shortest E···C_{aryl} distance *increases* from $As_2\mathbf{L}_3$ to $Sb_2\mathbf{L}_3$ to $Bi_2\mathbf{L}_3$. This is not an indication of a weaker E···π interaction, but is likely a consequence of the growing radius of E, the consequently longer E-S bonds, and the constricted position of the metals within the cryptand cavity.

Solution Structures. In solution each of the $E_2\mathbf{L}_3$ cryptands appears to be present in two different conformations. The first is a symmetric conformer similar to that in the solid state, in which each of the three ligands are equivalent and the complex has overall C_{3h} symmetry. Figure 4 shows the ^{1}H NMR spectra for each of the cryptands. The exterior aryl protons H_b and H_c are in very similar positions in each cryptand and are not affected by the identity of E, as shown by the almost identical resonance shifts for each cryptand. The resonance for interior proton H_a differs slightly depending on the pnictogen, shifting downfield from $P_2\mathbf{L}_3$ to $Bi_2\mathbf{L}_3$. The methylene protons, H_d and H_e, are significantly more affected by the identity of E. In $P_2\mathbf{L}_3$, the resonance for each of these

protons is split into a doublet of doublets due to splitting by the other methylene proton and the nearby phosphorus nucleus. In each of As_2L_3, Sb_2L_3, and Bi_2L_3, these methylene resonances appear as a single pair of doublets and are significantly shifted based on the identity of E. Similarly to proton H_a, the signals for H_d and H_e in Bi_2L_3 are shifted the farthest downfield.

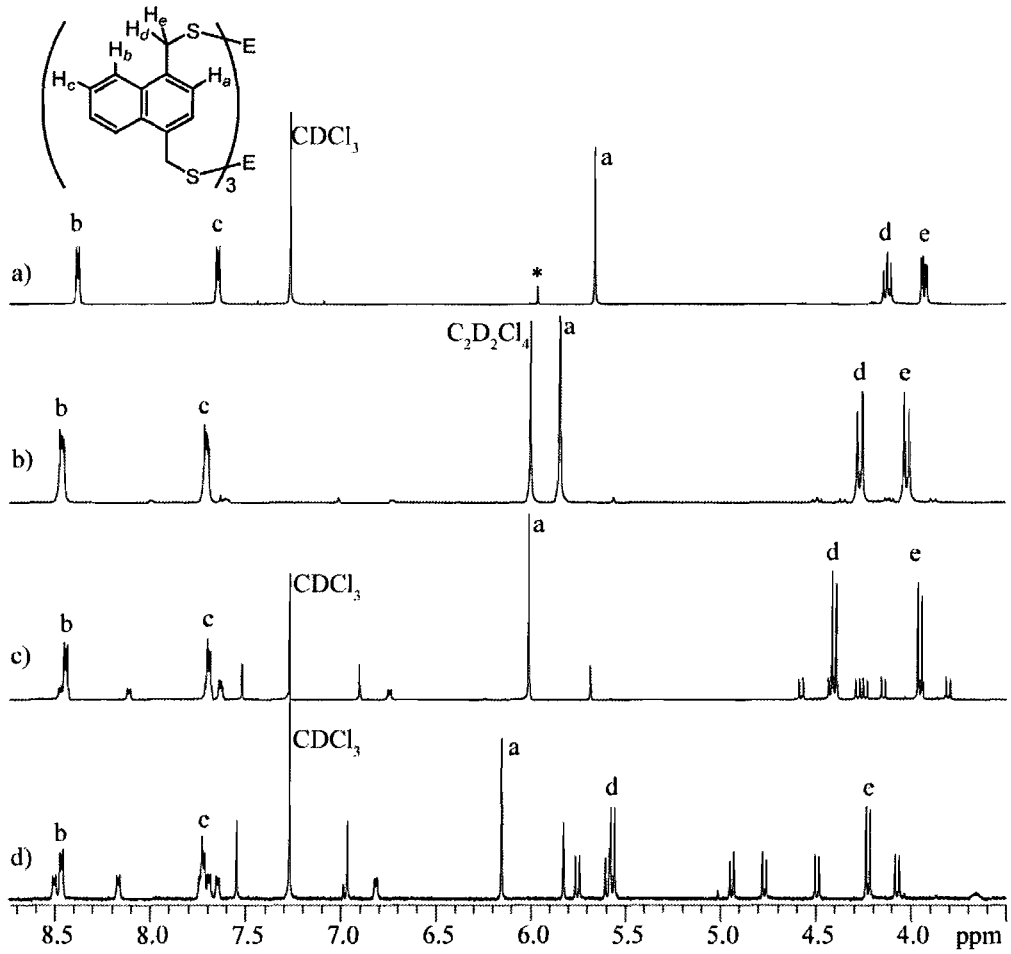

Figure 4. ^1H NMR spectra for P_2L_3 (a), As_2L_3 (b), Sb_2L_3 (c) and Bi_2L_3 (d). The signals from the symmetric cryptands are labeled, while those for the asymmetric cryptands are unlabeled (See Appendix B for complete labeling scheme). * denotes $C_2H_2Cl_4$ in the spectrum.

A glaring feature of these ^{1}H NMR spectra is the presence of a second, less-symmetric species in solution. The NMR samples were prepared by dissolving crystals of each symmetric cryptand. Initially, only the symmetric cryptand is observed. However, over the course of a half hour a conformational change establishes a new equilibrium between the symmetric E_2L_3 cryptand and an asymmetric species, E_2L_3-*asym*. *g*COSY and NOESY NMR (Appendix B) were used to identify this asymmetric species as a cryptand in which one ligand has "flipped" (Figure 5a), perturbing the C_3 symmetry of the complex and resulting in a conformation with only C_s symmetry. While less than 5% of

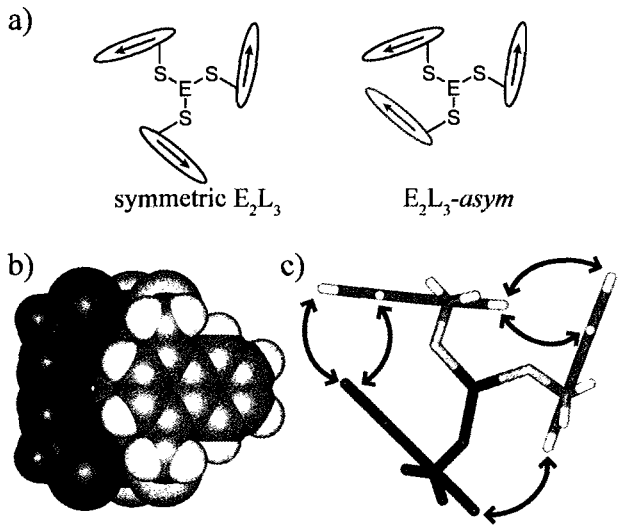

Figure 5. Cartoon representations of symmetric E_2L_3 (left) and E_2L_3-*asym* (right) in which the ligands are represented by arrows (a). In the symmetric cryptand all of the ligands point counterclockwise. In the asymmetric cryptand, two ligands point counterclockwise (black) and the one "flipped" ligand points clockwise (red). The DFT-calculated structure of Bi_2L_3-*asym* in space-filling (b) and stick (c) representations. The "flipped" ligand is shown in red. The blue arrows indicate the protons that were correlated by their NOEs in solution (See Appendix B for more information).

the As_2L_3 cryptand is in this asymmetric form, it comprises 47% of the Sb_2L_3 and 60% of the Bi_2L_3 samples based on ^1H NMR integrals. To confirm that the observed species was not actually a higher order assembly, liquid chromatography mass spectrometry was carried out on a sample of Sb_2L_3. As expected, two species with different retention times, yet the same mass-to-charge ratio, were present in solution (Figure 6, Appendix B). The relative amount of each did not match the ratio observed by ^1H NMR spectroscopy, but that could be a result of solvent effects or conformational change occurring over the course of the experiment.

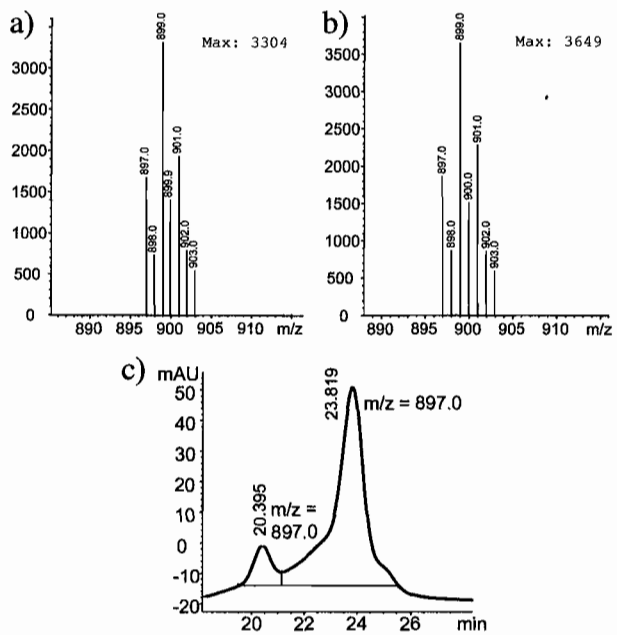

Figure 6. Liquid chromatography mass spectrometry data for the two conformers of $[Sb_2L_3+H]^+$ (a,b). LCMS trace showing two peaks with the same m/z (c). The isotope distribution verifies that these are both +1 charge states of a Sb_2L_3 cryptand.

DFT calculations were carried out to help visualize the likely structure of $E_2\mathbf{L}_3$-*asym*. First, to judge the ability of the chosen DFT method (with a 6-31+G* basis set for all atoms and with the B3LYP functional),[35,c,36] the structures of the symmetric $P_2\mathbf{L}_3$, $As_2\mathbf{L}_3$, $Sb_2\mathbf{L}_3$ and $Bi_2\mathbf{L}_3$ cryptands were calculated. These were found to match the crystal structures very closely (see overlays in Appendix B). The only minor difference is that in the DFT-calculated structures, the metals and ligands are not pulled quite as tightly into the cavity. However, it has been established that this functional is not well suited for describing the E···π interaction, which is likely a general limitation of DFT since dispersion forces account for at least some of this attractive interaction.[29,30] However, we have found DFT to be very useful in qualitatively predicting the overall structures of Group 15-containing assemblies.[35]

The structures of $P_2\mathbf{L}_3$-*asym*, $As_2\mathbf{L}_3$-*asym*, $Sb_2\mathbf{L}_3$-*asym* and $Bi_2\mathbf{L}_3$-*asym* were determined and it was found that in each case a stable structure was converged upon in which one ligand has "flipped" (Figure 5b-c for $Bi_2\mathbf{L}_3$-*asym*). In each case, the symmetric cryptand was found to be more stable than the asymmetric cryptand by 4-6 kcal/mol (6.6 for $P_2\mathbf{L}_3$, 5.3 for $As_2\mathbf{L}_3$, 4.0 for $Sb_2\mathbf{L}_3$ and 4.0 for $Bi_2\mathbf{L}_3$) (See Appendix B for exact energies). These energy differences are much larger than those observed by ^{1}H NMR spectroscopy, likely due to solvation effects and a limitation of DFT in predicting E···π interactions, but the general trend fits: the energy difference is smaller for the

---

[c] Models were minimized using Spartan '08.[36] The choice of functional and basis sets was based on those used in Ref. 35.

heavier pnictogens. However, these calculations do not show that $Bi_2\mathbf{L}_3$-*asym* is lower in energy than its symmetric counterpart even though we observe that it is 0.24 kcal/mol lower by ^{1}H NMR spectroscopy.

It is not immediately clear why the asymmetric cryptands are relatively more stable when compared to their symmetric counterparts for the heavier pnictogens. The simplest explanation is that it is a steric effect of the larger elements.[d] The larger pnictogens require more space within the cavity, and the "flipping" of one ligand provides that accommodation. The average of the six shortest E···C_{aryl} contacts in the DFT calculated model of $Sb_2\mathbf{L}_3$-*asym* (3.53 Å) was found to be slightly longer than that for the crystal structure of $Sb_2\mathbf{L}_3$ (3.46 Å), suggesting that the "flipping" does indeed open up more space. While we cannot confirm the accuracy of the models without a crystal structure of the asymmetric cryptand (which remains elusive), we can compare them to what is observed in solution. ^{1}H NMR spectroscopy shows that the proton resonances for $Bi_2\mathbf{L}_3$-*asym* and $Sb_2\mathbf{L}_3$-*asym* follow the same pattern but are significantly shifted based on proximity to the pnictogens. The similarity of these structures is corroborated by overlaying the DFT-calculated structures (See Appendix B).

Another possible explanation for the trend in the relative stability of the two conformations of cryptand is that the asymmetric conformation allows for stronger E···π interactions, and the strength of the E···π interaction increases down the group (Figure 3) (this would also explain the poor prediction of the conformational energy differences by

---

[d] The van der Waals radii are 1.8 Å for P, 1.85 Å for As, 2.0 Å for Sb, and 2.0 Å for Bi.[37]

DFT). Consequently, $Bi_2\mathbf{L}_3$-*asym* is stabilized more than $Sb_2\mathbf{L}_3$-*asym* and $As_2\mathbf{L}_3$-*asym* compared to their symmetric counterparts. In the symmetric cryptands, each pnictogen atom is involved in three E···π interactions, as evidenced by the short E···C_{aryl} contacts. Although the shortest E···C_{aryl} contacts for the "flipped" ligand are not as short as they are within the symmetric cryptand, the position of the ligand is thought to result in a stronger E···π interaction. The "flipped" ligand is positioned such that it is sitting deep into the cryptand cavity with *three* carbon atoms close to the pnictogen (within the sum of the van der Waals radii) allowing for an η^3-interaction (as compared to the η^2-interaction observed in the symmetric cryptand). Additionally, the S-E···C_{aryl} angle is larger in the asymmetric cryptands. This angle is 160° for $Sb_2\mathbf{L}_3$-*asym* and 155° in the symmetric cryptand. The larger angle allowed by the flipping of the ligand may result in a stronger Sb···π interaction. However, our laboratory has previously published a structural survey that shows that the average angle for non-constrained interactions is 155° for Sb.[30] The position of this ligand deep within the cryptand can also be observed in solution, as evidenced by the upfield-shifted resonance for H_c on this ligand (~6.8 ppm).

Mechanism of Ligand Flipping. Semi-empirical AM1 calculations were carried out to see if it was energetically feasible for a ligand to "flip" without breaking any bonds. Based on these calculations, and a look at the space-filling models, it is clear that this is not the route to interconversion between $E_2\mathbf{L}_3$ and $E_2\mathbf{L}_3$-*asym*. The cavity is far too sterically congested to allow even the short end of a naphthalene ring to pass through it. Rather, it seems far more likely that the mechanism to interconversion is through the breaking and reforming of an E-S bond. While that bond is broken, the ligand can rotate

freely without steric considerations. The strength of an As-S bond is estimated to be ~81 kcal/mol;[e] nonetheless, we have shown that these bonds are labile enough to allow for self-assembly and transmetallation.[11h,12]

Heterometallic $EE'L_3$ Cryptands

Further synthesis was carried out to determine whether or not this self-assembly process would result in self-sorting.[39-43] If self-sorting were to occur, it could be either "narcissistic"[44] (molecules display a high affinity for themselves), resulting in homometallic cryptands exclusively, or "social"[44-46] (molecules display a high affinity for others), resulting in heterometallic cryptands exclusively. If no self-sorting were occurring, a statistical 1:2:1 mixture of homo:hetero:homo cryptands would be expected to form. To test these possibilities, $H_2\mathbf{L}$ was treated with $AsCl_3$, DIPEA and either $SbCl_3$ or $BiCl_3$. Surprisingly, rather than a statistical mixture of cryptands, NMR spectroscopy on the crude reaction mixtures revealed that the heterometallic $AsSb\mathbf{L}_3$ and $AsBi\mathbf{L}_3$ cryptands were the dominant products of the reactions (>80% in each case), with the remainder of the product being homometallic cryptand. This result completely ruled out narcissistic self-sorting and implied that social self-sorting could be occurring, at least kinetically.

To follow up, the synthesis of $AsSb\mathbf{L}_3$ was carried out in $CDCl_3$ and monitored by ^{1}H NMR. This experiment showed that after 15 minutes $AsSb\mathbf{L}_3$, $As_2\mathbf{L}_3$, and $Sb_2\mathbf{L}_3$ were

---

[e] Bond strength approximated from As–S bond strengths in As_xS_y polyhedra.[38]

all present, but within two hours, $AsSb\mathbf{L}_3$ was the major product, implying social self-sorting. However, the reaction also produced a white precipitate which could not be identified, but was presumably a mixture of DIPEA-salts and coordination polymer containing ligand, As, and Sb. Over the next three days, reaction continued to occur between the soluble and insoluble components and the product ratio changed until it contained a ~1:2 ratio of $AsSb\mathbf{L}_3$ to $As_2\mathbf{L}_3$. There was no soluble $Sb_2\mathbf{L}_3$ present, implying that most of the Sb was tied up in the insoluble coordination polymer. While definitive conclusions cannot be drawn from this experiment, it does imply that initially social self-sorting results in the kinetic $AsSb\mathbf{L}_3$ and coordination polymer products, but, if given the opportunity, these will rearrange over time to give the thermodynamically stable $As_2\mathbf{L}_3$.[12] The precipitate in this above experiment is vital to the self-sorting observed: further NMR-scale experimentation showed that over time dissolved crystals of $AsSb\mathbf{L}_3$ will not rearrange to give $As_2\mathbf{L}_3$ and $Sb_2\mathbf{L}_3$ *and* dissolved crystals of $As_2\mathbf{L}_3$ and $Sb_2\mathbf{L}_3$ will not rearrange to give $AsSb\mathbf{L}_3$.

A heterometallic $PSb\mathbf{L}_3$ cryptand was also prepared, but was isolated from a transmetallation reaction involving the treatment of $Sb_2\mathbf{L}_3$ with PBr_3 that did not go to completion. X-ray quality crystals of each of $AsSb\mathbf{L}_3$, $AsBi\mathbf{L}_3$, and $PSb\mathbf{L}_3$ were grown by layering a chloroform solution of the complex with acetonitrile or pentane (Figure 7). Within each crystal, E and E′ are disordered over both positions, so all of the E···E′, E-S and S-E(E′)-S distances and angles are averaged for the two sides of the complex (Table 2). Still, the averaged distances and angles fit into the trend observed in the homometallic $E_2\mathbf{L}_3$ complexes. In each case, the E···E′ and E-S distances and S-E(E′)-S

angles fall between the values for the two homometallic complexes, but are closer to what is observed for the heavier E_2L_3 complex. This suggests that the larger metals have more of an effect on the geometry than the smaller metals. Like their homometallic analogues, each of the EE′L_3 cryptands exhibits six close E···C_{aryl} contacts in the solid state, suggesting stabilization of the cryptands through E···π interactions.

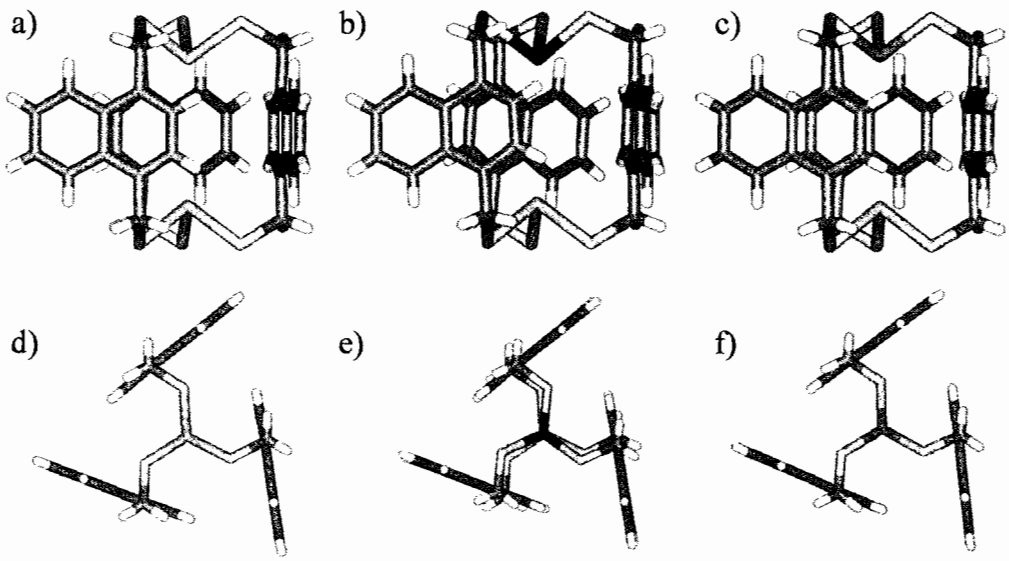

Figure 7. Stick representations of the X-ray crystal structures of $AsSbL_3$ (a, b), $AsBiL_3$ (c, d), and $PSbL_3$ (e, f). Phosphorus is shown in orange, arsenic in purple, antimony in teal, bismuth in blue, sulfur in yellow, carbon in grey and hydrogen in white.

Table 2. Select Distances and Bond Angles for EE′L_3 Cryptands.

	$AsSbL_3$	$AsBiL_3$	$PSbL_3$
E···E′ (Å)	4.944	4.685	4.960
E(E′)-S (Å)	2.3537(7)	2.4499(19) 2.376(2)	2.3212(7)
S-E(E′)-S (°)	92.10(2)	89.96(7) 91.42(8)	91.26(2)
E(E′)···C_{aryl} (Å)	3.302 3.553	3.278, 3.391 3.314, 3.570	3.263 3.524

In solution, the EE'$\mathbf{L}_3$ cryptands are C_3-symmetric, just as they are in the solid state (Figure 8). Unlike their homometallic counterparts, no asymmetric cryptand is observed. This could be a result of ligand strain caused by the size difference in the metals, or there could be too little asymmetric cryptand to observe by NMR spectroscopy. Because of the lack of σ_h-symmetry in the complex, the splitting for the asymmetric (and chiral) heterometallic cryptand would be quite complex and at a low concentration they might not appear in the spectra. For the symmetric heterometallic cryptand, the ^{1}H NMR resonances for H_b and $H_{b'}$ and H_c and $H_{c'}$ are relatively unchanged from their homometallic analogues, but the resonance for H_a and $H_{a'}$ is split into an AB_q. This is due

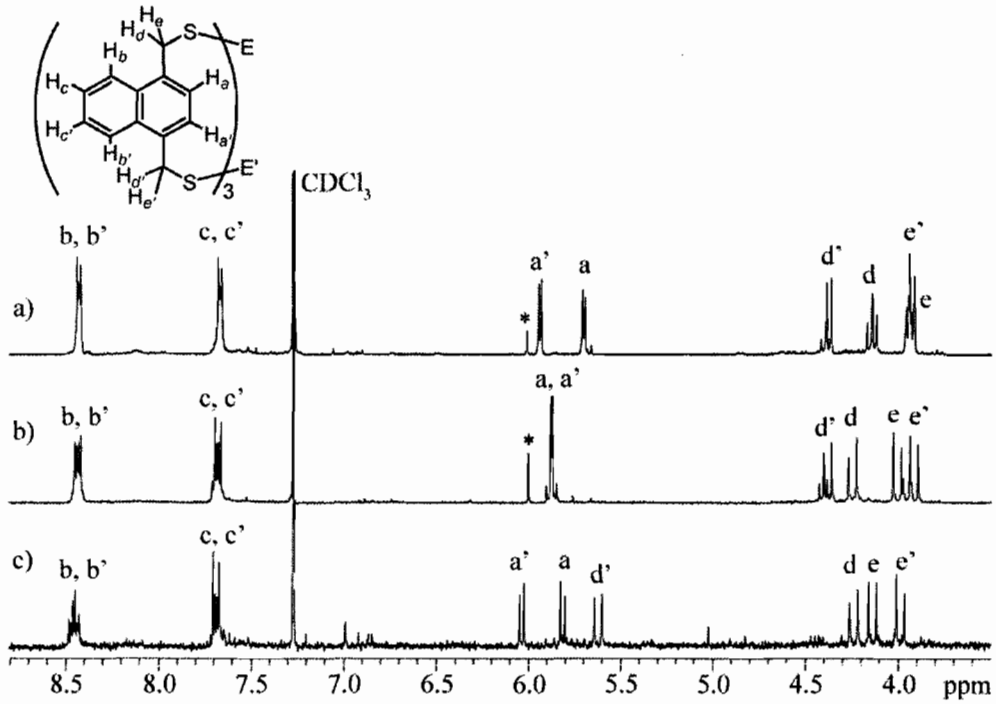

Figure 8. ^{1}H NMR spectra of EE'$\mathbf{L}_3$ heterometallic cryptands: PSb$\mathbf{L}_3$ (a), AsSb$\mathbf{L}_3$ (b), and AsBi$\mathbf{L}_3$ (c). * denotes $Sb_2\mathbf{L}_3$ cryptand impurity.

to the lack of σ_h symmetry in the heterometallic cryptands, making H_a and $H_{a'}$ inequivalent (and diastereotopic due to chirality of assembly). Additionally, the methylene protons at each end of the cryptand appear as separate sets of doublets (or two doublets of doublets for the P end of $PSbL_3$). Each of these resonances is shifted only slightly from where they appear for the homometallic complexes suggesting that in solution, as in the solid state, the geometries around the metals are very similar to what they are for the homometallic complexes.

The heterometallic $EE'L_3$ cryptands are chiral, due to a right-handed or left-handed twist of the ligands around the chirality axis of the two metals. This chirality is different from that in most supramolecular helicates, where both (identical) metals experience the same handedness of the ligands connecting them.[47] Here, the metals experience different handedness, but if the two metals were swapped, one would be left with the enantiomer of the original molecule. While spontaneous resolution of one enantiomer was not obtained upon crystallization, it may be possible to separate the enantiomers on a chiral HPLC column. These cryptands are too small to fit guest molecules, but larger P-containing cryptands may be able to serve as host molecules with potential applications in chiral catalysis. We are exploring their use as a new class of trans-directing phosphine ligands.

Conclusion

A series of homometallic (P_2L_3, As_2L_3, Sb_2L_3, Bi_2L_3) and heterometallic ($PSbL_3$, $AsSbL_3$, $AsBiL_3$) cryptands were prepared directly from H_2L and ECl_3 or by

transmetallation of $Sb_2\mathbf{L}_3$, showing that P, As, Sb, and Bi can be used almost interchangeably in "metal"-directed self-assembly. Within this supramolecular framework, the geometries of P, As, Sb, and Bi with thiolate ligands can be directly compared, giving insight into the bonding preferences of these pnictogens. As expected, the E-S bonds lengthen and the S-E-S bond angles contract down the group. Surprisingly, in solution the homometallic C_{3h}-symmetric $E_2\mathbf{L}_3$ cryptands rearrange into asymmetric conformers ($E_2\mathbf{L}_3$-*asym*). Heterometallic cryptands were prepared in higher than a statistical ratio, implying a self-sorting mechanism. $PSb\mathbf{L}_3$ is a rare example of a chiral trans-directing phosphine and $AsBi\mathbf{L}_3$ is a rare example of a chiral bismuth compound with axial chirality at each pnictogen. This work exemplifies the utility of Group 15 elements as "metals" in metal-directed supramolecular self-assembly.

Experimental Section

General Procedures

^{1}H NMR spectra were measured using Varian INOVA-300 and 500 spectrometers and ^{13}C NMR spectra were collected on a Varian INOVA-500 spectrometer in $CDCl_3$. Spectra were referenced using the residual solvent resonances as internal standards and reported in ppm. Mass spectrometry data were collected by directly injecting a $CHCl_3$ solution of cryptand into the spray chamber. Single crystal X-ray diffraction studies were performed on a Bruker SMART APEX diffractometer. Commercially available reagents were used as received. The reported yields below are for isolated crystals. *Caution: Arsenic and antimony compounds are hazardous and should be handled with care!* (This

accounts for the small scale of the reactions reported herein.) The preparation of 1,4-bis(mercaptomethyl)naphthalene (H_2**L**),[48] P_2**L**$_3$ and As_2**L**$_3$ via transmetallation, and Sb_2**L**$_3$ and Bi_2**L**$_3$ were previously reported.[12]

Synthetic Procedures

AsSbL$_3$. $AsCl_3$ (8.16 μL, 95.6 μmol), $SbCl_3$ (21.8 mg, 95.6 μmol), and diisopropylethylamine (DIPEA) (474 μL, 2.87 mmol) were dissolved in $CHCl_3$ (50 mL) under N_2 at 50 °C. H_2**L** (70.0 mg, 320 μmol) was added and the solution was stirred for 3 hours. After cooling the reaction mixture to 25 °C, it was washed with H_2O (20 mL) and 2 M NaOH (20 mL) and dried with brine (20 mL) and $MgSO_4$. The solution was layered with CH_3CN resulting in clear, colorless needles after 1 day (7.22 mg, 8.09 μmol, 8% crystalline yield). The crystals were dissolved in $CDCl_3$ and the ^{1}H NMR spectrum revealed that the product is 87% AsSb**L**$_3$·CH_3CN and 13% Sb_2**L**$_3$·CH_3CN. ^{1}H NMR (300 MHz, $CDCl_3$): δ 8.43 (m, 6H, C*H*), 7.68 (m, 6H, C*H*), 5.87 (AB*q*, 6H, C*H*, *J* = 7.0 Hz), 4.37 (d, 3H, CH_2, *J* = 13.0 Hz), 4.24 (d, 3H, CH_2, *J* = 13.0 Hz), 3.99 (d, 3H, CH_2, *J* = 13.0 Hz), 3.91 (d, 3H, CH_2, *J* = 13.0 Hz). ^{13}C{^{1}H} NMR (125 MHz, $CDCl_3$): δ = 136.3, 133.6, 132.0, 131.6, 126.43, 126.37, 126.35, 125.9, 125.2, 124.4, 33.8, 32.3 ppm. APCI-MS: $[H\{AsSbL_3\}]^+$ calcd 850.9, found 851.0.

AsBiL$_3$. $AsCl_3$ (11.8 μL, 138 μmol) and $BiCl_3$ (43.5 mg, 138 μmol) were dissolved in dry MeOH (10 mL) and THF (40 mL) and placed under N_2. DIPEA (684 μL, 4.14 mmol) was added, followed by H_2**L** (94.9 mg, 430 μmol) and the solution was stirred at 25 °C overnight. $CHCl_3$ (30 mL) was added, then the mixture was washed with

H_2O (20 mL) and 2 M NaOH (20 mL) and dried with brine (20 mL) and $MgSO_4$. The solution was concentrated to yield a bright yellow solid which was suspended in $CHCl_3$ (10 mL), filtered, and layered with pentane to yield pale yellow needles of $AsBiL_3 \cdot 2CHCl_3$ after a day (12 mg, 10.2 μmol, 7% crystalline yield). ^1H NMR (300 MHz, $CDCl_3$): δ 8.45 (m, 6H, C*H*), 7.68 (m, 6H, C*H*), 6.02 (d, 3H, C*H*, J = 7.0 Hz), 5.80 (d, 3H, C*H*, J = 7.0 Hz), 5.61 (d, 3H, CH_2, J = 12.3 Hz), 4.23 (d, 3H, CH_2, J = 12.8 Hz), 4.13 (d, 3H, CH_2, J = 12.3 Hz), 3.98 (d, 3H, CH_2, J = 12.8 Hz). $^{13}C\{^1H\}$ NMR (125 MHz, $CDCl_3$): δ = 139.1, 133.8, 132.2, 131.5, 126.7, 126.6, 126.5, 125.9, 125.3, 123.2, 33.9, 31.9 ppm. APCI-MS: $[H\{AsBiL_3\}]^+$ calcd 939.0, found 939.1.

$PSbL_3$. Clear, colorless X-ray quality needles of $PSbL_3 \cdot CH_3CN$ were isolated from the previously reported[12] synthesis of P_2L_3 from $Sb_2L_3 \cdot CH_3CN$ with PBr_3. These were dissolved in $CDCl_3$ for further analysis. ^1H NMR (500 MHz, $CDCl_3$): δ 8.43 (m, 6H, C*H*), 7.67 (m, 6H, C*H*), 5.94 (d, 3H, C*H*, J = 6.8 Hz), 5.70 (d, 3H, C*H*, J = 7.2 Hz), 4.37 (d, 3H, CH_2, J = 12.4 Hz), 4.17 (d, 1.5H, CH_2, J = 13.0 Hz), 4.15 (d, 1.5H, CH_2, J = 12.5 Hz), 3.96 (d, 1.5H, CH_2, J = 13.0 Hz), 3.95 (d, 1.5H, CH_2, J = 12.5 Hz), 3.93 (d, 3H, CH_2, J = 12.4 Hz). ^{31}P NMR (500 MHz, $CDCl_3$): δ 86.7 (s). $^{13}C\{^1H\}$ NMR (125 MHz, $CDCl_3$): δ = 136.1, 132.4, 132.2, 131.4, 126.4, 126.3, 126.2, 126.05, 125.8, 124.5, 34.38 (d, $^2J_{CP}$ = 9 Hz), 32.2 ppm. APCI-MS: $[H\{SbPL_3\}]^+$ calcd 807.0, found 807.0.

X-Ray Crystallography

Diffraction intensities for $AsSbL_3$, $AsBiL_3$ and $SbPL_3$ were collected at 173(2) K on a Bruker Apex CCD diffractometer using MoKα radiation λ = 0.71073 Å. Space

groups were determined based on systematic absences. Absorption corrections were applied by SADABS.[49] Structures were solved by direct methods and Fourier techniques and refined on F^2 using full matrix least-squares procedures. All non-H atoms were refined with anisotropic thermal parameters. All H atoms in $AsSbL_3$ and $AsBiL_3$ were refined in calculated positions in a rigid group model. H atoms in $SbPL_3$ were found from the F-map and refined with isotropic thermal parameters. In the crystal structures of $AsSbL_3$ and $SbPL_3$ there were solvent molecules, CH_3CN, disordered over two positions related by a mirror plane. These molecules were isolated in the crystal packing and were not involved in specific interactions with the cryptand molecules. These disordered molecules were treated by SQUEEZE.[50] Corrections of the X-ray data by SQUEEZE (42 and 44 electron/cell, respectively for $AsSbL_3$ and $SbPL_3$) were close to the required values of 44 electrons/cell for two molecules in the full unit cells. In the crystal structure of $AsBiL_3$ there were two solvent $CHCl_3$ molecules. One of these molecules was disordered over two positions related by a mirror plane. The disordered $CHCl_3$ molecule was refined with restrictions; the value of 1.75 Å was used as a target for the C-Cl distances in the refinement. H atoms in the disordered solvent molecules were not taken into consideration. In the structures of $AsSbL_3$ and $SbPL_3$ the Sb/As and Sb/P atoms, respectively, shared two positions related by a mirror plane. The refinement of occupation factors provided a ratio for these atoms: $As_{0.92}Sb_{1.08}$ in $AsSbL_3$ and $Sb_{1.01}P_{0.99}$ in $SbPL_3$. In the structure of $AsBiL_3$, the Bi and As atoms disordered over two symmetrically independent positions. The refinement occupation factors for a model in which the Bi and As atoms shared these two positions provided a ratio for the Bi/Sb

atoms of 0.565/0.435 and 0.417/0.583, respectively for the two positions, and the total ratio was $As_{1.02}Bi_{0.98}$. All calculations were performed by the Bruker SHELXTL (v. 6.10) package.[51]

Crystallographic Information Files will be available from the ACS website after publication at pubs.acs. org.

Crystallographic Data for $AsSbL_3{\cdot}CH_3CN$. $C_{38}H_{33}As_{0.92}NS_6Sb_{1.08}$, M = 896.66, 0.42 × 0.08 × 0.07 mm, T = 173(2) K, hexagonal, space group $P6_3/m$, $a = b =$ 11.4342(7) Å, c = 16.131(2) Å, V = 1826.5(3) $Å^3$, $Z = 2$, D_c = 1.630 Mg/m^3, μ = 2.012 mm^{-1}, $F(000)$ = 899, $2\theta_{max}$ = 54.00°, 18014 reflections, 1387 independent reflections [R_{int} = 0.0574], R_1 = 0.0318, wR_2 = 0.0722 and GOF = 1.108 for 1387 reflections (69 parameters) with $I > 2\sigma(I)$, R_1 = 0.0399, wR_2 = 0.0761 and GOF = 1.108 for all reflections, max/min residual electron density +0.520/-0.226 $eÅ^3$.

Crystallographic Data for $AsBiL_3{\cdot}2(CHCl_3)$. $C_{38}H_{32}As_{1.02}Bi_{0.98}Cl_6S_6$, M = 1177.60, 0.17 × 0.14 × 0.09 mm, T = 173(2) K cubic, space group $P2_13$, $a = b = c =$ 16.4744(8) Å, V = 4471.2(4) $Å^3$, Z = 4, D_c = 1.749 Mg/m^3, μ = 5.344 mm^{-1}, $F(000)$ = 2296, $2\theta_{max}$ = 54.00°, 9348 reflections, 3177 independent reflections [R_{int} = 0.0553], the Flack parameter is 0.037(11), R_1 = 0.0449, wR_2 = 0.1023 and GOF = 1.016 for 3177 reflections (164 parameters) with $I > 2\sigma(I)$, R_1 = 0.0530, wR_2 = 0.1053 and GOF = 1.026 for all reflections, max/min residual electron density +01.089/-0.619 $eÅ^3$.

Crystallographic Data for $SbPL_3{\cdot}CH_3CN$. $C_{38}H_{33}NPS_6Sb$, M = 848.73, 0.32 × 0.10 × 0.09 mm, T = 173(2) K, hexagonal, space group $P6_3/m$, $a = b$ = 11.3830(6) Å, c =

16.1453(18) Å, V = 1811.7(2) Å^3, Z = 2, D_c = 1.556 Mg/m^3, μ = 1.181 mm^{-1}, $F(000)$ = 860, $2\theta_{max}$ = 54.00°, 10291 reflections, 1382 independent reflections [R_{int} = 0.0319], R_1 = 0.0334, wR_2 = 0.0810 and GOF = 1.114 for 1382 reflections (89 parameters) with $I > 2\sigma(I)$, R_1 = 0.0405, wR_2 = 0.0849 and GOF = 1.114 for all reflections, max/min residual electron density +0.726/-0.211 eÅ^3.

Bridge to Chapter VII

Chapters V and VI analyzed the solid-state and solution structures of several Group 15-containing cryptands. Chapter VII will put this chapter into the context of the entire dissertation by tying together the conclusions from all of the previous chapters. It will also give a brief outlook on future directions for the project.

CHAPTER VII

CONCLUSIONS AND FUTURE OUTLOOK

Introduction

A supramolecular approach to toxic ion chelation can give unique insight into the chemistry of that ion. As a worldwide contaminant of human drinking water supplies, arsenic is an important target for chelator design. This dissertation described a supramolecular design strategy for the coordination of arsenic with thiolate ligands. Over the course of this research, much was revealed much about the bonding preferences, kinetics and reactivity of the As(III) ion.

Specifically, Chapters II and III showed that the As···π interaction is strong enough to influence the diastereoselectivity of a self-assembly reaction and affect the preferred bonding geometry of the products. In Chapter IV, As(III)-thiolate bonds were revealed to be kinetically labile on a timescale that allows for effective, albeit slow, self-assembly. The relatively leisurely rate of the self-assembly of $As_2L_2Cl_2$ macrocycles allowed for the characterization of reaction intermediates and oligomeric kinetic mistakes, both of which elude observation and characterization in most transition metal-directed self-assembly reactions. Finally, in Chapters V and VI, the reactivity of arsenic,

along with phosphorus, antimony, and bismuth, was exemplified through a supramolecular transmetallation reaction. Overall, this dissertation has provided insight into the chemistry of the As(III)-thiolate bond, but there is still more to be learned. Here, I will describe several potential future directions.

Potential Future Directions

Transmetallation Reactions

The work described in Chapters V and VI of this dissertation reveal the reactivity of the Group 15 ions, E(III), with thiolate ligands. Transmetallation was found to occur between cryptand congeners establishing the reactivity trends: Bi_2L_3 → Sb_2L_3 → As_2L_3 and Sb_2L_3 → P_2L_3. It is still unclear as to whether As_2L_3 will react with PBr_3 to form P_2L_3 or if As(III)-thiolate bonds are a thermodynamic sink and no reaction will occur. In fact, P_2L_3 may react with $AsCl_3$ to give As_2L_3. Establishment of this reactivity is important from a basic science perspective.

Transmetallation reactions between these cryptands and other metal ions may give access to new assembly stoichiometries. Mercury, lead, zinc, platinum, palladium, gold, cadmium, and tin are all reasonable targets. Additionally, the "transmetallation" with the non-metal phosphorus and the metalloid arsenic suggest that other non-metals may participate equally well in "metal"-directed self-assembly. Some suggestions are selenium, nitrogen, and boron. The differences in preferred bonding geometries of these ions could result in the formation of higher-order assemblies than the E_2L_3 cryptands reported here.

Guest Inclusion

One goal of supramolecular chemistry is to study molecules in isolated environments, such as within host cavities. To date, all of the assemblies prepared by our laboratory have been too small to allow for complete encapsulation of a guest molecule. Several macrocycles have shown partial guest encapsulation and guest identity has been shown to affect the structure of the host (Chapter III). However, complete encapsulation will necessitate the design of larger assemblies or the use of smaller guests.

Lewis basicity decreases down Group 15 as the lone pair of electrons becomes increasingly diffuse and inaccessible. Consequently, complexes containing the heavier elements make for worse ligands toward Lewis acidic ions. However, phosphines are commonly used as ligands for transition metals and the previously discussed transmetallation reaction has allowed for incorporation of P(III) into our assemblies. Still, the cavity of the P_2L_3 assembly is too small to fit most guests. Some targets that may be complementary in size are H^+, Au^+, Cu^+, BH_3, or Ga^+. Preliminary screening suggests no reaction between P_2L_3 and H^+, Cu^+, or BH_3, but Au^+ and Ga^+ show some reaction. Still, preparation of P(III)-containing cryptands with larger cavities may be necessary.

Self-Sorting

The high-yielding preparation of heterometallic cryptands presented in Chapter VI suggests that social self-sorting between metal ions may be occurring during self-assembly. If this is case, then this would be one of only a handful of examples of social

self-sorting and unique in that the metal ions, rather than the ligands, are being selected for. By following the reaction of H_2L, $AsCl_3$, $SbCl_3$, and base by ^1H NMR, Dr. Justin L. Crossland was able to get some preliminary indication that social self-sorting may be kinetic, but the loss of reactants to an uncharacterized coordination polymer made it impossible to draw any final conclusions. It would be very interesting to monitor this experiment under conditions that favor discrete species formation over polymerization (lower concentration and higher temperatures) and follow the product distribution.

APPENDIX A

ADDITIONAL NMR SPECTROSCOPY AND MALDI MASS SPECTROMETRY DATA FOR THE SELF-ASSEMBLY OF $As_2L_2Cl_2$ MACROCYCLES

This appendix contains the ^1H NMR spectra and MALDI Mass Spectrometry data for the self-assembly of $As_2\mathbf{L^b}_2Cl_2$ macrocycle from Chapter IV. This co-authored material was previously published as Supporting Information (*Chemical Comunications* **2009**, 5606-5608, © Royal Society of Chemistry).[1] Dr. Timothy G. Carter performed all MALDI mass spectrometry experiments and I performed all NMR spectroscopy experiments.

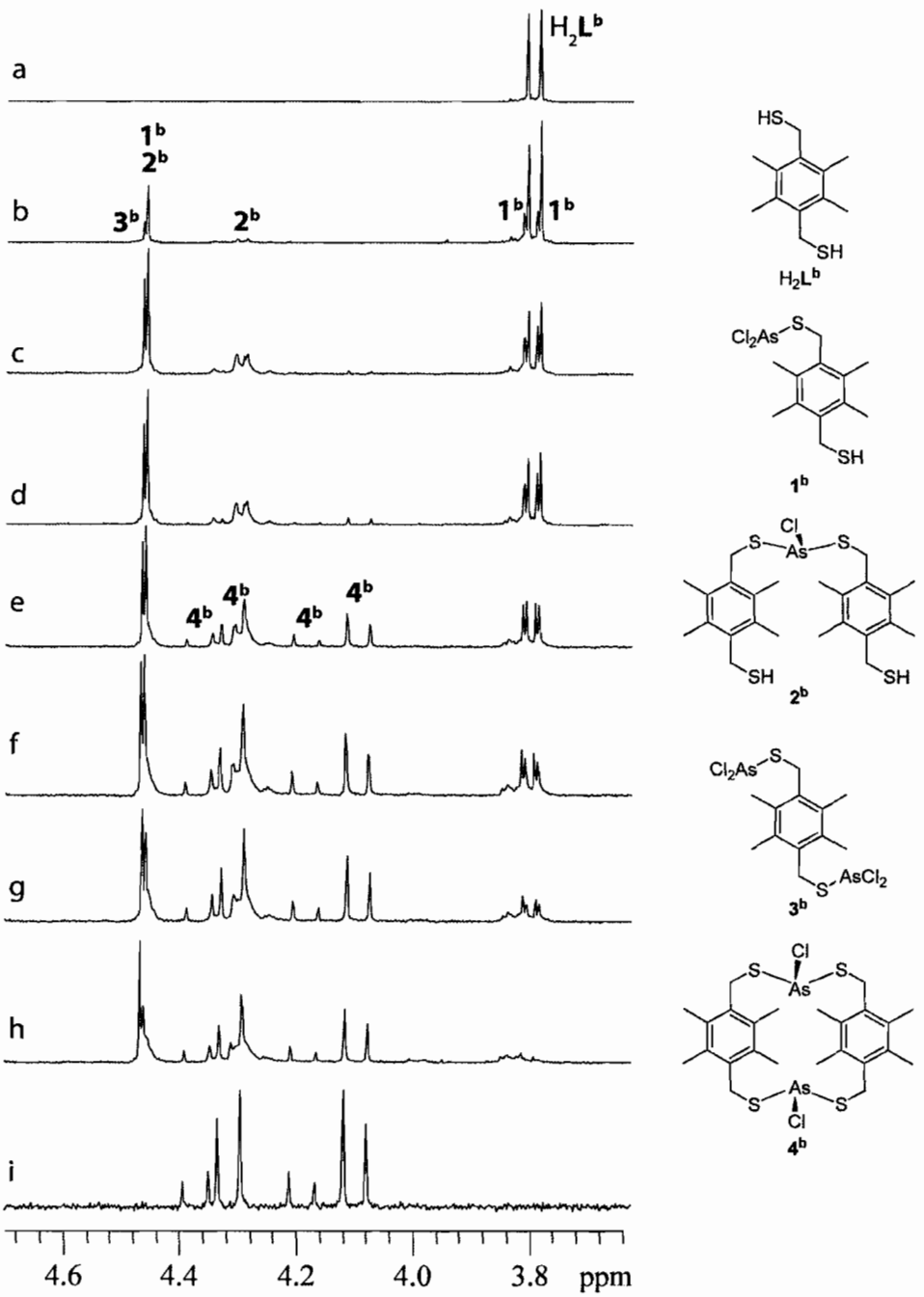

Figure 1. CH_2 region of ^1H NMR spectra of reaction of $H_2\mathbf{L}^b$ with $AsCl_3$ after 0 (a), 4 (b), 75 (c), 147 (d), 1559 (e), 2666 (f), 3995 (g), and 8395 (h) minutes. Dissolved crystals of $As_2\mathbf{L}^b{}_2Cl_2$ (**4b**) (i).

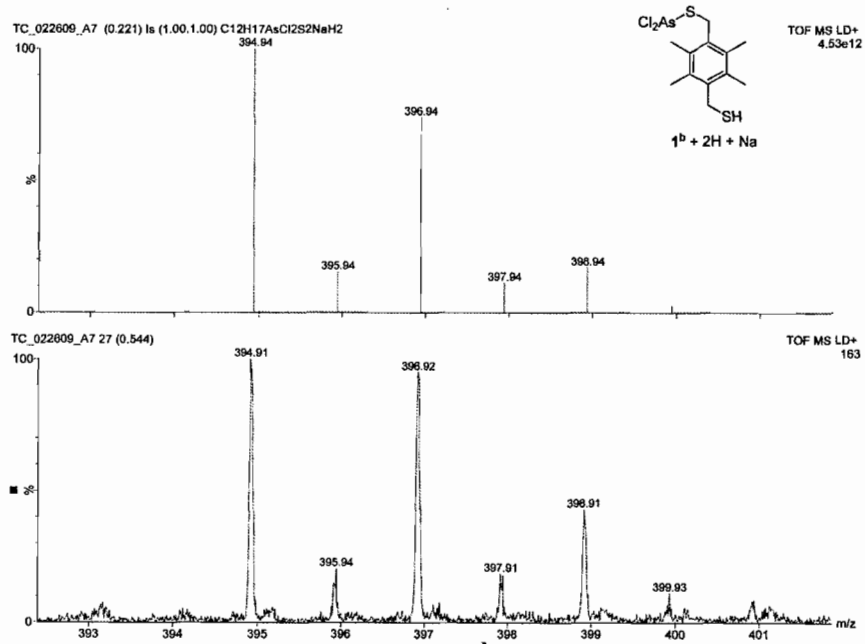

Figure 2. MALDI mass spectrometry data for $\mathbf{1^b}$. Predicted data shown on top and actual data shown on the bottom.

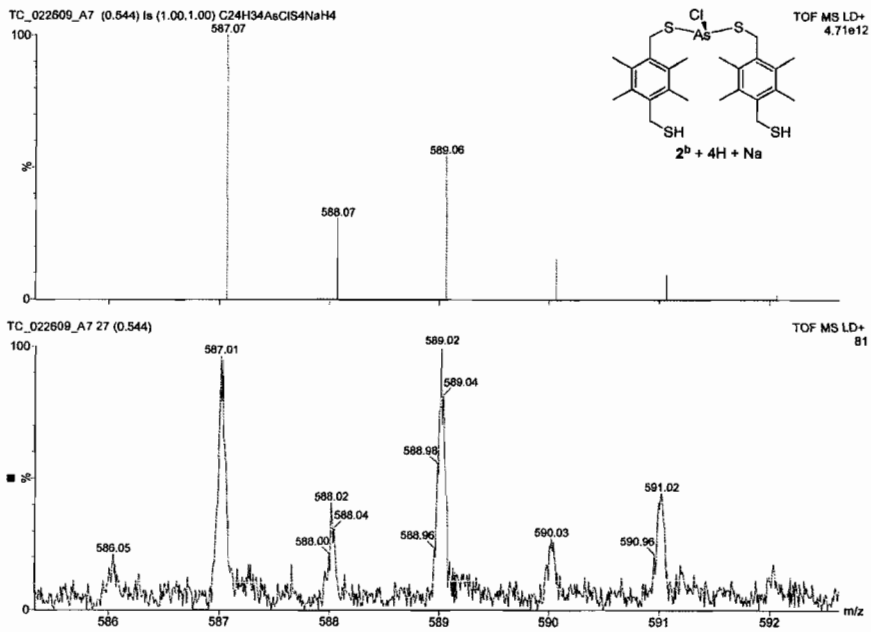

Figure 3. MALDI mass spectrometry data for $\mathbf{2^b}$. Predicted data shown on top and actual data shown on the bottom.

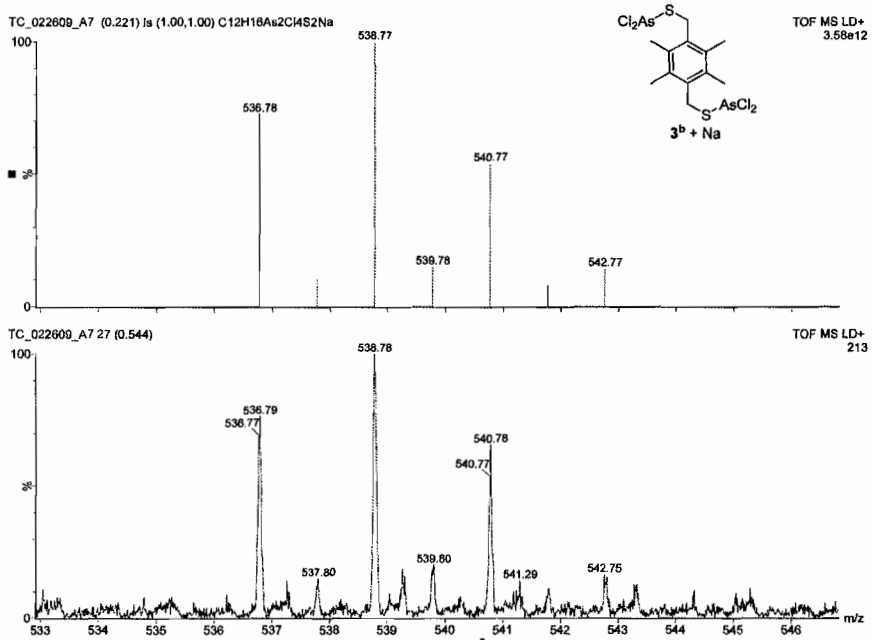

Figure 4. MALDI mass spectrometry data for 3^b. Predicted data shown on top and actual data shown on the bottom.

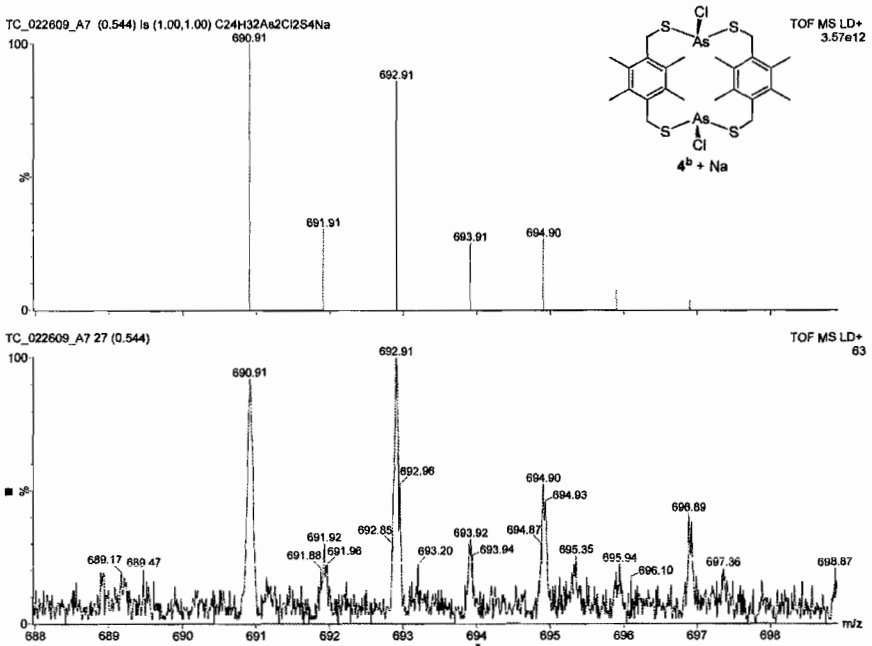

Figure 5. MALDI mass spectrometry data for 4^b. Predicted data shown on top and actual data shown on the bottom.

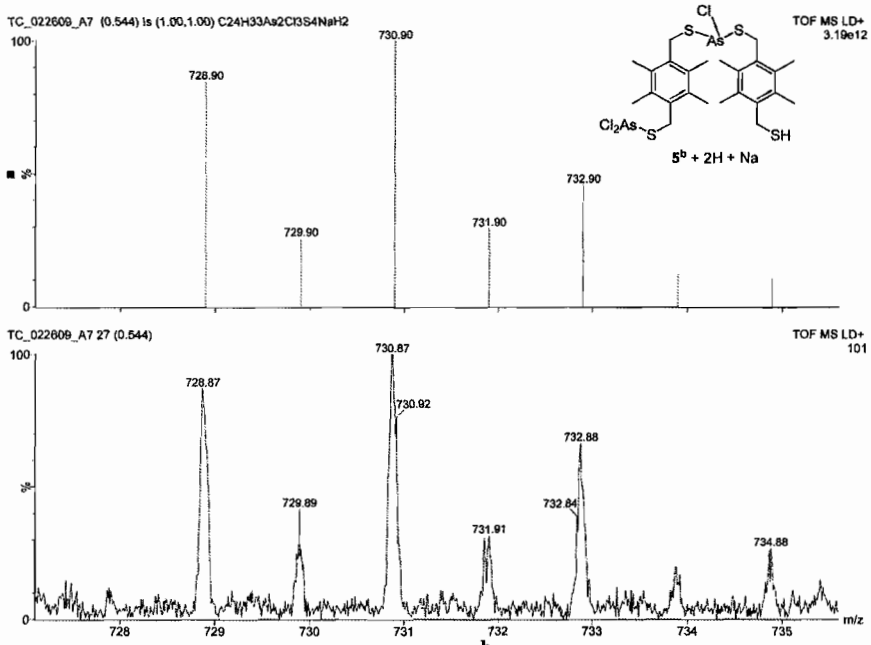

Figure 6. MALDI mass spectrometry data for **5**[b]. Predicted data shown on top and actual data shown on the bottom.

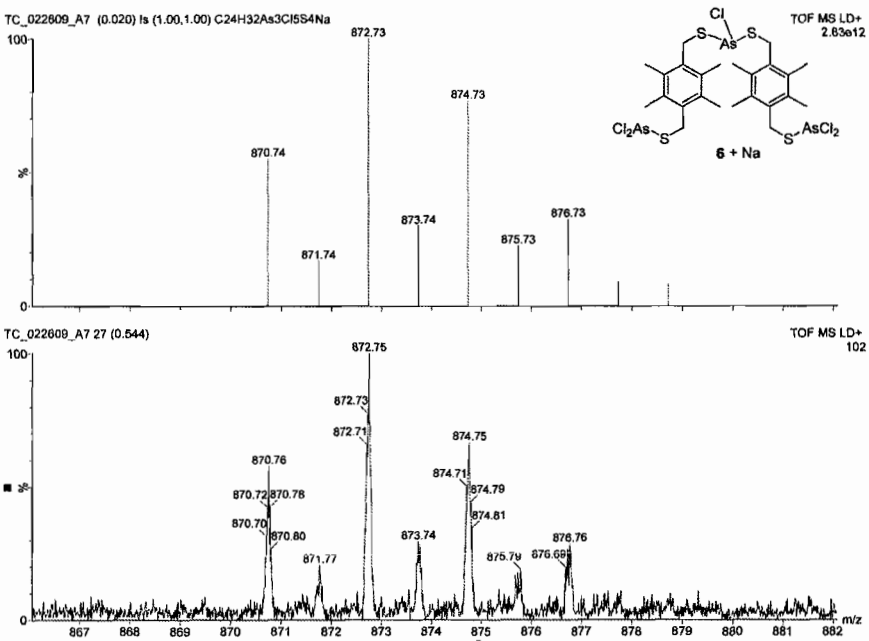

Figure 7. MALDI mass spectrometry data for **6**[b]. Predicted data shown on top and actual data shown on the bottom.

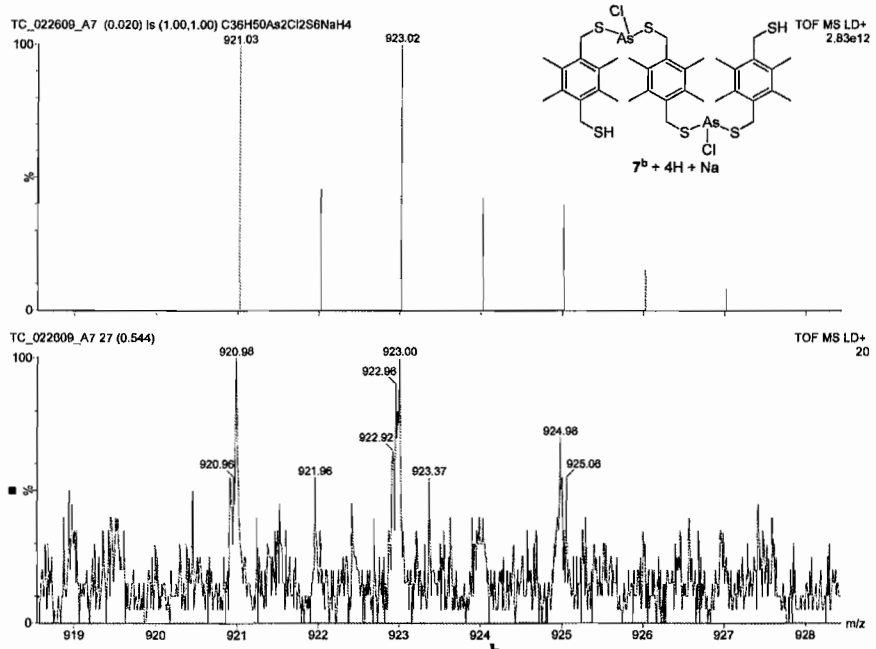

Figure 8. MALDI mass spectrometry data for 7^{b}. Predicted data shown on top and actual data shown on the bottom.

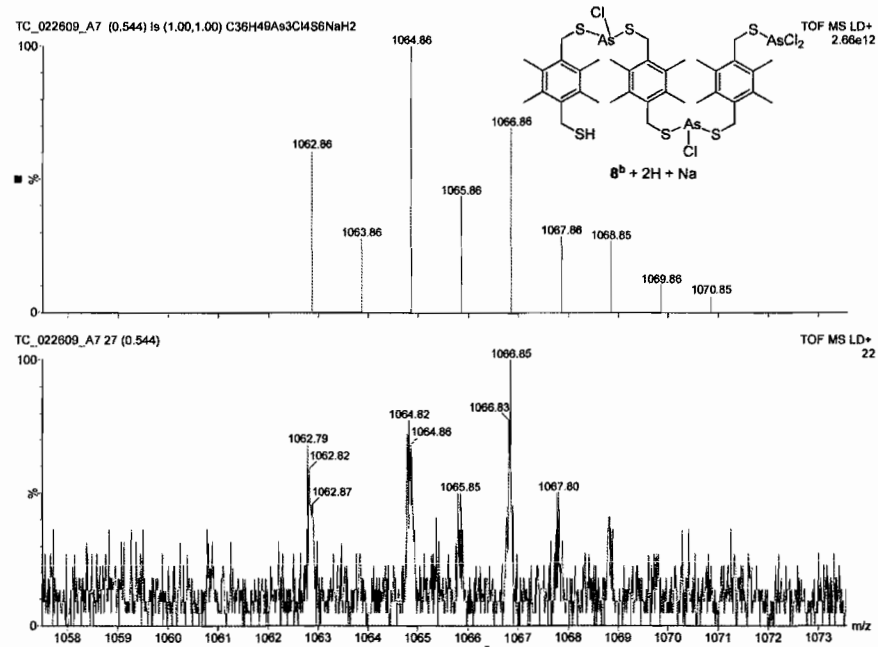

Figure 9. MALDI mass spectrometry data for 8^{b}. Predicted data shown on top and actual data shown on the bottom.

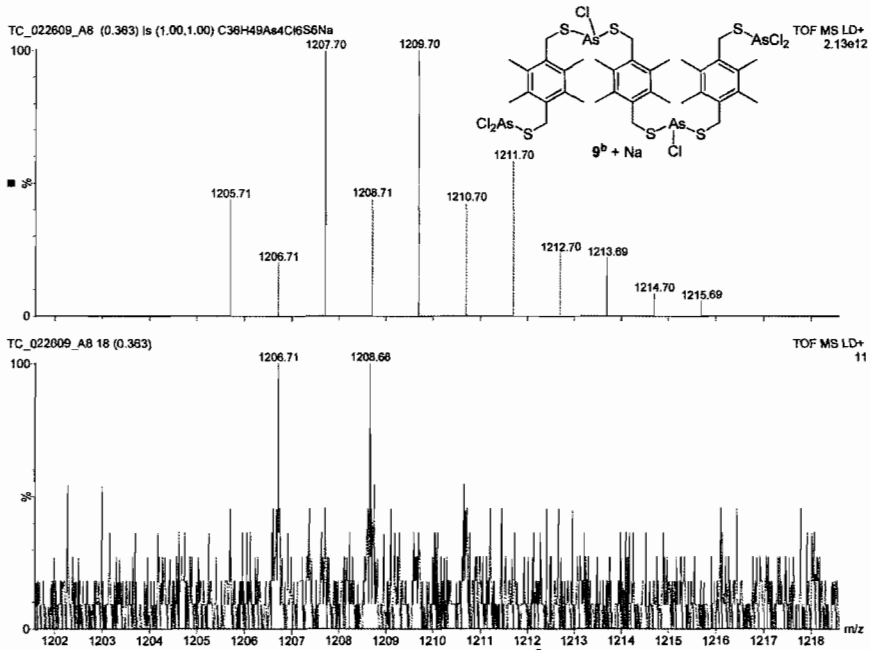

Figure 10. MALDI mass spectrometry data for **9**[b]. Predicted data shown on top and actual data shown on the bottom.

APPENDIX B

SUPPLEMENTARY DATA FOR THE CHARACTERIZATION OF GROUP 15-CONTAINING CRYPTANDS

This appendix contains the co-authored supplementary data from Chapter VI and has been submitted for publication in *Inorganic Chemistry*.[1] Dr. Timothy G. Carter performed the electrospray mass spectrometry experiment on Sb_2L_3 and Sb_2L_3-*asym*. Dr. Justin L. Crossland performed all other mass spectrometry characterization and ^{13}C NMR spectroscopy. Dr. Lev N. Zakharov carried out all X-ray diffraction experiments. Professor Darren W. Johnson provided intellectual and editorial contributions. I carried out all ^{1}H NMR, DFT calculations, searches of the Cambridge Structural Database, synthesis, and crystal growth.

Cambridge Structural Database (CSD) Searches

Several comprehensive searches of the Cambridge Structural Database (CSD) were carried out to establish structural parameters for Group 15 complexes.

CSD Search for E-S complexes

A CSD search for complexes containing Group 15 elements with three thiolate bonds was carried out (Chart 1). The data from this search was used to establish the CSD average E-S distances and S-E-S angles reported in Chapter VI. Refcodes for structures used in determining these averages are reported in Table 1. Searches were performed using ConQuest version 1.10 with CSD database version 5.29 updates (Jan 2008). The following filters were applied to each search: not disordered, no errors, and no powder structures. The substructures $E(SC)_3$ (E = P, As, Sb, Bi) were searched for (Chart 1). The E atoms were constrained to only 3 bonds. Only structures with three separate ligands were analyzed; macrocyclic structures were discarded due to ring strain. Each E-S bond distance and S-E-S bond angle was measured and the results were averaged.

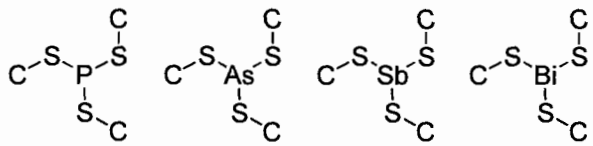

Chart 1. $E(SC)_3$ structures.

Table 1. Refcodes From the Cambridge Structural Database Included in the Structural Survey Used to Determine Average E-S Distances and S-E-S Angles.

P	As		Sb		Bi
CUMLIF	ASMTBZ02	DEDLUT	CIBKAZ	XIHNIL	OKOSAI
DOYXAQ	ASXANT	IBAYAM	CIBKAZ01	XIHNIL	YUKRUR
ETCBPS	ASXANT01	JACMUW	CIDWIV	YUSFUN	ZAHDUH
JUFROR	BOZFIF	JACNAD	CUYKIQ	ZAZYII	ZUMSAB
SEJRUU	BOZFIF01	NEJRAW	SQNLSB10	ZAZYOO	ZUMSAB
SEJRUU01	BOZFIF02	QIFKIZ	TIDGOC		ZUMSAB
SEJRUU02	BOZFIF02	QIFLAS	TIDHAP		ZUMSAB
TCBMPH	CATJOW	ULICAT	TIDHAP		ZUMSEF
TCBMPH	CUBVIE	ZAHDIV	XAVYEY		ZUMSEF

CSD Search for P···π Contacts

The second CSD search carried out was to establish if there was a directional preference for close contacts between phosphorus and aryl rings. The refcodes for the structures used are reported in Table 2. No directional preference was found, suggesting that there is no favorable interaction between phosphorus and aryl rings. The search was performed using ConQuest version 1.10 with CSD database version 5.29 updates (Jan 2008). The following filters were applied to each search: not disordered, no errors, and no powder structures. The searches screened for C_6-arene rings and neutral, three-coordinate phosphorus with intermolecular contacts that were shorter than the sum of the van der Waals radii (1.70 Å for aryl C + 1.80 Å for P = 3.50 Å). Structures were excluded if the phosphorus atom was bonded to another phosphorus or metal, charged, or part of a cluster. After excluding one structure, there were 20 hits. No correlation was found between the bond angle and distance.

Table 2. Refcodes From the Cambridge Structural Database Included in the Structural Survey.

Phosphorus			
BAVRIZ	CEWGIU	IQIMEA	WOPJOA
BILVIB	CIGJOR	JOBFUB	YEQDEE
BUFZIL	FAGLII	NETNEF	ZEWWAZ
BUSLEG	HUMRAI	PAMWIJ	GIHTOH
CAYLAP	ICULIC	WOJMOX	SIHVEL

NMR Experiments

Several ^{1}H NMR experiments were carried out to established the solution structures of E_2L_3 cryptands. By dissolving crystals of the cryptands in chloroform and waiting until the samples had reached equilibrium, it was observed that two species were present in solution: the symmetric E_2L_3 cryptand and E_2L_3-*asym* (Figure 1).

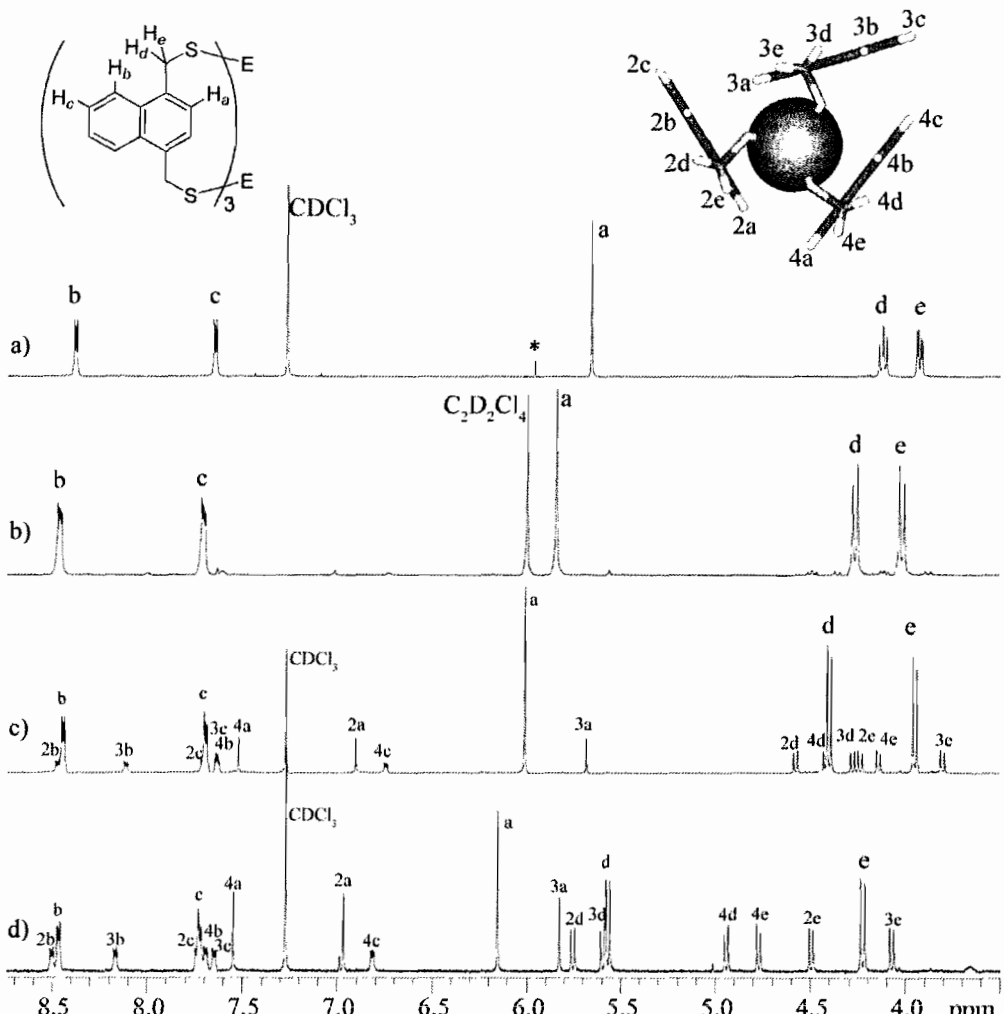

Figure 1. Fully labeled ^{1}H NMR spectra for P_2L_3 (a), As_2L_3 (b), Sb_2L_3 (c) and Bi_2L_3 (d). The resonances for the symmetric cryptand are labeled with letters and the resonances corresponding to the asymmetric cryptand are labeled with numbers and letters. * denotes $C_2H_2Cl_4$ in the spectrum.

Sb_2L_3 Cryptands

In order to identify which protons belonged to which ligand in the Sb_2L_3 cryptands, *g*-COSY (Figure 2) and NOESY (Figures 3-7) experiments were carried out.

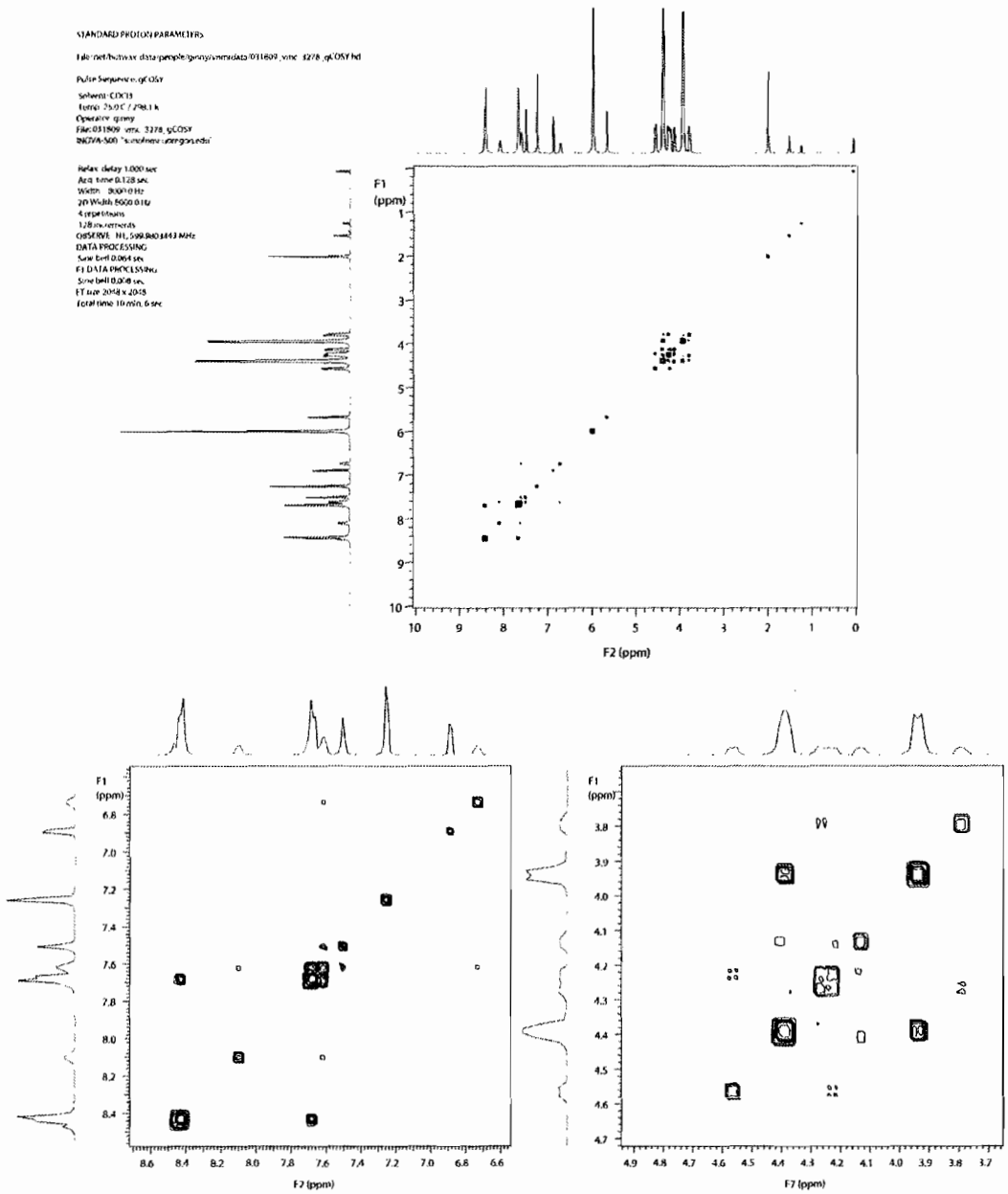

Figure 2. *g*COSY spectra for Sb_2L_3 in $CDCl_3$: full spectrum (top), CH region (bottom left), CH_2 region (bottom right). See Figure 1c for labeling scheme.

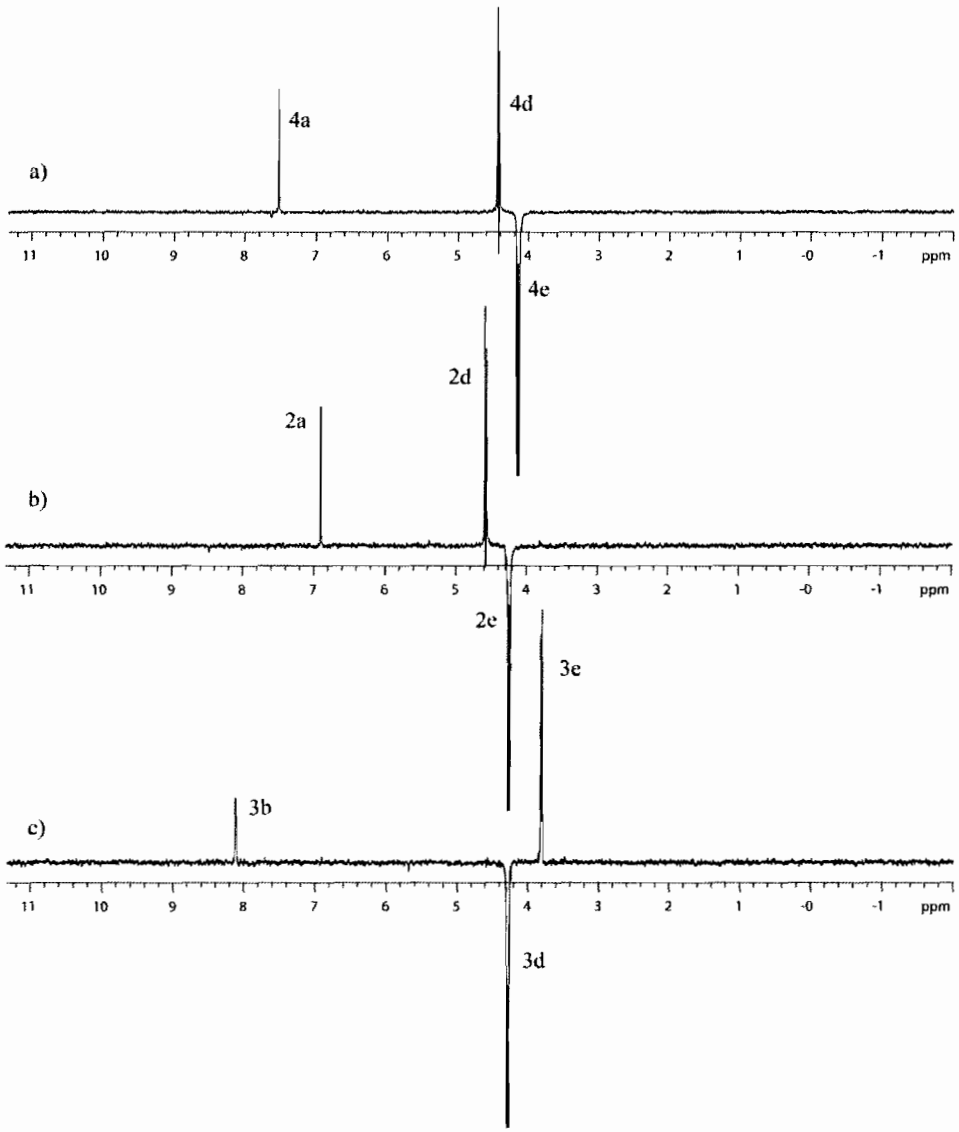

Figure 3. 1D NOESY spectra for $Sb_2\mathbf{L_3}$ in $CDCl_3$ with irradiation of the following protons: 4e (a), 2e (b), and 3d (c). See Figure 1c for labeling scheme.

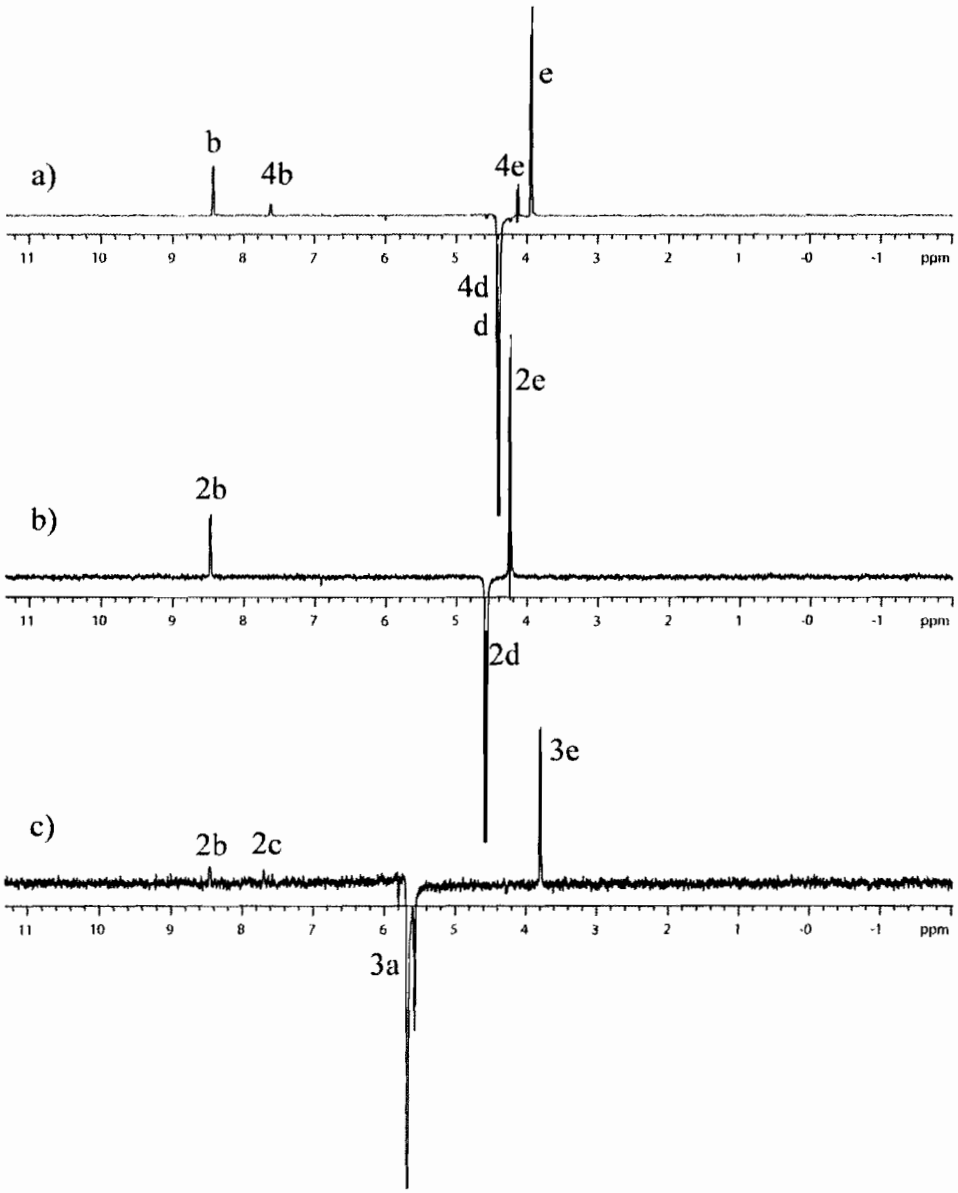

Figure 4. 1D NOESY spectra for Sb_2L_3 in $CDCl_3$ with irradiation of the following protons: d and 4d (a), 2d (b), and 3a (c). See Figure 1c for labeling scheme.

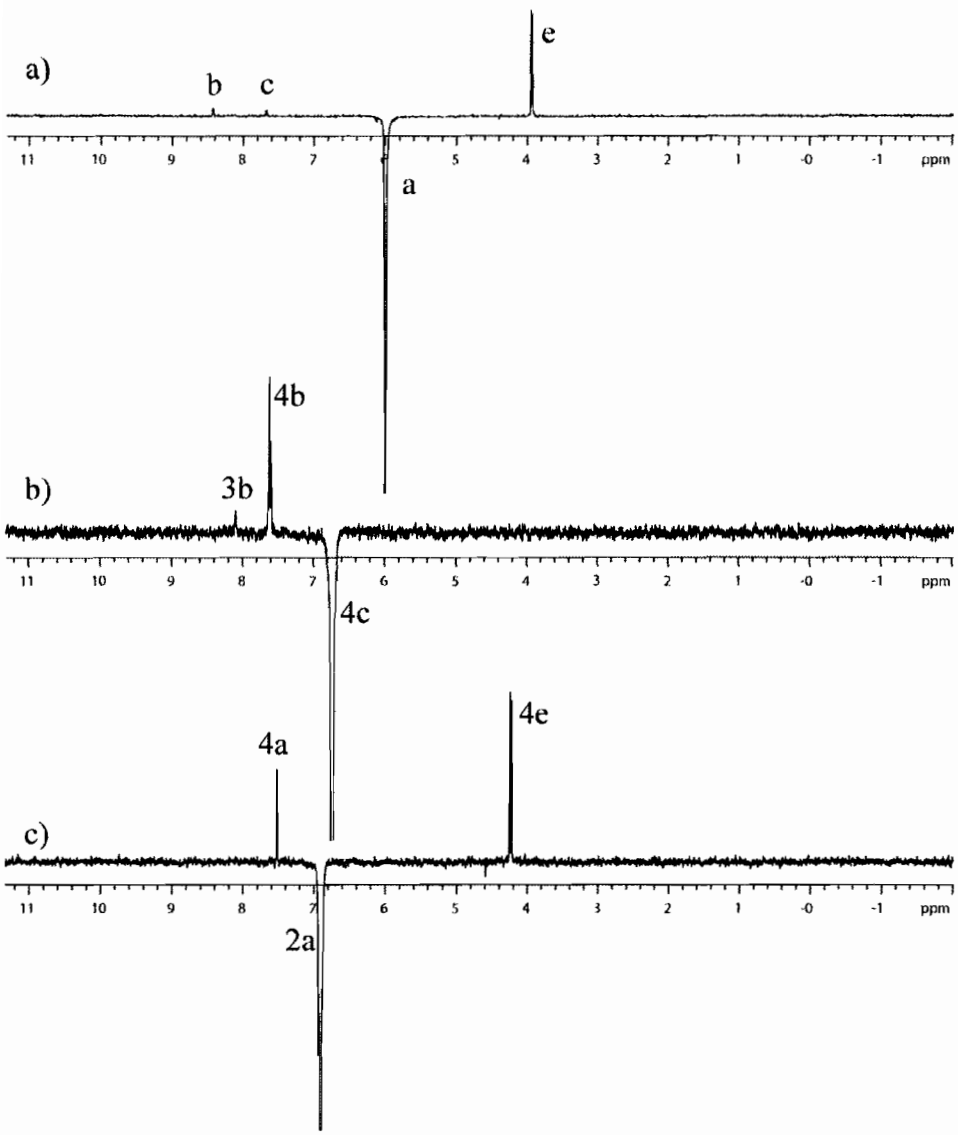

Figure 5. 1D NOESY spectra for Sb_2L_3 in $CDCl_3$ with irradiation of the following protons: a (a), 4c (b), and 2a (c). See Figure 1c for labeling scheme.

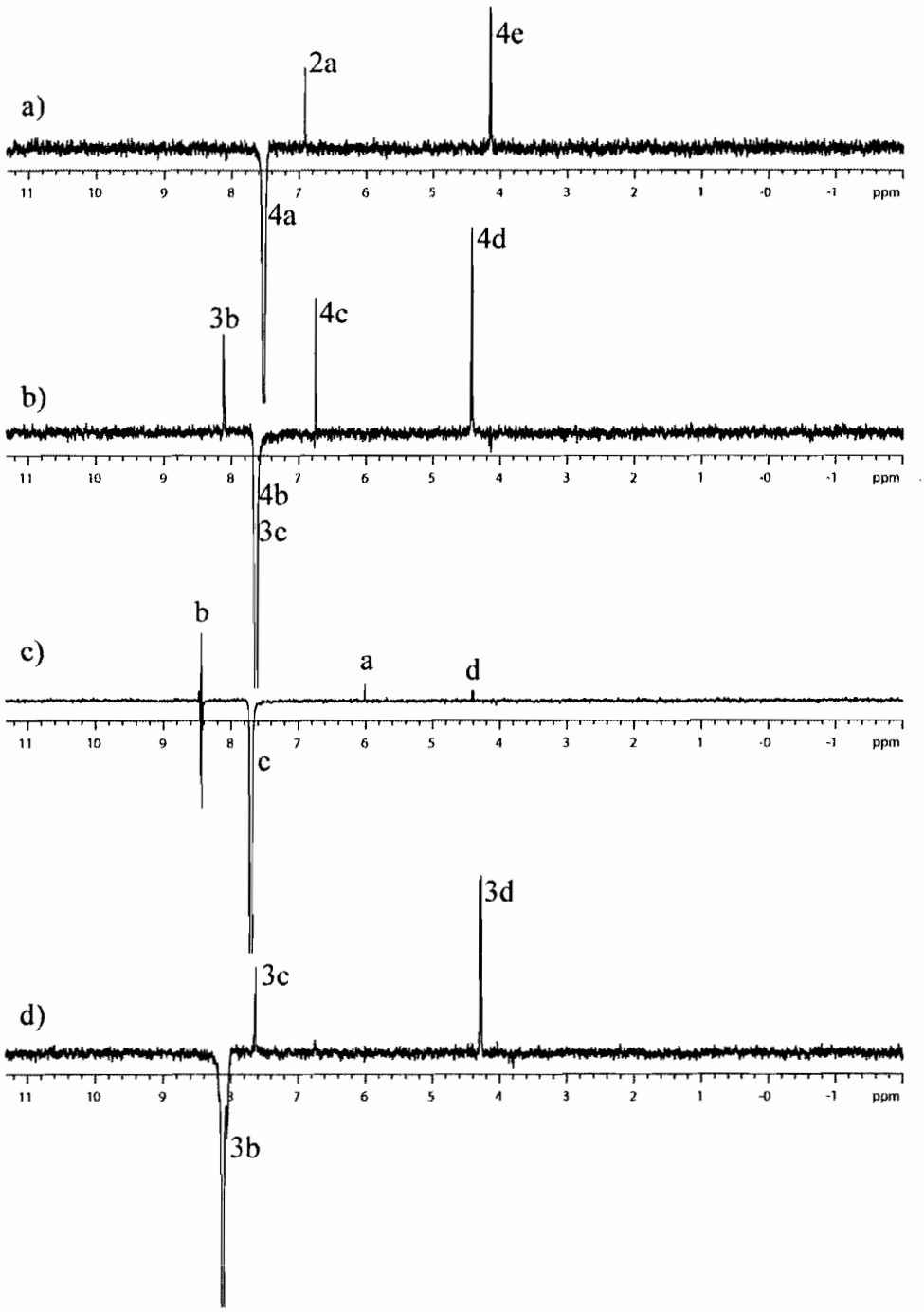

Figure 6. 1D NOESY spectra for Sb_2L_3 in $CDCl_3$ with irradiation of the following protons: 4a (a), 4b and 3c (b), c (c), and 3b (d). See Figure 1c for labeling scheme.

Bi_2L_3 Cryptands

In order to identify which protons were part of which ligand in Bi_2L_3, *g*-COSY (Figures 7) and NOESY (Figures 8 and 9) experiments were carried out.

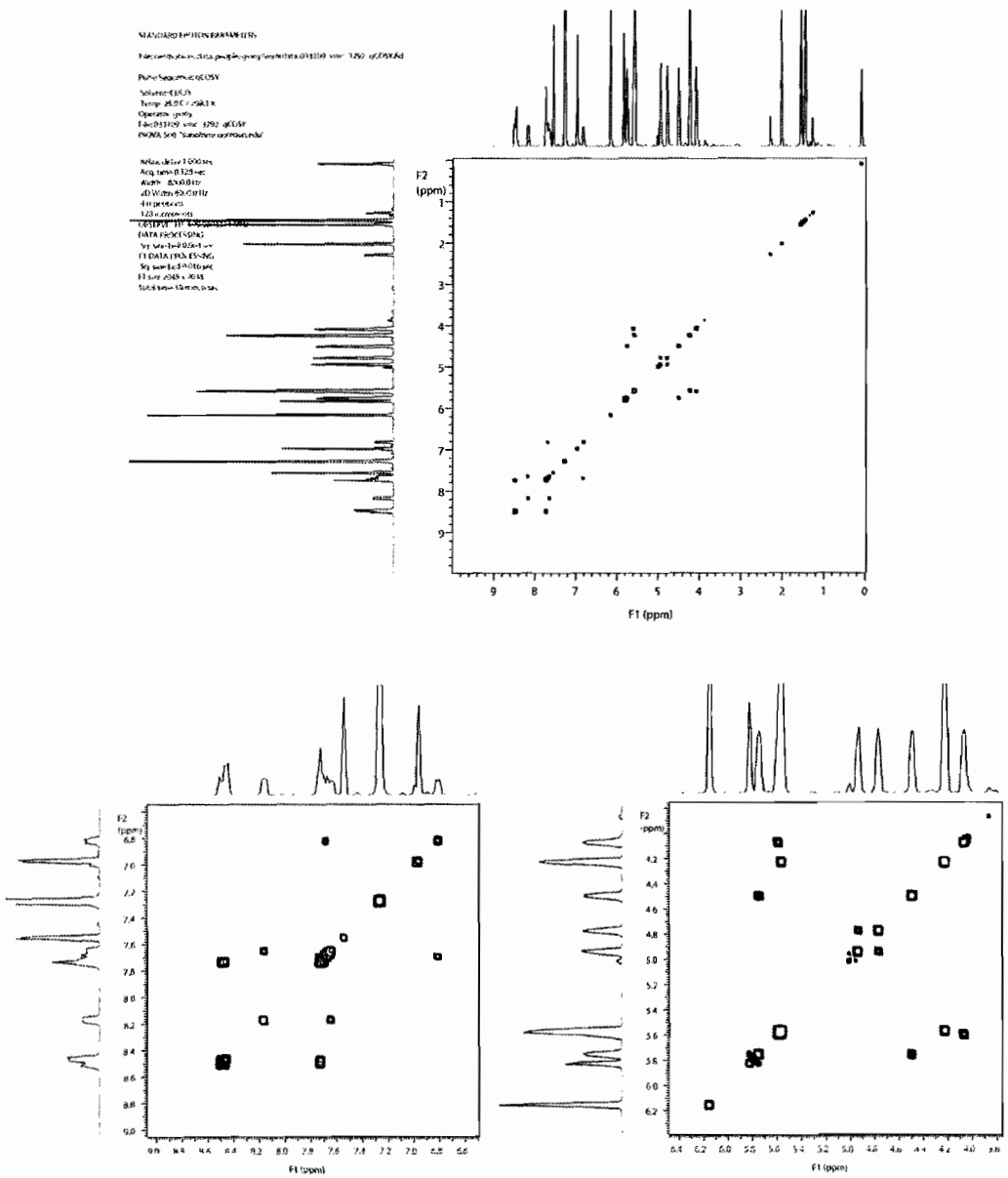

Figure 7. *g*COSY spectra for Bi_2L_3 in $CDCl_3$: full spectrum (top), CH region (bottom left), CH_2 region (bottom right). See Figure 1c for labeling scheme.

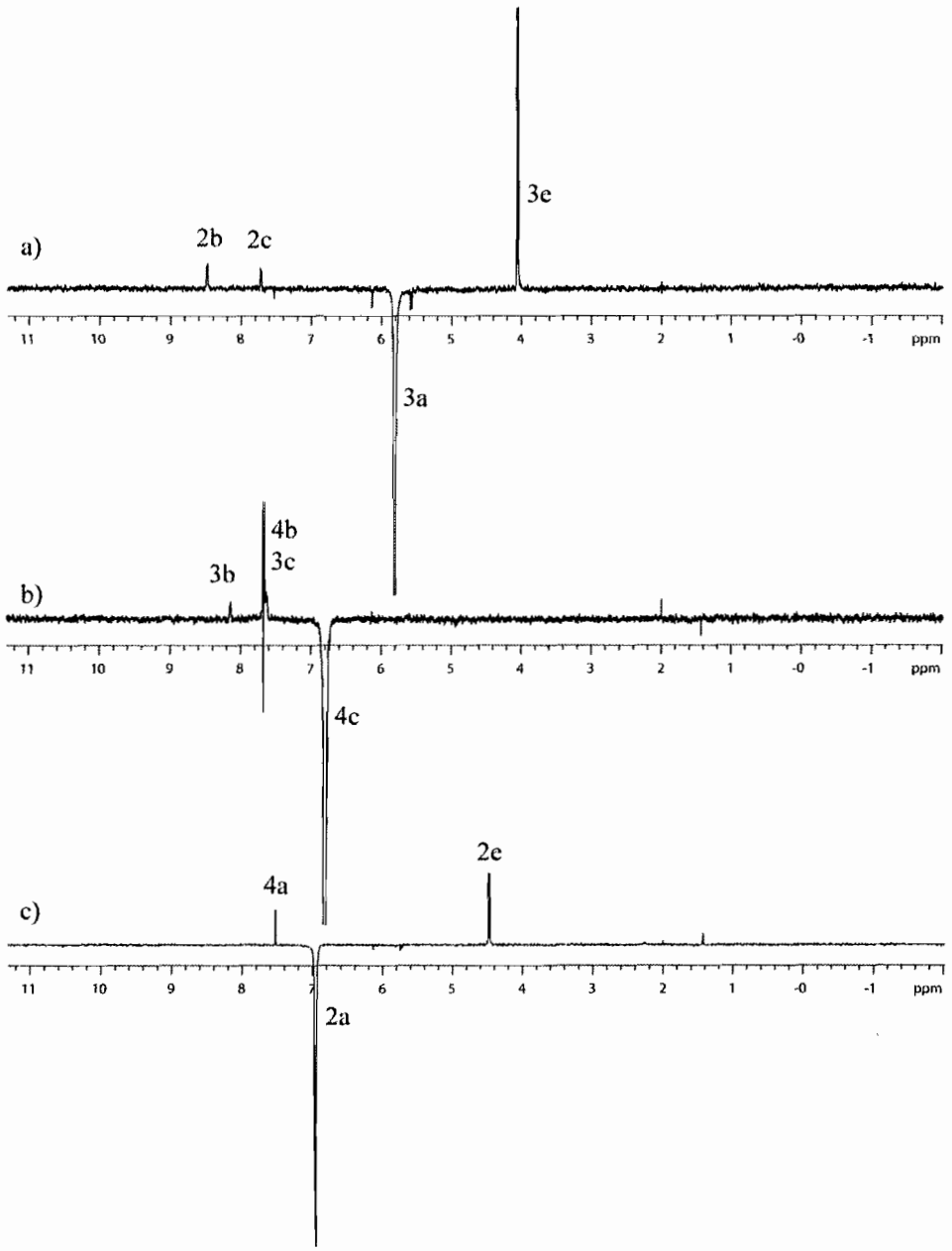

Figure 8. 1D NOESY spectra for $Bi_2\mathbf{L}_3$ in $CDCl_3$ with irradiation of the following protons: 3a (a), 4c (b), and 2a (c). See Figure 1d for labeling scheme.

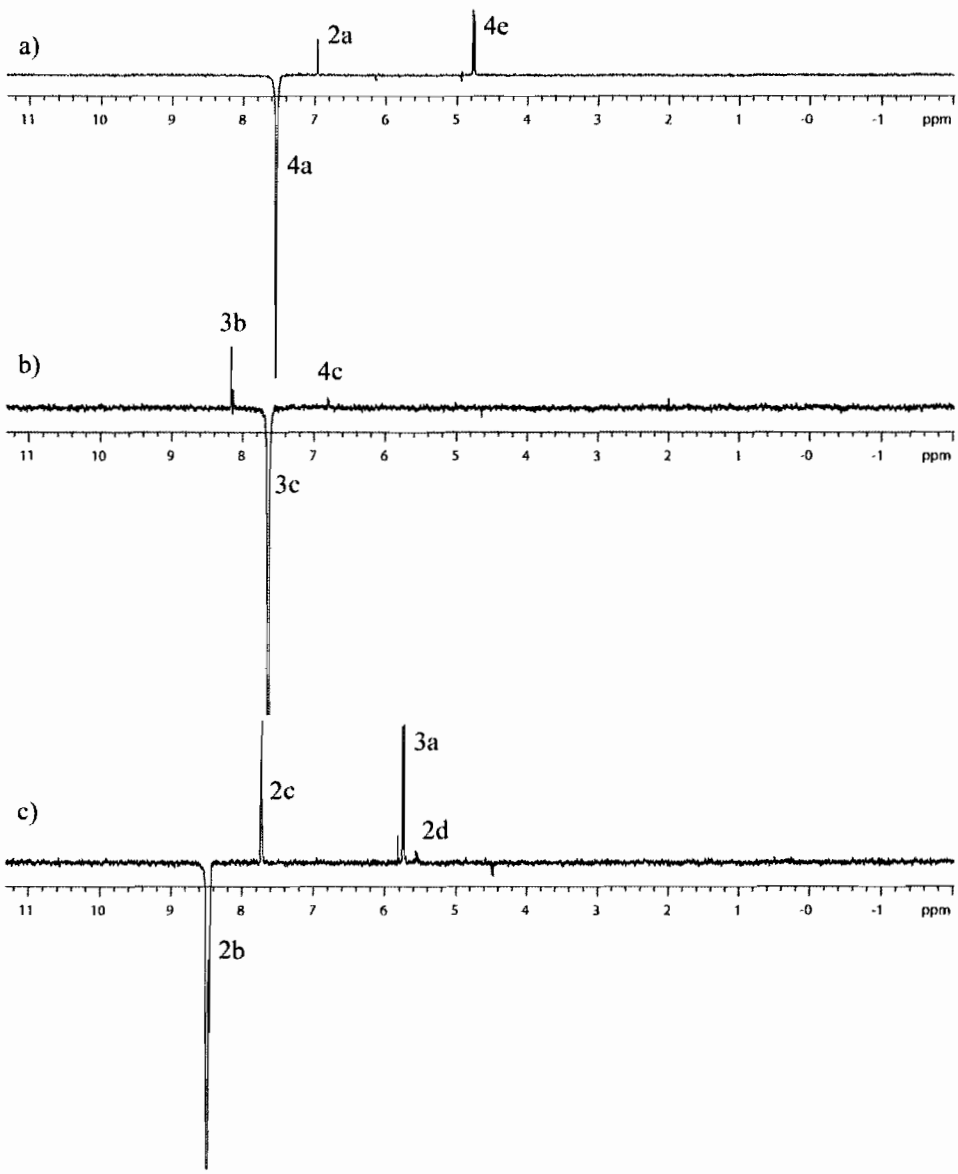

Figure 9. 1D NOESY spectra for Bi_2L_3 in $CDCl_3$ with irradiation of the following protons: 4a (a), 3c (b), and 2b (c). See Figure 1d for labeling scheme.

Phosphorus NMR

Routine characterization of $PSbL_3$ included ^{31}P NMR (Figure 10).

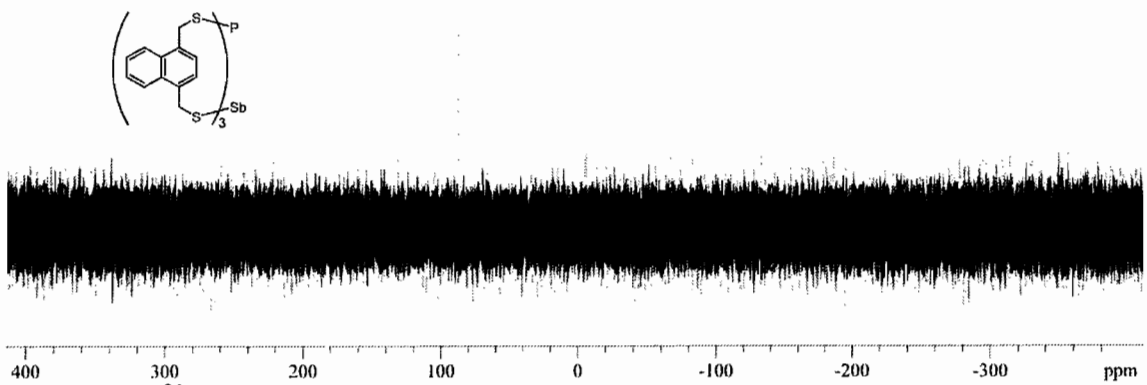

Figure 10. ^{31}P NMR spectrum for $PSbL_3$, externally referenced to H_3PO_4 (0 ppm).

Density Functional Theory Calculations

Density Functional Theory (DFT) calculations were carried out on the symmetric (Figures 11 and 12) and asymmetric cryptand structures (Figure 13). The energies derived from these calculations are reported in Table 3.

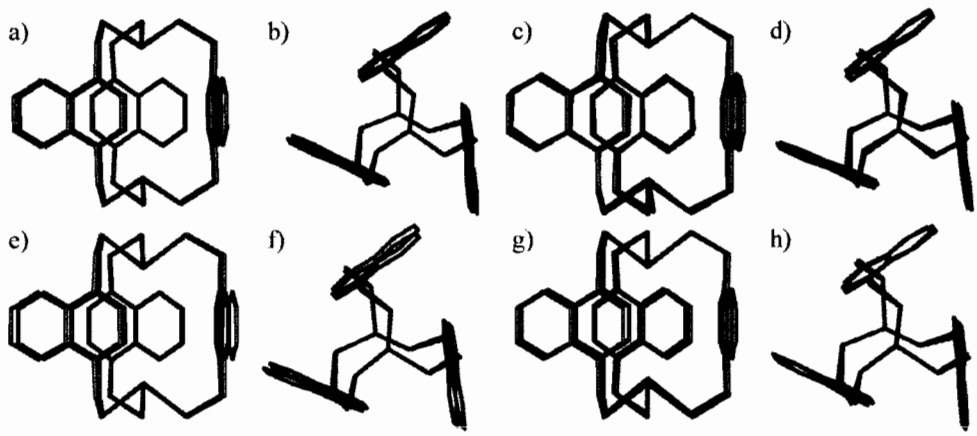

Figure 11. Overlayed stick-representations of the X-ray crystal structures (blue) and DFT-calculated structures (red) of P_2L_3 (a,b), As_2L_3 (c,d), Sb_2L_3 (e,f) and Bi_2L_3 (g,h).

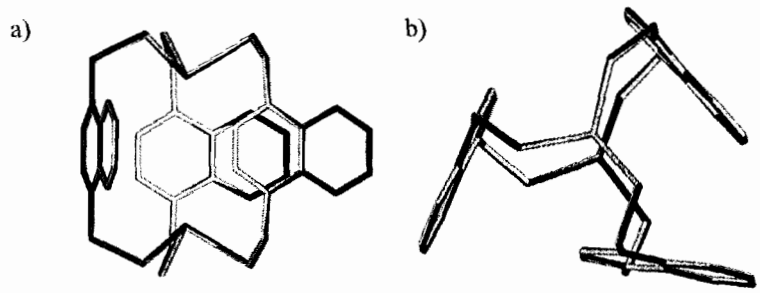

Figure 12. Overlayed stick-representations of the DFT-calculated structures of Sb_2L_3 (teal) and Bi_2L_3 (blue) from side (a) and top (b).

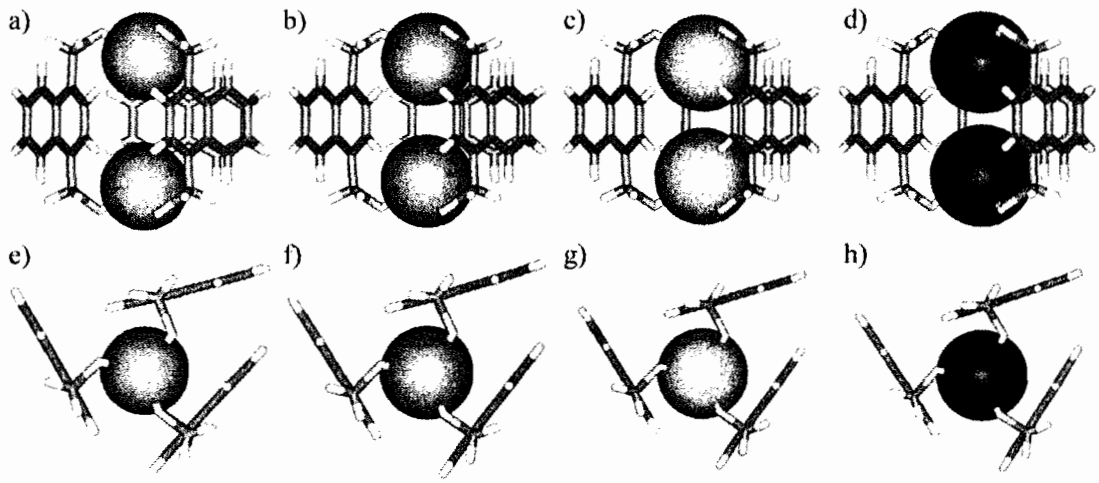

Figure 13. DFT-calculated structures of P_2L_3-*asym* (a,e), As_2L_3-*asym* (b,f), Sb_2L_3-*asym* (c,g) and Bi_2L_3-*asym* (d,h).

Table 3. Energies Derived From DFT-Calculations and ^{1}H NMR Spectroscopy Experiments for Symmetric and Asymmetric E_2L_3 Cryptands.

	DFT Calculations			^{1}H NMR Experiments			
Cryptand	Energy *sym* (kcal/mol)	Energy *asym* (kcal/mol)	Energy dif. (ΔG) (kcal/mol)	Eq. *sym*	Eq. *asym*	Ratio	ΔG_{calc} (kcal/mol)
P_2L_3	-2799891.361	-2799884.752	-6.6083	1	0	NA	NA
As_2L_3	-2379204.541	-2379199.236	-5.30559	60	3	0.5	0.148588
Sb_2L_3	-2378314.07	-2378310.028	-4.04242	0.53	0.47	0.89	0.005959
Bi_2L_3	-2378372.83	-2378368.762	-4.06814	2	3	1.5	-0.02011

Mass Spectrometry Experiments

Liquid Chromatography Mass Spectrometry experiments were carried out on the Sb_2L_3 cryptand to show that two species were present in solution with the same mass-to charge ratio (Figure 14). Routine Electrospray Mass Spectrometry was carried out on all of the heterometallic cryptands (Figures 15-17).

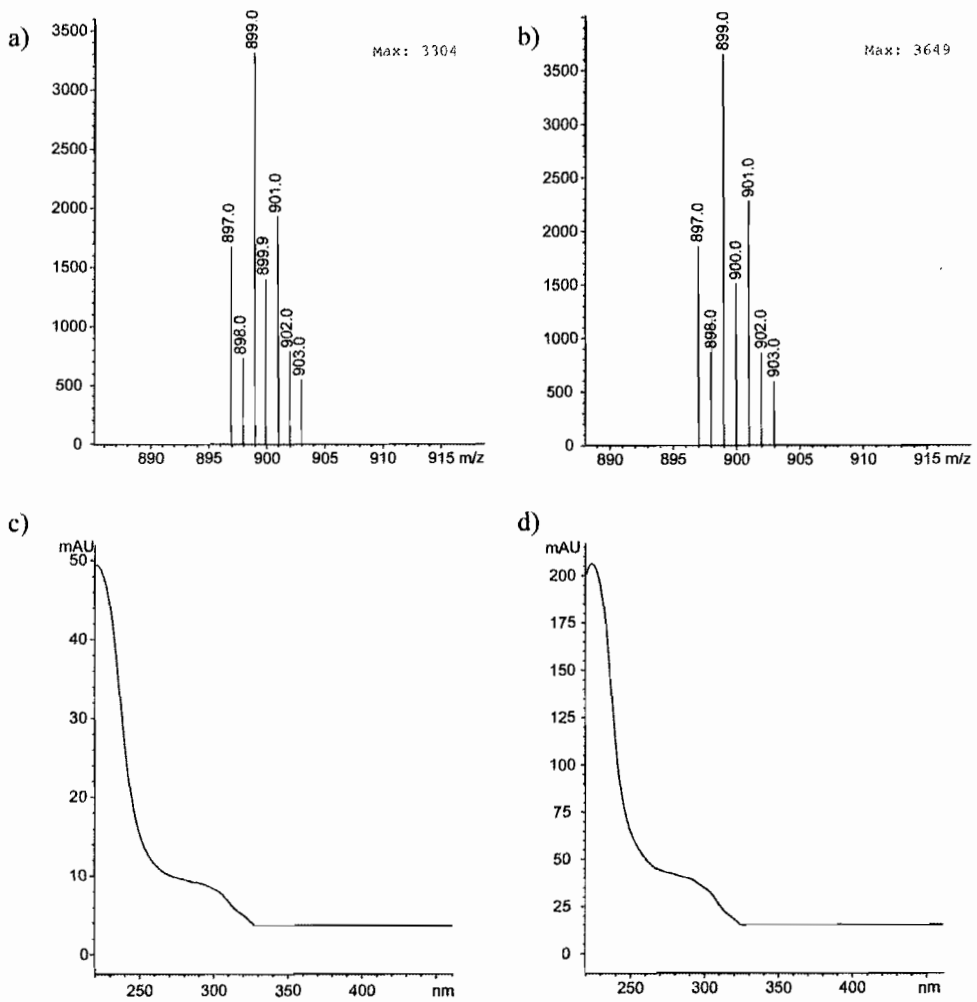

Figure 14. Liquid chromatography mass spectrometry data for $[Sb_2L_3+H]^+$ showing that symmetric and asymmetric cryptands have identical masses (a,b) and UV/vis spectra (c,d).

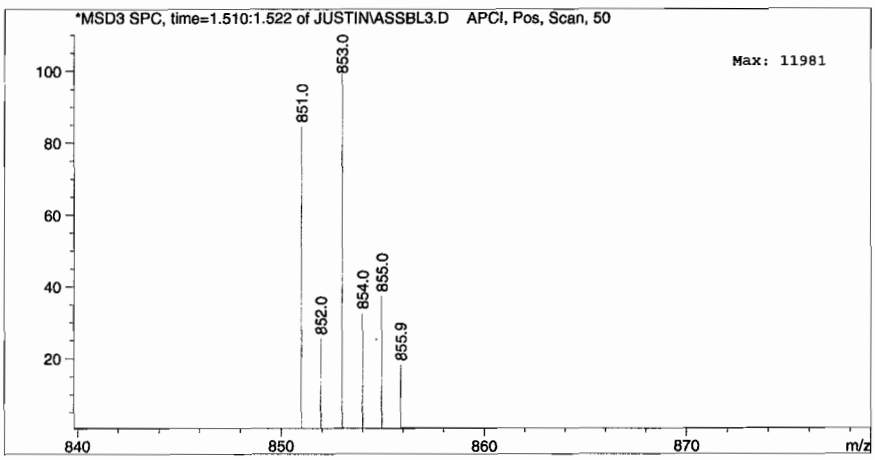

Figure 15. LCMS spectrometry data for $[AsSbL_3+H]^+$.

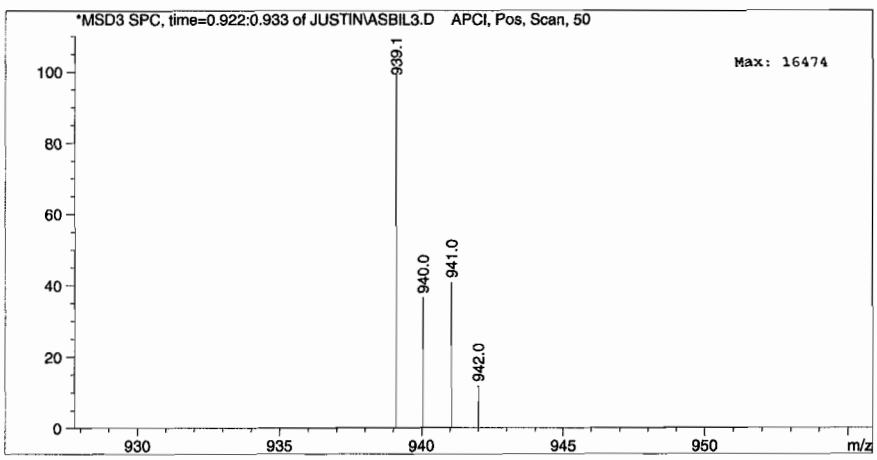

Figure 16. LCMS spectrometry data for $[AsBiL_3+H]^+$.

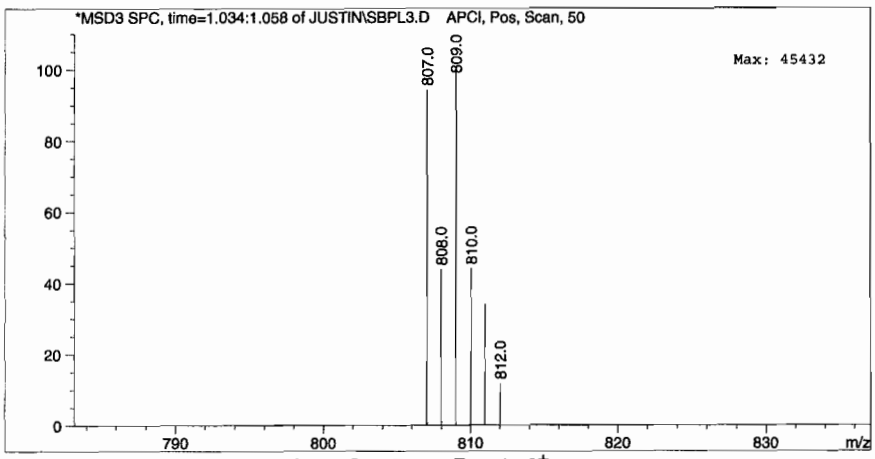

Figure 17. LCMS spectrometry data for $[PSbL_3+H]^+$.

X-Ray Crystallography

The X-ray crystal structures of all heterometallic cryptands were determined (Figure 18).

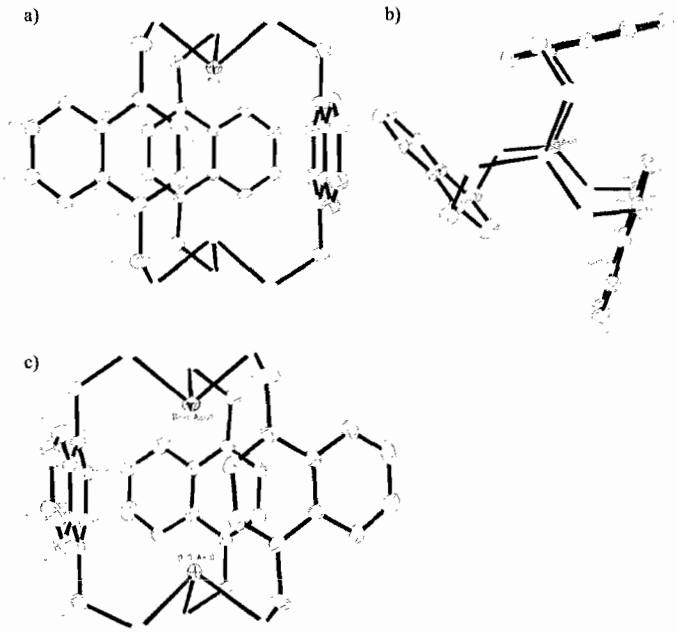

Figure 18. ORTEP representations (30% ellipsoids) of the X-ray crystal structures of $PSbL_3$ (a), $AsSbL_3$ (b), and $AsBi_2L_3$ (c).

REFERENCES

Chapter I

(1) Ratnaike, R. N. *Postgrad. Med. J.* **2003**, *79*, 391-396.

(2) Ng, J. C.; Wang, J. P.; Shraim, A. *Chemosphere* **2003**, *52*, 1353-1359.

(3) Mandal, B. K.; Suzuki, K. T. *Talanta* **2002**, *58*, 201-235.

(4) Sharma, V. K.; Sohn, M. *Environ. Int.* **2009**, *35*, 743-759.

(5) Roy, P.; Saha, A. *Curr. Sci.* **2002**, *82*, 38-45.

(6) Drahota, P.; Filippi, M. *Environ. Int.* **2009**, *35*, 1243-1255.

(7) Hering, J. G. *J. Hazard. Mater.* **1996**, *45*, 175-184.

(8) Smedley, P. L.; Kinniburgh, D. G. *Appl. Geochem.* **2002**, *17*, 517-568.

(9) Dhar, R. K.; Biswas, B. K.; Samanta, G.; Mandal, B. K.; Chakraborti, D.; Roy, S.; Jafar, A.; Islam, A.; Ara, G.; Kabir, S.; Khan, A. W.; Ahmed, S. A.; Hadi, S. A. *Curr. Sci.* **1997**, *73*, 48-59.

(10) Ahmad, K. *Lancet* **2001**, *358*, 133-133.

(11) Berg, M.; Tran, H. C.; Nguyen, T. C.; Pham, H. V.; Schertenleib, R.; Giger, W. *Environ. Sci. Technol.* **2001**, *35*, 2621-2626.

(12) Welch, A. H.; Lico, M. S.; Hughes, J. L. *Ground Water* **1988**, *26*, 333-347.

(13) An, D.; He, Y. G.; Hu, Q. X. *Fluoride* **1997**, *30*, 29-32.

(14) Sakuma, A. M.; De Capitani, E. M.; Figueiredo, B. R.; De Maio, F. D.; Paoliello, M. M. B.; da Cunha, F. G.; Duran, M. C. *Cad. Saude Publica* **2010**, *26*, 391-398.

(15) Jones, F. T. *Poult. Sci.* **2007**, *86*, 2-14.

(16) Cullen, W. R. *Is Arsenic an Aphrodisiac? The Sociochemistry of an Element*; Thr Royal Society of Chemistry: Cambridge, UK, 2008.

(17) Steverding, D. *Parasite Vector* **2010**, *3*, 15-23.

(18) Ferrara, F. *Expert Opin. Pharmacother.* **2010**, *11*, 587-596.

(19) Pepin, J.; Milord, F.; Khonde, A. N.; Niyonsenga, T.; Loko, L.; Mpia, B.; Dewals, P. *Trans. Roy. Soc. Trop. Med. Hyg.* **1995**, *89*, 92-97.

(20) Ivan, M. K.; Dermot, A. H. *Angew. Chem., Int. Ed.* **2010**, DOI: 10.1002/anie.200906594.

(21) Lech, T.; Trela, F. *Forensic Sci.Int.* **2005**, *151*, 273-277.

(22) Morales, K. H.; Ryan, L.; Kuo, T. L.; Wu, M. M.; Chen, C. J. *Environ. Health Perspect.* **2000**, *108*, 655-661.

(23) Smith, A. H.; Biggs, M. L.; Moore, L.; Haque, R.; Steinmaus, C.; Chung, J.; Hernandez, A.; Lopipero, P.; Willard, R. C.; Charles, O. A.; Rebecca, L. C. In *Arsenic Exposure and Health Effects III*; Elsevier Science Ltd: Oxford, 1999, p 191-199.

(24) Tseng, W. P. *Environ. Health Perspect.* **1977**, *19*, 109-119.

(25) Tchounwou, P. B.; Patlolla, A. K.; Centeno, J. A. *Toxicol. Pathol.* **2003**, *31*, 575-588.

(26) Ferguson, J. F.; Gavis, J. *Water Res.* **1972**, *6*, 1259-1274.

(27) Mizumura, A.; Watanabe, T.; Kobayashi, Y.; Hirano, S. *Toxicol. Appl. Pharmacol.*, *242*, 119-125.

(28) Loffredo, C. A.; Aposhian, H. V.; Cebrian, M. E.; Yamauchi, H.; Silbergeld, E. K. *Environ. Res.* **2003**, *92*, 85-91.

(29) Petrick, J. S.; Jagadish, B.; Mash, E. A.; Aposhian, H. V. *Chem. Res. Toxicol.* **2001**, *14*, 651-656.

(30) Labes, R. *Arch. ezp. Path. u. Pharmakol.* **1929**, *141*, 148.

(31) Johnson, J. M.; Voegtlin, C. *J. Biol. Chem.* **1930**, *89*, 27-31.

(32) Gailer, J.; Lindner, W. *J. Chromatogr., B: Anal. Technol. Biomed. Life Sci.* **1998**, *716*, 83-93.

(33) Percy, A. J.; Gailer, J. *Bioinorg. Chem. Appl.* **2008**, 539082.

(34) Serves, S. V.; Charalambidis, Y. C.; Sotiropoulos, D. N.; Ioannou, P. V. *Phosphorus Sulfur* **1995**, *105*, 109-116.

(35) Delnomdedieu, M.; Basti, M. M.; Otvos, J. D.; Thomas, D. J. *Chem.-Biol. Interact.* **1994**, *90*, 139-155.

(36) Scott, N.; Hatlelid, K. M.; MacKenzie, N. E.; Carter, D. E. *Chem. Res. Toxicol.* **1993**, *6*, 102-106.

(37) Burford, N.; Eelman, M. D.; Groom, K. *J. Inorg. Biochem.* **2005**, *99*, 1992-1997.

(38) Ramadan, D.; Cline, D. J.; Bai, S.; Thorpe, C.; Schneider, J. P. *J. Am. Chem. Soc.* **2007**, *129*, 2981-2988.

(39) Kitchin, K. T.; Wallace, K. *Toxicol. Appl. Pharmacol.* **2005**, *206*, 66-72.

(40) Merrifield, M. E.; Ngu, T.; Stillman, M. J. *Biochem. Biophys. Res. Commun.* **2004**, *324*, 127-132.

(41) Toyama, M.; Yamashita, M.; Hirayama, N.; Murooka, Y. *J. Biochem.* **2002**, *132*, 217-221.

(42) Jiang, G.; Gong, Z.; Li, X.-F.; Cullen, W. R.; Le, X. C. *Chem. Res. Toxicol.* **2003**, *16*, 873-880.

(43) Kreppel, H.; Bauman, J. W.; Liu, J.; McKim, J. M.; Klaassen, C. D. *Fundam. Appl. Toxicol.* **1993**, *20*, 184-189.

(44) Hochadel, J. F.; Waalkes, M. P. *Toxicology* **1997**, *116*, 89-98.

(45) Swaran, J. S. F.; Neelima, T. *IUBMB Life* **1998**, *45*, 1121-1127.

(46) Falnoga, I.; Stilbilj, V.; Tusek-Znidaric, M.; Slejkovec, Z.; Mazej, D.; Jacimovic, R.; Scancar, J. *Biol. Trace Elem. Res.* **2000**, *78*, 241-254.

(47) Romach, E. H.; Zhao, C. Q.; Del Razo, L. M.; Cebrian, M. E.; Waalkes, M. P. *Toxicol. Sci.* **2000**, *54*, 500-508.

(48) Liu, J.; Kadiiska, M. B.; Liu, Y.; Lu, T.; Qu, W.; Waalkes, M. P. *Toxicol. Sci.* **2001**, *61*, 314-320.

(49) Lu, M. L.; Wang, H. L.; Li, X. F.; Lu, X. F.; Cullen, W. R.; Arnold, L. L.; Cohen, S. M.; Le, X. C. *Chem. Res. Toxicol.* **2004**, *17*, 1733-1742.

(50) Shi, W. P.; Dong, J.; Scott, R. A.; Ksenzenko, M. Y.; Rosen, B. P. *J. Biol. Chem.* **1996**, *271*, 9291-9297.

(51) Liu, J. Y.; Rosen, B. P. *J. Biol. Chem.* **1997**, *272*, 21084-21089.

(52) Chang, K. N.; Lee, T. C.; Tam, M. F.; Chen, Y. C.; Lee, L. W.; Lee, S. Y.; Lin, P. J.; Huang, R. N. *Biochem. J.* **2003**, *371*, 495-503.

(53) Lin, C. H.; Huang, C. F.; Chen, W. Y.; Chang, Y. Y.; Ding, W. H.; Lin, M. S.; Wu, S. H.; Huang, R. N. *Chem. Res. Toxicol.* **2006**, *19*, 469-474.

(54) Hoffman, R. D.; Lane, M. D. *J. Biol. Chem.* **1992**, *267*, 14005-14011.

(55) Menzel, D. B.; Hamadeh, H. K.; Lee, E.; Meacher, D. M.; Said, V.; Rasmussen, R. E.; Greene, H.; Roth, R. N. *Toxicol. Lett.* **1999**, *105*, 89-101.

(56) Yan, H. M.; Wang, N.; Weinfeld, M.; Cullen, W. R.; Le, X. C. *Anal. Chem.* **2009**, *81*, 4144-4152.

(57) Zahler, W. L.; Cleland, W. W. *J. Biol. Chem.* **1968**, *243*, 716-719.

(58) Cruse, W. B. T.; James, M. N. G. *Acta. Crystall. B-Stru.* **1972**, *B 28*, 1325-1331.

(59) Seong-Ho, S.; Tudor, L.; Stephen, C.; Orit, B.; Hagan, B. *Angew. Chem., Int. Ed.* **2002**, *41*, 3707-3709.

(60) Shin, S. H.; Steffensen, M. B.; Claridge, T. D. W.; Bayley, H. *Angew. Chem., Int. Ed.* **2007**, *46*, 7412-7416.

(61) Ramadan, D.; Rancy, P. C.; Nagarkar, R. P.; Schneider, J. P.; Thorpe, C. *Biochemistry* **2009**, *48*, 424-432.

(62) Ngu, T. T.; Stillman, M. J. *J. Am. Chem. Soc.* **2006**, *128*, 12473-12483.

(63) Ngu, T. T.; Easton, A.; Stillman, M. J. *J. Am. Chem. Soc.* **2008**, *130*, 17016-17028.

(64) Ngu, T. T.; Lee, J. A.; Rushton, M. K.; Stillman, M. J. *Biochemistry* **2009**, *48*, 8806-8816.

(65) Ngu, T. T.; Lee, J. A.; Pinter, T. B. J.; Stillman, M. J. *J. Inorg. Biochem.* **2010**, *104*, 232-244.

(66) Whittaker, V. P. *Biochem. J.* **1947**, *41*, 56-62.

(67) Delnomdedieu, M.; Basti, M. M.; Otvos, J. D.; Thomas, D. J. *Chem. Res. Toxicol.* **1993**, *6*, 598-602.

(68) Dill, K.; Adams, E. R.; Oconnor, R. J.; Chong, S.; McGown, E. L. *Arch. Biochem. Biophys.* **1987**, *257*, 293-301.

(69) Kobayashi, Y.; Cui, X.; Hirano, S. *Toxicology* **2005**, *211*, 115-123.

(70) Rey, N. A.; Howarth, O. W.; Pereira-Maia, E. C. *J. Inorg. Biochem.* **2004**, *98*, 1151-1159.

(71) Spuches, A. M.; Kruszyna, H. G.; Rich, A. M.; Wilcox, D. E. *Inorg. Chem.* **2005**, *44*, 2964-2972.

(72) Baechler, R. D.; Mislow, K. *J. Am. Chem. Soc.* **1970**, *92*, 3090-3093.

(73) *Chemistry of Arsenic, Antimony, and Bismuth*; Norman, N. C., Ed.; Blackie Academic and Professional: New York, 1998.

(74) Senkler, G. H.; Mislow, K. *J. Am. Chem. Soc.* **1972**, *94*, 291.

(75) Weston, R. E. *J. Am. Chem. Soc.* **1954**, *76*, 2645-2648.

(76) Koeppl, G. W.; Sagatys, D. S.; Krishnam.Gs; Miller, S. I. *J. Am. Chem. Soc.* **1967**, *89*, 3396-3405.

(77) von Döllen, A.; Strasdeit, H. *Eur. J. Inorg. Chem.* **1998**, 61-66.

(78) Dill, K.; Huang, L. H.; Bearden, D. W.; McGown, E. L.; Oconnor, R. J. *Chem. Res. Toxicol.* **1991**, *4*, 295-299.

(79) Cangelosi, V. M.; Sather, A. C.; Zakharov, L. N.; Berryman, O. B.; Johnson, D. W. *Inorg. Chem.* **2007**, *46*, 9278-9284.

(80) Casey, J. P.; Mislow, K. *J. Chem. Soc. Chem. Comm.* **1970**, 999b.

(81) Aksnes, D. W.; Bjoroy, M. *Acta. Chem. Scand. A* **1975**, *29*, 672-676.

(82) Vickaryous, W. J.; Healey, E. R.; Berryman, O. B.; Johnson, D. W. *Inorg. Chem.* **2005**, *44*, 9247-9252.

(83) Cangelosi, V. M.; Zakharov, L. N.; Crossland, J. L.; Franklin, B. C.; Johnson, D. W. *Cryst. Growth Des.* **2010**, *10*, 1471-1473.

(84) Vickaryous, W. J.; Herges, R.; Johnson, D. W. *Angew. Chem., Int. Ed. Engl.* **2004**, *43*, 5831-5833.

(85) Carter, T. G.; Healey, E. R.; Pitt, M. A.; Johnson, D. W. *Inorg. Chem.* **2005**, *44*, 9634-9636.

(86) Carter, T. G.; Vickaryous, W. J.; Cangelosi, V. M.; Johnson, D. W. *Comments Inorg. Chem.* **2007**, *28*, 97-122.

(87) Schmidbaur, H.; Schier, A. *Organometallics* **2008**, *27*, 2361-2395.

(88) Schmidbaur, H.; Bublak, W.; Huber, B.; Muller, G. *Angew. Chem.* **1987**, *99*, 248-249.

(89) Schmidbaur, H.; Bublak, W.; Huber, B.; Muller, G. *Angew. Chem., Int. Ed. Engl.* **1987**, *26*, 234-236.

(90) Schmidbaur, H.; Nowak, R.; Steigelmann, O.; Muller, G. *Chem. Ber.* **1990**, *123*, 1221-1226.

(91) Hill, N. J.; Levason, W.; Reid, G. *Inorg. Chem.* **2002**, *41*, 2070-2076.

(92) Tani, K.; Hanabusa, S.; Kato, S.; Mutoh, S.; Suzuki, S.; Ishida, M. *J. Chem. Soc., Dalton Trans.* **2001**, 518-527.

(93) Petrie, S.; Stranger, R.; Rae, A. D.; Willis, A. C.; Zhou, X.; Wild, S. B. *Organometallics* **2006**, *25*, 164-171.

(94) Pappalardo, G. C.; Chakravorty, R.; Irgolic, K. J.; Meyers, E. A. *Acta Crystallogr. Sect. C-Cryst. Struct. Commun.* **1983**, *39*, 1618-1620.

(95) Pappalardo, G. C.; Irgolic, K. J.; Pyles, R. A.; Montoneri, E. *Spectroc. Acta Pt. A-Molec. Biomolec. Spectr.* **1982**, *38*, 363-366.

(96) Shaikh, T. A.; Bakus, R. C.; Parkin, S.; Atwood, D. A. *J. Organomet. Chem.* **2006**, *691*, 1825-1833.

(97) Shaikh, T. A.; Parkin, S.; Atwood, D. A. *J. Organomet. Chem.* **2006**, *691*, 4167-4171.

(98) Cangelosi, V. M.; Pitt, M. A.; Vickaryous, W. J.; Allen, C. A.; Zakharov, L. N.; Johnson, D. W. *Cryst. Growth Des.* **2010**, *in press*.

(99) Burford, N.; Parks, T. M.; Royan, B. W.; Borecka, B.; Cameron, T. S.; Richardson, J. F.; Gabe, E. J.; Hynes, R. *J. Am. Chem. Soc.* **1992**, *114*, 8147-8153.

(100) Osborne, A. G.; Hollands, R. E.; Bryan, R. F.; Lockhart, S. *J. Organomet. Chem.* **1985**, *288*, 207-217.

(101) Adams, E.; Jeter, D.; Cordes, A. W.; Kolis, J. W. *Inorg. Chem.* **1990**, *29*, 1500-1503.

(102) Aksnes, D. W. *Acta. Chem. Scand. A* **1974**, *A 28*, 1175-1179.

(103) Lu, C.-S.; Donohue, J. *J. Am. Chem. Soc.* **1944**, *66*, 818-827.

(104) Christian, B. H.; Gillespie, R. J.; Sawyer, J. F. *Inorg. Chem.* **1981**, *20*, 3410-3420.

(105) Bergerhoff, G.; Namgung, H. *Z. Kristall.* **1979**, *150*, 209-213.

(106) Cordes, A. W.; Gwinup, P. D.; Malmstrom, M. C. *Inorg. Chem.* **1972**, *11*, 836-838.

(107) DiMaio, A. J.; Rheingold, A. L. *Inorg. Chem.* **1990**, *29*, 798-804.

(108) Burford, N.; Parks, T. M.; Royan, B. W.; Richardson, J. F.; White, P. S. *Can. J. Chem.-Rev. Can. Chim.* **1992**, *70*, 703-709.

(109) Burford, N.; Landry, J. C.; Ferguson, M. J.; McDonald, R. *Inorg. Chem.* **2005**, *44*, 5897-5902.

(110) Cea-Olivares, R.; Garcia-Montalvo, V.; Moya-Cabrera, M. M. *Coord. Chem. Rev.* **2005**, *249*, 859-872.

(111) Gonzilez-Montiel, S.; Andrade-Lopez, N.; Alvarado-Rodriguez, J. G. *Eur. J. Inorg. Chem.* **2006**, 3762-3768.

(112) Sherlock, D. J.; Chandrasekaran, A.; Day, R. O.; Holmes, R. R. *Inorg. Chem.* **1997**, *36*, 5082-5089.

(113) Timosheva, N. V.; Chandrasekaran, A.; Day, R. O.; Holmes, R. R. *Inorg. Chem.* **1998**, *37*, 3862-3867.

(114) Chandrasekaran, A.; Sood, P.; Day, R. O.; Holmes, R. R. *Inorg. Chem.* **1999**, *38*, 3369-3376.

(115) Pauling, L. *The Nature of the Chemical Bond*; 3rd ed.; Cornell University Press: Ithaca, NY, 1960.

(116) Britton, D.; Dunitz, J. D. *J. Am. Chem. Soc.* **1981**, *103*, 2971-2979.

(117) Kolb, U.; Beuter, M.; Gerner, M.; Drager, M. *Organometallics* **1994**, *13*, 4413-4425.

(118) Ezeh, V. C.; Patra, A. K.; Harrop, T. C. *Inorg. Chem.* **2010**, *49*, 2586-2588.

(119) Raston, C. L.; Skelton, B. W.; Tolhurst, V. A.; White, A. H. *J. Chem. Soc.-Dalton Trans.* **2000**, *8*, 1279-1285.

(120) Bott, R. C.; Smith, G.; Sagatys, D. S.; Lynch, D. E.; Kennard, C. H. L. *Aust. J. Chem.* **2000**, *53*, 917-924.

(121) Klapotke, T. M.; Noth, H.; Schutt, T.; Suter, M. *Eur. J. Inorg. Chem.* **2002**, 2511-2517.

(122) Green, S. P.; Jones, C.; Jin, G. X.; Stasch, A. *Inorg. Chem.* **2007**, *46*, 8-10.

(123) Hitchcock, P. B.; Lappert, M. F.; Li, G.; Protchenko, A. V. *Chem. Commun.* **2009**, 428-429.

(124) Farrer, B. T.; McClure, C. P.; Penner-Hahn, J. E.; Pecoraro, V. L. *Inorg. Chem.* **2000**, *39*, 5422-5423.

(125) Matzapetakis, M.; Farrer, B. T.; Weng, T. C.; Hemmingsen, L.; Penner-Hahn, J. E.; Pecoraro, V. L. *J. Am. Chem. Soc.* **2002**, *124*, 8042-8054.

(126) Dieckmann, G. R.; McRorie, D. K.; Tierney, D. L.; Utschig, L. M.; Singer, C. P.; Ohalloran, T. V.; PennerHahn, J. E.; DeGrado, W. F.; Pecoraro, V. L. *J. Am. Chem. Soc.* **1997**, *119*, 6195-6196.

(127) Farrer, B. T.; Pecoraro, V. L. *Curr. Opin. Drug Discovery Dev.* **2002**, *5*, 937-943.

(128) Touw, D. S.; Nordman, C. E.; Stuckey, J. A.; Pecoraro, V. L. *Proc. Natl. Acad. Sci. U. S. A.* **2007**, *104*, 11969-11974.

(129) Cline, D. J.; Thorpe, C.; Schneider, J. P. *J. Am. Chem. Soc.* **2003**, *125*, 2923-2929.

(130) Lehn, J. M. *Science* **1993**, *260*, 1762-1763.

(131) MacGillivray, L. R.; Atwood, J. L. *Angew. Chem., Int. Ed.* **1999**, *38*, 1019-1034.

(132) Wyler, R.; Demendoza, J.; Rebek, J. *Angew. Chem., Int. Ed.* **1993**, *32*, 1699-1701.

(133) Branda, N.; Wyler, R.; Rebek, J. *Science* **1994**, *263*, 1267-1268.

(134) Caulder, D. L.; Raymond, K. N. *Acc. Chem. Res.* **1999**, *32*, 975-982.

(135) Caulder, D. L.; Raymond, K. N. *Dalton Trans.* **1999**, 1185-1200.

(136) Hunter, C. A.; Sanders, J. K. M. *J. Am. Chem. Soc.* **1990**, *112*, 5525-5534.

(137) Ma, J. C.; Dougherty, D. A. *Chem. Rev.* **1997**, *97*, 1303-1324.

(138) Piatnitski, E. L.; Flowers, R. A.; Deshayes, K. *Chem.-Eur. J.* **2000**, *6*, 999-1006.

(139) Greenwood, N. N. *J. Chem. Soc.-Dalton Trans.* **1991**, 565-573.

(140) Greenwood, N. N. *J. Chem. Soc.-Dalton Trans.* **2001**, 2055-2066.

(141) Pitt, M. A.; Johnson, D. W. *Chem. Soc. Rev.* **2007**, *36*, 1441-1453.

(142) Cangelosi, V. M.; Zakharov, L. N.; Fontenot, S. A.; Pitt, M. A.; Johnson, D. W. *Dalton Trans.* **2008**, 3447-3453.

(143) Pitt, M. A.; Zakharov, L. N.; Vanka, K.; Thompson, W. H.; Laird, B. B.; Johnson, D. W. *Chem. Commun.* **2008**, 3936-3938.

(144) Auer, A. A.; Mansfeld, D.; Nolde, C.; Schneider, W.; Schurmann, M.; Mehring, M. *Organometallics* **2009**, *28*, 5405-5411.

(145) Cangelosi, V. M.; Zakharov, L. N.; Johnson, D. W. *Angew. Chem., Int. Ed.* **2010**, *49*, 1248-1251.

(146) Cangelosi, V. M.; Carter, T. G.; Crossland, J. L.; Zakharov, L. N.; Johnson, D. W. *submitted to Inorg. Chem.*

(147) Cangelosi, V. M.; Carter, T. G.; Zakharov, L. N.; Johnson, D. W. *Chem. Commun.* **2009**, 5606-5608.

(148) Lindquist, N. R.; Carter, T. G.; Cangelosi, V. M.; Zakharov, L. N.; Johnson, D. W. *Chem. Commun.* **2010**, *46*, 3505-3507.

Chapter II

(1) Cangelosi, V. M.; Sather, A. C.; Zakharov, L. N.; Berryman, O. B.; Johnson, D. W. *Inorg. Chem.* **2007**, *46*, 9278-9284.

(2) Healey, E. R.; Vickaryous, W. J.; Berryman, O. B.; Johnson, D. W. In *Bottom-up Nanofabrication: Supramolecules, Self-Assemblies, and Organized Films*; Nalwa, H. S., Ed.; American Scientific Publishers, 2007.

(3) Pitt, M. A.; Johnson, D. W. *Chem. Soc. Rev.* **2007**, *36*, 1441-1453.

(4) Cook, V. C.; Willis, A. C.; Zank, J.; Wild, S. B. *Inorg. Chem.* **2002**, *41*, 1897-1906.

(5) Vickaryous, W. J.; Herges, R.; Johnson, D. W. *Angew. Chem. Int. Ed.* **2004**, *43*, 5831-5833.

(6) Vickaryous, W. J.; Healey, E. R.; Berryman, O. B.; Johnson, D. W. *Inorg. Chem.* **2005**, *44*, 9247-9252.

(7) Schmidbaur, H.; Bublak, W.; Huber, B.; Muller, G. *Angew. Chem., Int. Ed. Engl.* **1987**, *26*, 234-236.

(8) Schmidbaur, H.; Nowak, R.; Steigelmann, O.; Muller, G. *Chem. Ber.* **1990**, *123*, 1221-1226.

(9) Hamilton, T. D.; MacGillivray, L. R. *Cryst. Growth Des.* **2004**, *4*, 419-430.

(10) Seeber, G. T., Bryan E. F.; Raymond, Kenneth N. In *Top. Curr. Chem.*; Springer Berlin: Heidelberg, 2006; Vol. 265, pp 147-183.

(11) Beissel, T.; Powers, R. E.; Parac, T. N.; Raymond, K. N. *J. Am. Chem. Soc* **1999**, *121*, 4200-4206.

(12) Fiedler, D.; Leung, D. H.; Bergman, R. G.; Raymond, K. N. *Acc. Chem. Res.* **2005**, *38*, 349-358.

(13) (a) Givens, R. S.; Venkatramanan, M. K.; Figard, J. *Tetrahedron Lett.* **1984**, *25*, 2187-2190; (b) Givens, R. S.; Olsen, R. J.; Wylie, P. L. *J. Org. Chem.* **1979**, *44*, 1608-1613; (c) Haenel, M. W. *Chem. Ber.* **1982**, *115*, 1425-1436.

(14) Schmidbaur, H.; Bublak, W.; Huber, B.; Muller, G. *Angew. Chem.* **1987**, *99*, 248-249.

(15) Cainelli, G.; Giacomini, D.; Galletti, P. *Eur. J. Org. Chem.* **1999**, 61-65.

(16) Yamamoto, T.; Arif, A. M.; Stang, P. J. *J. Am. Chem. Soc* **2003**, *125*, 12309-12317.

(17) Nagase, S. *The Chemistry of Organic Arsenic, Antimony, and Bismuth Compounds*; Wiley: Chichester, U.K., 1994.

(18) Cross, W. I.; Godfrey, S. M.; McAuliffe, C. A.; Mackie, A. G.; Pritchard, R. B. In *Chemistry of Arsenic, Antimony, and Bismuth*; Norman, N. C., Ed.; Blackie Academic & Professional: London, 1998.

(19) Doak, G. O.; Freedman, L. D. *Organometallic Compounds of Arsenic, Antimony, and Bismuth*; Wiley Intersciences: New York, 1970.

(20) Westheimer, F. H. *Acc. Chem. Res.* **1968**, *1*, 70-78.

(21) Godfrey, S. M.; McAuliffe, C. A.; Mackie, A. G.; Pritchard, R. G. In *Chemistry of Arsenic, Antimony, and Bismuth*; Norman, N. C., Ed.; Blackie Academic & Professional: London, 1998, p 94.

(22) Gutmann, V. *Quart. Revs.* **1956**, *10*, 451-462.

(23) George M. Sheldrick, *Gottingen University*.

Chapter III

(1) Cangelosi, V. M.; Zakharov, L. N.; Fontenot, S. A.; Pitt, M. A.; Johnson, D. W. *Dalton Trans.* **2008**, 3447-3453.

(2) Pitt, M. A.; Johnson, D. W. *Chem. Soc. Rev.* **2007**, *36*, 1441-1453.

(3) Caulder, D. L.; Raymond, K. N. *J. Chem. Soc., Dalton Trans.* **1999**, 1185-1200.

(4) Fujita, M.; Tominaga, M.; Hori, A.; Therrien, B. *Acc. Chem. Res.* **2005**, *38*, 369-378.

(5) Leininger, S.; Olenyuk, S.; Stang, P. J. *Chem. Rev.* **2000**, *100*, 853-908.

(6) Swiegers, G. F.; Malefetse, T. J. *Chem. Rev.* **2000**, *100*, 3483-3538.

(7) Goto, K.; Okazaki, R. *Liebigs Ann. Chem.* **1997**, 2393-2407.

(8) Atwood, J. L.; Barbour, L. J.; Jerga, A. *Proc. Natl. Acad. Sci. U. S. A.* **2002**, *99*, 4837-4841.

(9) Laughrey, Z. R.; Gibb, B. C. *J. Org. Chem.* **2006**, *71*, 1289-1294.

(10) Srinivasan, K.; Gibb, B. C. *Org. Lett.* **2007**, *9*, 745-748.

(11) Purse, B. W.; Rebek, J. *Proc. Natl. Acad. Sci. U. S. A.* **2005**, *102*, 10777-10782.

(12) Renslo, A. R.; Rebek, J. *Angew. Chem. Int. Ed.* **2000**, *39*, 3281-3283.

(13) Butterfield, S. M.; Rebek, J. *Angew. Chem Int. Ed.* **2000**, *112*, 3419-3421.

(14) Iwasawa, T.; Hooley, R. J.; Rebek, J., *Science* **2007**, *317*, 493-496.

(15) Rowan, S. J.; Cantrill, S. J.; Cousins, G. R. L.; Sanders, J. K. M.; Stoddart, J. F. *Angew. Chem. Int. Ed.* **2002**, *41*, 898-952.

(16) Carter, T. G.; Vickaryous, W. J.; Cangelosi, V. M.; Johnson, D. W. *Comments Inorg. Chem.* **2007**, *28*, 97-122.

(17) (a) Vickaryous, W. J.; Healey, E. R.; Berryman, O. B.; Johnson, D. W. *Inorg. Chem.* **2005**, *44*, 9247-9252. (b) Cangelosi, V. M.; Sather, A. C.; Zakharov, L. N.; Berryman, O. B.; Johnson, D. W. *Inorg. Chem.* **2007**, *46*, 9278-9284.

(18) Schmidbaur, H.; Bublak, W.; Huber, B.; Muller, G. *Angew. Chem., Int. Ed. Engl.* **1987**, *26*, 234-236.

(19) Schmidbaur, H.; Nowak, R.; Steigelmann, O.; Muller, G. *Chem. Ber.* **1990**, *123*, 1221-1226.

(20) Vickaryous, W. J.; Herges, R.; Johnson, D. W. *Angew. Chem. Int. Ed.* **2004**, *43*, 5831-5833.

(21) Conquest Version 1.7, February 2005 Release.

(22) WebLab ViewerPro 4.0, December 1, 2000 release.

(23) Nakamura, T.; Ren, J. J.; Zhu, K. M.; Kawara, S.; Jin, B. K. *Anal. Sci.* **2006**, *22*, 1261-1264.

(24) *Brit. Pat.* 807720 (January 21, 1959).

(25) *Chem. Abstr.* **1960**, *54*, P413b.

(26) Azehara, H.; Liang, T. T.; Ishida, T.; Naitoh, Y.; Mizutani, W. *Jpn. J. Appl. Phys. Part 1*, **2004**, *43*, 4511-4516.

(27) Elandaloussi, E. H.; Frere, P.; Richomme, P.; Orduna, J.; Garin, J.; Roncali, J. *J. Am. Chem. Soc.* **1997**, *119*, 10774-10784.

(28) Feast, W. J.; Lovenich, P. W.; Puschmann, H.; Taliani, C. *Chem. Commun.* **2001**, 505-506.

(29) Sheldrick, G. M. SADABS, 1995, University of Göttingen, Germany.

(30) Henkel & Cie GmbH. *Br. Pat.*, 807,720, 1959; *Chem. Abstr.* **1995**, *123*, 2870.

(31) Nicholls, A.; Sharp, K. A.; Honig, B. *Proteins: Struc., Func. and Genet.* **1991**, *11*, 281-296.

(32) Bruker SMART (Version 5.631), SAINT (Version 6.63) and SHELXTL (Version 6.10), 2000, Bruker AXS Inc., Madison, Wisconsin, USA.

Chapter IV

(1) Cangelosi, V. M.; Carter, T. G.; Zakharov, L. N.; Johnson, D. W. *Chem. Commun.* **2009**, 5606-5608.

(2) (a) Piguet, C.; Bernardinelli, G.; Hopfgartner, G. *Chem. Rev.* **1997**, *97*, 2005-2062. (b) Albrecht, M. *Chem. Rev.* **2001**, *101*, 3457-3498. (c) Elhabiri, M.; Albrecht-Gary, A.-M. *Coord. Chem. Rev.* **2008**, *252*, 1079-1092.

(3) (a) Saalfrank, R. W.; Scheurer, H. M. A. *Angew. Chem., Int. Ed.* **2008**, *47*, 8794-8824. (b) Leininger, S.; Olenyuk, B.; Stang, P. J. *Chem. Rev.* **2000**, *100*, 853-908. (c) Swiegers, G. F.; Malefetse, T. J. *Chem. Rev.* **2000**, *100*, 3483-3538. (d) Caulder, D. L.; Raymond, K. N. *Dalton Trans.* **1999**, 1185-1200.

(4) (a) Davis, A. V.; Yeh, R. M.; Raymond, K. N. *Proc. Natl. Acad. Sci. U. S. A.* **2002**, *99*, 4793-4796. (b) Lehn, J. M. *Proc. Natl. Acad. Sci. U. S. A.* **2002**, *99*, 4763-4768.

(5) (a) Fujita, M.; Nagao, S.; Ogura, K. *J. Am. Chem. Soc.* **1995**, *117*, 1649-1650. (b) Baxter, P.; Lehn, J. M.; Decian, A.; Fischer, J. *Angew. Chem., Int. Ed. Engl.* **1993**, *32*, 69-72.

(6) (a) Pak, J. J.; Greaves, J.; McCord, D. J.; Shea, K. J. *Organometallics* **2002**, *21*, 3552-3561. (b) Sato, S.; Ishido, Y.; Fujita, M. *J. Am. Chem. Soc.* **2009**, *131*, 6064-6065.

(7) (a) Pfeil, A.; Lehn, J. M. *Chem. Commun.* **1992**, 838-840. (b) Fatin-Rouge, N.; Blanc, S.; Leize, E.; Van Dorsselaer, A.; Baret, P.; Pierre, J. L.; Albrecht-Gary, A. M. *Inorg. Chem.* **2000**, *39*, 5771-5778. (c) Fatin-Rouge, N.; Blanc, S.; Pfeil, A.; Rigault, A.; Albrecht-Gary, A. M.; Lehn, J. M. *Helv. Chim. Acta* **2001**, *84*, 1694-1711. (d) Marquis, A.; Kintzinger, J. P.; Graff, R.; Baxter, P. N. W.; Lehn, J. M. *Angew. Chem., Int. Ed.* **2002**, *41*, 2760-2764. (e) Hamacek, J.; Blanc, S.; Elhabiri, M.; Leize, E.; Van Dorsselaer, A.; Piguet, C.; Albrecht-Gary, A. M. *J. Am. Chem. Soc.* **2003**, *125*, 1541-1550. (f) Elhabiri, M.; Hamacek, J.; Bunzli, J. C. G.; Albrecht-Gary, A. M. *Eur. J. Inorg. Chem.* **2004**, 51-62. (g) Leize, E.; Dorsselaer, A. V.; Krämer, R.; Lehn, J. M. *Chem. Commun.* **1993**, 990-993.

(8) Takeda, N.; Umemoto, K.; Yamaguchi, K.; Fujita, M. *Nature* **1999**, *398*, 794-796.

(9) (a) Hasenknopf, B.; Lehn, J. M.; Boumediene, N.; Leize, E.; Van Dorsselaer, A. *Angew. Chem., Int. Ed.* **1998**, *37*, 3265-3268. (b) Albrecht, M.; Dehn, S.; Frohlich, R. *Angew. Chem., Int. Ed.* **2006**, *45*, 2792-2794.

(10) Vickaryous, W. J.; Healey, E. R.; Berryman, O. B.; Johnson, D. W. *Inorg. Chem.* **2005**, *44*, 9247-9252.

(11) Cangelosi, V. M.; Zakharov, L. N.; Fontenot, S. A.; Pitt, M. A.; Johnson, D. W. *Dalton Trans.* **2008**, 3447-3453.

(12) Carter, T. G.; Healey, E. R.; Pitt, M. A.; Johnson, D. W. *Inorg. Chem.* **2005**, *44*, 9634-9636.

(13) Schmidbaur, H.; Schier, A. *Organometallics* **2008**, *27*, 2361-2395.

(14) (a) Rowan, S. J.; Cantrill, S. J.; Cousins, G. R. L.; Sanders, J. K. M.; Stoddart, J. F. *Angew. Chem., Int. Ed.* **2002**, *41*, 898-952. (b) Campbell, V. E.; de Hatten, X.; Delsuc, N.; Kauffmann, B.; Huc, I.; Nitschke, J. R. *Chem.-Eur. J.* **2009**, *15*, 6138-6142.

(15) Pitt, M. A.; Johnson, D. W. *Chem. Soc. Rev.* **2007**, *36*, 1441-1453.

(16) Watzky, M. A.; Finney, E. E.; Finke, R. G. *J. Am. Chem. Soc.* **2008**, *130*, 11959-11969.

(17) Alberto, C. *Macromol. Rapid Commun.* **2002**, *23*, 511-529.

(18) Schwartz, D. K. *Annu. Rev. Phys. Chem.* **2001**, *52*, 107-137.

(19) Zhang, P.; Bundle, D. R. *Isr. J. Chem.* **2000**, *40*, 189-208.

(20) Rohrbach, W. D.; Boekelheide, V. *J. Org. Chem.* **1983**, *48*, 3673-3678.

(21) Zenobi, R.; Knochenmuss, R. *Mass Spectrom. Rev.* **1998**, *17*, 337-366.

Chapter V

(1) Cangelosi, V. M.; Zakharov, L. N.; Johnson, D. W. *Angew. Chem., Int. Ed.* **2010**, *49*, 1248-1251.

(2) Farrer, B. T.; McClure, C. P.; Penner-Hahn, J. E.; Pecoraro, V. L. *Inorg. Chem.* **2000**, *39*, 5422-5423.

(3) (a) Escudero-Adan, E. C.; Benet-Buchholz, J.; Kleij, A. W. *Inorg. Chem.* **2007**, *46*, 7265-7267. (b) Wezenberg, S. J.; Metselaar, G. A.; Escudero-Adan, E. C.; Benet-Buchholz, J.; Kleij, A. W. *Inorg. Chim. Acta* **2009**, *362*, 1053-1057. (c) Vilaplana, R. A.; Gonzalezvilchez, F. *Dalton Trans.* **1993**, 1779-1781. (d) Siddiqui, K. A.; Mehrotra, G. K.; Mrozinski, J.; Butcher, R. J. *Eur. J. Inorg. Chem.* **2008**, 4166-4172..

(4) Osakada, K.; Yamamoto, T. *Coord. Chem. Rev.* **2000**, *198*, 379-399.

(5) Chow, C. F.; Fujii, S.; Lehn, J. M. *Chem.-Asian J.* **2008**, *3*, 1324-1335.

(6) Caulder, D. L.; Raymond, K. N. *Dalton Trans.* **1999**, 1185-1200.

(7) (a) Cangelosi, V. M.; Carter, T. G.; Zakharov, L. N.; Johnson, D. W. *Chem. Commun.* **2009**, 5606-5608. (b) Davis, A. V.; Yeh, R. M.; Raymond, K. N. *Proc. Natl. Acad. Sci. U. S. A.* **2002**, *99*, 4793-4796. (c) Saalfrank, R. W.; Scheurer, H. M. A. *Angew. Chem., Int. Ed.* **2008**, *47*, 8794-8824.

(8) Campbell, V. E.; de Hatten, X.; Delsuc, N.; Kauffmann, B.; Huc, I.; Nitschke, J. R. *Chem.-Eur. J.* **2009**, *15*, 6138-6142.

(9) (a) Sato, S.; Ishido, Y.; Fujita, M. *J. Am. Chem. Soc.* **2009**, *131*, 6064-6065. (c) Schmittel, M.; Mahata, K. *Chem. Commun.* **2008**, 2550-2552. (d) Ziegler, M.; Davis, A. V.; Johnson, D. W.; Raymond, K. N. *Angew. Chem., Int. Ed.* **2003**, *42*, 665-668.

(10) (a) Umemoto, K.; Yamaguchi, K.; Fujita, M. *J. Am. Chem. Soc.* **2000**, *122*, 7150-7151. (b) Scherer, M.; Caulder, D. L.; Johnson, D. W.; Raymond, K. N. *Angew. Chem., Int. Ed.* **1999**, *38*, 1588-1592.

(11) (a) Schmittel, M.; Kalsani, V.; Kishore, R. S. K.; Colfen, H.; Bats, J. W. *J. Am. Chem. Soc.* **2005**, *127*, 11544-11545. (b) Jimenez-Molero, M. C.; Dietrich-Buchecker, C.; Sauvage, J. P. *Chem. Commun.* **2003**, 1613-1616. (c) Schmittel, M.; Kalsani, V.; Michel, C.; Mal, P.; Ammon, H.; Jackel, F.; Rabe, J. P. *Chem.-Eur. J.* **2007**, *13*, 6223-6237. (d) Akine, S.; Taniguchi, T.; Nabeshima, T. *Angew. Chem., Int. Ed.* **2002**, *41*, 4670-4673.

(12) Cangelosi, V. M.; Sather, A. C.; Zakharov, L. N.; Berryman, O. B.; Johnson, D. W. *Inorg. Chem.* **2007**, *46*, 9278-9284.

(13) (a) Carter, T. G.; Vickaryous, W. J.; Cangelosi, V. M.; Johnson, D. W. *Comments Inorg. Chem.* **2007**, *28*, 97-122. (b) Pitt, M. A.; Zakharov, L. N.; Vanka, K.; Thompson, W. H.; Laird, B. B.; Johnson, D. W. *Chem. Commun.* **2008**, 3936-3938. (c) Vickaryous, W. J.; Herges, R.; Johnson, D. W. *Angew. Chem., Int. Ed. Engl.* **2004**, *43*, 5831-5833.

(14) Vickaryous, W. J.; Zakharov, L. N.; Johnson, D. W. *Main Group Chem.* **2006**, *5*, 51-59.

(15) (a) Liu, L.; Zakharov, L. N.; Golen, J. A.; Rheingold, A. L.; Hanna, T. A. *Inorg. Chem.* **2008**, *47*, 11143-11153. (b) Geisselmann, A.; Klufers, P.; Kropfgans, C.; Mayer, P.; Piotrowski, H. *Angew. Chem., Int. Ed.* **2005**, *44*, 924-927.

(16) Schmidbaur, H.; Schier, A. *Organometallics* **2008**, *27*, 2361-2395.

(17) Carmalt, C. J.; Norman, N. C. *Chemistry of Arsenic, Antimony, and Bismuth*, Thomas Science, New York, **1998**.

(18) Kataeva, O. N.; Krivolapov, D. B.; Gubaidullin, A. T.; Litvinov, I. A.; Kursheva, L. I.; Katsyuba, S. A. *J. Mol. Struct.* **2000**, *554*, 127-140.

(19) (a) Burford, N.; Royan, B. W.; White, P. S. *Acta Crystallogr. Sect. C-Cryst. Struct. Commun.* **1990**, *46*, 274-276. (b) Milyukov, V. A.; Zverev, A. V.; Podlesnov, S. M.; Krivolapov, D. B.; Litvinov, I. A.; Gubaidullin, A. T.; Kataeva, O. N.; Ginzburg, A. G.; Sinyashin, O. G. *Eur. J. Inorg. Chem.* **2000**, 225-228.

(20) WebLab ViewerPro 4.0, December 1, 2000 release.

(21) Strasser, C. E.; Cronje, S.; Schmidbaur, H.; Raubenheimer, H. G. *J. Organomet. Chem.* **2006**, *691*, 4788-4796.

(22) (a) Ge, R. G.; Sun, H. Z. *Acc. Chem. Res.* **2007**, *40*, 267-274. (b) Yang, N.; Sun, H. *Coord. Chem. Rev.* **2007**, *251*, 2354-2366.

(23) Sheldrick, G. M. *Bruker/Siemens Area Detector Absorption Correction Program*, Bruker AXS, Madison, WI, 1998.

(24) Van der Sluis, P.; Spek, A. L. *Acta Cryst., Sect. A,* **1990**, *A46*, 194-201.

(25) SHELXTL-6.10 "Program for Structure Solution, Refinement and Presentation" BRUKER AXS Inc., 5465 East Cheryl Parkway, Madison, WI 53711-5373 USA.

Chapter VI

(1) Cangelosi, V. M.; Carter, T. G.; Crossland, J. L.; Zakharov, L. N.; Johnson, D. W. *submitted to Inorg. Chem.*

(2) Yang, N.; Sun, H. *Coord. Chem. Rev.* **2007**, *251*, 2354-2366.

(3) (a) Pitt, M. A.; Johnson, D. W. *Chem. Soc. Rev.* **2007**, *36*, 1441-1453 and references therein; (b) Carter, T. G.; Vickaryous, W. J.; Cangelosi, V. M.; Johnson, D. W. *Comments Inorg. Chem.* **2007**, *28*, 97-122.

(4) (a) Milios, C. J.; Ioannou, P. V.; Raptopoulou, C. P.; Papaefstathiou, G. S. *Polyhedron* **2009**, *28*, 3199-3202. (b) Morsali, A.; Masoomi, M. Y. *Coord. Chem. Rev.* **2009**, *253*, 1882-1905.

(5) Santacruz-Juarez, E.; Cruz-Huerta, J.; Hernandez-Ahuactzi, I. F.; Reyes-Martinez, R.; Tlahuext, H.; Morales-Rojas, H.; Hopfl, H. *Inorg. Chem.* **2008**, *47*, 9804-9812.

(6) Cruz-Huerta, J.; Carillo-Morales, M.; Santacruz-Juarez, E.; Hernandez-Ahuactzi, I. F.; Escalante-Garcia, J.; Godoy-Alcantar, C.; Guerrero-Alvarez, J. A.; Hopfl, H.; Morales-Rojas, H.; Sanchez, M. *Inorg. Chem.* **2008**, *47*, 9874-9885.

(7) Hernandez-Ahuactzi, I. F.; Hopfl, H.; Barba, V.; Roman-Bravo, P.; Zamudio-Rivera, L. S.; Beltran, H. I. *Eur. J. Inorg. Chem.* **2008**, 2746-2755.

(8) Kua, J.; Daly, R. C.; Tomlin, K. M.; Duin, A. C. T. v.; Brill, T. B.; Beal, R. W.; Rheingold, A. L. *J. Phys. Chem. A* **2009**, *113*, 11443-11453.

(9) (a) Marcovich, D.; Tapscott, R. E. *J. Am. Chem. Soc.* **1980**, *102*, 5712-5717. (b) Marcovich, D.; Duesler, E. N.; Tapscott, R. E.; Them, T. F. *Inorg. Chem.* **1982**, *21*, 3336-3341.

(10) Biros, S. M.; Yeh, R. M.; Raymond, K. N. *Angew. Chem., Int. Ed.* **2008**, *47*, 6062-6064.

(11) (a) Vickaryous, W. J.; Herges, R.; Johnson, D. W. *Angew. Chem., Int. Ed. Engl.* **2004**, *43*, 5831-5833; (b) Vickaryous, W. J.; Healey, E. R.; Berryman, O. B.; Johnson, D. W. *Inorg. Chem.* **2005**, *44*, 9247-9252; (c) Vickaryous, W. J.; Zakharov, L. N.; Johnson, D. W. *Main Group Chem.* **2006**, *5*, 51-59; (d) Cangelosi, V. M.; Sather, A. C.; Zakharov, L. N.; Berryman, O. B.; Johnson, D. W. *Inorg. Chem.* **2007**, *46*, 9278-9284; (e) Cangelosi, V. M.; Zakharov, L. N.; Fontenot, S. A.; Pitt, M. A.; Johnson, D. W. *Dalton Trans.* **2008**, 3447-3453. (f) Pitt, M. A.; Zakharov, L. N.; Vanka, K.; Thompson, W. H.; Laird, B. B.; Johnson, D. W. *Chem. Commun.* **2008**, 3936-3938; (g) Allen, C. A.; Cangelosi, V. M.; Zakharov, L. N.; Johnson, D. W. *Cryst. Growth Des.* **2009**, *9*, 3011-3013; (h) Cangelosi, V. M.; Carter, T. G.; Zakharov, L. N.; Johnson, D. W. *Chem. Commun.* **2009**, 5606-5608.; (i) Cangelosi, V. M.; Zakharov, L. N.; Crossland, J. L.; Franklin, B. C.; Johnson, D. W. *Cryst. Growth Des.* **2010**, *10*, 1471-1473; (j) Lindquist, N. R.; Carter, T. G.; Cangelosi, V. M.; Zakharov, L. N.; Johnson, D. W. *Chem. Commun.* **2010**, *46*, 3505-3507.

(12) Cangelosi, V. M.; Zakharov, L. N.; Johnson, D. W. *Angew. Chem., Int. Ed.* **2010**, *49*, 1248-1251.

(13) Piguet, C.; Bernardinelli, G.; Williams, A. F.; Bocquet, B. *Angew. Chem., Int. Ed. Engl.* **1995**, *34*, 582-584.

(14) Riis-Johannessen, T.; Bernardinelli, G.; Filinchuk, Y.; Clifford, S.; Favera, N. D.; Piguet, C. *Inorg. Chem.* **2009**, *48*, 5512-5525.

(15) Akine, S.; Taniguchi, T.; Nabeshima, T. *Angew. Chem., Int. Ed.* **2002**, *41*, 4670-4673.

(16) Albrecht, M.; Liu, Y. F.; Zhu, S. C. S.; Schalley, C. A.; Frohlich, R. *Chem. Commun.* **2009**, 1195-1197.

(17) Andruh, M. *Chem. Commun.* **2007**, 2565-2577 and references therein.

(18) Petitjean, A.; Kyritsakas, N.; Lehn, J.-M. *Chem.-Eur. J.* **2005**, *11*, 6818-6828.

(19) Dietrich-Buchecker, C.; Colasson, B.; Fujita, M.; Hori, A.; Geum, N.; Sakamoto, S.; Yamaguchi, K.; Sauvage, J.-P. *J. Am. Chem. Soc.* **2003**, *125*, 5717-5725.

(20) Piguet, C.; Hopfgartner, G.; Bocquet, B.; Schaad, O.; Williams, A. F. *J. Am. Chem. Soc.* **1994**, *116*, 9092-9102.

(21) Hahn, F. E.; Offermann, M.; Schulze Isfort, C.; Pape, T.; Fröhlich, R. *Angew. Chem., Int. Ed.* **2008**, *47*, 6794-6797.

(22) (a) Funeriu, D. P.; Lehn, J.-M.; Fromm, K. M.; Fenske, D. *Chem.-Eur. J.* **2000**, *6*, 2103-2111. (b) Stulz, E.; Scott, S. M.; Bond, A. D.; Teat, S. J.; Sanders, J. K. M. *Chem.-Eur. J.* **2003**, *9*, 6039-6048.

(23) (a) Tanya , K. R.; Jane, N.; Geoffrey , B. J.; John , C. J.; Sally, B. *Eur. J. Inorg. Chem.* **2004**, *2004*, 2570-2584. (b) Lindsay, H. U.; Jean-Paul, G.; Nathalie, K.; Kalle, N.; Kari, R.; Jean-Marie, L. *Chem.-Eur. J.* **2005**, *11*, 2549-2565. (c) Cari , D. P.; Kelly , S. C.; Andrea , J. P.; Gareth , W. V. C.; Stuart , J. C.; Stoddart, J. F. *Angew. Chem., Int. Ed.* **2007**, *46*, 218-222.

(24) (a) Kunze, A.; Bethke, S.; Gleiter, R.; Rominger, F. *Org. Lett.* **2000**, *2*, 609–612. (b) Kunze, A.; Gleiter, R. Rominger, F. *Chem. Commun.* **1999**, 171–172.

(25) Klieser, B.; Vögtle, F. *Angew. Chem., Int. Ed. Engl.* **1982**, *21*, 618.

(26) Vögtle, F.; Pawlitzki, G.; Hahn, U. In *Modern Cyclophane Chemistry*, ed. R. Gleiter and H. Hopf, Wiley-VCH, Weinheim, 2004, pp. 41–80.

(27) Schmidbaur, H.; Schier, A. *Organometallics* **2008**, *27*, 2361-2395 and references therein.

(28) Carter, T. G.; Vickaryous, W. J.; Cangelosi, V. M.; Johnson, D. W. *Comments Inorg. Chem.* **2007**, *28*, 97-122.

(29) Auer, A. A.; Mansfeld, D.; Nolde, C.; Schneider, W.; Schurmann, M.; Mehring, M. *Organometallics* **2009**, *28*, 5405-5411.

(30) Cangelosi, V. M.; Pitt, M. A.; Vickaryous, W. J.; Allen, C. A.; Zakharov, L. N.; Johnson, D. W. *Cryst. Growth Des.* **2010**, *in press*.

(31) Burford, N.; Clyburne, J. A. C.; Bakshi, P. K.; Cameron, T. S. *J. Am. Chem. Soc.* **1993**, *115*, 8829-8830.

(32) Schmidbaur, H.; Nowak, R.; Steigelmann, O.; Muller, G. *Chem. Ber.* **1990**, *123*, 1221-1226.

(33) Schmidbaur, H.; Nowak, R.; Schier, A.; Wallis, J. M.; Huber, B.; Muller, G. *Chem. Ber.* **1987**, *120*, 1829-1835.

(34) Schier, A.; Wallis, J. M.; Muller, G.; Schmidbaur, H. *Angew. Chem., Int. Ed. Engl.* **1986**, *25*, 757-759.

(35) Pitt, M. A.; Zakharov, L. N.; Vanka, K.; Thompson, W. H.; Laird, B. B.; Johnson, D. W. *Chem. Commun.* **2008**, 3936-3938.

(36) Spartan '08, Wave function, Inc., 182 Irvine,CA, 2008.

(37) Bondi, A. *J. Phys. Chem.* **1964**, *68*, 441-451.

(38) Babíc, D.; Rabii, S.; Bernholc, *J. Phys. Rev. B: Condens. Matter Mater. Phys.*, **1989**, *39*, 10831-10838.

(39) Wu, A.; Isaacs, L. *J. Am. Chem. Soc.* **2003**, *125*, 4831-4835.

(40) Kramer, R.; Lehn, J. M.; Marquisrigault, A. *Proc. Natl. Acad. Sci. U. S. A.* **1993**, *90*, 5394-5398.

(41) Nitschke, J. R.; Lehn, J. M. *Proc. Natl. Acad. Sci. U. S. A.* **2003**, *100*, 11970-11974.

(42) Ajami, D.; Hou, J. L.; Dale, T. J.; Barrett, E.; Rebek, J. *Proc. Natl. Acad. Sci. U. S. A.* **2009**, *106*, 10430-10434.

(43) Jiang, W.; Schafer, A.; Mohr, P. C.; Schalley, C. A. *J. Am. Chem. Soc.*, *132*, 2309-2320.

(44) Mukhopadhyay, P.; Wu, A. X.; Isaacs, L. *J. Org. Chem.* **2004**, *69*, 6157-6164.

(45) Tomimasu, N.; Kanaya, A.; Takashima, Y.; Yamaguchi, H.; Harada, A. *J. Am. Chem. Soc.* **2009**, *131*, 12339-12343.

(46) Shivanyuk, A.; Rebek, J. *J. Am. Chem. Soc.* **2002**, *124*, 12074-12075.

(47) Seeber, G. T., Bryan E. F.; Raymond, Kenneth N. In *Top. Curr. Chem.*; Springer Berlin: Heidelberg, 2006; Vol. 265, p 147-183.

(48) Cangelosi, V. M.; Sather, A. C.; Zakharov, L. N.; Berryman, O. B.; Johnson, D. W. *Inorg. Chem.* **2007**, *46*, 9278-9284.

(49) G. M. Sheldrick, Bruker/Siemens Area Detector Absorption Correction Program, Bruker AXS, Madison, WI, 1998.

(50) Van der Sluis, P.; Spek, A. L. *Acta Cryst., Sect. A*, **1990**, *A46*, 194-201.

(51) SHELXTL-6.10 "Program for Structure Solution, Refinement and Presentation" BRUKER AXS Inc., 5465 East Cheryl Parkway, Madison, WI 53711-5373 USA.

Appendix A

(1) Cangelosi, V. M.; Carter, T. G.; Zakharov, L. N.; Johnson, D. W. *Chem. Commun.* **2009**, 5606-5608.

Appendix B

(1) Cangelosi, V. M.; Carter, T. G.; Crossland, J. L.; Zakharov, L. N.; Johnson, D. W. *submitted to Inorg. Chem.*